Temperature Compensation of Surface Acoustic Waves on Berlinite.

by

David Michael Marshall Searle, BSc.

Thesis submitted for the degree of Doctor of Philosophy of the University of London.

Bedford College

July 1980

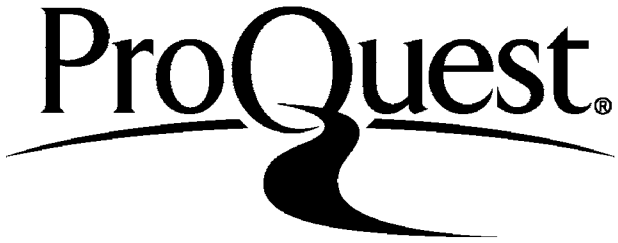

Abstract

The surface acoustic wave properties of Berlinite (α-$AlPO_4$) have been investigated theoretically and experimentally,for a variety of crystallographic orientations,to evaluate its possible use as a substrate material for temperature compensated surface acoustic wave devices.

A computer program has been developed to calculate the surface wave properties of a material from its elastic,piezoelectric, dielectric and lattice constants and their temperature derivatives. The program calculates the temperature coefficient of delay,the velocity of the surface wave, the direction of power flow and a measure of the electro-mechanical coupling. These calculations have been performed for a large number of orientations using a modified form of the data given by Chang and Barsch for Berlinite and predict several new temperature compensated directions.

Experimental measurements have been made of the frequency-temperature response of a surface acoustic wave oscillator on an 80° X axis boule cut which show it to be temperature compensated in qualitative agreement with the theoretical predictions. This orientation shows a cubic frequency-temperature dependence instead of the expected parabolic response. Measurements of the electro-mechanical coupling coefficient k^2gave a value lower than predicted. Similar measurements on a Y cut plate gave a value which is approximately twice that of ST cut quartz, but again lower than predicted. The surface wave velocity on both these cuts was measured to be slightly higher than predicted by the computer program.

Experimental measurements of the lattice parameters a and c are also presented for a range of temperatures from 25°C to just above the α-β transition at 584°C. These results are compared with the values obtained by Chang and Barsch.

The results of this work indicate that Berlinite should become a useful substrate material for the construction of temperature compensated surface acoustic wave devices.

Contents.

List of Tables in text.

List of Figures in text.

Chapter 1. Introduction.

Section 1. Introduction to SAW.

Lord Rayleigh first showed in 1885 that it was possible to propogate an acoustic wave on the free surface of an isotropic, homogeneous and elastic solid occupying an infinite half-space. This surface acoustic wave (usually abreviated to SAW) is confined to a superficial region of the solid comparable to the wavelength of the wave. The amplitude of this surface wave decays exponentially into the solid. Lord Rayleigh suggested at the end of his paper [1] that these waves might play an important part in earthquakes and the collisions of elastic solids. The study of these 'Rayleigh Waves' on the earths crust was in fact one of the first major applications of the theory and has led to a better understanding of earthquake phenomena.

Similar surface acoustic waves may also propogate on the surface of an anisotropic material such as a crystal. In particular we are interested in the use of piezoelectric crystals to allow coupling between electromagnetic and mechanical signals through the piezoelectric effect. The use of surface acoustic waves on piezoelectric crystals has led to the realisation of many devices in the field of electronic signal processing. Such devices as broad band delay lines, bandpass filters, matched filters and oscillators can all be designed using surface acoustic waves. The velocity of a surface wave is of the order of 10^{-5} of that of an electromagnetic wave. Hence the wavelength of the SAW for a given frequency is five orders of magnitude smaller than that of an electromagnetic wave of the same frequency, thus promising a reasonably compact electronic delay line. If we can obtain piezoelectric crystal substrates up to a few centimeters in length, then we can fabricate devices relatively easily for frequencies from about 10MHz to around 2GHz.

Section 2. Requirements for useful devices.

The electromagnetic signal must be converted into an acoustic wave. This is done by means of an interdigital transducer which utilises the piezoelectric effect. An interdigital transducer (IDT) consists of a pair of interlaced metal finger sets which have

been deposited on the surface of the crystal. A schematic diagram of two IDTs forming a delay line is shown in Fig.1.1. When an AC signal at a frequency corresponding to v/λ is applied at A then a reduced signal is received at B, L/v seconds later.

To obtain a useful device we need a material with good efficiency and stability. The efficiency of a piezoelectric crystal is measured by its coupling coefficient. We thus seek materials such as Lithium Niobate ($LiNbO_3$) which has a high coupling coefficient of about 4.5% and is available commercially as large crystals. The coupling coefficient k^2 is in fact related to the difference in velocity between a surface wave on a free surface and one on a metallised surface and can be written [2] :

$$k^2 = 2.(1 + \frac{1}{\varepsilon^T_{PR}}).\ \Delta v/v.(1 - \Delta v/v)^{-1} \qquad (1.1)$$

where $\Delta v/v = (v_{free} - v_{metallised})/v_{free}$, [3] (1.2)

and ε^T_{PR} is the relative dielectric constant for the orientation considered and is given by :

$$\varepsilon^T_{PR} = (\varepsilon_{11}\varepsilon_{33} - \varepsilon^2_{13})^{\frac{1}{2}}/\varepsilon_o \qquad (1.3)$$

However, for many materials equation (1.1) can be approximated by :

$$k^2 \simeq 2\Delta v/v \qquad (1.4)$$

Slobodnik [4] gives a table of values of k^2 for commonly used SAW materials.

Stability is also important and it is usually temperature stability that is required for SAW devices. Often devices are needed to work with precision in extended temperature ranges, so that materials that are temperature stable are required. Temperature changes can affect SAW devices in three ways, thermal expansion, thermal variation of effective elastic constants and thermal variation of density. The thermal variation of density is related to the thermal expansion and both are quite easy to evaluate for a given orientation of crystal. However, the thermal variation of the effective elastic constants is much more complicated. There is no simple analytic expression giving these effective elastic constants in terms of the fundamental crystal constants for an arbitrary orientation of a

Fig. 1.1

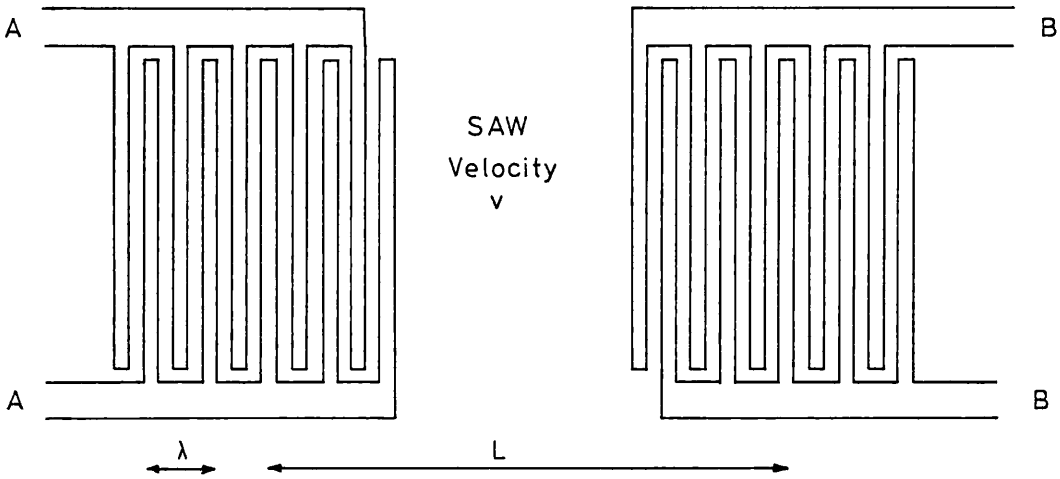

Schematic diagram of delay line.

Fig. 1.2

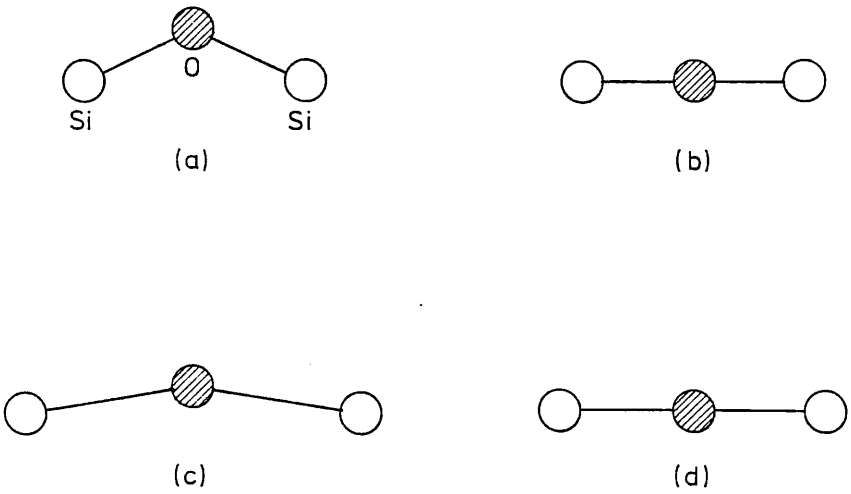

Diagrams of Si-O-Si bonds.

crystal, so the evaluation of a temperature coefficient must be performed iteratively. The orientation of the crystal is usually defined in terms of the Euler angles (α,β,γ) which are described in Chapter 2. A temperature coefficient of delay (TCD) is calculated by evaluating the delay, D(T), at three temperatures and using :

$$TCD = \frac{D(T_o + \Delta T) - D(T_o - \Delta T)}{2.\,\Delta T.D(T_o)} \qquad (1.5)$$

In the case of the computer program described in Chapter 4, T_o is 25°C and ΔT is 0.5°C. However, other writers [5] have used ΔT of 50°C.

As $\Delta T \to 0$, equation (1.5) reduces to :

$$TCD = \frac{1}{D_o}\frac{\partial D}{\partial T}\bigg|_{T_o} \qquad (1.6)$$

where D represents the time delay as a function of temperature. It is often easier to measure a temperature coefficient of frequency (TCF) which is defined at a frequency f_o at T_o as :

$$TCF = \frac{1}{f_o}\frac{\partial f}{\partial T}\bigg|_{T_o} \qquad (1.7)$$

$$= -\frac{1}{D_o}\frac{\partial D}{\partial T}\bigg|_{T_o} \qquad = -\,TCD \qquad (1.8)$$

A material that has a temperature coefficient of delay (or frequency) which is equal to zero at some temperature T_o is said to be "temperature compensated" at that temperature. The first material known to possess a temperature compensated cut was quartz on the ST cut [5]. However, the coupling coefficient k^2 for ST cut quartz is about 0.16%, so the present search for new materials which combine a high coupling coefficient and temperature compensation was begun. Unfortunately the material with the highest coupling coefficient, Lithium Niobate (4.5%), also has a large temperature coefficient of delay of $90\times10^{-6}°C^{-1}$ [4] (often written as 90ppm/°C).

Another factor that can affect the efficiency of a device is the angle of the power flow between the transducers. If the power flow direction and the propagation direction are co-linear then the

maximum proportion of power is transfered. If they are not co-linear, then clearly a reduced proportion of the power passes between the transducers and the output signal drops. The angle of power flow, ϕ, can be calculated, as shown in Chapter 2, and for an efficient device is zero (called a "pure mode axis"). Even if the power flow angle is zero, a slight misallignment between the transducers and the pure mode axis can still cause losses. Thus we need to know the slope of the power flow angle, $\frac{\partial\phi}{\partial\theta}$, with respect to misallignment. Slobodnik [4] gives an approximation valid for small angles of misorientation θ from a pure mode axis θ_o [6] :

$$\frac{v(\theta)}{v_o} \simeq 1 + \frac{1}{2}\frac{\partial\phi}{\partial\theta}(\theta - \theta_o)^2 \qquad (1.9)$$

where $v(\theta)$ is the revised surface wave velocity and v_o is the pure mode velocity. Equation (1.9) derives from :

$$\tan(\phi) \simeq \frac{1}{v}\frac{\partial v}{\partial\theta} \qquad (1.10)$$

using the small angle approximation, $\tan(\theta) \simeq \theta$.

Temperature compensation has been obtained by using many methods [7] and some of them will be outlined in the rest of this chapter.

Section 3. A phenomenological model for temperature compensation

Newnham [8] has suggested a phenomenological model to explain why some known materials are temperature compensated and to suggest areas to investigate to find new temperature compensated materials.

The time delay of a signal travelling with a velocity v over a distance L is given by :

$$D = L/v \qquad (1.11)$$

We can express the velocity v as a function of some effective elastic constant c and the density of the material ρ. Thus equation (1.11)

becomes :

$$D = L.(c/\rho)^{-\frac{1}{2}} \tag{1.12}$$

If we now take natural logarithms :

$$\ln(D) = \ln(L) + \tfrac{1}{2}\ln(\rho) - \tfrac{1}{2}\ln(c) \tag{1.13}$$

The first order differential temperature coefficient of a function x is :

$$T_x^{(1)} = \frac{1}{x}\frac{\partial x}{\partial T} = \frac{\partial}{\partial T}(\ln(x)) \tag{1.14}$$

Thus differentiating equation (1.13) with respect to T gives :

$$T_D^{(1)} = T_L^{(1)} + \tfrac{1}{2}T_\rho^{(1)} - \tfrac{1}{2}T_c^{(1)} \tag{1.15}$$

Generally $T_L^{(1)}$ is of the order of $+10^{-5}\,°C^{-1}$, $T_\rho^{(1)}$ is of the order of $-10^{-5}\,°C^{-1}$ and $T_c^{(1)}$ is of the order of $-2\times10^{-4}\,°C^{-1}$ giving an overall $T_D^{(1)}$ of the order of $10^{-4}\,°C^{-1}$. From this we note that $T_c^{(1)}$ is the dominant factor in determining $T_D^{(1)}$ and we look for materials that have unusual values of $T_c^{(1)}$ to compensate $T_L^{(1)}$ and $T_\rho^{(1)}$ in equation (1.15) and give us a temperature compensated material ($T_D^{(1)} = 0$).

If we consider quartz, we have two elastic constants c_{14} and c_{66} which have positive temperature coefficients [9] :

$$T_{c_{14}}^{(1)} = +1.78\times10^{-4}\,°C^{-1} \tag{1.16}$$

$$T_{c_{66}}^{(1)} = +1.01\times10^{-4}\,°C^{-1} \tag{1.17}$$

Thus it is likely that an orientation can be found with an effective elastic constant whose temperature coefficient sets equation (1.15) to zero. This occurs in the well known case of the ST cut of quartz.

The structures of the α and β phases of quartz provide an understanding of the unusual behaviour of $T_{c_{14}}^{(1)}$ and $T_{c_{66}}^{(1)}$, since α quartz is a partially collapsed derivative of β quartz. At high temperatures the SiO_4 tetrahedra of the α quartz structure rotate to form a fully expanded structure, undergoing a phase transition to β quartz at 573°C (see Chapter 3). The thermal expansion coefficient $T_L^{(1)}$ of quartz increases rapidly with temperature to until just below the transition temperature when it decreases abruptly to zero once the fully expanded structure is achieved. The unusual positive value of $T_{c_{66}}^{(1)}$ is related to

the rotation effect, since c_{66} relates the shear stress T_{12} about the 3 axis (z axis) to the shear strain S_{12} about the same axis. This movement is the same as that involved in the tetrahedral rotation occuring during the phase transition from α to β quartz. Similarly, c_{14} relates the shear stress T_{13} to the shear strain S_{12} which gives a twist to the tetrahedra, which is also seen to occur as the transition temperature is approached.

At room temperature the Si-O-Si bonds are bent (Fig.1.2a) in α quartz. As the structure grows closer to β quartz (Fig.1.2b), the bonds straighten with temperature (Fig.1.2c). When stressed bonds of type (a) go to type (c) where the bonds both lengthen and rotate. When bonds of type (b) are stressed they can only go to type (d) where only lengthening takes place. Structure (c) shows a larger overall change in length than type (d), hence the lower temperature structure is less elastic than the higher temperature structure and $T_C^{(1)}$ is positive. The difference between (c) and (d) also explains the abrupt change in $T_L^{(1)}$ at the α - β transition.

To sum up, Newnham's model suggests that a temperature compensated material has either of two properties,

(a) A positive temperature coefficient of an elastic constant.

or (b) A negative coefficient of thermal expansion.

This then sugests the following qualities of temperature compensated materials :

(i) Open lattice structure with an associated bending moment.

(ii) The existance of a structural phase transition.

Section 4. Temperature compensated materials.

(a) Quartz. (i) The ST cut.

The best known temperature compensated crystal is α quartz, when used in the ST cut [5,10,11,12].

Large crystals of both natural and synthetic quartz have been available for some time and several temperature compensated cuts have been found for bulk wave resonators. These include the well known AT and BT cuts [13,14]. The work on temperature compensated bulk waves prompted Schulz et al. [5] to investigate the possibility of a temperature compensated surface acoustic wave cut. They calculated the temperature dependence of surface waves for several sets of orientations using the computer model of Campbell and Jones [3] and used data from Bechmann et al. [9]. They also tried to verify their calculations experimentally. The orientations that they investigated were on the X,Y,AC and AT cuts using various directions of propagation and also along the X axis of several other rotated Y cuts (the 'X axis boule cuts'). The data that they used [9] included temperature coefficients to the third order for density and elastic constants, and they used values calculated at 50°C above and below room temperature to evaluate the temperature coefficients of delay.

Their results suggested that the best temperature compensated orientation of the ones that they found was X direction propogation on a $42\frac{1}{2}^{\circ}$ rotated Y cut, which they designated the ST cut. In a later paper [11] this was modified to a $42\frac{3}{4}^{\circ}$ rotated Y cut with a first order temperature coefficient of delay equal to zero at 25°C and a second order temperature coefficient of delay of $31.5\times10^{-9}\,°C^{-2}$. They calculated a coupling coefficient k^2 of 0.17% which is about 1/30 of that for Lithium Niobate. The SAW velocity was found to be 3158 m/s and the orientation is a pure mode axis (power flow angle, $\phi = 0$)

Hauden et al. [15] calculated the first and second order frequency-temperature coefficients for the ST cut from the experimental values obtained by Hartemann [16] and Henaff [17]. They obtained a first order TCF of -0.24 ppm/°C (parts per million per °C) and a second order coefficient of frequency of $-40\times10^{-9}\,°C^{-2}$ at 25°C.

(ii) Other cuts on quartz.

A number of authors have carried out searches to try to improve on the ST cuts performance. Table 1.1 lists the suggested cuts that are temperature compensated and have a coupling coefficient larger than that of the ST cut. A few of the orientations listed here have been checked using the computer program described in Chapter 4 with data from [9] and were found to be in good agreement with the values quoted.

Several workers have tried to find temperature compensated directions by propagating in different directions on an ST cut plate rather than the usual X axis propagation. However, the orientation found [24,25,15] which is approximately 50° away from the X axis has a greatly reduced coupling coefficient.

Schulz et al. [5], as mentioned above, investigated the X cut, the Y cut, the X axis boule, AC and AT cuts, but failed to find any orientation that improved on the ST cut. Two sets of workers [26, 10] commented on discrepancies between the calculations and the experiments caused by the use of data which did not satisfy the symmetry conditions for class 32 crystals at all temperatures. They presented improved calculations for the AC and AT cuts which agreed with the experimental results [5]. Hauden [15] also provided improved calculations for the Y cut plate which again agreed with the experimental results [5].

Jhunjhunwala et al. [27] quote some results from Slobodnik [unpublished] but these show no improvement over the ST cut.

Four major attempts to find all the theoretical temperature compensated orientations of quartz have been made [19,21,22,23]. The cuts listed in Table 1.1 are the best of those reported, but the results seem to depend on the method of calculation and data used. Sinha and Tiersten [19] use a method [20,26] involving a non-linearly based formalism where the reference geometry remains fixed whilst the temperature varies. The data that they used [28] is a modified form of [29] for use with this formalism.

Shimizu et al. [23] use an average of the data in [14] and [30], although it is a little unclear from their paper how they obtained their rotation angles. Feldmann and Henaff [21] use the elastic constants of Bechmann [29] and their temperature derivatives from Koga et al. [30]. Newton [22] uses a modified form of [9].

Hauden et al. [18] found a useful cut with reasonable

Table 1.1 Temperature compensated cuts on quartz with good coupling.

α	β (deg)	γ	v(SAW) (m/s)	$\Delta v/v$ (10^{-4})	ϕ (deg)	$\partial\phi/\partial\theta$ (deg/deg)	refs	checked by us
0	132.75	0	3158.8	5.81	0	0.378	5 ST cut	yes
55	128	37	3589.2	~5.8	3.7	-	18	
34.29	120	-19.1	3397.1	6.6	-2.5	-	19	yes
30	124.25	-16.2	3331.4	6.6	-0.9	-	19,20	yes
22.4	124.3	-15.0	3257.8	6.2	-1.5	-	19	yes
0	40.78	23	3650.5	6.8	<0.5	-	19	yes
135	45	20	3493.9	k =0.17%	3.86	-	21	
74.25	54	0	3326.7	6.5	0.02	0.20	22	
0	0	48	3157.4	5.8	0	0.37	22	
θ	ϕ	ψ						
49	133	19	3522	7.8	-1.9	-	23	
42	133	18	3531	7.7	-4.7	-	23	
53	133	20	3520	7.6	-0.2	-	23	
49	135	19	3498	7.5	-2.3	-	23	
54	134	20	3510	7.5	0.06	-	23	
53	137	19	3478	7.4	-0.7	-	23	
60	135	21	3508	7.0	2.7	-	23	
40	120	23	3654	6.8	-1.8	-	23	
60	130	23	3529	6.7	-3.2	-	23	
50	120	24	3594	6.6	-2.2	-	23	
30	150	7	3383	6.3	-8.6	-	23	
60	120	25	3521	6.1	5.7	-	23	
50	168	9	3183	5.9	-0.6	-	23	
40	0	27	3641	5.9	-4.0	-	23	
70	150	22	3422	5.9	7.0	-	23	

coupling and a second order temperature coefficient of delay much smaller than that of the ST cut. Browning and Lewis [31] found a cut giving improved temperature stability but with lower coupling than the ST cut. Lukaszek and Ballato [32] list some cuts with good coupling but which are temperature compensated in the region of 100°- 175°C. Williams and Cho [33] analysed doubly rotated cuts and found no new cuts with coupling better than ST cut quartz, although some had better temperature stability.

O'Connell has found an orientation [24,25,34] near the ST cut which has two orthogonal temperature compensated directions which could be useful for reflection grating devices such as the reflective array compressor (the RAC cut).

(b) Paratellurite, TeO_2.

Jipson et al. [35] and Jhunjhunwala et al. [27] quote results from Slobodnik [unpublished] for temperature compensated cuts on TeO_2 , which unfortunately have a coupling coefficient much lower than that of ST cut quartz. Data for TeO_2 comes from [36,37] with reference [36] showing that c_{66} increases with temperature and [37] showing that c_{13} also increases with temperature. The cuts found were :

X cut and Y cut	39°,	v = 1424 m/s,	$\Delta v/v = 8 \times 10^{-4}$,	ϕ = 37.5°
X and Y axis boule	58.2°,	v = 1387 m/s,	$\Delta v/v = 2 \times 10^{-5}$,	ϕ = 0°

(c) Thallium Vanadium Sulphide, Tl_3VS_4.

Isaacs et al. [38] measured the surface wave velocity for the ⟨110⟩ direction on Tl_3VS_4 as 870 m/s with a coupling coefficient k^2 of 1.4% which is intermediate between ST cut quartz and Lithium Niobate. For this cut they obtained a temperature coefficient of delay of -54 ppm/°C which implies the possibility of a temperature compensated cut. Prompted by this result Jhunjhunwala et al. [27,39] presented temperature compensated cuts for Tl_3VS_4 by calculation and experiment. Their computer program searched for cuts with temperature compensation and zero power flow angle simultaneously. Henaff and Feldmann [40,41, 21] computed the complete atlas of all orientations in terms of the coupling coefficient and the temperature coefficient of frequency. They found four cuts not listed by [39], although two of the cuts,

B and C, are related by symmetry. The results (excluding the cut C) are listed in Table 1.2. O'Connell and Carr [42,43,44] quote these results. The basic data for the calculations comes from [45].

(d) Thallium Tantalum Selenide, Tl_3TaSe_4.

Isaacs and Weinert [45] give the elastic constants and their first order temperature coefficients for Tl_3TaSe_4. They found a temperature compensated cut on the ⟨110⟩ plate with propogation 26° from the ⟨100⟩ direction. Jhunjhunwala et al. [27,39] also report temperature compensated cuts, as do Henaff and Feldmann [41,46] who again present the complete atlas of orientations. Henaff [46] found seven new cuts and concluded that Tl_3TaSe_4 was a better material than Tl_3VS_4 for surface wave devices since the coupling coefficients are higher. The results are shown in Table 1.3. O'Connell and Carr quote a modified result from [39].

(e) β - Eucryptite, $LiAlSiO_4$.

O'Connell and Carr [43,47] and Jhunjhunwala et al. [27] suggested that $LiAlSiO_4$ could be temperature compensated, based on Newnham's model [8]. When suitable new crystal constants became available [48] O'Connell and Carr [42,49] were able to present their theoretical results, finding two temperature compensated cuts. They noted that the material has an anomalous negative coefficient of thermal expansion in the direction of the hexagonal c axis [50,51]. This material has the highest SAW velocity of the temperature compensated materials at present known. The cuts found were :

X cut 69°, (90,90,69), v = 3662 m/s, $\Delta v/v$ = 0.1 %, ϕ = 18°
Doubly rotated (0,57,62), v = 3258 m/s, $\Delta v/v$ = 0.035%, ϕ = 0°, $\frac{\partial \phi}{\partial \theta}$ =0.32

β - Eucryptite has the structure of β quartz and has the space group $P6_422$ [52].

(f) Nepheline, $(KAlSiO_4)(NaAlSiO_4)_3$.

The elastic and thermoelastic constants of Nepheline were measured by Bonczar and Barsch [53] and they found that both c_{11} and c_{66}

Table 1.2 Temperature compensated cuts on Tl_3VS_4.

Orientation	α	β (deg)	γ	v(SAW) (m/s)	k^2 (%)	φ (deg)	references
(110) cut 70° (theory)	-45	90	70	931.3	2.0	17.7	21,27,39,40, 42,43,44
79° (expt)	-45	90	79	931.3	2.0	17.7	39
(110) cyl 24°	45	24	90	1010	1.234	0	21,39,40,41, 42,44
" " 53°	45	53	90	1033	0.8	0	21,39,40,41
A	45	36.5	62	976.9	3.02	17.8	21,40
B	0	54	30	970.5	2.44	14.7	21,40
D	30	66.6	11	984	2.98	18.0	21,40

Table 1.3 Temperature compensated cuts on Tl_3TaSe_4.

Orientation	α	β (deg)	γ	v(SAW) (m/s)	k^2 (%)	φ (deg)	T_o (°C)	references
X cut 26°	90	90	26	800	2.4	12.8	25	27,39
(110) cut 75°	45	90	75	790.4	2.8	18.0	25	27,39
" " 72°,C	45	90	72	798.4	3.35	19.48	19	46
(110) cyl 19°,A	45	19	90	866.3	1.85	0	38	39,41,46
" " 53°,B	45	53	90	890.2	1.08	0	35.5	39,41,42,46
D	30	60	9	847.1	4.17	14.57	25	46
E	60	45	51	847.1	4.01	13.59	23	46
F	40	68	60	852.5	4.02	-12.74	17	46
G	45	39.5	60	843.6	4.16	15.68	24	46
H	25	60	70	843.6	4.17	-15.93	30	46
J	32	38	70.5	849.9	4.17	16.57	21	46
K	0	62.75	50	870.8	2.12	0	20	41,46

Table 1.4 Temperature compensated cuts on $Pb_2KNb_5O_{15}$.

Orientation	α	β (deg)	γ	v(SAW) (m/s)	$\Delta v/v$ (10^{-4})	φ (deg)	$\partial\phi/\partial\theta$ (deg/deg)	
X cut 10.6°	90	90	10.6	2493	84	-2.5	-	44,57,58
Z axis cyl	24.4	90	0	2516	3.3	0	0.150	44,57,58
" "	74.4	90	0	2505	73	0	-0.268	44,57,58
Y axis boule	90	66.6	0	2525	94	0	-0.241	44,57,58

had positive temperature coefficients. This led O'Connell and Carr [42,43 47] and Juhnjhunwala et al. [27] to suggest that it might be temperature compensated. However, little further work appears to have been carried out.

(g) Lead Potassium Niobate, ($Pb_2KNb_5O_{15}$).

Lead Potassium Niobate was suggested by O'Connell and Carr [42,43,47] as a temperature compensated material on the basis that some cuts that are used for bulk wave devices had temperature coefficients of frequency with opposite signs. The material also has large coupling coefficients for bulk waves [54,55]. Using the data from references [54,56], O'Connell calculated [44,57,58] four temperature compensated cuts shown in Table 1.4. Yamuchi [59] noted strong electromechanical coupling of SAWs but did not perform any temperature calculations.

(h) Lead Titanate Ceramic, ($PbTiO_3$).

Lead Titanate ceramics with additions of Nd_2O_3, In_2O_3 and MnO_2 have been shown to be temperature compensated [60] with a SAW velocity of 2554 m/s, a coupling coefficient k^2 of 2.6% and a second order temperature coefficient of delay of about one quarter that of ST cut quartz.

(i) Other Crystals.

Several other crystals have been suggested as possibly having temperature compensated orientations. The quartz isomorphs [27, 47], $AlPO_4$, $AlAsO_4$, BPO_4, $BAsO_4$, $GaPO_4$ and $GaAsO_4$ will be discussed in Chapter 3, together with $FePO_4$, $FeAsO_4$, $MnPO_4$, $MnAsO_4$, $AlVO_4$ and GeO_2. These are mostly 'half breed' derivatives of quartz. Jhunjhunwala et al. [27] also suggest various 'stuffed' derivatives of quartz, where one or more of the silicon atoms is replaced by an atom of lower valency, the valence being supplied by an alkali atom or atoms in interstitial spaces of the structure. Such materials are, $LiAlSiO_4$ (β - Eucryptite, see section 4e above), $NaAlSiO_4$, $KAlSiO_4$, $SrAl_2O_4$, $BaAl_2O_4$, $K_2Al_2O_4$, $BaFeO_4$, $PbFe_2O_4$, $SrFe_2O_4$, $K_2Fe_2O_4$, $Rb_2Fe_2O_4$ and $NaCaSiO_4$. Some more complicated formulae include $(KAlSiO_4)(NaAlSiO_4)_3$ (Nepheline, see section 4f above) and $NaCaAl_3Si_{15}O_{36}$ (natural Tridymite).

Carr [47] also suggested the ferroelectrics Bi_2WO_6, $Bi_4Ti_3O_{12}$, Ba_2GeTiO_2, $Ba_2NaNb_5O_{15}$, $Pb_5Ge_3O_{11}$ and $Pb_2KNb_5O_{15}$ (Lead Potassium Niobate, see section 4g above). $Ba_2NaNb_5O_{15}$ is known to have positive temperature coefficients of c_{44} and c_{55} [61], but $\Delta v/v$ is not much larger than that of quartz [62]. The temperature coefficients of c_{11}, c_{12}, c_{13} and c_{33} of $Pb_5Ge_3O_{11}$ are all positive above the ferroelectric Currie temperature of 177°C [63], but this is only for a 20°C temperature range. The material also has low coupling coefficients and high losses which implies that the crystal will not be very useful for our purposes. The similar crystal $Ba_2Si_2TiO_8$ [64,65,66,67] was found not to be temperature compensated.

Lithium Iodate ($LiIO_3$) was thought to possess temperature compensated cuts [35] due to an error in the published data [68]. When the error was corrected no temperature compensated cuts were found which is in agreement with the experimental findings [69].

Section 5. Other methods of obtaining temperature compensation.

Several other methods of obtaining temperature compensation have been suggested [7]. Jhunjhunwala et al. mention temperature compensation in ceramics and in composite materials such as layers of quartz deposited on lithium niobate or lithium tantalate, or even bonded slabs of quartz and lithium niobate [27]

(a) Overlays.

Carr and O'Connell [42,43,47] quote the results obtained by Parker et al. [70,71] for a thin film of SiO_2 overlaid on YZ cut $LiTaO_3$ [72,73,74] and on YZ cut $LiNbO_3$. These results give a coupling coefficient k^2 of 6.2% for SiO_2 on $LiNbO_3$ and k^2 of 1.6% for SiO_2 on $LiTaO_3$. The SiO_2 layer compensates for the large coefficient of delay of $LiNbO_3$ or $LiTaO_3$. The SiO_2 on $LiTaO_3$ structure has a second order temperature coefficient of delay which is much smaller than that of ST cut quartz. However it is quite difficult to fabricate devices since the thickness of the quartz overlay has to be critically controlled. The film also causes dispersion and increases propogation losses.

Two groups have looked at SiO_2 on other orientations of $LiTaO_3$. Parker and Wichansky [74] found five other suitable temperature compensated orientations and Yamanouchi et al. [75] tried SiO_2 on the

36° and 126° rotated Y cut, X propogating, $LiTaO_3$ giving k^2 of 5.1% and 2.7% respectively.

Another overlaid composite is ZnO film on Pyrex [76,77], this has a coupling coefficient k^2 of 1%. A film of ZnO on Z cut quartz [78] gives k^2 of 0.45% and overlaying SiO_2 on top of that gives an improved second order temperature coefficient. ZnO on glass [79] gave a temperature coefficient of delay of -10 ppm/°C and could be modified to achieve temperature compensation.

(b) Bonded structures.

Carr [47] refers to a bonded structure of $LiNbO_3$- SiO_2- $LiNbO_3$ made by Wauk [80,81] with a zero first order temperature coefficient of delay and a second order coefficient similar to that of ST cut quartz. However, losses occuring across the bonds put an upper frequency limit on any device constructed and the composite substrate is also difficult to fabricate.

(c) Other methods.

Temperature compensation has also been achieved by both electrical and mechanical means. Hohkawa and Yoshikawa [82] have used multiple parallel connected SAW resonators of different temperature characteristics to obtain less than 2 ppm frequency change over a temperature range of 60°C. They used 35° and 46° X axis boule cuts with turnover temperatures of 65°C and -15°C respectively. Coldren [83] used multiple coupling paths on a single crystal to give temperature stability over a wider range of temperatures than ST cut quartz. Kinsman [84] used two series varactors driven by a linear voltage versus temperature function to obtain less than 4 ppm variation on ST cut quartz between -40°C and 70°C. Lee [85] suggested thermal compensation by electronic control of a phase shift element in a feedback loop to obtain temperature stability for resonators.

Toda and Osaka [86] have used a $LiNbO_3$- bimetallic strip to obtain temperature compensation with good coupling.

Section 6. Conclusions and Discussion.

It can be seen from the above survey that there is, as yet, no easily obtainable material or method which improves substantially on the properties of the widely used ST cut of quartz. Several promising materials have been identified, but much work still remains to be done to verify experimentally the theoretical predictions. In many cases it is difficult to obtain good quality crystals of any useful size, or else the fabrication techniques are difficult to carry out with any degree of accuracy and consistancy. Many of the materials also introduce more losses into the device which negates any improvement achieved in the coupling coefficient.

Berlinite has been excluded from the above survey since the results obtained by other workers are discussed in Chapters 3,4 and 5 and our results are the subject of this study. Berlinite seems to be one of the most promising of the new materials which are temperature compensated. A great deal of effort is being put into the growth of high quality crystals of berlinite and into the measurement of the SAW properties of various orientations, ensuring that the study of berlinite is rather more advanced than most of the other materials mentioned above.

Chapter 2. Theory of surface acoustic waves.

Section 1. Introduction.

We wish to be able to calculate the surface acoustic wave properties for any crystal for any arbitrary orientation of that crystal. We start from the elastic, piezoelectric and dielectric constants of the crystal together with its density. These constants are used in the piezoelectric constitutive equations, which together with Maxwell's electromagnetic field equations, enable us to derive a wave equation for the surface wave. This gives us a set of equations involving the surface wave velocity and the decay coefficients of its propogation vector. When the boundary conditions of the problem are introduced, we can then use an iterative method to solve for the surface wave velocity and the decay coefficients simultaneously.

Section 2. Axis rotation.

To calculate the surface wave properties of an arbitrary orientation of a crystal we must first define a rotation matrix. This transforms the crystal constants from the standard X,Y,Z (x_1,x_2,x_3) reference frame to a new, primed, reference frame (x_1',x_2',x_3'). Figure 2.1 shows the convention used to obtain the Euler rotation angles (α,β,γ). The rotation matrix for this transformation is :

$$V_{ij} = \begin{bmatrix} \cos\alpha\cos\gamma - \sin\alpha\cos\beta\sin\gamma, & \sin\alpha\cos\gamma + \cos\alpha\cos\beta\sin\gamma, & \sin\beta\sin\gamma \\ -\cos\alpha\sin\gamma - \sin\alpha\cos\beta\cos\gamma, & -\sin\alpha\sin\gamma + \cos\alpha\cos\beta\cos\gamma, & \sin\beta\cos\gamma \\ \sin\alpha\sin\beta, & -\cos\alpha\sin\beta, & \cos\beta \end{bmatrix} \quad (2.1)$$

We have chosen x_1' as the propogation direction, x_3' as the outward plate normal and x_2' lying on the surface of the plate as shown in figure 2.2 [27,87]. Other workers have defined x_3' to be the inward plate normal [3,4,42]. This means that to achieve consistancy in notation for the orientation we must replace β by $\beta-180^\circ$ and α by $-\alpha$ in equation (2.1). This has been done for our computer program (see Appendix 1).

We now have the following transformations for the elastic stiffness tensor c_{ijkl}', the piezoelectric tensor e_{ijk}', the dielectric tensor ϵ_{ij}' and the thermal expansion coefficient α_{ij}' :

Figure 2.1

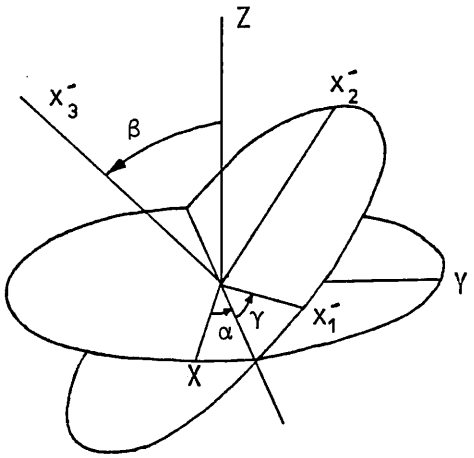

Euler rotation angles (α,β,γ).

Figure 2.2

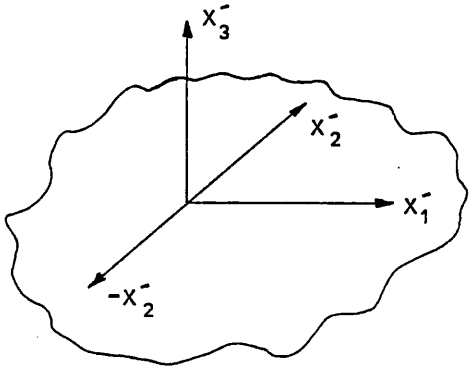

Axis reference frame.

$$c'_{ijkl} = \sum_{pqtu} V_{ip}V_{jq}V_{kt}V_{lu}\, c_{pqtu} \qquad i,j,k,l,p,q,t,u=1,2,3 \quad (2.2)$$

$$e'_{ijk} = \sum_{pqt} V_{ip}V_{jq}V_{kt}\, e_{pqt} \qquad i,j,k,p,q,t=1,2,3 \quad (2.3)$$

$$\varepsilon'_{ij} = \sum_{pq} V_{ip}V_{jq}\, \varepsilon_{pq} \qquad i,j,p,q=1,2,3 \quad (2.4)$$

$$\alpha'_{ij} = \sum_{pq} V_{ip}V_{jq}\, \alpha_{pq} \qquad i,j,p,q=1,2,3 \quad (2.5)$$

These equations will be used to calculate the new values of these constants in the chosen orientation described by the Euler angles (α,β,γ).

Section 3. Surface acoustic wave equations.

We will use the repeated index summation notation, the comma notation for differentiation with respect to a direction and the dot notation for differentiation with respect to time. The primes refer to the new, rotated reference frame but will be dropped later.

In a solid the field equations governing the motion of a particle are :

$$\dot{p}'_i = T'_{ij,j} + F'_i \quad (2.6)$$

where $p'_i = \rho v'_i$ and $v'_i = \dot{u}'_i$, where u'_i is the particle displacement field and v'_i is the particle velocity field, p'_i is the momentum density, ρ is the mass density, F'_i is the external force per unit area and T'_{ij} is the mechanical stress tensor.

Maxwell's electromagnetic field equations relating the electric field intensity, E, the electric flux density, D, the current density, J, the magnetic field intensity, H, the magnetic flux density, B, and the free charge density, σ_E , can be written :

$$D'_{i,i} = \sigma_E \quad (2.7)$$

$$-\varepsilon_{ijk}E'_{j,k} = -\dot{B}'_i \quad (2.8)$$

$$-\varepsilon_{ijk}H'_{j,k} = J'_i + \dot{D}'_i \quad (2.9)$$

$$B'_{i,i} = 0 \quad (2.10)$$

where ε_{ijk} is the Levi-Civita pseudotensor ($\varepsilon_{123} = \varepsilon_{231} = \varepsilon_{312} = 1$, $\varepsilon_{132} = \varepsilon_{321} = \varepsilon_{213} = -1$, $\varepsilon_{ijk} = 0$ otherwise).

We will assume that there is no external force F_i^- acting and that there are no magnetic fields present. Since the surface wave velocity is several orders of magnitude less than the velocity of light we can assume a quasi-static approximation is valid. Thus :

$$B_i^- = H_i^- = 0 \tag{2.11}$$

$$E_i^- = -u_{4,i} \tag{2.12}$$

$$F_i^- = 0 \tag{2.13}$$

where u_4^- is the quasi-static electric potential (often written as ϕ) in the crystal.

The piezoelectric constitutive equations for the rotated crystal are :

$$D_i^- = \varepsilon_{ij}^- E_j^- + e_{ijk}^- S_{jk}^- \tag{2.14}$$

and

$$T_{jk}^- = -e_{ijk}^- E_i^- + c_{jkil}^- S_{il}^- \tag{2.15}$$

where T_{jk}^- is the stress tensor and S_{jk}^- is the strain tensor. The strain in the solid is given by :

$$S_{ij}^- = \tfrac{1}{2}(u_{i,j}^- + u_{j,i}^-) \tag{2.16}$$

We will assume from now on that all equations refer to the rotated reference frame and we will drop the use of primes.

If we now substitute equations (2.15) and (2.16) into equation (2.6) :

$$\rho \ddot{u}_i = T_{ij,j} \tag{2.17}$$

$$= -e_{kij} E_{k,j} + c_{ijkl} S_{kl,j} \tag{2.18}$$

$$= e_{kij} u_{4,kj} + c_{ijkl} \cdot \tfrac{1}{2}(u_{k,li} + u_{l,ki}) \tag{2.19}$$

thus

$$\rho \ddot{u}_i = e_{kij} u_{4,kj} + c_{ijkl} u_{k,lj} \tag{2.20}$$

since $c_{ijkl} = c_{ijlk}$.

If the surface charge density σ_E is zero then :

$$D_{i,i} = 0 \tag{2.21}$$

and we can substitute equation (2.14) into equation (2.21) and we obtain :

$$-\varepsilon_{ij}\, u_{4,ij} + e_{ijk} S_{jk,i} = 0 \tag{2.22}$$

$$-\varepsilon_{ij}\, u_{4,ij} + e_{ijk} u_{j,ki} = 0 \tag{2.23}$$

since $e_{ijk} = e_{ikj}$.

Equations (2.20) and (2.23) give us the field equations in terms of the crystal constants. We can now try a plane wave solution of the form :

$$u_r = a_r \exp\{i(k_p x_p - \omega t)\} \qquad r=1,2,3,4 \tag{2.24}$$

and we can write k_p in the form $k_p = K\ell_p$, where K is the wave vector in the propagation direction (x_1) and ℓ_p are the direction cosines. We can choose $\ell_1 = 1$, $\ell_2 = 0$ and $\ell_3 = \ell_3$ if we assume that the wave is uniform in the x_2 direction. This reduces the plane wave solution to :

$$u_r = a_r \exp\{iK(\ell_p x_p - vt)\} \qquad r=1,2,3,4 \tag{2.25}$$

$$= a_r \exp\{iK(x_1 + \ell_3 x_3 - vt)\} \tag{2.26}$$

where $\omega = Kv$. Now substitute this into the field equations (2.20) and (2.23) :

$$c_{ijkl} a_k \ell_l \ell_j + e_{kij} a_4 \ell_k \ell_j = \rho v^2 a_i \tag{2.27}$$

$$e_{ijk} a_j \ell_k \ell_i - \varepsilon_{ij} a_4 \ell_i \ell_j = 0 \tag{2.28}$$

or rewriting equation (2.28) with a change of subscripts :

$$e_{jkl} a_k \ell_l \ell_j - \varepsilon_{jk} a_4 \ell_j \ell_k = 0 \tag{2.29}$$

This gives us a set of four equations :

$$(A_{rs} - \delta'_{rs}\rho v^2)a_r = 0 \qquad r,s=1,2,3,4 \qquad (2.30)$$

where $A_{pq} = \ell_i c_{ipql}\ell_l \qquad p,q=1,2,3 \qquad (2.31)$

$$A_{p4} = A_{4p} = e_{ipj}\ell_i\ell_j \qquad (2.32)$$

$$A_{44} = -\epsilon_{ik}\ell_i\ell_k \qquad (2.33)$$

$$\delta'_{rs} = \delta_{rs} - \delta_{r4}\delta_{s4} \qquad r,s=1,2,3,4 \qquad (2.34)$$

If we now solve equation (2.30) for ℓ_3 (using $\ell_1 = 1$, $\ell_2 = 0$) we find that, for a non-trivial solution, ℓ_3 is the solution of :

$$|A_{rs} - \delta'_{rs}\rho v^2| = 0 \qquad (2.35)$$

In general ℓ_3 is complex and the solution of equation (2.35) gives eight possible values of ℓ_3 which occur in complex conjugate pairs. Four of these solutions will have the imaginary part of ℓ_3 less than zero, which corresponds to a wave decaying into the substrate. These solutions will be denoted by $\ell_3^{(m)}$ with corresponding eigenvectors $a_r^{(m)}$ (m=1,2,3,4). We now have trial solutions formed by a linear superposition of the plane wave solutions (2.25) :

$$u_r = \sum_{m=1}^{4} C_m a_r^{(m)} \exp\{iK(x_1 + \ell_3^{(m)} x_3 - vt)\} \qquad r=1,2,3,4 \qquad (2.36)$$

These trial solutions are general solutions to which we must now introduce the boundary conditions.

Section 4. Boundary conditions.

The boundary conditions that we have are for a stress free surface which is either 'free' or covered with a massless metallisation (the metallisation is massless so that it only affects the electrical conditions). The electric flux density must also be continuous across the boundary at the surface.

The stress free condition gives :

$$T_{3j} = 0 \qquad = c_{3jkl}u_{k,l} + e_{k3j}u_{4,k} \qquad x_3 = 0 \qquad (2.37)$$

For a metallised surface :

$$u_4 = 0 \qquad x_3 = 0 \qquad (2.38)$$

and for a free surface :

$$u_{4,ii} = 0 \qquad \text{for } x_3 > 0 \qquad (2.39)$$

since $\sigma_E = 0$ in equation (2.7) which is then differentiated with respect to i and $\varepsilon_o E_i$ is substituted for D_i , followed by the use of equation (2.12).

Equation (2.39) implies the exponential decay of u_4 above the surface of the crystal :

$$u_4(x_1,x_2,x_3,t) = u\,(x_1,x_2,0,\,t).\exp(-Kx_3) \qquad (2.40)$$

The continuity of the electric flux density across the boundary for a free surface gives us :

$$D_3 = \varepsilon_o E_3 \qquad (2.41)$$

$$= -\varepsilon_o u_{4,3} \qquad \text{for } x_3 > 0 \qquad (2.42)$$

$$= e_{3kl}u_{k,l} - \varepsilon_{3k}u_{4,k} \qquad \text{for } x_3 < 0 \qquad (2.43)$$

Thus :

$$e_{3kl}u_{k,l} - \varepsilon_{3k}u_{4,k} - K\varepsilon_o u_4 = 0 \qquad x_3 = 0 \qquad (2.44)$$

The continuity of D_3 across the boundary for a metallised surface is implicit in equation (2.38).

When these conditions are imposed upon the trial solutions we find :

$$d_{mn}C_n = 0 \qquad m,n=1,2,3,4 \qquad (2.45)$$

where $$d_{jn} = c_{3jkl}\ell_l^{(n)} a_k^{(n)} + e_{k3j}\ell_k^{(n)} a_j^{(n)} \qquad k,j,l=1,2,3 \qquad (2.46)$$

and $$d_{4n} = a_4^{(n)} \qquad \text{for a metallised surface} \qquad (2.47)$$

or $$d_{4n} = e_{3kl}\ell_l^{(n)} a_k^{(n)} - (\varepsilon_{3k}\ell_k^{(n)} - i\varepsilon_o)a_4^{(n)} \quad \text{for a free surface} \tag{2.48}$$

Thus the equation to solve for the surface wave velocity is, for a non-trivial solution :

$$|d_{mn}| = 0 \tag{2.49}$$

When this has been solved by an iterative process for v, $\ell_k^{(m)}$, $a_r^{(m)}$, C_m we can calculate other useful quantities such as the direction of power flow from the plane wave superpositions, u_r.

Section 5. Time averaged power flow vector.

We wish to calculate the direction in which the power is transmitted by the surface wave since this is not always co-linear with the propogation direction. This is found by calculating the time averaged power flow from the plane wave superpositions (2.36). If the surface power flow angle (2.63) is zero we have a pure mode axis. It is also useful to know the slope of the power flow angle, $\partial\phi/\partial\theta$, to see the effects of any accidental transducer misallignment. The power flow angle is usually denoted by ϕ.

Section 6. Derivation of power flow angles.

We have the plane wave superpositions (2.36) which in general can be written :

$$u_r = \sum_{m=1}^{4} C_m a_r^{(m)} \exp\{iK(\ell_p^{(m)} x_p - vt)\} \tag{2.50}$$

where $\ell_1^{(m)} = 1$, and $\ell_2^{(m)} = 0$.

The time averaged power flow vector in the crystal is given by [4,64] :

$$W_q = -\tfrac{1}{2}\mathrm{Re}\left(\int_{-\infty}^{0} T_{qj}\, \dot{u}_j^{*}\, dx_3 - \int_{-\infty}^{0} \dot{D}_q^{*}\, u_4\, dx_3 \right) \tag{2.51}$$

$$= -\tfrac{1}{2}\mathrm{Re}\left(\mathrm{Re}\{P_{qM}\} - \mathrm{Re}\{P_{qE}\}\right) \tag{2.52}$$

where P_{qM} is the mechanical power flow in the q direction and P_{qE} is the electrical power flow in the q direction.

Substituting equation (2.50) into equation (2.15) we

obtain :

$$T_{qj} = \sum_{m=1}^{4} C_m iK\left(e_{kqj} a_4^{(m)} \ell_k^{(m)} + c_{qjkl} a_k^{(m)} \ell_l^{(m)}\right) \exp\{iK(\ell_p^{(m)} x_p - vt)\} \tag{2.53}$$

Differentiating equation (2.50) with respect to time and taking complex conjugates gives :

$$(\dot{u}_j)^* = \sum_{n=1}^{4} C_n^* (a_j^{(n)})^* (iKv) \exp\{-iK(\ell_p^{(n)*} x_p - vt)\} \tag{2.54}$$

Now substituting these two equations (2.53) and (2.54) into the mechanical term in equation (2.52) gives :

$$P_{qM} = \int_{-\infty}^{0} T_{qj} \dot{u}_j^* \, dx_3 \tag{2.55}$$

$$= \int_{-\infty}^{0} \sum_{m=1}^{4} \sum_{n=1}^{4} C_n^* C_m (a_j^{(n)})^* (iKv)(iK)\left(e_{kqj} a_4^{(m)} \ell_k^{(m)} + c_{qjkl} a_k^{(m)} \ell_l^{(m)}\right) . \exp\{iK(\ell_3^{(m)} - \ell_3^{(n)*}) x_3\} dx_3 \tag{2.56}$$

for $\ell_3^{(m)} \neq (\ell_3^{(n)})^*$.

$$P_{qM} = \sum_{m=1}^{4} \sum_{n=1}^{4} C_n^* C_m (a_j^{(n)})^* (iKv)(iK)\left(e_{kqj} a_4^{(m)} \ell_k^{(m)} + c_{qjkl} a_k^{(m)} \ell_l^{(m)}\right) . \int_{-\infty}^{0} \exp\{iK(\ell_3^{(m)} - \ell_3^{(n)*}) x_3\} dx_3 \tag{2.57}$$

Now the integral term gives :

$$\int_{-\infty}^{0} \exp\{iK(\ell_3^{(m)} - \ell_3^{(n)*}) x_3\} dx_3 = \frac{1}{iK(\ell_3^{(m)} - \ell_3^{(n)*})} \{-e^{-i\infty} + e^{i0}\} \tag{2.58}$$

$$= \frac{1}{iK(\ell_3^{(m)} - \ell_3^{(n)*})} \tag{2.59}$$

Thus the mechanical power flow is given by :

$$P_{qM} = \sum_{m=1}^{4} \sum_{n=1}^{4} \frac{C_n^* C_m (a_j^{(n)})^* (iKv)}{(\ell_3^{(m)} - \ell_3^{(n)*})} \{e_{kqj} a_4^{(m)} \ell_k^{(m)} + c_{qjkl} a_k^{(m)} \ell_l^{(m)}\} \tag{2.60}$$

Similarily for the second term in equation (2.52), the electrical power flow is given by :

$$P_{qE} = \int_{-\infty}^{0} u_4 \dot{D}_q^* \, dx_3 \tag{2.61}$$

$$= \sum_{m=1}^{4} \sum_{n=1}^{4} \frac{C_n^* C_m a_4^{(m)} (iKv) \{\varepsilon_{qj} (a_4^{(n)})^* (\ell_j^{(n)})^* - e_{qjk} (a_j^{(n)})^* (\ell_k^{(n)})^*\}}{(\ell_3^{(m)} - \ell_3^{(n)*})} \tag{2.62}$$

So when equations (2.60) and (2,62) are substituted into equation (2.52) we obtain the components W_q of the power flow vector. Note that in equations (2.59), (2.60) and (2.62) the factor $(\ell_3^{(m)} - \ell_3^{(n)*})$ is only evaluated if it is non zero, since zero terms disappear in equation (2.56) before the integrations are performed. This avoids the possibilities of singularities occuring in W_q.

The power flow angle in the surface is given by :

$$\phi_1 = \tan^{-1}(W_2/W_1) \tag{2.63}$$

The leakage of power into the bulk of the material is given by $-W_3$ and hence the angle of power flow into the bulk is :

$$\phi_2 = \tan^{-1}(-W_3/W_1) \tag{2.64}$$

For a surface wave ϕ_2 should be zero and this is a useful check that a pseudosurface wave or a bulk wave solution has not been found.

Section 7. Pseudosurface waves.

In general a surface wave on a crystal has a phase velocity which is lower than that of the slowest bulk wave in the same direction. However, a mode of propagation, similar to that of the surface wave, but with a phase velocity in excess of that of the slowest bulk wave, has been identified for some orientations of various crystals [88]. This has been shown [89] to contain a bulk wave component together with components decaying with depth that a normal surface wave contains. The wave radiates energy into the bulk of the crystal and also suffers attenuation in the direction of propagation.

Lim and Farnell [88] have shown that the boundary conditions cannot be satisfied by the choice of the $\ell_i^{(n)}$ made in equation (2.26) for this new wave. The magnitude of the boundary condition determinant decreases rapidly near this phase velocity but cannot be made arbitrarily small, as it can for a true surface wave, by using real values of $\ell_1^{(n)}$ and $\ell_2^{(n)}$. They found at this phase velocity that a pair

of the complex roots $\ell_3^{(n)}$ of equation (2.35) lay on the real axis and correspond to terms in equation (2.25) that do not decay with depth. They modified their calculations to allow for complex values of $\ell_1^{(n)}$ and $\ell_2^{(n)}$ and found that by adding a small imaginary part to both $\ell_1^{(n)}$ and $\ell_2^{(n)}$ that they could make the magnitude of the boundary condition determinant arbitrarily small corresponding to a 'pseudosurface wave' solution. This modification made the coefficients of $\ell_3^{(n)}$, in equation (2.35), complex and thus removed the constraint that the $\ell_3^{(n)}$ must occur in exact complex conjugate pairs. One of the $\ell_3^{(n)}$ pairs now have extra small real parts corresponding to a bulk wave with its propogation vector tilted into the solid.

This mode of propogation can cause confusion in surface wave calculations, since sometimes during the iterative search for a minimum in the magnitude of the boundary condition determinant, the computer program tries to find a solution near a pseudosurface wave velocity. In this case the boundary condition determinant cannot be made zero and the program fails to find a solution to equation (2.35).

Another mode of propogation that can cause computational problems is a bulk wave with a velocity near that of the surface wave. For certain orientations of some crystals the surface wave can degenerate into this bulk wave which satisfies the boundary conditions by itself [87]. This has been noticed for a range of orientations along the X axis boule of Berlinite (see Chapter 4).

For certain special directions, the psuedosurface wave is a true surface wave with a velocity higher than that of the slowest bulk wave in the same direction. This seems to occur at orientations for which the normal surface wave velocity is at a maximum or minimum and the imaginary parts of the roots $\ell_1^{(n)}$ and $\ell_2^{(n)}$ are zero. This is often a symmetry direction and corresponds with a pure mode axis.

Chapter 3. Quartz isomorphs and Berlinite.

Section 1. The crystal structure of quartz.

The crystal structure of α quartz is well known, it belongs to the crystal class 32 and has either of the space groups $P3_121$ or $P3_221$ corresponding to 'right' or 'left' quartz [90]. The elastic, piezoelectric and dielectric constants have been measured several times [9,29,30] together with their temperature derivatives [9,30]. Three authors [28,91,92] have recalculated the values of these temperature derivatives to give greater accuracy in calculations. The lattice constants [9,93] and thermal expansion coefficients [9,94] have also been measured. This gives us a full set of crystal data for use in surface wave calculations (see Chapter 1).

Quartz sometimes suffers from electrical or 'Dauphine' twinning which consists of a region in which there is a 180° crystal rotation about the c axis giving a reversal of sign of both the x and y axes [95,96,97].

Quartz undergoes a phase transformation from its trigonal (class 32) form to its β quartz structure which is hexagonal (class 62) at about 573°C [98,99,100,101] to 579°C [94]. β quartz can also exist in 'left' (space group $P6_422$) or 'right' forms (space group $P6_222$). During the phase transformation the SiO_4 tetrahedra, that can be considered to make up the basic structure of quartz, rotate slightly and alter the symmetry of the crystal (see Chapter 1) to a more ordered hexagonal form [8]. The angle of this rotation has been measured and found to be about 16° [98,102,103]. Taylor [104] gives the angle of rotation from the ideal, i.e. β structure, as 16.2° at 27°C, 8° at 570°C and 0° at 600°C showing how rapidly the structure rotates at higher temperatures near the α-β transition.

Quartz was the first material that was discovered to possess temperature compensated surface acoustic wave orientations, [5] although it had been known to possess temperature stable bulk wave orientations. Following Newnham's model [8] some authors [27,47] have suggested that quartz isomorphs should be investigated to see if they also possess temperature compensated orientations. Jhunjhunwala et al. [27] suggested the isomorphs where alternate silicon atoms of the quartz crystal are replaced by atoms of valence 5 and 3. They suggested $AlAsO_4$, $AlPO_4$ (Berlinite), $BAsO_4$, BPO_4, $GaAsO_4$ and $GaPO_4$. Other similar isomorphs are $AlVO_4$, $FePO_4$, $FeAsO_4$, $MnPO_4$, $MnAsO_4$ and GeO_2. Table 3.1

Table 3.1 Quartz isomorphs.

Isomorph	α quartz structure	a (Å)	c (Å)	refs	comments
$AlAsO_4$	✓	5.03	11.22	105,106,107	ρ=3.34 gm/cc
	✓	5.030	11.23	106	
$AlPO_4$	(see Table 3.2)				
$AlVO_4$	-			108	
$BAsO_4$	X	4.458	6.796	108,109	ρ=3.660 gm/cc
	?	4.562	10.33	106,110	Trigonal
BPO_4	X	4.332	6.640	109	Trigonal, ρ=2.802gm/cc
	?	4.94	11.08	108	uncertain
	?	4.47	9.93	110	Trigonal
$FeAsO_4$	-			108	
$FePO_4$	✓	5.035	11.176	108	α→β at 707°C
	✓	5.04	11.24	106,108	
	✓	5.051	11.27	106	α→β at 707°C
$GaAsO_4$	✓	5.00	11.36	106,107,111	
	✓	4.996	11.39	106	
$GaPO_4$	✓	4.917	11.10	112	
	✓	4.92	11.00	106,107,111	
	✓	4.910	11.07	106	
GeO_2	✓			113	
$MnAsO_4$	-			108	
$MnPO_4$	✓	4.94	10.96	108	α→β at 813°C

lists some of the properties of these suggested isomorphs and indicates that $AlAsO_4$, $AlPO_4$, $GaAsO_4$, $GaPO_4$, $FePO_4$, $MnPO_4$ and GeO_2 have all been shown to be quartz isomorphs.

Section 2. Berlinite crystal growth.

Berlinite has been found naturally at only two locations, in the Westana in Sweden [114] and in the Buranga pegmatite from Rwanda [115]. Since then it has been synthesised by Huttenlocher [116], Jahn and Kordes [117] and Stanley [118]. Stanley used an homogeneous, acidic solution and slowly increased the temperature. More recently other workers have used the method of Stanley but with some slight modifications [107,119,120,121,122]. Chai et al. [123,124] have tried a different method using a transport growth system similar to that used for synthetic quartz crystal growth.

The crystals used for the work described below were grown by D.F. Croxall at the GEC Hirst Research Centre (Wembley) [125] and the method used will be described here.

Since the solubility of berlinite is retrograde, unsaturated nutrient solutions can be brought to saturation by heating from room temperature, leading to either spontaneous nucleation of new crystal seeds or an overgrowth on an existing seed crystal in the system. A rapid temperature rise to near the saturation point followed by a very slow rise in temperature of about 1°C per day was used followed by a rapid cooling. The rapid heating and cooling stages either side of the growth stage are needed to minimise the dissolution of the seed or crystals in the high solubility low temperature region. In the initial heating stage the seed plate thins due to this dissolution, but thickens rapidly during the slow heating growth stage. Towards the end of this slow heating stage the rate of thickening gradually decreases, and then during the rapid cooling some more dissolution occurs. This final dissolution leaves the crystals with heavily etched surfaces.

Three types of crystal have been grown at the GEC Hirst Research Centre. Spontaneously nucleated crystals have enabled crystals up to 40mm along the c axis to be grown by repeated overgrowth. However, interfaces caused by the repeated cycling of the crystal have led to low quality which has been improved by single runs of extended duration. Seeds cut parallel to basal plane were also tried but rapidly flawed after reaching a thickness of about 2mm. Crystals

grown on rhombohedral seed plates give satisfactory growth although at a slower rate.

Initially both Dauphine (electrical) and Brazil (optical) twinning was observed, but the amount of twinning has decreased with better crystals (see Chapter 5 for details of the crystals used for SAW measurements). Twinning has also been observed by Kolb et al. [122] who reported twinning revealed by etching. Chai et al. [124] show photographs of the etched surface of a crystal revealing both types of twinning. Van Tenderloo et al. [96,97] also report Dauphine twinning near the α-β transition. Brill and de Bretteville [126] also report electrical twinning and Lang et al. [127] describe irreversibly twinned crystals.

It can be seen from the above that twin free crystals are not easily grown and it is felt that the later examples of the crystals grown at the GEC Hirst Research Centre are amongst the best currently available for crystal property measurements.

Section 3. Lattice constants of berlinite.

The lattice parameters a and c of berlinite have been measured by several authors and the results are shown in Table 3.2 with comments on the crystals used (if known). The method used is generally that of X-ray diffraction of a powder sample taken at about room temperature (20°C or 25°C). The first result presented by us was made on an early sample of a spontaneously nucleated crystal grown by D.F. Croxall at the GEC Hirst Research Centre. This provided reasonable agreement with the measurements made by Croxall et al. [125] at GEC on a similar crystal. We also show in Table 3.2 the room temperature value for another crystal which was measured over a range of temperatures from 25°C to 600°C. The complete results of this set of measurements is shown in Table 3.3 and graphically in Figure 3.1.

In Table 3.3 our results are compared with results read from the graphs of Chang and Barsch [128] over a similar range of temperatures. Our powder photograph was taken by staff at Birkbeck College and was measured by us. The results do not agree very well with [128] which may be explained by uncertainties in the calibration of the platinum thermocouple temperature scale. Figure 3.1 shows our results as points with associated error bars calculated from a standard crystallographic computer program [129]. The results read from Chang and Barsch [128] are shown as circles (no errors were indicated on

Table 3.2 $AlPO_4$ lattice parameters.

date	a (Å)	c (Å)	refs	comments
1935	4.93	10.94	112,115,116, 130	ρ=2.560 gm/cc
1941	4.92	10.91	114,115	Natural crystal from Westana.
1950	4.95	10.94	131,132	
1955	4.97	10.84	126	Crystal grown by Stanley [118].
1960	4.942	10.97	115,133,134, 135	T=25°C
1963	4.943 ±.002	10.948 ±.004	115	ρ=2.66 gm/cc, Natural crystal from Rwanda.
1964	4.9416	10.957	136	Powder from Riedel de Haen, Germany.
1966	4.94291 ±.00016	10.94761 ±.00046	106,107,137, 138,139	T=25°C, ρ=2.64 gm/cc [114].
1976	4.943 ±.001	10.974 ±.005	128,48	ρ=2.620 gm/cc, Stanley's crystal.
1979	4.9434	10.9480	125	GEC grown crystal.
1980	4.9425	10.951	106	T=20°C
1981	4.9447 ±.0010	10.9536 ±.0030	This work	T=25°C, GEC grown crystal.
1981	4.961 ±.003	11.022 ±.010	This work	T=25°C, GEC grown crystal.

Table 3.3 $AlPO_4$ lattice parameters at elevated temperatures.

T (°C)	a (Å) (reference [128])	c (Å) (reference [128])	a (Å) (This work)		c (Å) (This work)	
25	4.944	10.972	4.961	±.003	11.022	±.010
75	4.948	10.980	4.964	±.003	11.031	±.013
100	4.952	10.981				
150			4.967	±.004	11.043	±.015
200	4.959	11.003	4.970	±.004	11.051	±.016
	4.959	10.990				
250			4.970	±.004	11.060	±.016
300	4.967	11.012	4.976	±.004	11.073	±.017
350			4.982	±.005	11.088	±.018
400	4.978	11.018	4.987	±.004	11.085	±.017
475	4.990	11.043				
500			4.993	±.005	11.077	±.019
550	5.010	11.052	5.000	±.007	11.090	±.026
600	5.043	11.205	5.019	±.008	11.151	±.030
700	5.043	11.210				
800	5.045	11.210				

Figure 3.1

THERMAL EXPANSION OF BERLINITE

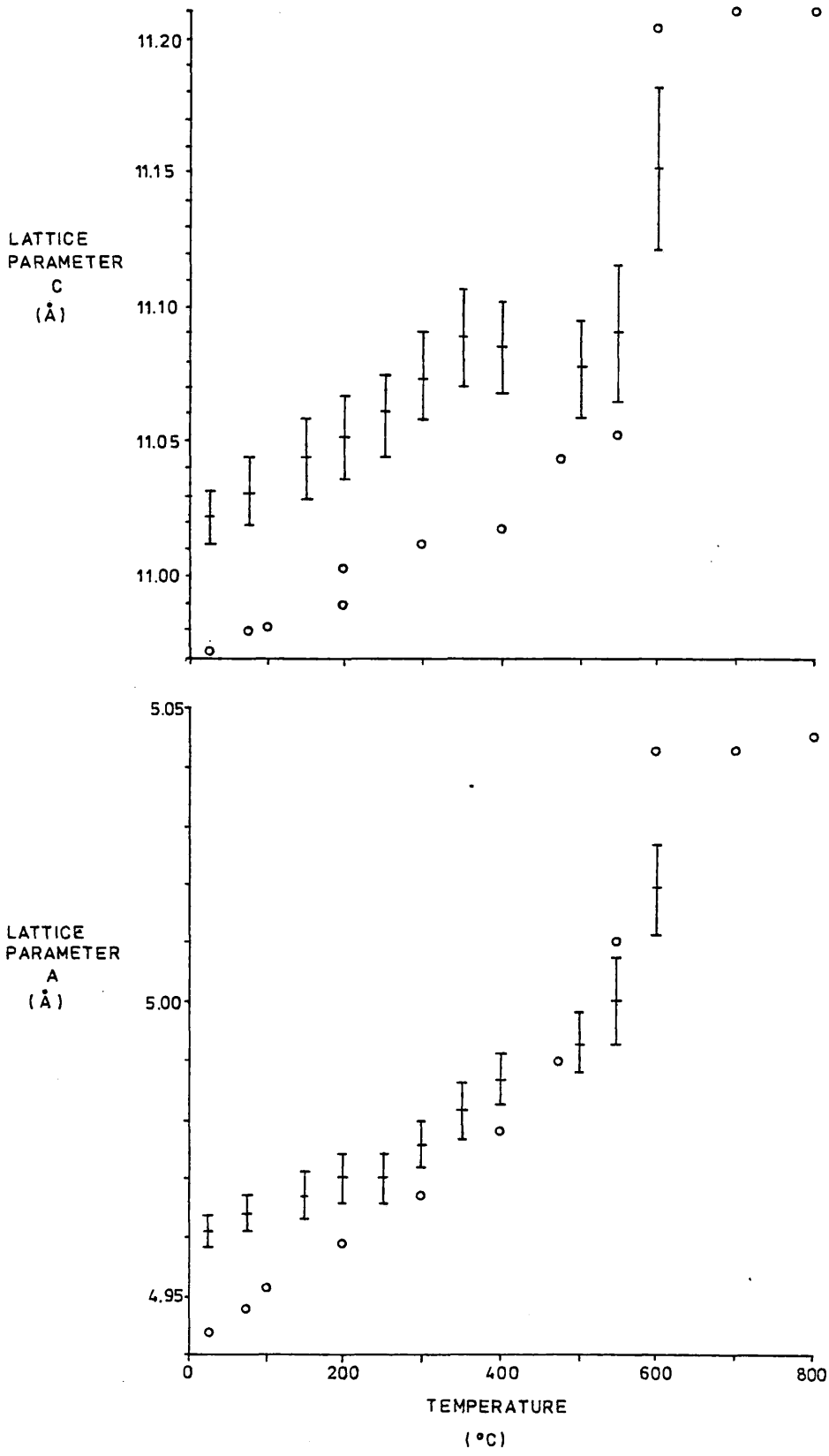

Table 3.4 Temperature of α-β transition for berlinite.

T (°C)	reference	quoted by	comments
579	127	141,142	McMaster crystal grown by Lang [127]
"	143	144 (586°C)	" " " "
580	106		
"	145	141	
"	119		
581	146		Airtron and Naval Weapons Centre crystal.
"	147		
584	141	120,128	
"	128,48		Stanley's crystal.
585	148		
586 ±2	130	141,124 (580°C)	
581 ±1	163	101,141,149 (586°C)	

their graphs). Our experimental results show the same general trend as [128] but without as large a change in the lattice parameters just below the α-β transition at about 584°C [128]. The temperature calibration was somewhat unreliable since it indicates that the α-β transition occurs at a temperature of over 600°C which conflicts with other results (see Table 3.4)

Four platinum lines were found on the X-ray powder photograph and these were used to calibrate the angles that the X-rays were deflected through. The calibration factor obtained was 1.00769 mm/°C. This was used to find the scattering angles and hence the d spacings and the lattice parameters a and c using the computer program [129]. A temperature scale was provided with the photograph but seems to give unreliable results.

Section 4. α-β transition temperature and density of berlinite.

The α-β transition in berlinite has been observed by several authors and their measurements have been quoted by others. The range of results is from 579°C to 586°C as shown in Table 3.4. As mentioned for quartz this is a structural phase transition from a trigonal (class 32) structure to an hexagonal structure (class 62).

Five measurements of the density of berlinite have been made. Huttenlocher [91] found a density of 2.56 gm/cc, Gallagher and Gerrard [115] found 2.64 gm/cc, Mason [140] gives 2.57 gm/cc and Chang and Barsch found a density of 2.62 gm/cc. These results seem to be in reasonable agreement with each other with only a 4% or so variation.

Section 5. The elastic, piezoelectric and dielectric matrices.

The elastic constants c_{ijkl}, the piezoelectric constants e_{ijk} and the dielectric constants ε_{ij} used in Chapter 2 are expressed in their mathematical form. For real crystals symmetry requirements reduce the number of independent constants. It is possible for any crystal class to reduce the number of independent elastic constants to a maximum of 36, the piezoelectric constants to a maximum of 18 and the dielectric constants remain as before [162]. We have the following relationships to enable the reduction of the mathematical matrices to two dimensional matrices :

$$c_{pq} = c_{ijkl} \qquad p,q=1,2,3,4,5,6 \qquad (3.1)$$

subject to the conditions that when :

$$i = j \text{ , then } p = i \tag{3.2}$$

and $$i \neq j \text{ , then } p = 9 - (i + j) \tag{3.3}$$

Similarily when :

$$k = l \text{ , then } q = k \tag{3.4}$$

and $$k \neq l \text{ , then } q = 9 - (k + l) \tag{3.5}$$

For the piezoelectric constant we have a similar type of relationship :

$$e_{ip} = e_{ijk} \tag{3.6}$$

subject to the conditions that when :

$$j = k \text{ , then } p = j \tag{3.7}$$

and $$j \neq k \text{ , then } p = 9 - (j + k) \tag{3.8}$$

These reductions in the elastic and piezoelectric constant matrices are general for any class of crystal. In the specific case of crystals of class 32, such as quartz and berlinite, some of the constants c_{pq} and e_{ip} and ε_{ij} are equivalent and some are identically zero due to the symmetry of the class of crystal. Class 32 crystals have only 6 independent c_{pq} and 2 independent e_{ip} and 2 indepedent ε_{ij} . These are illustrated in Figure 3.2. Note that c_{66} is not independent since :

$$c_{66} = \tfrac{1}{2}(c_{11} - c_{12}) \tag{3.9}$$

Section 6. Elastic, piezoelectric and dielectric constants of berlinite.

The elastic compliances s_{pq}, the piezoelectric strains d_{ij} and the dielectric constant ε_{11} of berlinite were first measured by Mason [140]. The corresponding values of the elastic stiffness constant c_{pq} and the piezoelectric stress constant e_{ip} are shown in Table 3.5.

The next, and to date only other, measurements of the elastic stiffness constants and the piezoelectric stress constants

Figure 3.2

Elastic constants of class 32: c_{ij}

i \ j						
	c_{11}	c_{12}	c_{13}	c_{14}	0	0
	c_{12}	c_{11}	c_{13}	$-c_{14}$	0	0
	c_{13}	c_{13}	c_{33}	0	0	0
	c_{14}	$-c_{14}$	0	c_{44}	0	0
	0	0	0	0	c_{44}	c_{14}
	0	0	0	0	c_{14}	c_{66}

Note $c_{66} = \frac{1}{2}(c_{11} - c_{12})$.

Dielectric constants of class 32: ε_{ij}

i \ j			
	ε_{11}	0	0
	0	ε_{11}	0
	0	0	ε_{33}

Piezoelectric constants of class 32: e_{ji}

i \ j			
	e_{11}	0	0
	$-e_{11}$	0	0
	0	0	0
	e_{14}	0	0
	0	$-e_{14}$	0
	0	$-e_{11}$	0

were made by Chang and Barsch [128], who also published the temperature variation of these constants over the range 80°K to 293°K at about 20°K intervals. These measurements have enabled us and Detaint et al. [119] to try to fit cubic curves to the data for the elastic stiffnesses c_{pq}. The results of these two attempts at a least squares cubic fit are tabulated in Table 3.5 and shown graphically in Figures 3.3 to 3.9. The graphs show the experimental points from Chang and Barsch [128] including their quoted errors, the Chang and Barsch straight line fit at 25°C (dashed line), the Detaint et al. least squares cubic fit (dotted line) and our own least squares cubic fit (solid line). It is clear that our fit is in closest agreement with the experimental results.

A similar attempt to find a cubic fit for the piezoelectric stress constants e_{ip} was tried but abandoned since the errors in the data points swamp any temperature variation.

The dielectric constant ε_{11} has only been measured by Mason [140] and ε_{33} has not been measured at all. In their paper Chang and Barsch [128] assume $\varepsilon_{33} = \varepsilon_{11}$ and then use the temperature coefficients of the dielectric constants of <u>quartz</u> to calculate the bulk wave responses of berlinite!

Table 3.5 Elastic, piezoelectric and dielectric constants of berlinite and their temperature derivatives.

constant	ref [128]	ref [119]	this work	ref [140]
c_{11}	6.40 x10^{10} Nm^{-2}	6.4013x10^{10} Nm^{-2}	6.4015x10^{10} Nm^{-2}	10.5032x10^{10} Nm^{-2}
c_{12}	7.20 x10^{9} "	7.2400x10^{9} "	7.2454x10^{9} "	2.9337x10^{10} "
c_{13}	9.60 x10^{9} "	9.5500x10^{9} "	9.5703x10^{9} "	6.9271x10^{10} "
c_{14} †	-1.24 x10^{10} "	-1.2347x10^{10} "	-1.2350x10^{10} "	-7.4278x10^{10} "
c_{33}	8.58 x10^{10} "	8.5754x10^{10} "	8.5764x10^{10} "	13.3534x10^{10} "
c_{44}	4.32 x10^{10} "	4.3171x10^{10} "	4.3173x10^{10} "	2.3137x10^{10} "
c_{66}	2.84 x10^{10} "	2.8381x10^{10} "	2.8385x10^{10} "	3.7847x10^{10} "
$T_{c_{11}}^{(1)}$	-7.5781x10^{-5} °C^{-1}	-7.7800x10^{-5} °C^{-1}	-7.2300x10^{-5} °C^{-1}	
$T_{c_{12}}^{(1)}$	-1.4861x10^{-3} "	-1.4090x10^{-3} "	-1.4678x10^{-3} "	
$T_{c_{13}}^{(1)}$	-3.9583x10^{-4} "	-1.2720x10^{-4} "	-4.0084x10^{-4} "	
$T_{c_{14}}^{(1)}$	7.1774x10^{-5} "	6.2400x10^{-5} "	1.0212x10^{-4} "	
$T_{c_{33}}^{(1)}$	-2.1795x10^{-4} "	-2.2350x10^{-4} "	-2.0648x10^{-4} "	
$T_{c_{44}}^{(1)}$	-1.5671x10^{-4} "	-1.6974x10^{-4} "	-1.6355x10^{-4} "	
$T_{c_{66}}^{(1)}$	1.0282x10^{-4} "	8.8740x10^{-5} "	1.0595x10^{-4} "	
$T_{c_{11}}^{(2)}$		3.5300x10^{-7} °C^{-2}	-2.0944x10^{-7} °C^{-2}	
$T_{c_{12}}^{(2)}$		3.8000x10^{-6} "	2.0235x10^{-6} "	
$T_{c_{13}}^{(2)}$		8.4190x10^{-6} "	-3.7364x10^{-7} "	
$T_{c_{14}}^{(2)}$		-1.5580x10^{-6} "	-6.5660x10^{-7} "	
$T_{c_{33}}^{(2)}$		-3.8800x10^{-7} "	-1.8651x10^{-9} "	
$T_{c_{44}}^{(2)}$		-5.5500x10^{-7} "	-4.1474x10^{-7} "	
$T_{c_{66}}^{(2)}$		-8.8500x10^{-7} "	-4.9466x10^{-7} "	
$T_{c_{11}}^{(3)}$		-1.4950x10^{-9} °C^{-3}	-3.1696x10^{-10} °C^{-3}	
$T_{c_{12}}^{(3)}$		2.7037x10^{-8} "	1.2688x10^{-8} "	
$T_{c_{13}}^{(3)}$		6.7000x10^{-8} "	1.6353x10^{-10} "	
$T_{c_{14}}^{(3)}$		-9.2720x10^{-9} "	-2.6763x10^{-9} "	
$T_{c_{33}}^{(3)}$		2.1380x10^{-9} "	6.9210x10^{-10} "	
$T_{c_{44}}^{(3)}$		-1.6030x10^{-9} "	-5.7701x10^{-10} "	
$T_{c_{66}}^{(3)}$		4.8350x10^{-9} "	-1.9781x10^{-9} "	

† reference [119] quotes c_{14} = +1.2347x10^{10} Nm^{-2} instead of -1.2347x10^{10}

Table 3.5 (continued).

constant	ref[128]	ref[119]	this work	ref[140]
e_{11}	-0.3000 Cm^{-2}	-0.3000 Cm^{-2}	-0.3000 Cm^{-2}	0.1369 Cm^{-2}
e_{14}	0.1300 "	0.1300 "	0.1300 "	-0.4588 "
$T_{c_{11}}^{(1)}$	-2.6667×10^{-4} °C^{-1}	-2.6600×10^{-4} °C^{-1}	-2.6667×10^{-4} °C^{-1}	
$T_{c_{14}}^{(1)}$	-5.6154×10^{-4} "	-5.6100×10^{-4} "	-5.6154×10^{-4} "	
ε_{11}	5.2063×10^{-11} Fm^{-1}	5.1900×10^{-11} Fm^{-1}	5.2063×10^{-11} Fm^{-1}	5.2063×10^{-11} Fm^{-1}
ε_{33}	5.2063×10^{-11} "	5.1900×10^{-11} "	5.2063×10^{-11} "	
$T_{\varepsilon}^{(1)}$	2.8000×10^{-5} °C^{-1}		2.8000×10^{-5} °C^{-1}	
$T_{\varepsilon_{33}}^{(1)}$	3.9000×10^{-5} "		3.9000×10^{-5} "	
α_{11}	1.5900×10^{-5} °C^{-1}	1.5900×10^{-5} °C^{-1}	1.5900×10^{-5} °C^{-1}	
α_{33}	9.7000×10^{-6} "	9.7000×10^{-6} "	9.7000×10^{-6} "	
$T_{\alpha_{11}}^{(1)}$	7.6264×10^{-9} °C^{-2}	7.6200×10^{-9} °C^{-2}	7.6264×10^{-9} °C^{-2}	
$T_{\alpha_{33}}^{(1)}$	7.5470×10^{-9} "	7.5400×10^{-9} "	7.5470×10^{-9} "	
ρ	2.6200 gm/cc		2.620 gm/cc	2.57 gm/cc
$T_{\rho}^{(1)}$	-4.1500×10^{-5} °C^{-1}		-4.1500×10^{-5} °C^{-1}	
$T_{\rho}^{(2)}$	-2.1639×10^{-8} °C^{-2}		-2.1639×10^{-8} °C^{-2}	

Figure 3.3

ELASTIC CONSTANT c_{11} FROM CHANG AND BARSCH DATA

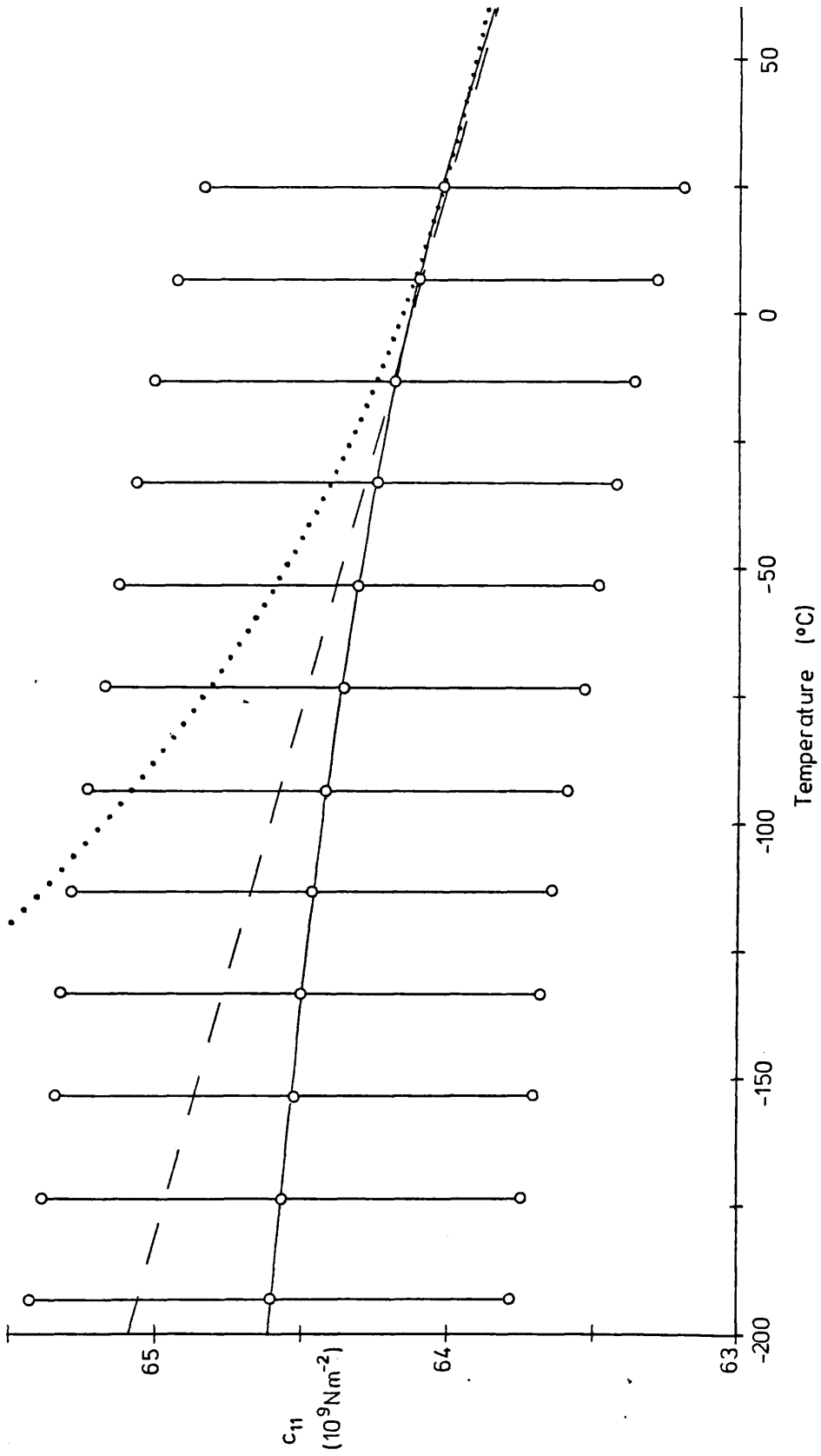

Figure 3.4

ELASTIC CONSTANT $c_{11}-2c_{66}$ FROM CHANG AND BARSCH DATA

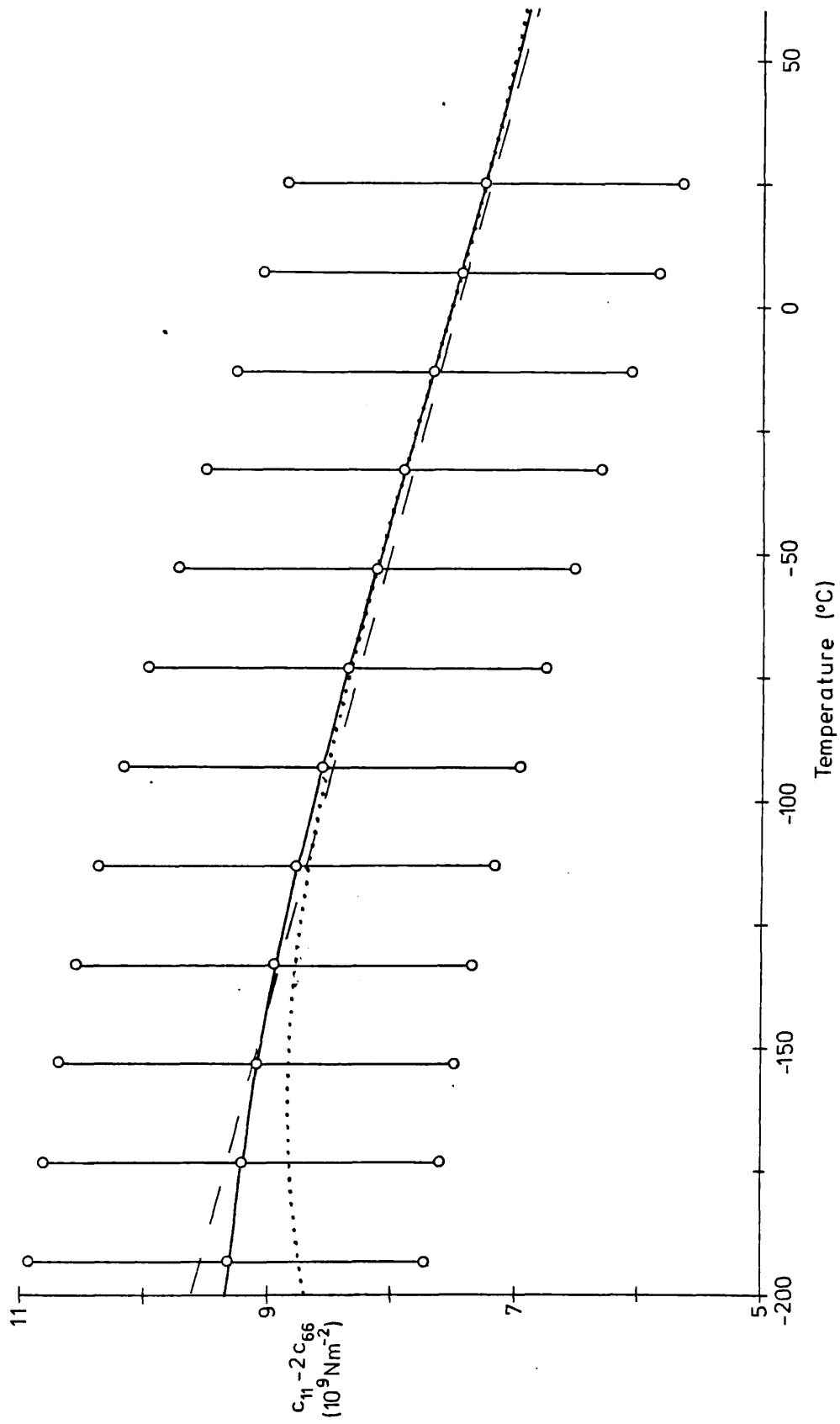

Figure3.5

ELASTIC CONSTANT c_{13} FROM CHANG AND BARSCH DATA

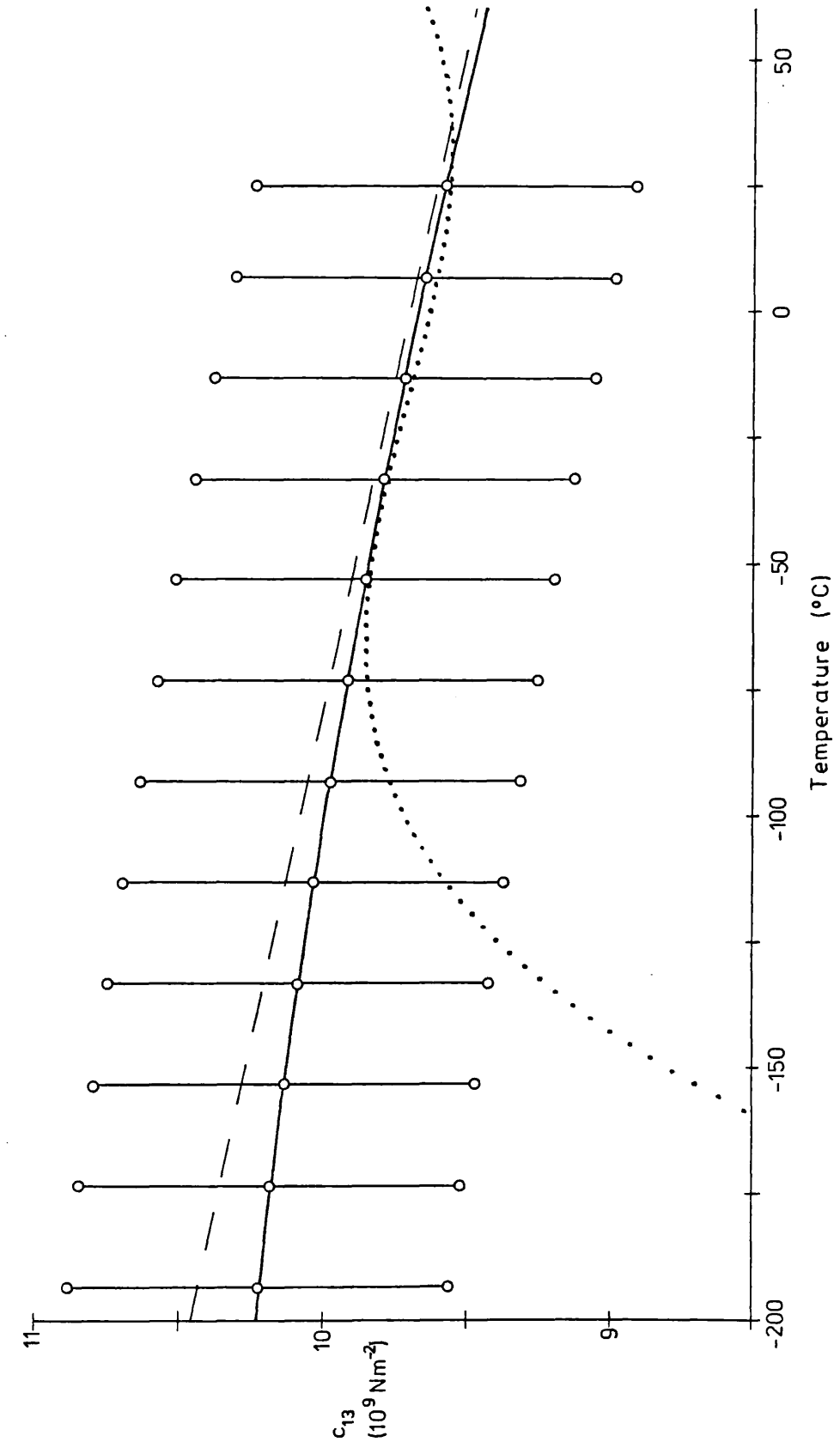

Figure 3.6

ELASTIC CONSTANT c_{14} FROM CHANG AND BARSCH DATA

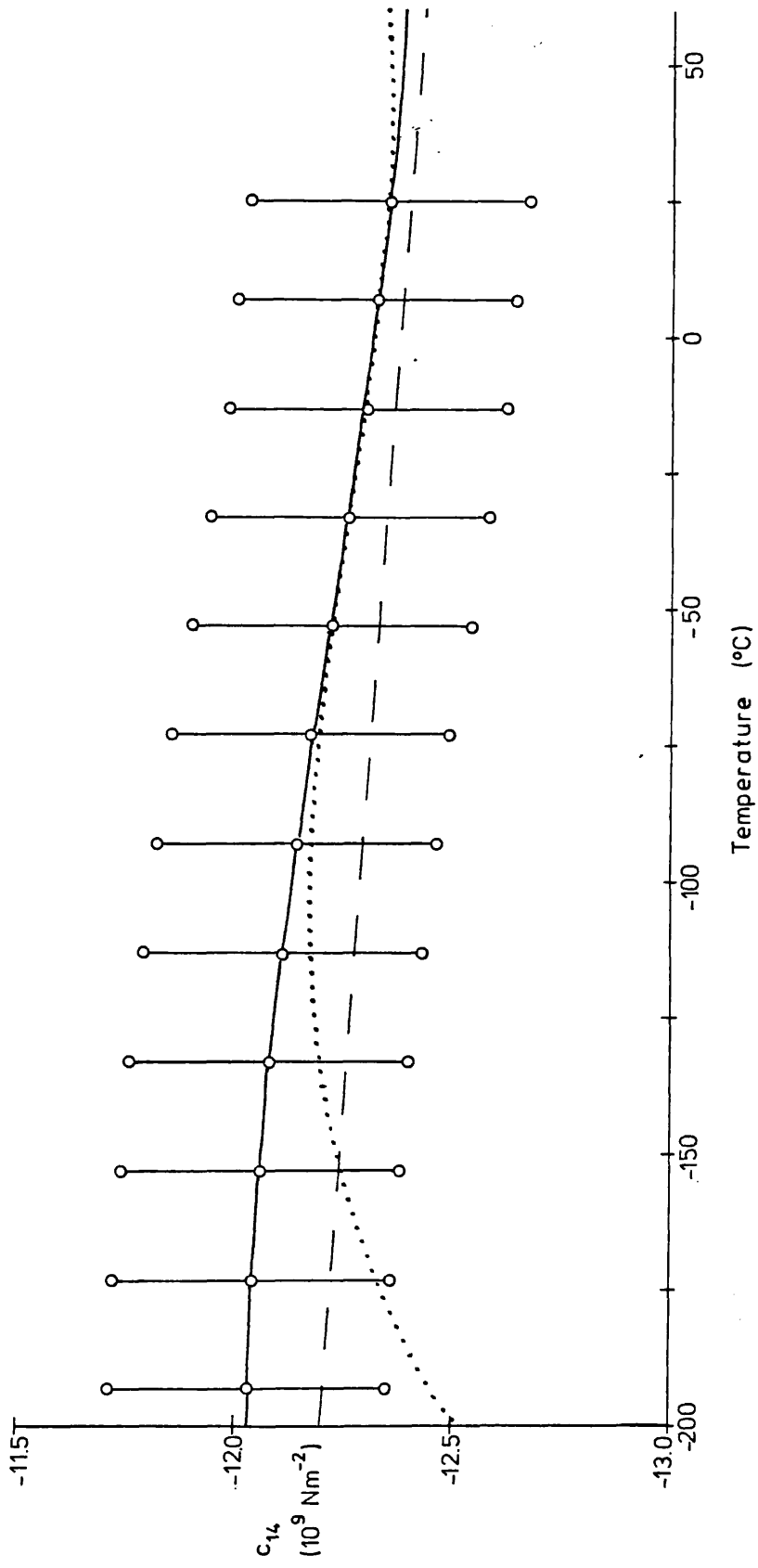

Figure 3.7

ELASTIC CONSTANT c_{33} FROM CHANG AND BARSCH DATA

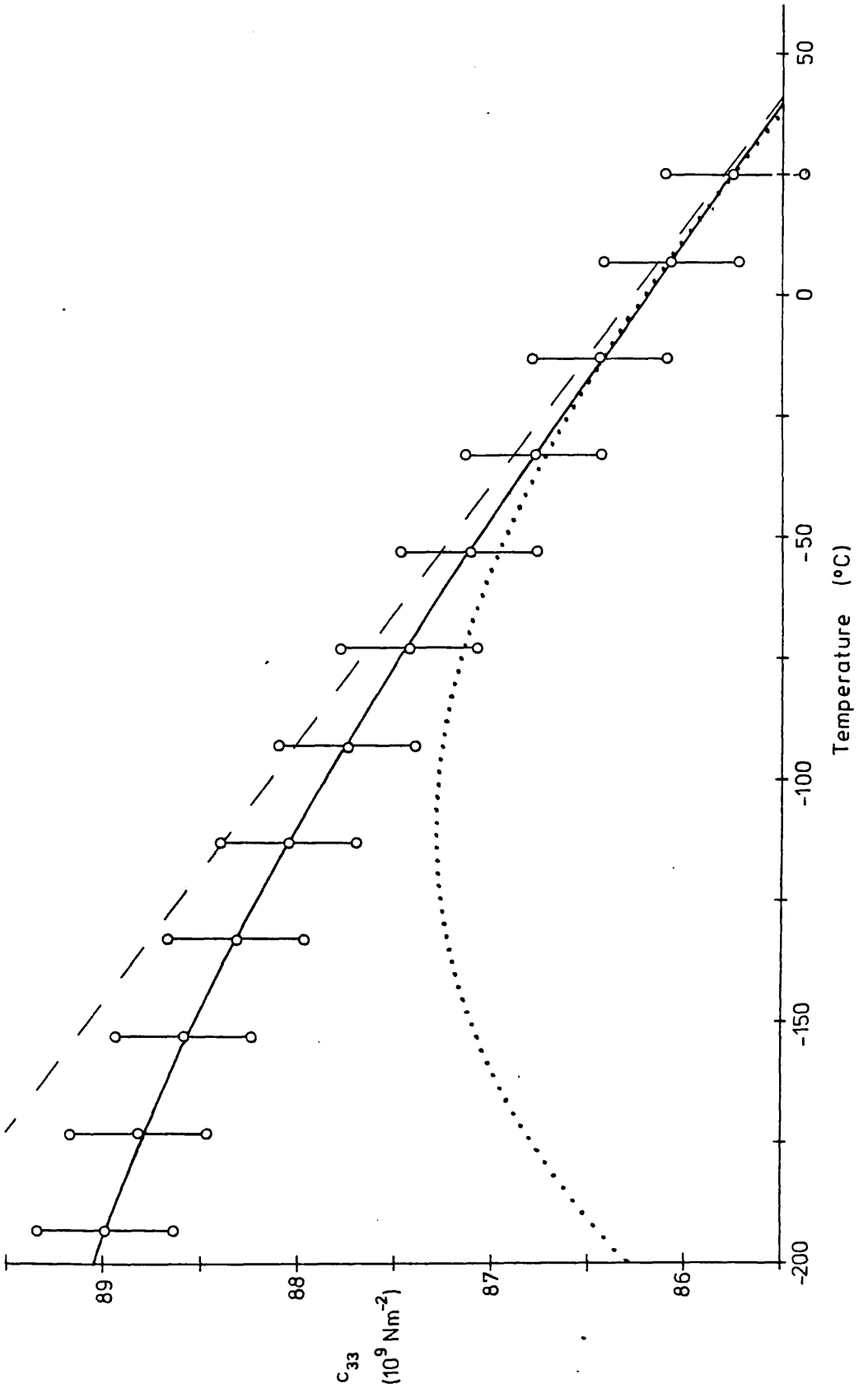

Figure 3.8

ELASTIC CONSTANT c_{44} FROM CHANG AND BARSCH DATA

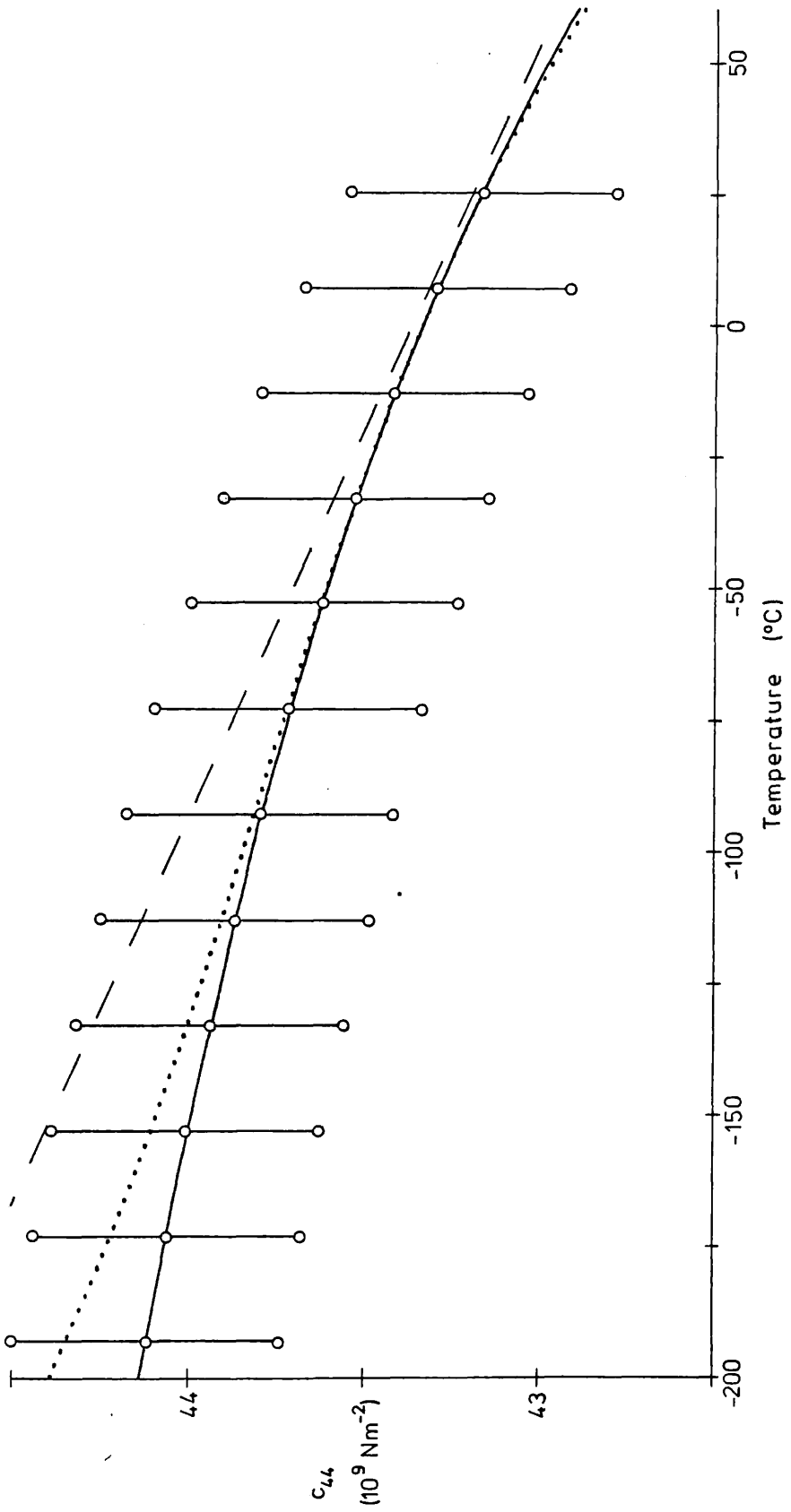

Figure 3.9

ELASTIC CONSTANT c_{66} FROM CHANG AND BARSCH DATA

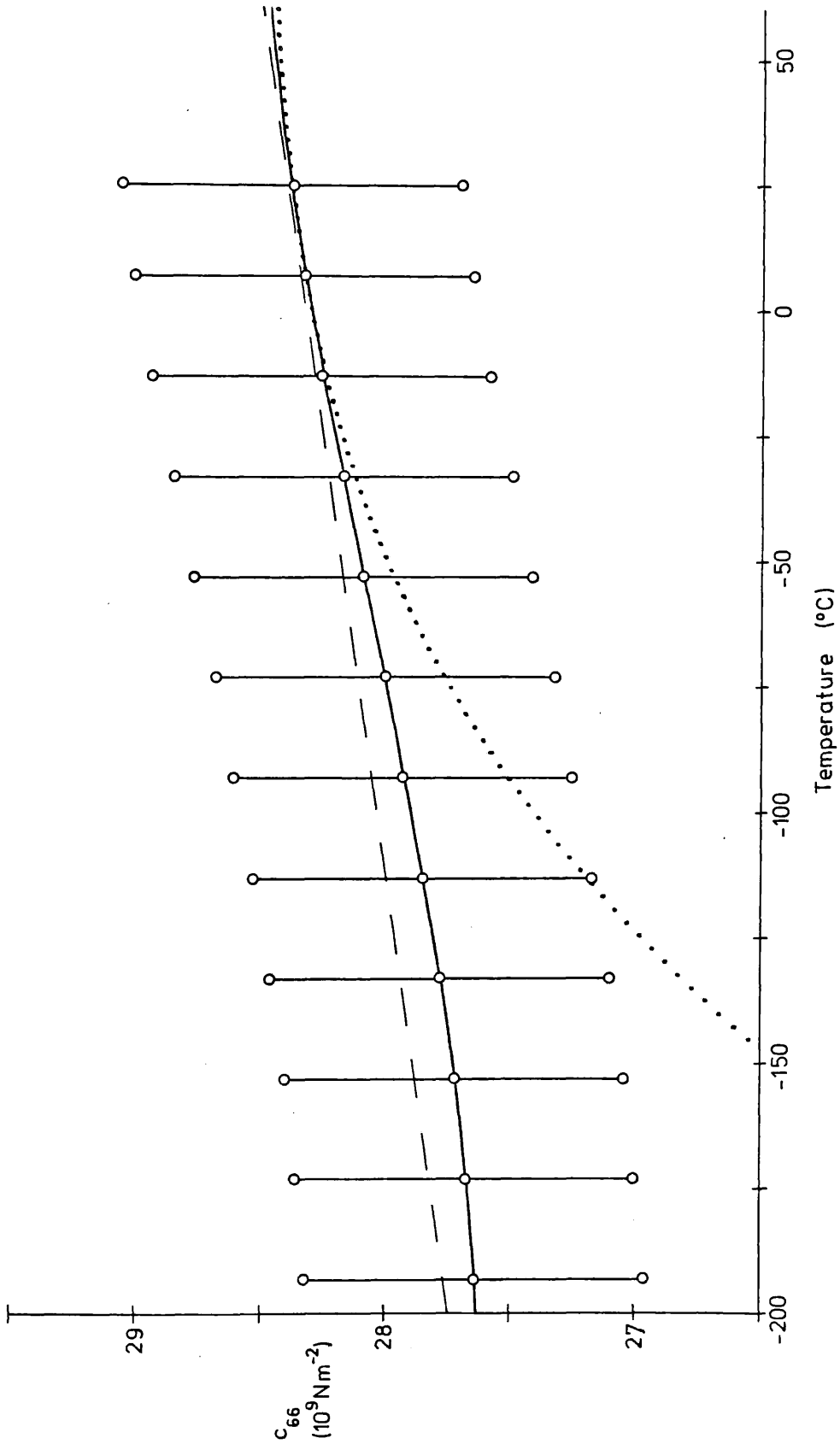

Chapter 4. Theoretical results for surface acoustic waves on berlinite

Section 1. The computer program.

The theory shown in Chapter 2 has been developed into a computer program to enable the prediction of surface acoustic wave properties for any orientation of a crystal. The program is written in FORTRAN and has been run on the University of London's CDC 7600 and 6600 computers. The program uses the elastic,piezoelectric, dielectric and lattice constants, the density and their temperature derivatives (to third order if available) as the input data for a given orientation. The calculated properties are the surface wave velocity for both free and metallised surfaces (and hence $\Delta v/v$ and k^2), the angle of power flow and its slope and the temperature coefficient of delay for that orientation.

Subroutines appropriate to the crystal class are used to generate the complete matrices of the constants for any given temperature. An orientation is selected and a sample starting velocity for the iteration process is chosen together with the number and size of the iteration steps. For any given orientation the calculations are performed six times to enable the temperature coefficient of delay (equation 1.5), the slope of the power flow angle (equation 4.3) and the velocities for both the free and metallised surfaces to be calculated. These calculations are indicated by the shaded regions in Figure 4.1.

The iteration process involves minimising the boundary condition determinant (equation 2.49), whilst ensuring that the surface wave velocity determinant is zero (equation 2.35). This is done by calculating the boundary condition determinant starting from an intelligent guess for the surface wave velocity, for a reasonable number of trial velocities and then selecting the velocity corresponding to the minimum value of $|d_{mn}|$ (equation 2.49). The search is then continued around this velocity with a reduced number of increments of much smaller size until the increment reaches a small value (in our case 10^{-4} m/s).

The iteration process has been optimised to provide rapid convergence whilst enabling the program to determine accurately the region of the minimum on the first iteration. The function $|d_{mn}(v)|$ does not always provide a simple, single minimum (see Section 4).

Fig. 4.1

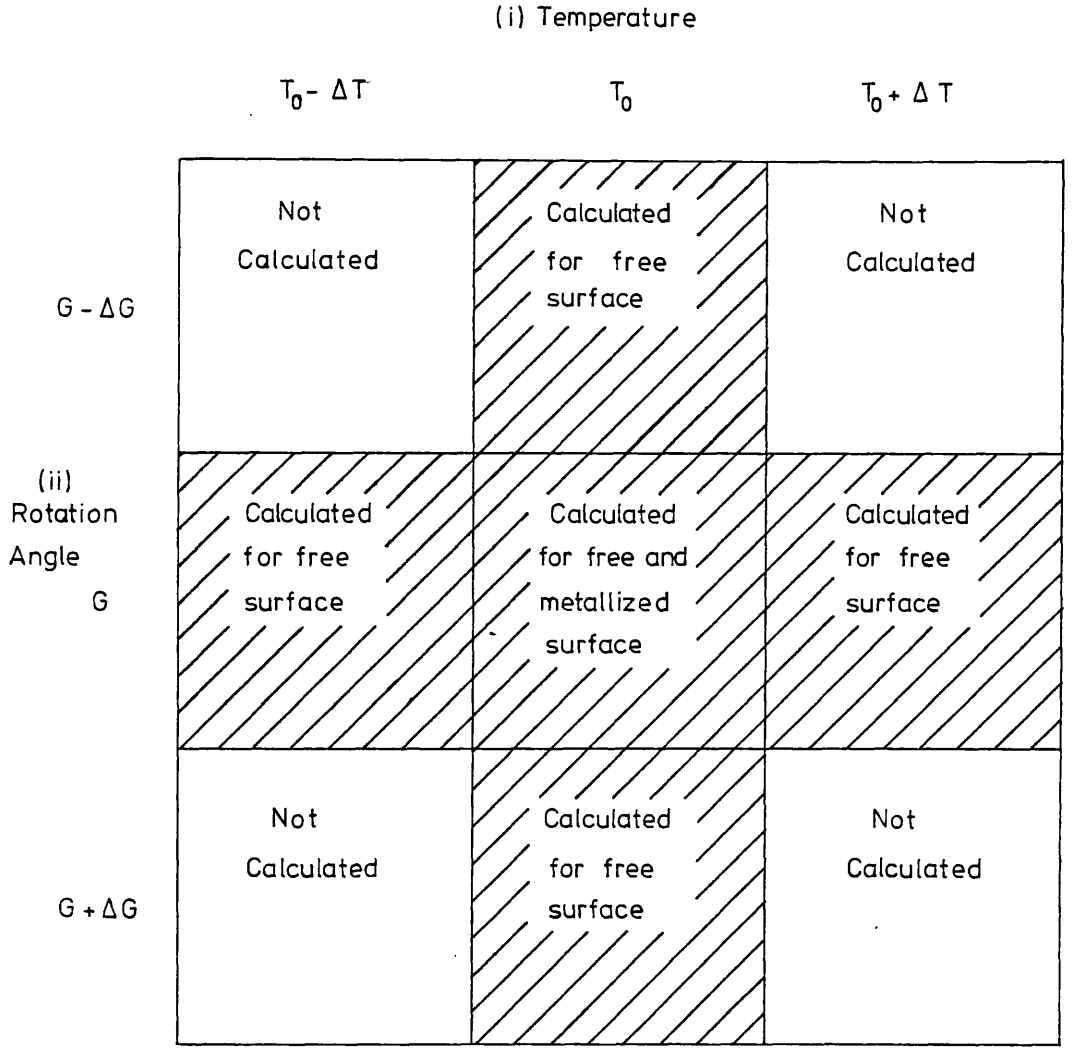

Calculations performed to obtain
(i) Temperature coefficient of delay
(ii) Slope of the power flow angle

This means that it is not practicable to use a standard method such as the Newton convergence method to find the minimum. We have found in several cases a number of turning points which could easily confuse such a standard method. It is felt that by stepping by a relatively small increment of 10 m/s over a range of 1000 m/s that the 'true' global minimum in the function will be found. Once this minimum has been found it can be rapidly converged upon. For berlinite we have found that a good starting velocity is 3500 m/s with an initial increment D of -10 m/s for 101 steps (this covers the range 2500-3500 m/s, which contains all the surface wave velocities for berlinite so far discovered). For the second and following increments we use a new increment calculated by :

$$D' = \frac{D}{\frac{1}{2}(I - 1)} \qquad (4.1)$$

where I (=7) is the number of increments of size D'. Iterations continue until $D' \leqslant 10^{-4}$m/s giving 11 complete levels of iteration. The first level of iteration gives a good approximation to the solution not only for the surface wave velocity for temperature T and angle $(\theta - \Delta\theta)$, (the first value to be calculated), but also for the velocities of the other regions shaded in Figure 4.1. The capture range of the iteration process is ±15 m/s from this velocity which is sufficient for berlinite calculations. Thus to save on calculation time this value of the velocity is used as the starting point for the second iterations for all 5 regions of interest together with the metallised surface wave velocity at (T,θ) giving a total of 6 sets of secondary iterations.

The total number of calculations to find the surface wave velocity to within 10^{-4} m/s in all regions of interest is thus :

$$101 + 6\{(11\times7) + 1\} = 569 \qquad (4.2)$$

The 11 iterations of 7 steps are followed by a further one to calculate the correct surface wave velocity (to within 10^{-4} m/s) and are performed 6 times, for all the regions in Figure 4.1 that we require solutions for. The 7 step iteration process was found to produce the required accuracy of convergence in the fewest calculations hence making the best use of the computer time available.

An outline flow diagram of the computer program is shown

in Figure 4.2 and a full listing is given in Appendix 1. The FORTRAN variable names corresponding to the algebraic variables in Chapter 2 are listed in Table 4.1. The program uses two standard subroutines from the NAG library [164]. One (C02AEF) finds the eight complex roots $\ell_3^{(n)}$ of the secular equation (2.35). Four of the roots with $Im(\ell_3^{(n)}) < 0$ are selected and substituted into DET(I,J) where another NAG subroutine (F02AKF) evaluates the complex eigenvectors. The corresponding eigenvalues are checked to select the zero one (i.e. the one that corresponds to a root of equation (2.35)) and its corresponding eigenvector (EIGVEC(K,J)). The determinant $|d_{mn}|$ (DMN(J,N)) is evaluated and then stored. The program then continues the iterations and selects the minimum stored value of $|d_{mn}|$ (ABSOL(IQ)) and its corresponding surface wave velocity (VS(IQ)).

After performing all the iterations, the final surface acoustic wave velocity is calculated along with the necessary eigenvalues $a_r^{(n)}$ and roots $\ell_3^{(n)}$. These are used to calculate the eigenvectors C_n for the displacement vectors u_r (equation 2.36), the power flow vector W_i and the power flow angles (surface wave power flow angle $\tan^{-1}(W_2/W_1)$, and bulk wave power flow angle $\tan^{-1}(-W_3/W_1)$. Since the program calculates both the metallised and free surface wave velocities we can calculate $\Delta v/v$ (equation 1.2) and k^2 (equation 1.1). The temperature coefficient of delay is calculated from equation (1.5) :

$$TCD = \frac{Delay(T+\Delta T) - Delay(T-\Delta T)}{2.\Delta T.Delay(T)} \qquad (1.5)$$

where Delay is the delay corresponding to 10 mm of wave travel, T = 25°C and ΔT = 0.5°C. Similarily the slope of the power flow angle comes from :

$$\frac{\partial \phi}{\partial \theta} = \frac{\phi(\theta+\Delta\theta) - \phi(\theta-\Delta\theta)}{2.\Delta\theta.\phi(\theta)} \qquad (4.3)$$

where $\Delta\theta = 0.05^{\circ}$.

Fig. 4.2

FLOW DIAGRAM

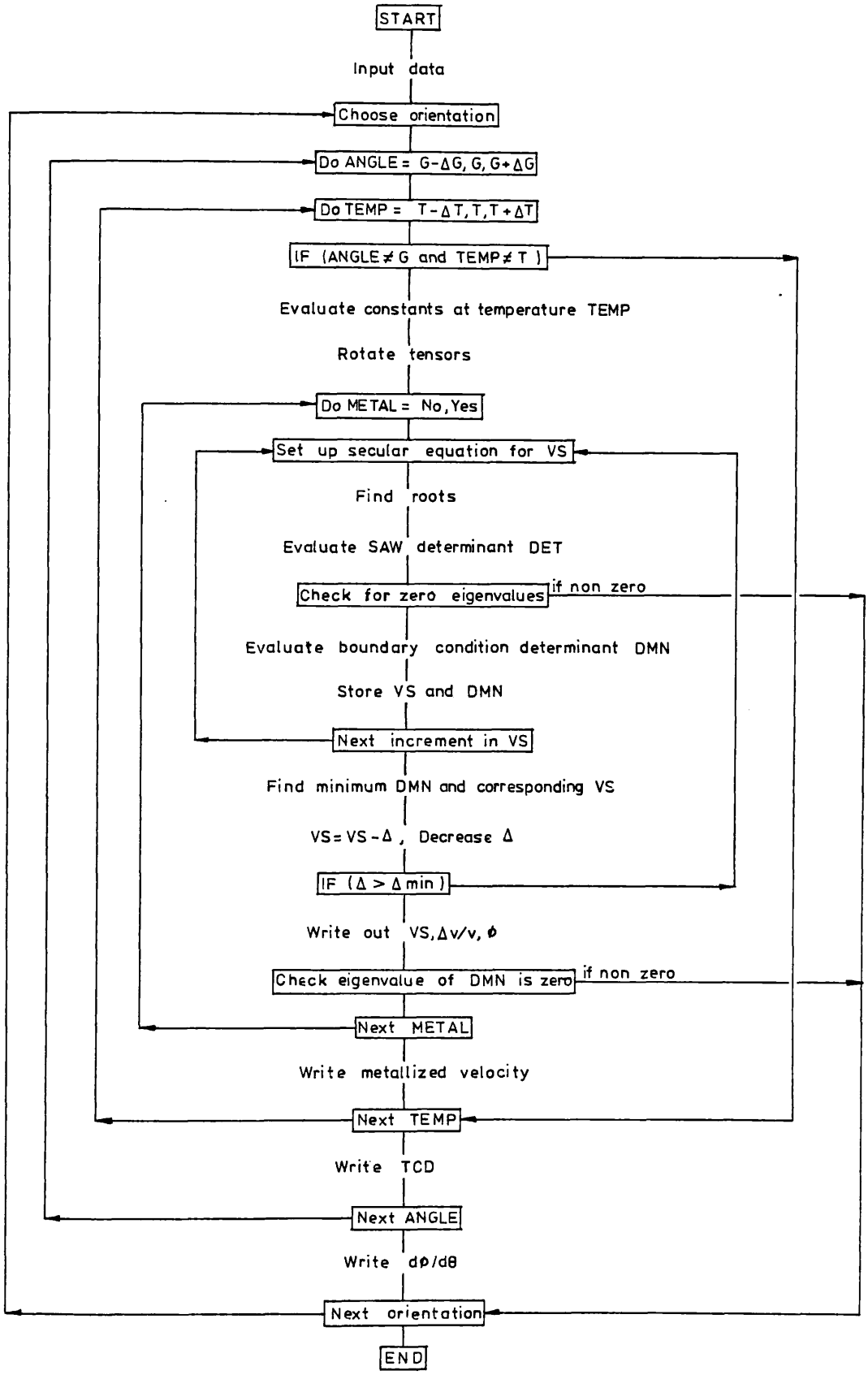

Table 4.1 Computer program variables.

Algebraic symbol	FORTRAN symbol	Comments
V_{ij}	V(I,J)	Rotation matrix.
c'_{ijkl}	CPRIME(IJKL)	Rotated elastic constant IJKL = 27(i-1)+9(j-1)+3(k-1)+l .
e'_{ijk}	EPRIME(I,J,K)	Rotated piezoelectric constant.
ϵ'_{ij}	EP(I,J)	Rotated dielectric constant.
α'_{ij}	ALPHA(I,J)	Rotated coefficient of thermal expansion.
u_r	UVECT(R)	Normalised displacement vector.
$\ell_j^{(n)}$	RL(J,N)	Roots of secular equation ROOTS = RL(3,N), RL(1,N) = 1, RL(2,N) = 0.
$\lvert A_{rs} - \delta'_{rs}\,\rho v^2 \rvert$	DET(R,S)	Equation (2.30)
$a_r^{(n)}$	EIGVEC(R,N)	Equation (2.30)
K	RKSP	Wave vector
d_{mn}	DMN(M,N)	$\lvert d_{mn} \rvert$ = ABSOL(IQ)
C_n	CVECT(N)	Normalised coefficients of displacement.
v	VS(IQ)	SAW velocity (VSTORE after completion of iterations).
W_i	RWPOW(I)	Power flow vector.
$\phi_1(\theta)$	PHI1(IANGLE)	Angle of power flow in surface.
$\phi_2(\theta)$	PHI2(IANGLE)	" " " " " bulk.
γ, θ	G	Euler angle.
α	A	" "
β	B	" "
ρ	RO	Density.
ΔT	DELTA	Change in temperature in equation(1.5).
	X3(I,J)	Coefficients of secular equation (2.30).
	METAL	= 0, free surface.
		= 1, metallised surface
	ITEMP	= 1 (T-ΔT), = 2 (T), = 3 (T+ΔT).
	IANGLE	= 1 (θ-$\Delta\theta$), = 2 (θ), = 3 (θ+$\Delta\theta$).

Section 2. Bulk waves.

A similar but much simpler program has been developed to calculate the bulk wave velocities for any given orientation of a crystal. This was developed from the theory of Tiersten [150] who gives an analytical solution to the problem. The solution is much faster than the surface wave solution since it involves solving only one eigenvalue problem. This program has been used to compare the bulk and surface wave velocities for identical orientations of berlinite. The results are shown on Figures 4.3 to 4.26 as dotted lines on the velocity graphs where the velocities fall into the ranges plotted.

Section 3. Results of computer calculations by other workers.

Three groups of workers other than ourselves have calculated some of the surface acoustic wave properties of berlinite. Carr [47] first suggested that berlinite could be a temperature compensated material. Later with O'Connell's computer program, they calculated the properties of some of the singly rotated cuts [46](see Appendix 2 for definitions of the singly rotated cuts) and one plane of doubly rotated cuts (α,90,γ) [43,151]. The data that they used was from Chang and Barsch [128] and the results are shown in Table 4.2. Some results are quoted by O'Connell and Carr in later papers [42,44,49].

Jhunjhunwala et al. [27,152] also calculated the surface acoustic wave properties for some of the singly rotated cuts using data from [128] and the results are included in Table 4.2. However, some of the results differ slightly fromm O'Connell and Carr [43]. Jhunjhunwala et al. [27,152] suggest that a slight difference in the input data, less than the experimental errors, could explain the differences. Carr and O'Connell [151] thought that Jhunjhunwala et al. may not have used the temperature coefficients of the piezoelectric and dielectric constants (which Chang and Barsch [128] admit are approximate). When O'Connell and Carr recalculated without these temperature coefficients, they claimed results similar to those of [27,152]. Jhunjhunwala et al. [27,152] claimed to have used "the temperature dependences of the elastic constants, piezoelectric constants, dielectric constants and lattice constants".

We have checked the properties of the orientations listed by both groups [27,152,43,151] using data taken from Chang and Barsch

Table 4.2 Berlinite SAW cuts from other workers.

Orientation (α,β,γ) (deg)	v(SAW) (m/s)	$\Delta v/v$ (10^{-4})	ϕ (deg)	$\partial\phi/\partial\theta$ (deg/deg)	TCD1 (ppm/°C)	TCD2	references
(0,0,24(36,84))	3090	11.7	±16.5	-	-	0	27,152
"	3089.9	12.9	±16.9	-0.444	-1.64	4.90	This work.
(0,37,0)	2855	1.5	0	-	-	0	27,152
"	no solution found						This work.
(0,46.6,0)	2847	12.8	0	2.97	-	0	151
"	2847.9	13.9	0	2.964	-4.24	-3.50	This work.
(0,80.4,0)	2751	24.5	0	0.901	-	0	42,44,49,151
"	2753.1	27.0	0	0.904	-6.12	-3.13	This work.
(0,87.1,0)	2736.5	28	0	-	-	0(19°C)	119
"	2741.5	25.4	0	0.747	-4.46	-1.50	This work.
(0,90,0)	2736	22.5	0	0.365	-	1	43
"	2739.6	29	0	-	-	0	119
"	2737.7	24.8	0	0.693	-3.58	-0.68	This work.
(0,90,6.75)	2752.6	28.5	4.36	-	-	0	119
(0,90,6.7)	2750.4	24.4	4.4	0.600	-2.76	0.16	This work.
(0,90,6.8)	2749	22.1	4.5	-	-	0	27,152
"	2750.8	24.4	4.5	0.597	-2.74	0.18	This work.
(0,90,8.8)	2761	21.8	5.6	0.511	-	0	43
"	2759.4	24.1	5.6	0.534	-2.19	0.74	This work.
(0,92.75,0)	2733	22	0	-	-	0	27,152
(0,92.7,0)	2734.9	24.1	0	0.648	-2.72	0.15	This work.
(11.2,90,0)	2759	23.6	4.1	0.335	-	0	43
"	2760.9	26.0	4.0	0.620	-4.94	-1.46	This work.
(18.5,90,0)	2792	25.5	6.3	-	-	0	151
"	2794.4	28.1	6.2	0.506	-7.37	-2.97	This work.
(76.8,90,11.5)	2756	25.0	0	0.372	-	0	42,49,151
"	2759.3	27.6	0.03	0.389	-7.30	-2.96	This work.
(79.7,90,15.5)	2758	24.7	0	0.221	-	0	42,44,49,151
"	2761.7	27.3	0.01	0.233	-7.682	-2.94	This work.
(90,9.5,0)	3113	16.2	10	-	-	0	27,152
"	3118.8	17.9	11.1	-1.636	-5.20	1.98	This work
(90,65.5,0)	2865	27.7	-2.9	-	-	0	27,152
"	2868.3	30.6	-3.0	-0.057	-4.80	0.55	This work.
(90,90,19.1)	2754	24.0	-1.6	-	-	0	151
"	2758.0	26.6	-1.6	0.236	-8.12	-2.88	This work.

Table 4.2 (continued).

Orientation (α,β,γ) (deg)	v(SAW) (m/s)	$\Delta v/v$ (10^{-4})	ϕ (deg)	$\partial\phi/\partial\theta$ (deg/deg)	TCD1 (ppm/°C)	TCD2	references
(90,90,22)	2751	20	-0.55	-	-	0	27,152
"	2754.9	24.0	-0.92	0.248	-5.01	-0.13	This work.
(90,90,22.3)	2756.6	27.5	0.76	-	-	0(18°C)	119
"	2754.7	23.7	-0.85	0.252	-4.62	0.21	This work.
(90,90,22.6)	2750	21.1	-0.68	0.266	-	0	43
"	2754.4	23.4	-0.77	0.256	-4.24	0.56	This work.
(90,90,168.7)	2926	22.2	-11.3	0.209	-	0	43
"	2928.9	25.1	-11.3	0.211	-2.94	2.04	This work.
(90,90,175.2)	2865	26.4	-9.6	-	-	0	151
"	2868.2	29.2	-9.5	0.314	-8.33	-2.90	This work.
(135,45,6.87)	3060.6	43	4.36	-	-	0(20°C)	119
(135,45,6.9)	3058.7	36.8	3.36	-1.501	-6.62	0.17	This work.

TCD1 uses α, $T_\rho^{(1)}$, $T_c^{(1)}$ only.
TCD2 uses α, $T_\rho^{(1)}$, $T_c^{(1)}$, $T_e^{(1)}$, $T_\varepsilon^{(1)}$, $T_\alpha^{(1)}$, $T_\rho^{(2)}$.

[128] and listed in the first column of Table 3.5 and our results are shown where appropriate in Table 4.2. TCD1 shows the results of our calculations for the orientations considered using only the first order temperature coefficients of the elastic constants $T_{C_{ij}}^{(1)}$ and density $T_{\rho}^{(1)}$ and the linear expansion α_{ij}. TCD2 shows results for the same calculations but this time using all the temperature coefficients obtained from Chang and Barsch [128] (α, $T_{\alpha}^{(1)}$, $T_{\rho}^{(1)}$, $T_{\rho}^{(2)}$, $T_{C}^{(1)}$, $T_{e}^{(1)}$ and $T_{\varepsilon}^{(1)}$). This includes some second order coefficients and also the temperature coefficients of the piezoelectric and dielectric constants. The calculations were performed using the two sets of temperature coefficients to see why there were differences in the results presented by the different groups.The results show that better agreement is obtained using all the temperature coefficients that are available.

Detaint et al. [119] recalculated the elastic constant data from Chang and Barsch [128] (see Chapter 3) by a polynomial least squares analysis to the third order in temperature and used these temperature coefficients to calculate the SAW properties of berlinite. They produced five orientations that were temperature compensated at different temperatures from 18° - 25°C. These have also been checked by our computer program and the results are also shown in Table 4.2.

All these other workers have found temperature compensated orientations for berlinite which have an electromechanical coupling which is up to five times that of ST cut quartz. However,the actual orientations obtained are affected by which of the basic constants and temperature coefficients are used to calculate them and ultimately upon the measurements themselves.

Section 4. Results of our calculations for surface waves on berlinite.

In Chapter 3 we explained how we obtained a cubic least squares fit to the elastic constant variation with temperature from the data of Chang and Barsch [128]. These values, together with the piezoelectric, dielectric and lattice and density parameters and their temperature derivatives (column 3 in Table 3.5) were used in the computer program described in Section 1 above. Eight standard crystallographic, singly rotated cuts sweeping through 180° of orientation were studied. For all the singly rotated cuts, except the X axis boule and the X cut, the properties were symmetrical about the

90° orientation (see Appendix 2 for definitions of the singly rotated cuts). These orientations are presented graphically in Figures 4.3, 4.4, 4.13, 4.22 - 4.26 and tabulated in Appendix 3 (3.1, 3.2, 3.11 and 3.20 - 3.24). The ninth standard cut, the X axis cylinder, was not calculated for all 180° since for this cut the electromechanical coupling is identically zero and for some orientations no surface wave solutions could be found.

The eight standard cuts yielded 12 temperature compensated orientations, however, due to the symmetry of the Z axis cylinder and the Z cut, each having three orientations that are equivalent, only 8 independent temperature compensated orientations were found. The results are presented in Table 4.3.

It was then decided to investigate some simple doubly rotated cuts that could be obtained simply by using a different propogation direction on a singly rotated cut. Thus the X axis boule singly rotated cut was selected and by using different propogation directions, γ, the plane described by the Euler angles $(0,\beta,\gamma)$ was investigated. This plane includes the Z cut $(0,0,\gamma)$, the Y cut $(0,90,\gamma)$, both of which have temperature compensated directions, and the X axis cylinder cut $(0,\beta,90)$. The orientations investigated are shown graphically in Figures 4.4 to 4.21 and are tabulated in Appendix 3 (3.2 - 3.19). The angle β was incremented by 10° and this gave 14 further temperature compensated directions directly which are listed in Table 4.3. These temperature compensated orientations together with the orientations for which the power flow angle is zero are plotted in Figure 4.27 and this suggested two further orientations which are both temperature compensated and have a power flow angle of zero. These two orientations are also listed in Table 4.3.

The cuts listed show only four with both a zero temperature coefficient of delay and an effectively zero power flow angle. The 71.8° X axis boule cut appears to have the best electromechanical coupling (about five times that of ST cut quartz) of these orientations and corresponds approximately to the orientations being investigated experimentally. However all four orientations have a larger value for the slope of the power flow angle than we would like (all are at least three times that of ST cut quarzt). This means that transducer orientation on a crystal slice must be accurate to reduce losses arising from misallignment (see Chapter 1).

Points of interest to note from the graphs are the correlation between maxima and minima on the velocity curves and pure mode

Table 4.3 Temperature compensated cuts on berlinite.

α	β (deg)	γ	v(SAW) (m/s)	Δv/v (10^{-4})	φ (deg)	∂φ/∂θ (deg/deg)	TCD (ppm/°C)	Cut	Fig
0	56.2	0	2825.0	24.9	0	2.155	0.05	X axis boule	4.3
0	71.8	0	2775.4	28.4	0	1.191	0.14	" " "	"
90	90	17.6	2761.3	27.8	-1.96	-2.139	-0.26	X cut	4.26
90	90	174.5	2874.8	28.9	-9.73	0.304	-0.06	" "	"
90	7.6	0	3131.2	17.1	10.47	-2.366	-0.07	Y axis boule	4.23
90	74.0	0	2849.0	31.1	-5.67	0.126	0.07	" " "	"
20.0	90	0	2802.7	28.7	6.60	0.478	0.05	Z axis cyl.	4.22
40.0	90	0	2802.7	28.7	6.60	0.478	0.07	" " "	"
80.0	90	0	2802.7	28.7	-6.60	0.478	0.05	" " "	"
0	0	26	3122.2	13.5	15.00	-1.631	-0.21	Z cut	4.4
0	0	34	3122.2	13.5	-15.00	-1.631	-0.17	" "	"
0	0	86	3122.2	13.5	15.00	-1.631	-0.23	" "	"
0	10	23.8	3195.2	10.3	17.08	-3.117	0.07	Doubly rotated	4.5
0	10	26.4	3221.9	13.6	0.85	-8.280	-0.26	" "	4.5
0	10	84.3	2988.3	10.6	9.92	-4.602	0.43	" "	"
0	30	15.6	3151.8	14.0	27.32	6.769	-0.05	" "	4.7
0	40	12.0	3044.3	20.8	26.48	-0.318	0.12	" "	4.8
0	40	17.0	3150.3	32.4	12.67	-3.831	-0.18	" "	"
0	50	9.0	2929.3	25.8	18.82	0.938	0.16	" "	4.9
0	50	14.3	3026.3	32.3	17.97	-1.253	-0.16	" "	"
0	60	6.5	2844.9	28.3	10.82	1.296	-0.07	" "	4.10
0	70	4	2789.1	28.5	4.93	1.160	0.21	" "	4.11
0	160	32.9	2986.9	17.7	3.28	-1.552	-0.08	" "	4.20
0	160	42	2952.5	6.5	-10.23	-0.522	-0.20	" "	"
0	170	29.1	3053.0	16.2	9.36	-1.695	0.32	" "	4.21
0	170	39.1	3016.0	8.3	-15.05	-0.777	0.05	" "	"
0	9.8	26.6	3221.2	13.9	-0.16	-8.126	-0.35	" "	4.27
0	155.2	35.6	2956.0	17.4	0.08	-1.174	-0.13	" "	"

axes, the bulk wave depression of the surface wave velocity and the regions where no surface wave solution has been found.

From equation (1.10) we can see clearly that when we have a maximum or minimum on the velocity curve (with respect to orientation θ), i.e. $\partial v/\partial\theta = 0$, then $\tan\phi = 0$ and hence $\phi = 0^\circ$ and we have a pure mode axis. This connection has been noticed by Browning and Lewis [31] and derived by Szabo and Slobodnik [6] from [153].

For some orientations the SAW velocity approaches that of the shear bulk wave in the same direction. The rate of decay of the surface wave into the substrate decreases with orientation until the surface wave becomes a pure bulk wave. A pseudosurface wave often appears near such degenerate cases [88]. This is a surface wave that decays in the propogation direction and radiates energy into the bulk of the material [87]. These pseudosurface waves give rise to secondary minima in the boundary condition determinent versus velocity curve. These minima cannot be made arbitrarily small with an appropriate choice of velocity without assuming a complex value for ℓ_1 in equation (2.25) which complicates the process of computing the roots $\ell_3^{(n)}$ which do not then occur in complex conjugate pairs. We have not calculated these pseudosurface wave solutions although Jhunjhunwala et al. [27, 152] show some results. Our computer program does not produce a solution unless the magnitude of the boundary condition determinant can be made sufficiently small, so the pseudosurface wave solutions are not shown, although near regions where no surface wave solutions were found some of the surface wave energy begins to radiate into the bulk.

Section 5. Comparison of results.

If we compare orientations having both a zero temperature coefficient of delay and a zero power flow angle (i.e. $|\phi| < 0.2^\circ$), using the results that we have calculated, then the cut with the highest electromechanical coupling is the (0,71.8,0) orientation. The cut with the smallest slope of the power flow angle is the (79.7, 90,15.5) orientation found by Carr and O'Connell [42,44,49,151]. This cut would appear to be the best compromise cut if we can accept a doubly rotated cut. Of the singly rotated cuts the (0,90,0) Y cut seems to be the best from the point of view of good electromechanical coupling and reasonably low power flow loss if misalligned.

The optimum singly rotated cut would seem to lie in the range 70° - 95° rotated X axis boule cuts, since the orientation is

dependent on the basic constants used in the calculation and it may well alter when further elastic, piezoelectric and dielectric data becomes available. All the calculations performed by other workers were done prior to any experimental results being known for surface waves on berlinite, but our work was completed after the experiments described in the next Chapter, so we have not been able to test the accuracy of our predictions for the temperature compensated cuts.

Figure 4.3

SAW PROPERTIES (0, B, 0)

X AXIS BOULE

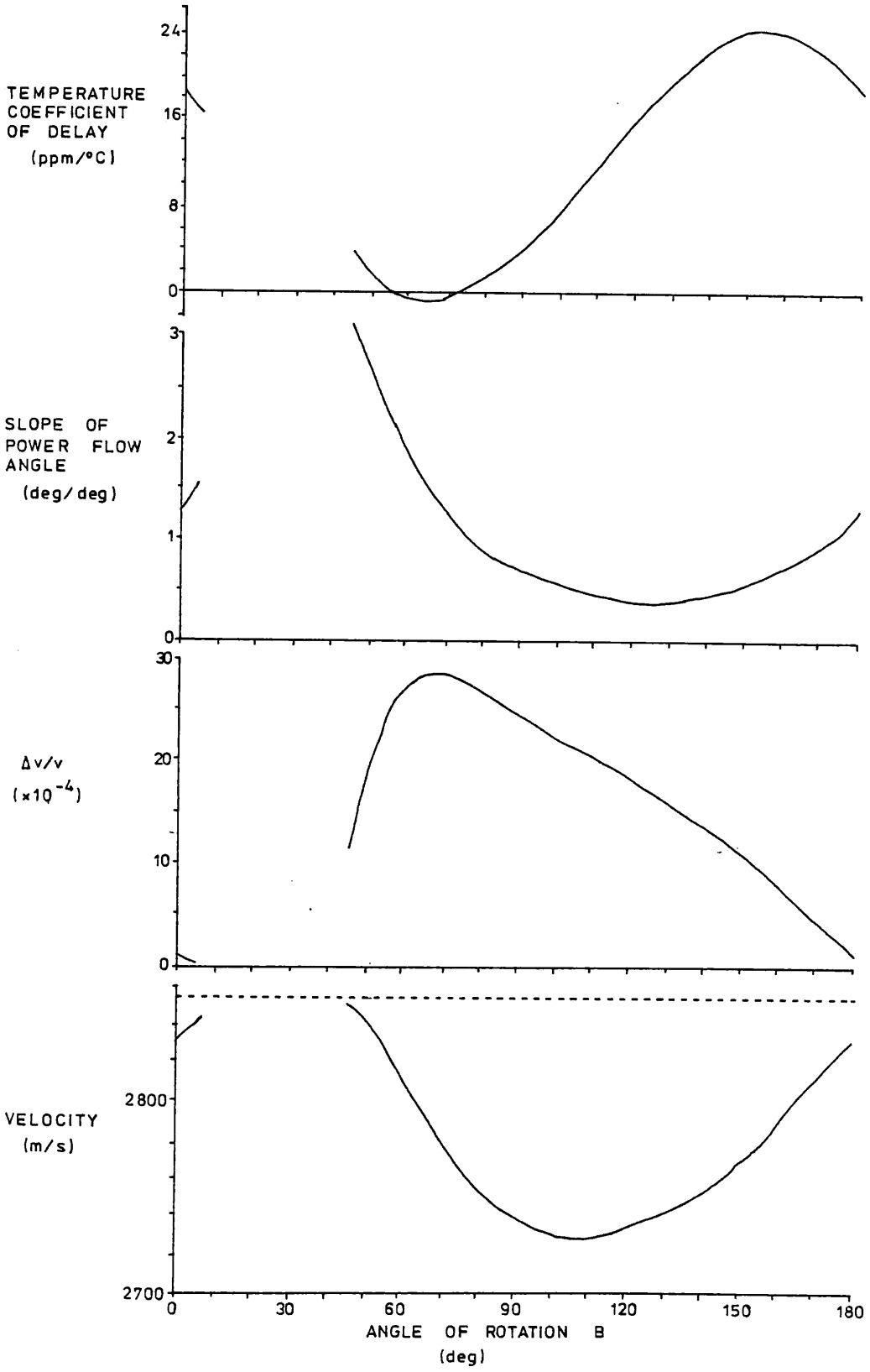

Figure 4.4

SAW PROPERTIES (0,0,G)

Z CUT

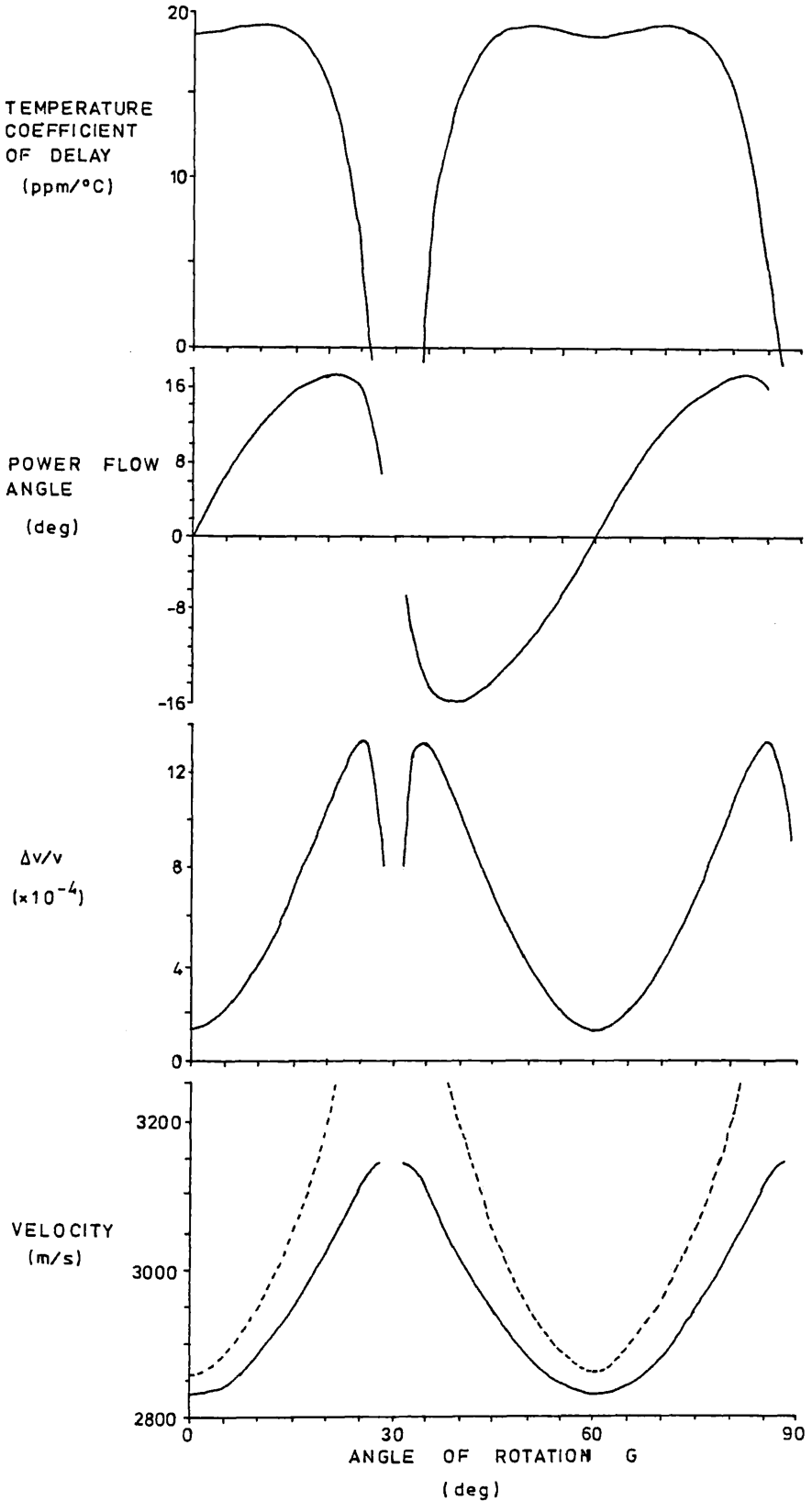

Figure 4.5

SAW PROPERTIES (0,10,G)

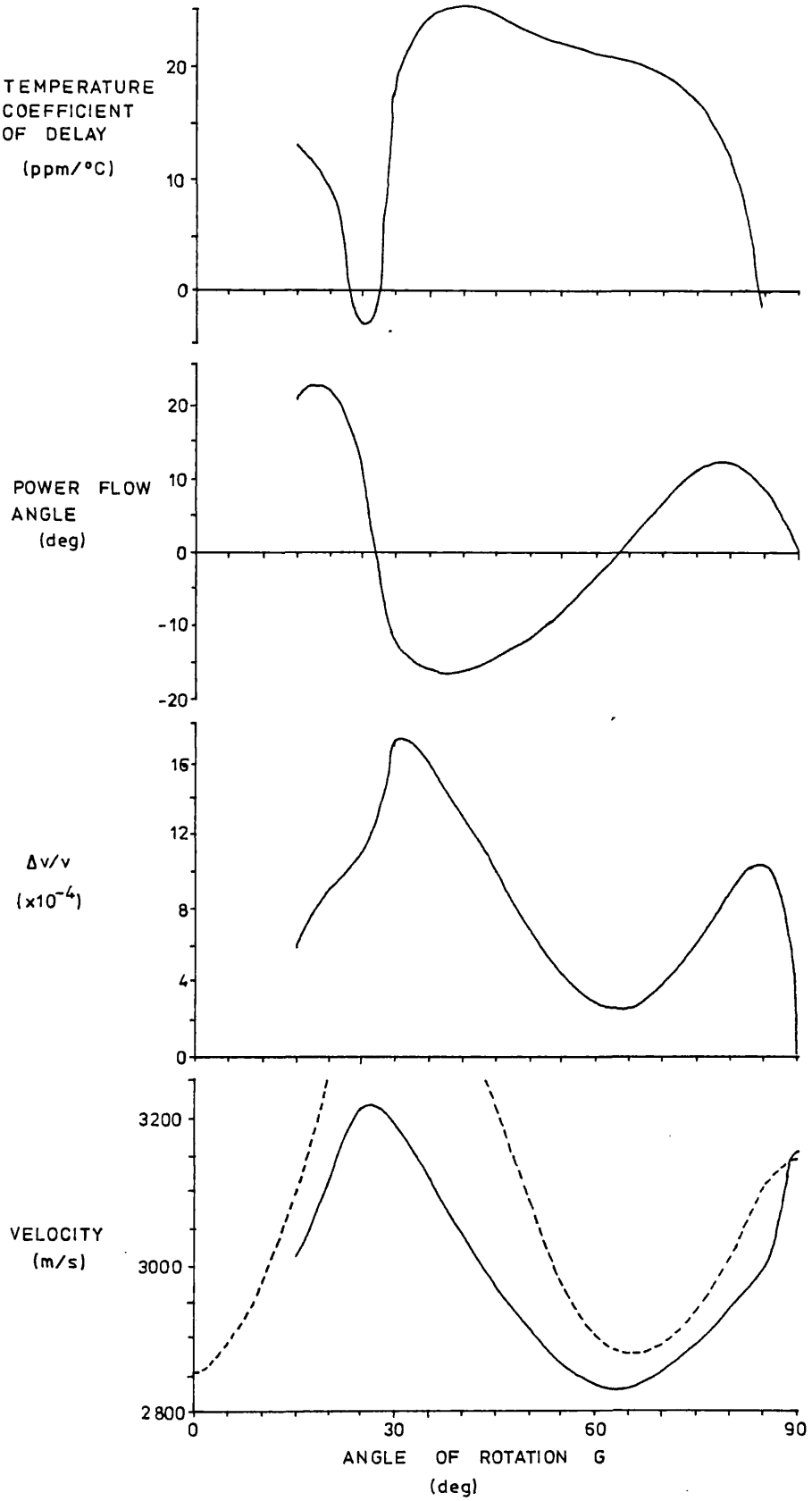

Figure 4.6

SAW PROPERTIES (0,20,G)

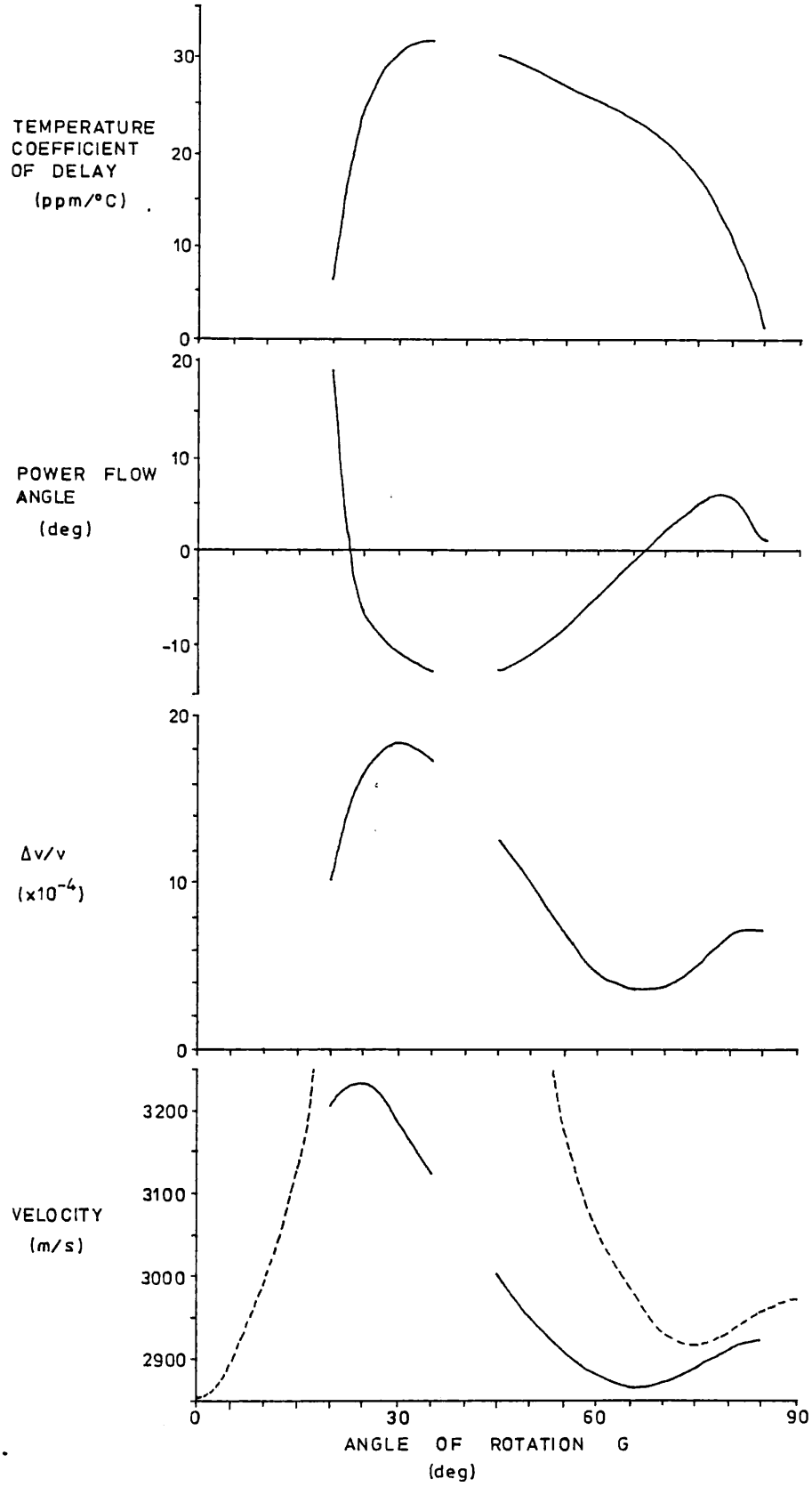

Figure 4.7

SAW PROPERTIES (0,30, G)

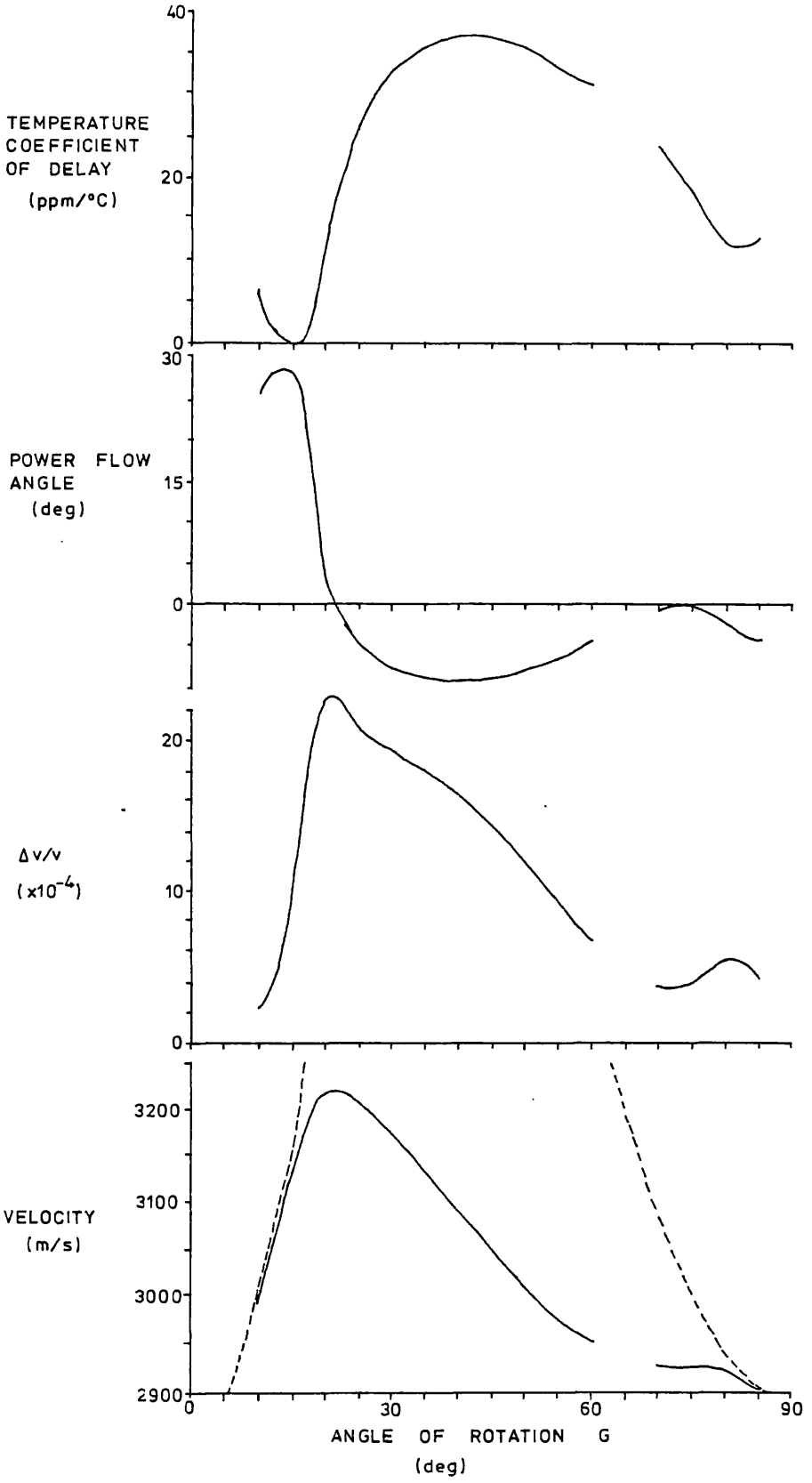

Figure 4.8

SAW PROPERTIES (0,40,G)

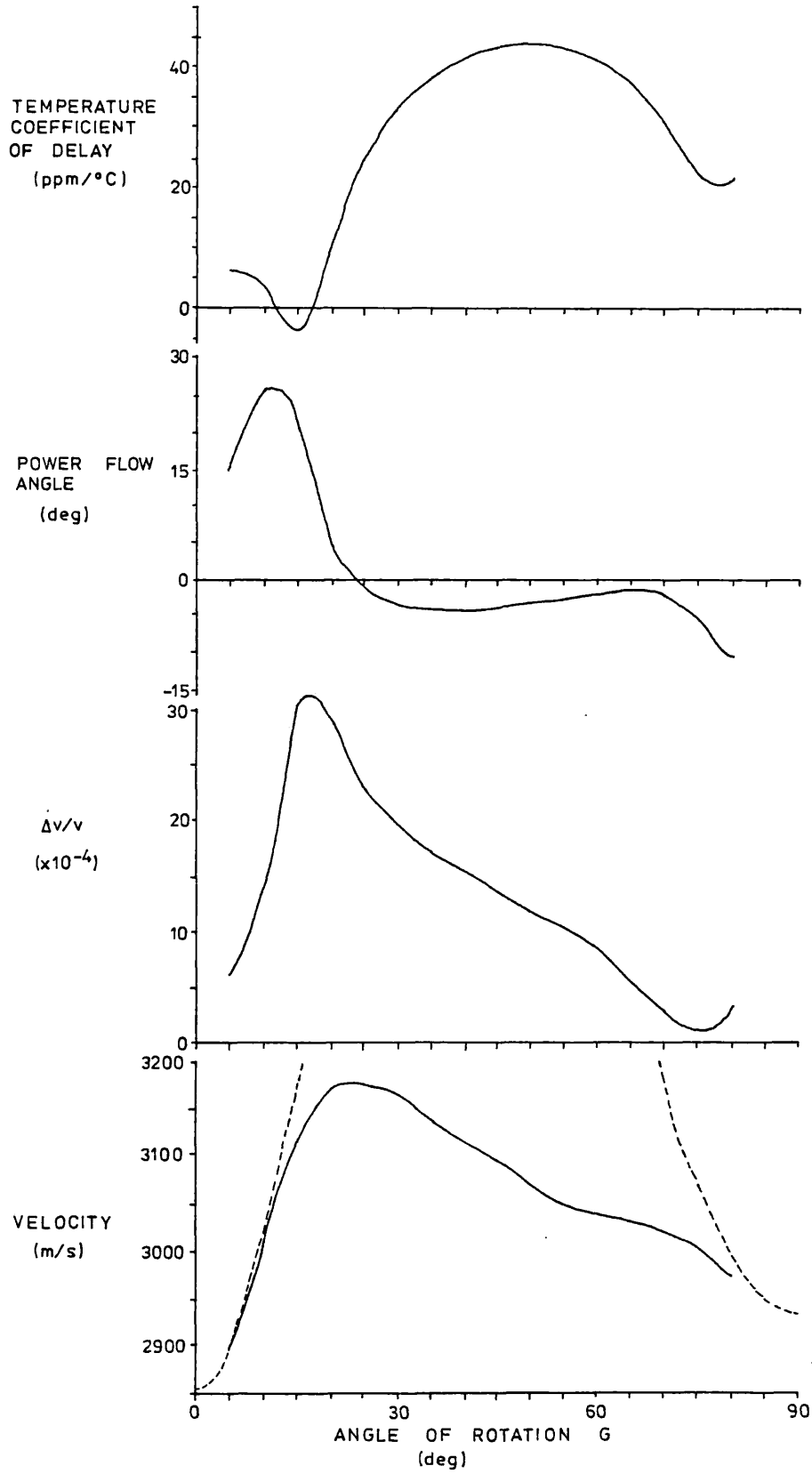

Figure 4.9

SAW PROPERTIES (0,50,G)

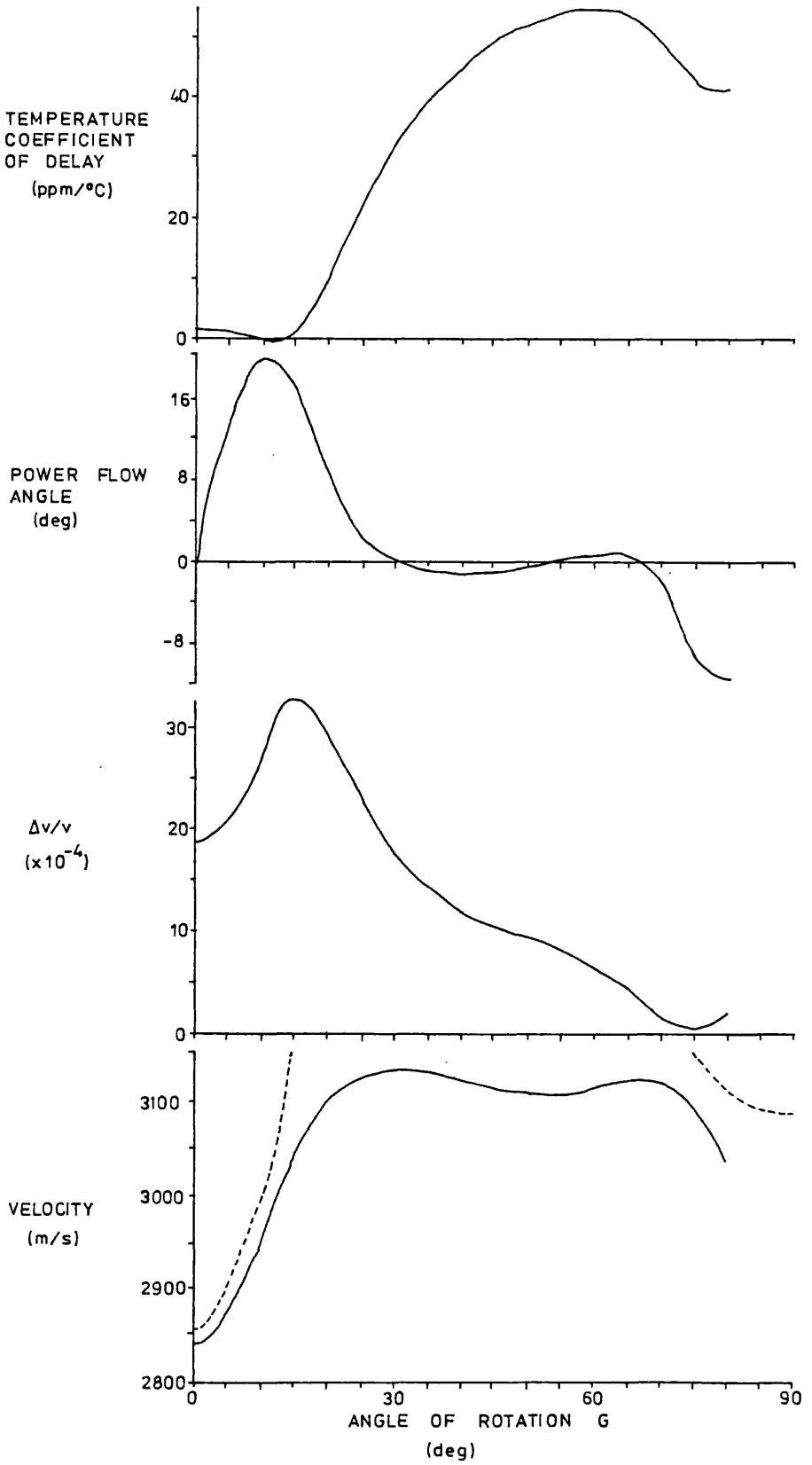

Figure 4.10

SAW PROPERTIES (0,60,G)

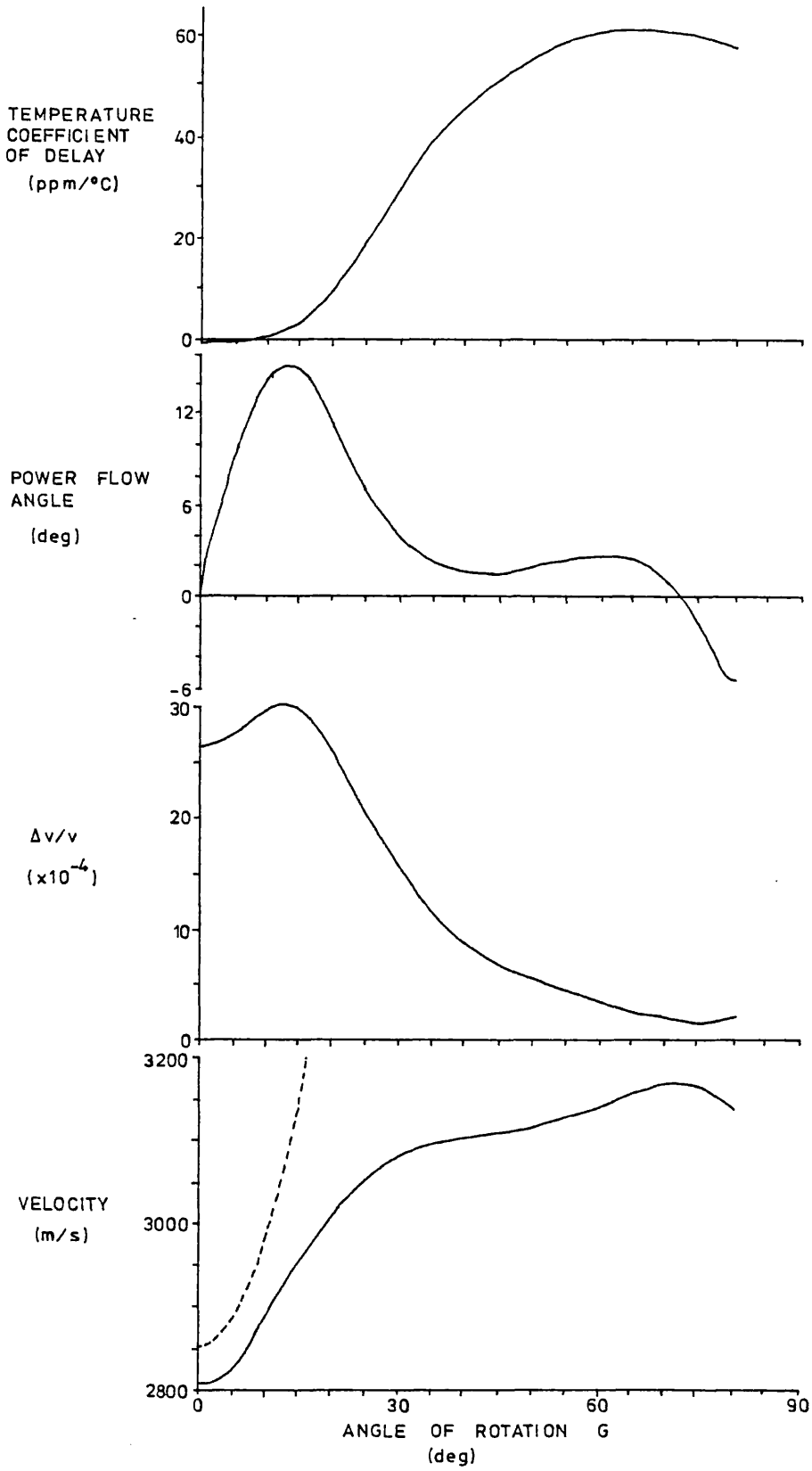

Figure 4.11

SAW PROPERTIES (0,70,G)

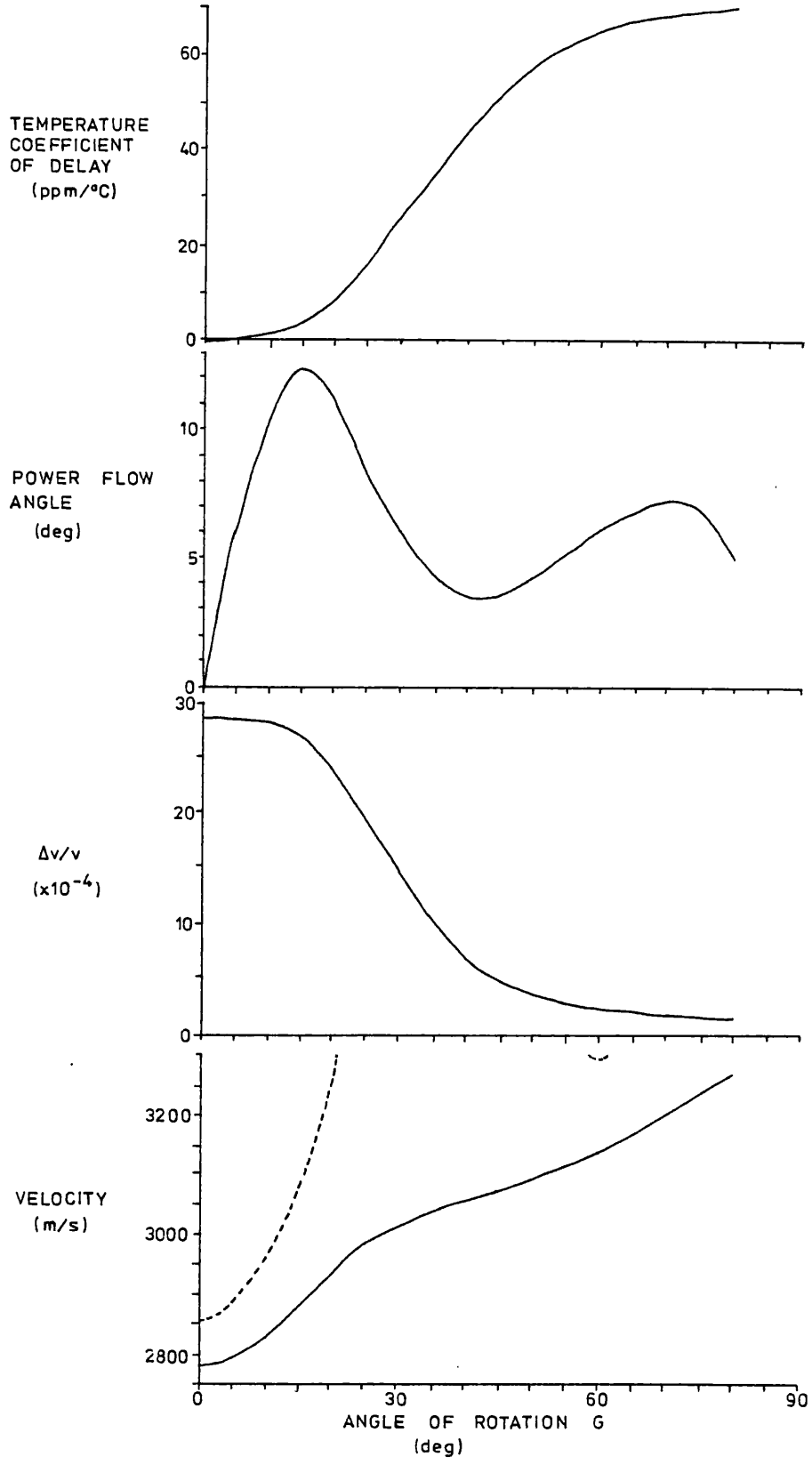

Figure 4.12

SAW PROPERTIES (0,80,G)

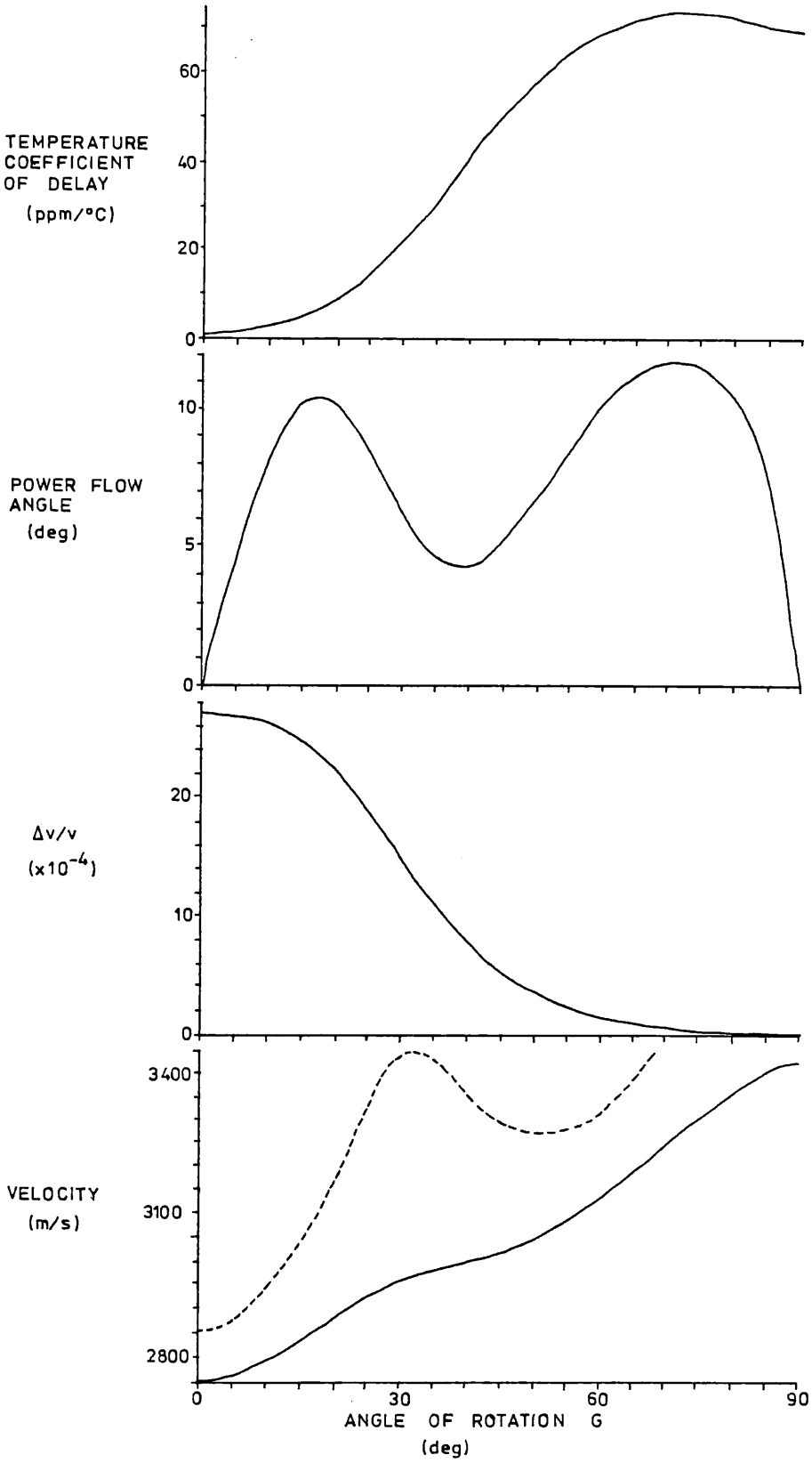

Figure 4.13

SAW PROPERTIES (0,90,G)

Y CUT

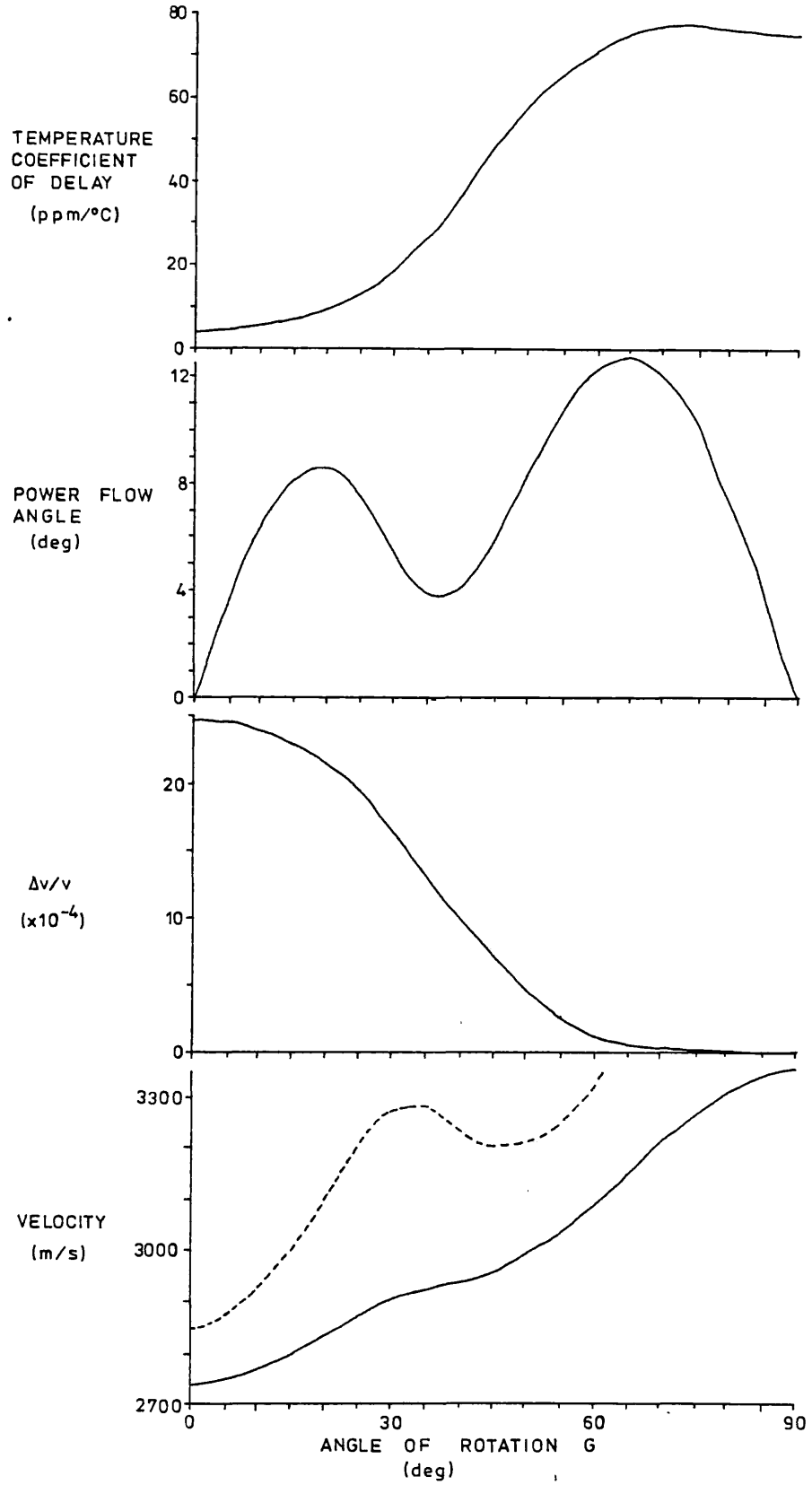

Figure 4.14

SAW PROPERTIES (0,100,G)

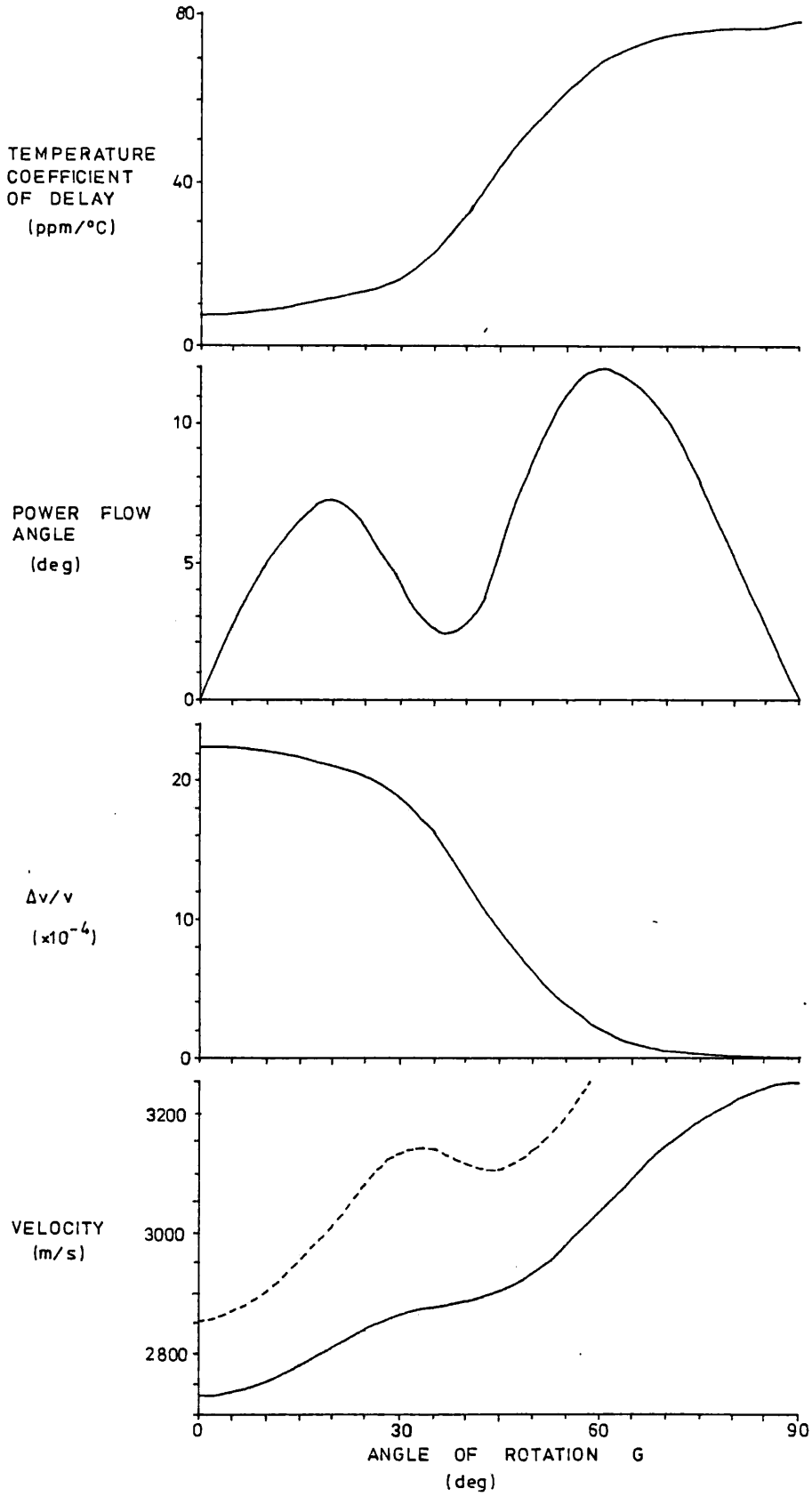

Figure 4.15

SAW PROPERTIES (0,110,G)

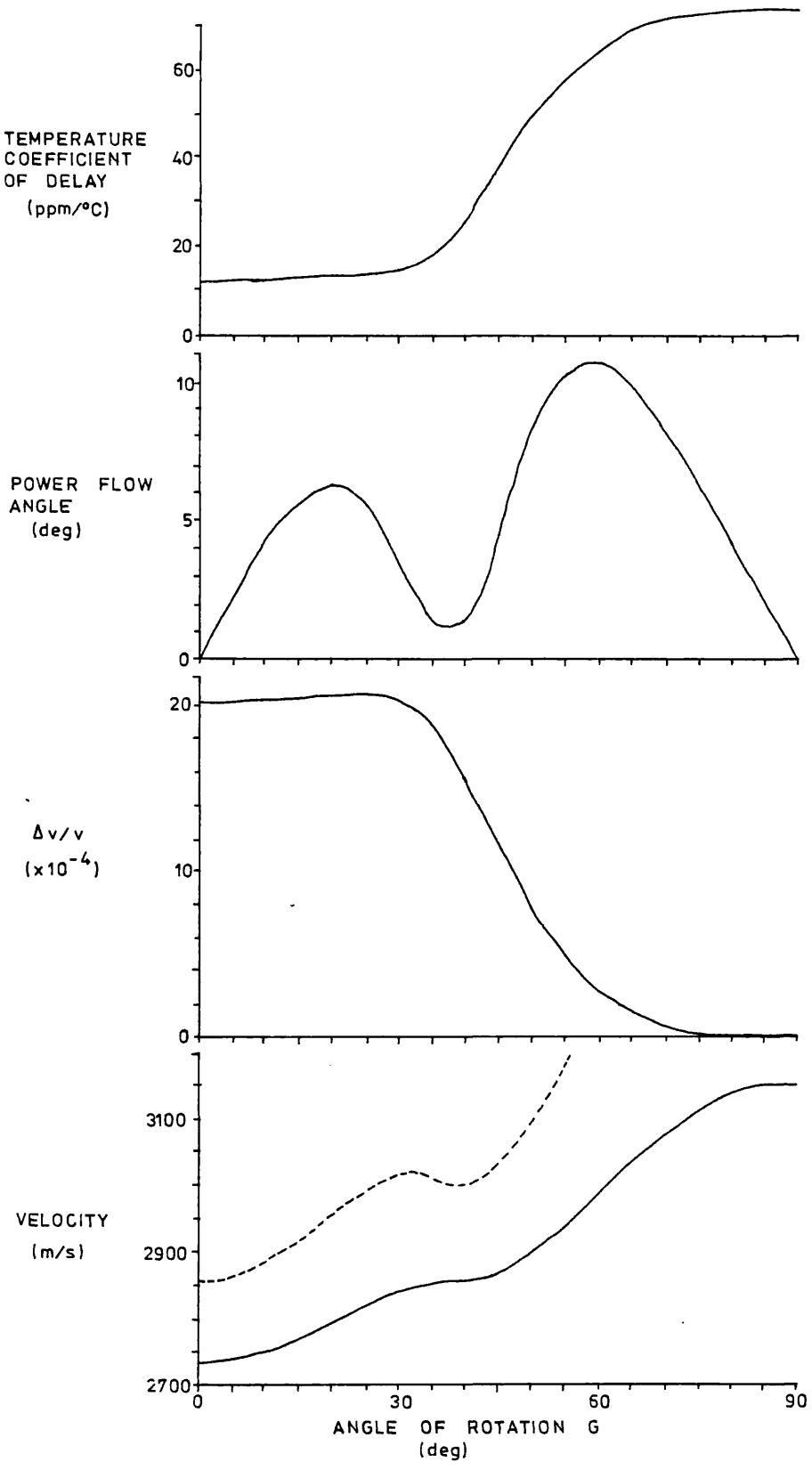

Figure 4.16

SAW PROPERTIES (0,120,G)

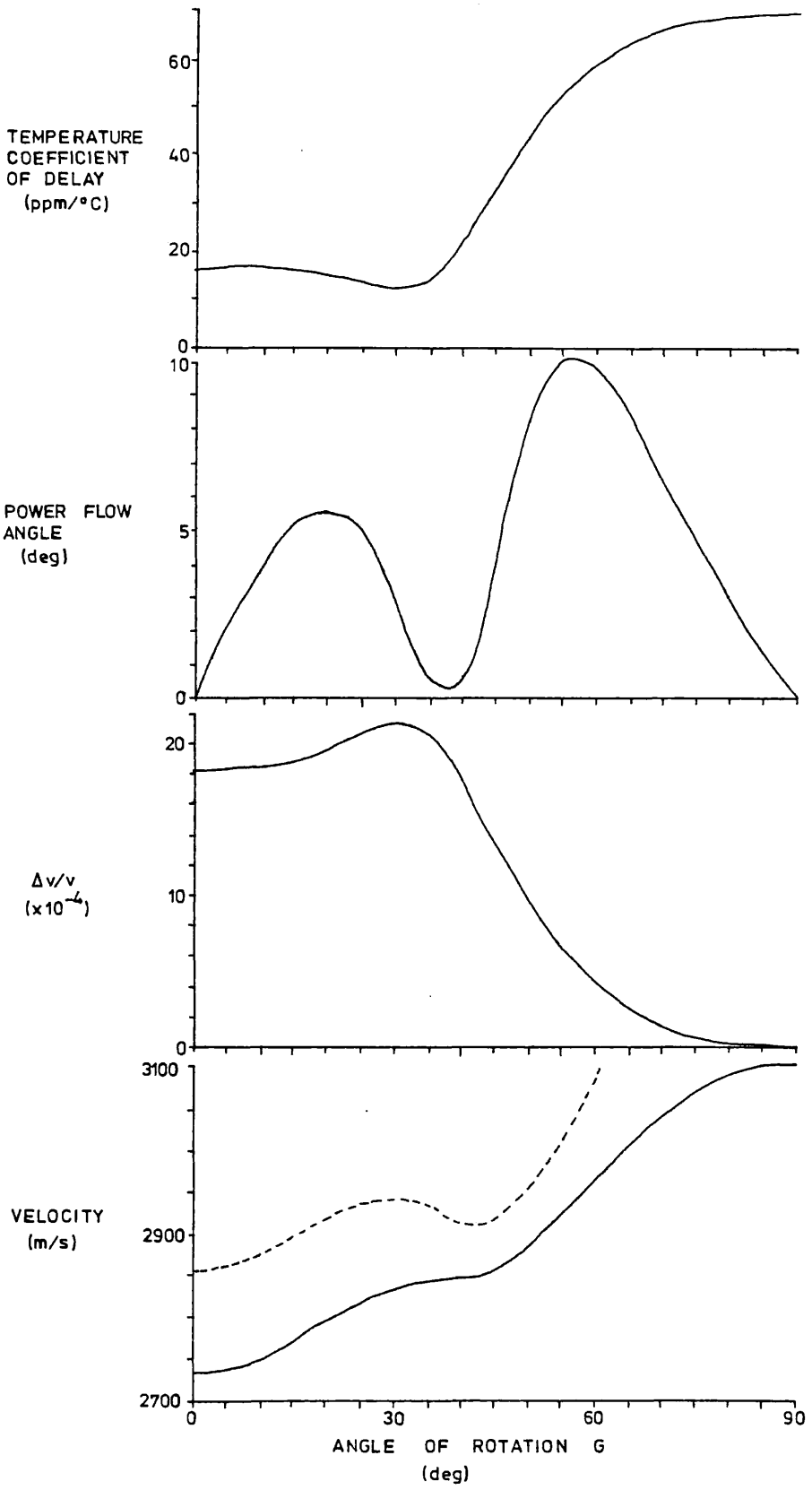

Figure 4.17

SAW PROPERTIES (0,130,G)

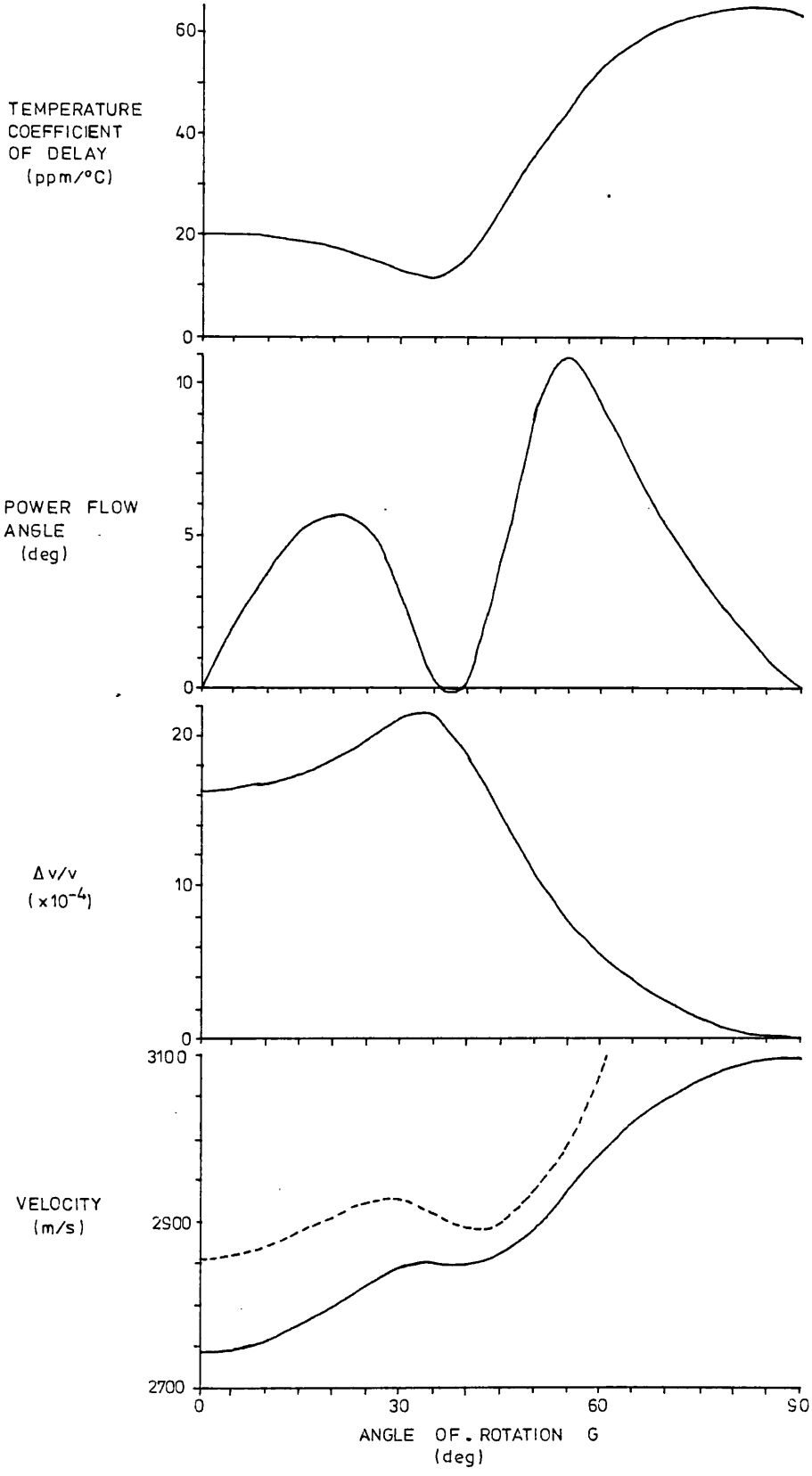

Figure 4.18

SAW PROPERTIES (0,140,G)

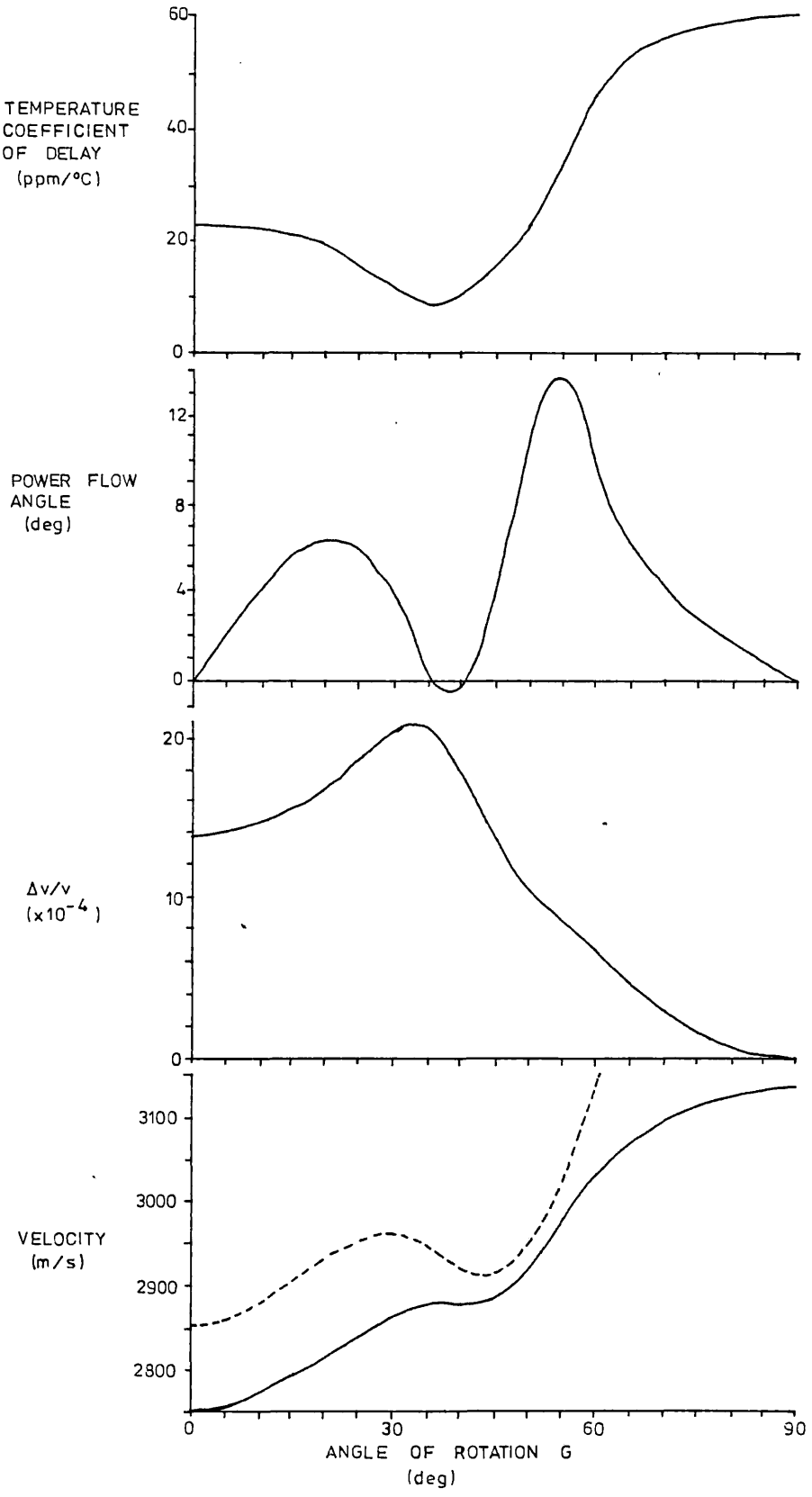

Figure 4.19

SAW PROPERTIES (0,150,G)

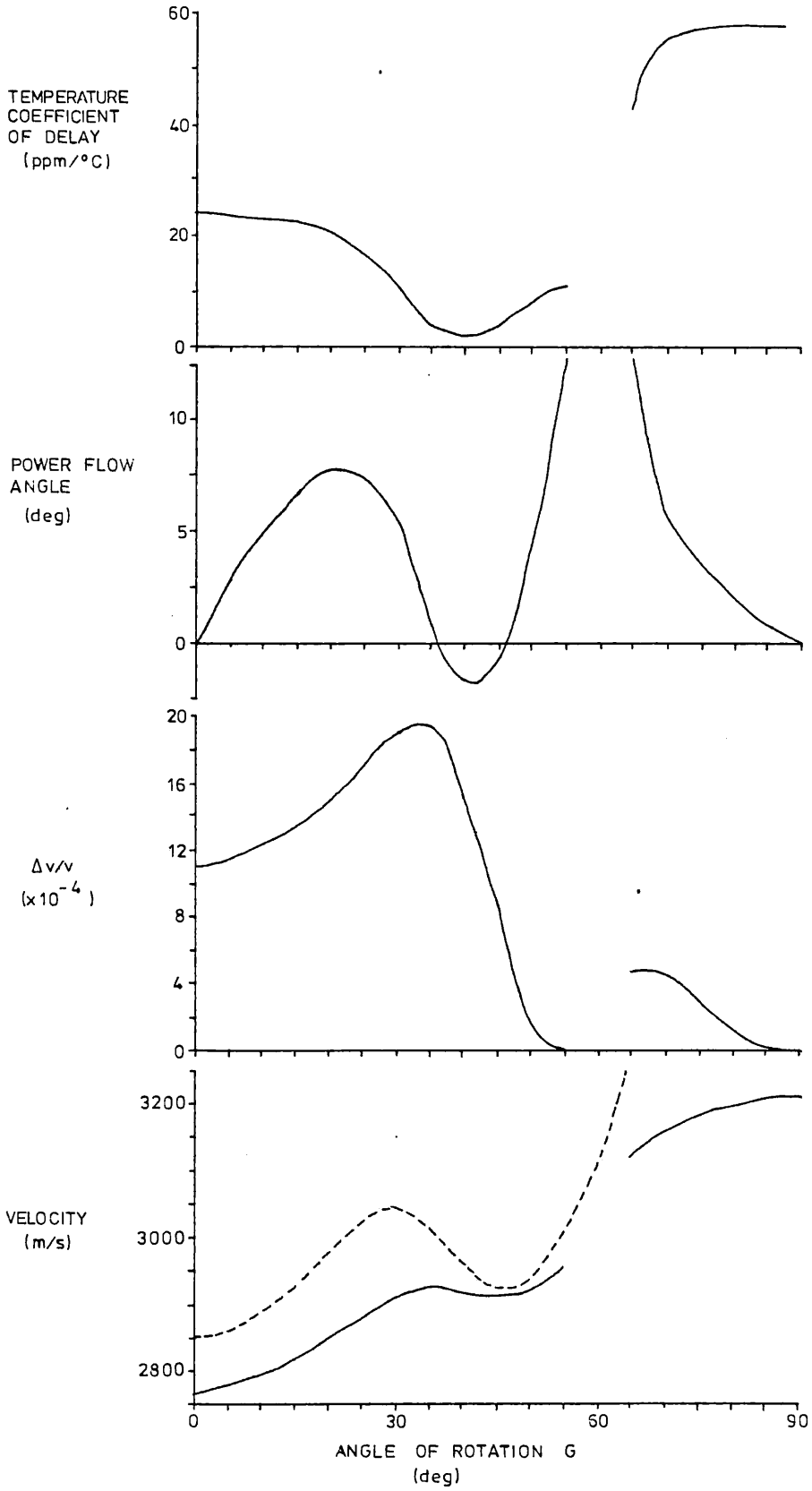

Figure 4.20

SAW PROPERTIES (0,160,G)

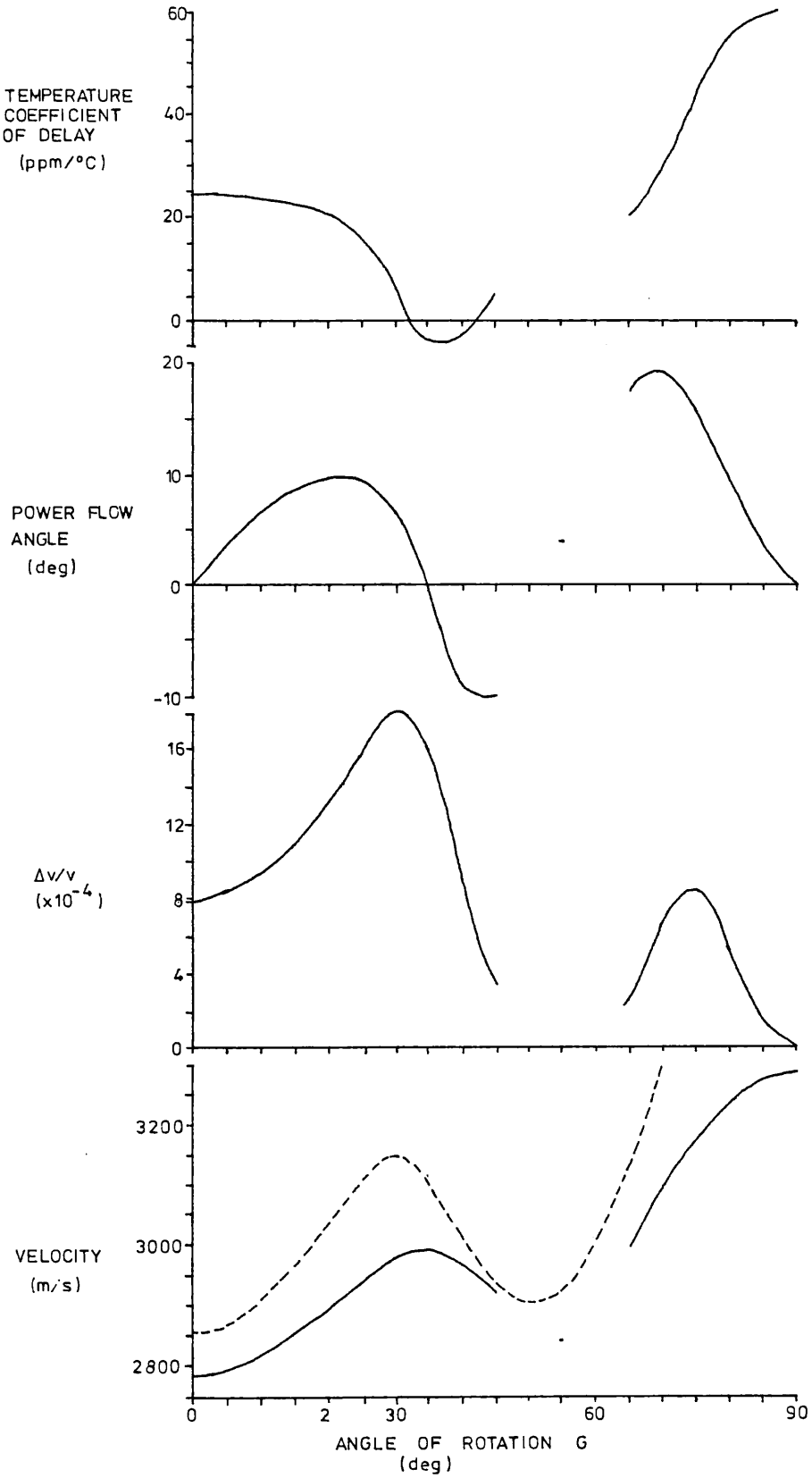

Figure 4.21

SAW PROPERTIES (0,170,G)

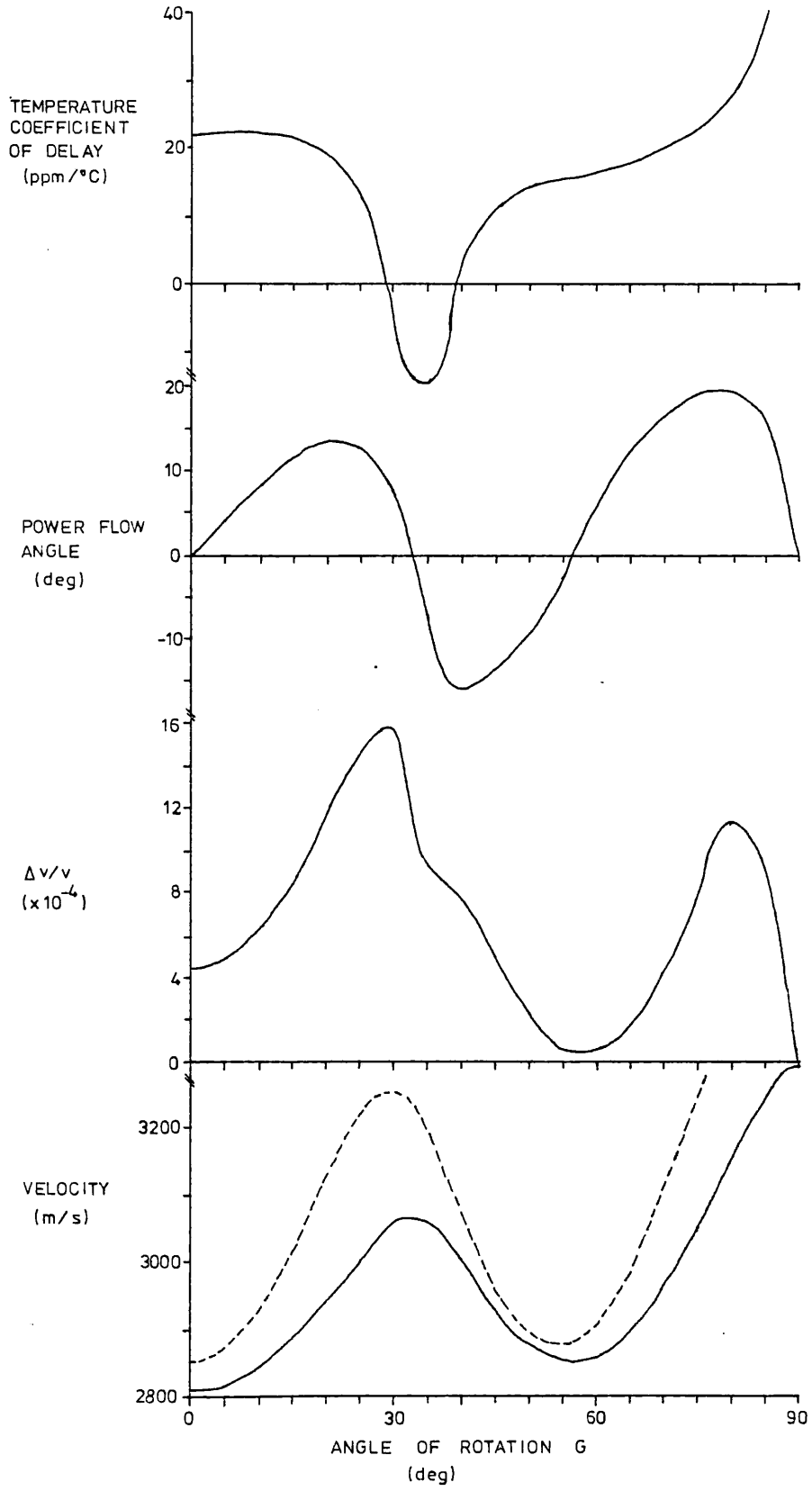

Figure 4.22

SAW PROPERTIES (A, 90,0)

Z AXIS CYLINDER

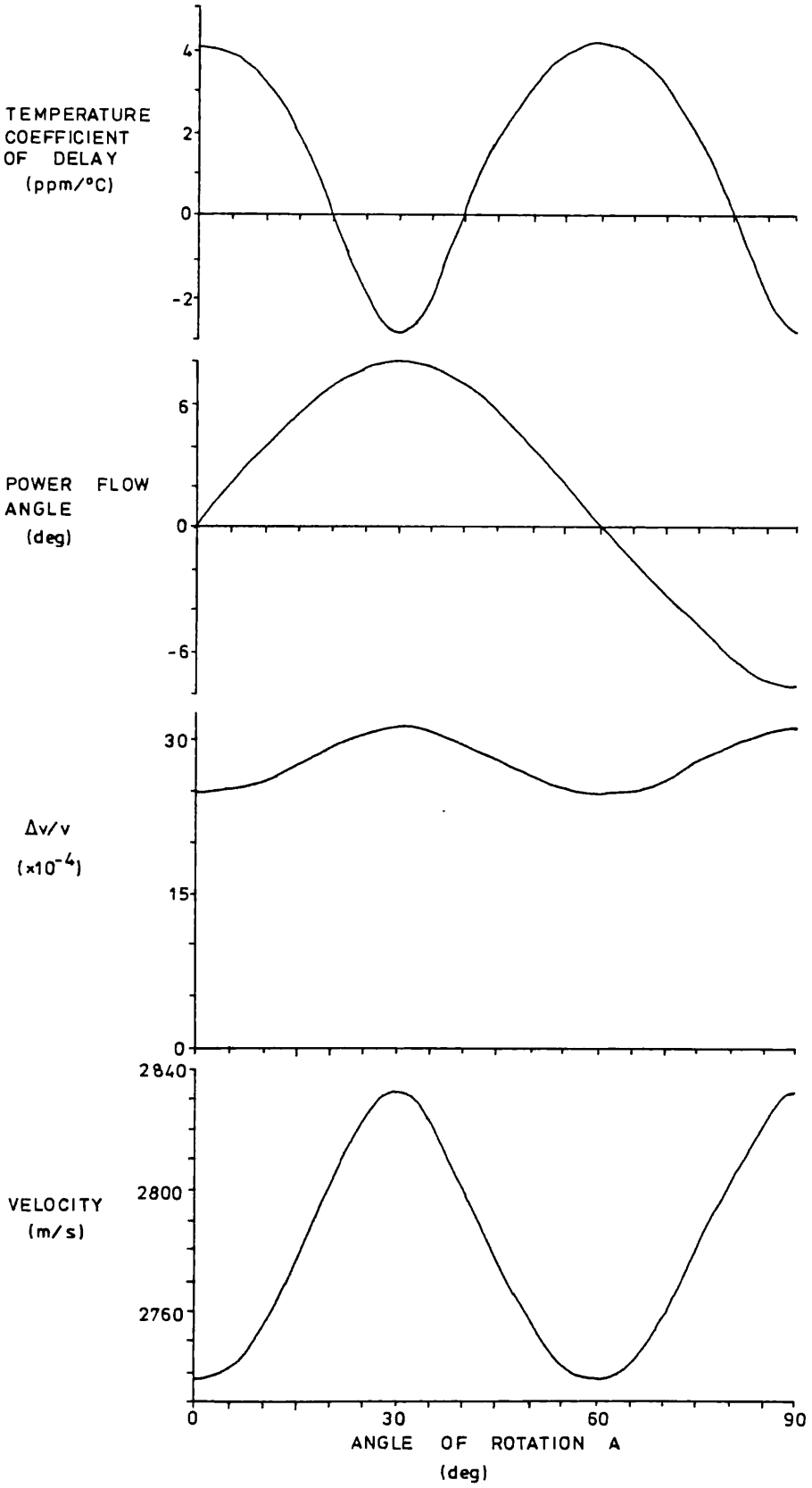

Figure 4.23

SAW PROPERTIES (90, B, 0)

Y AXIS BOULE

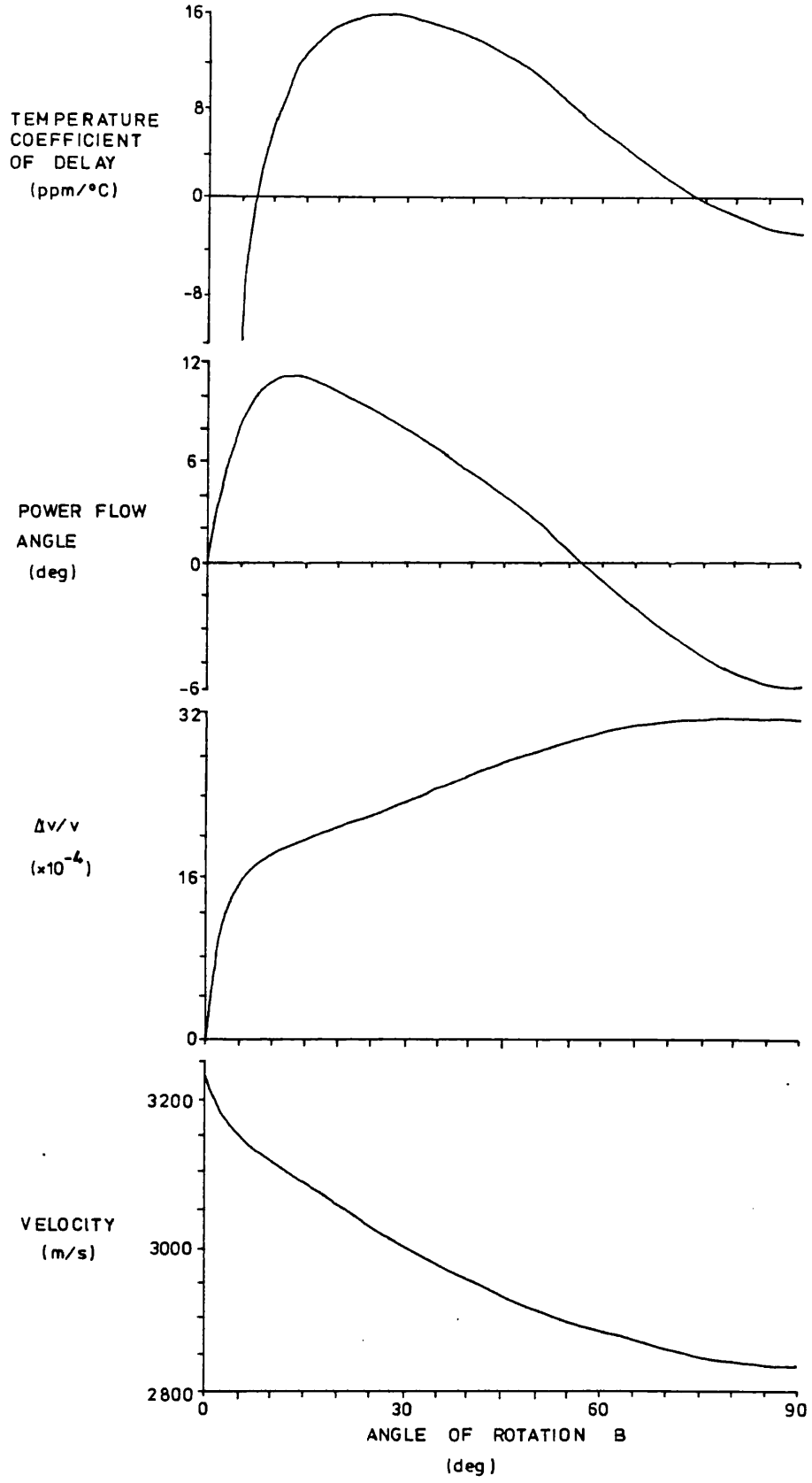

Figure 4.24

SAW PROPERTIES (90,B,90)

Y AXIS CYLINDER

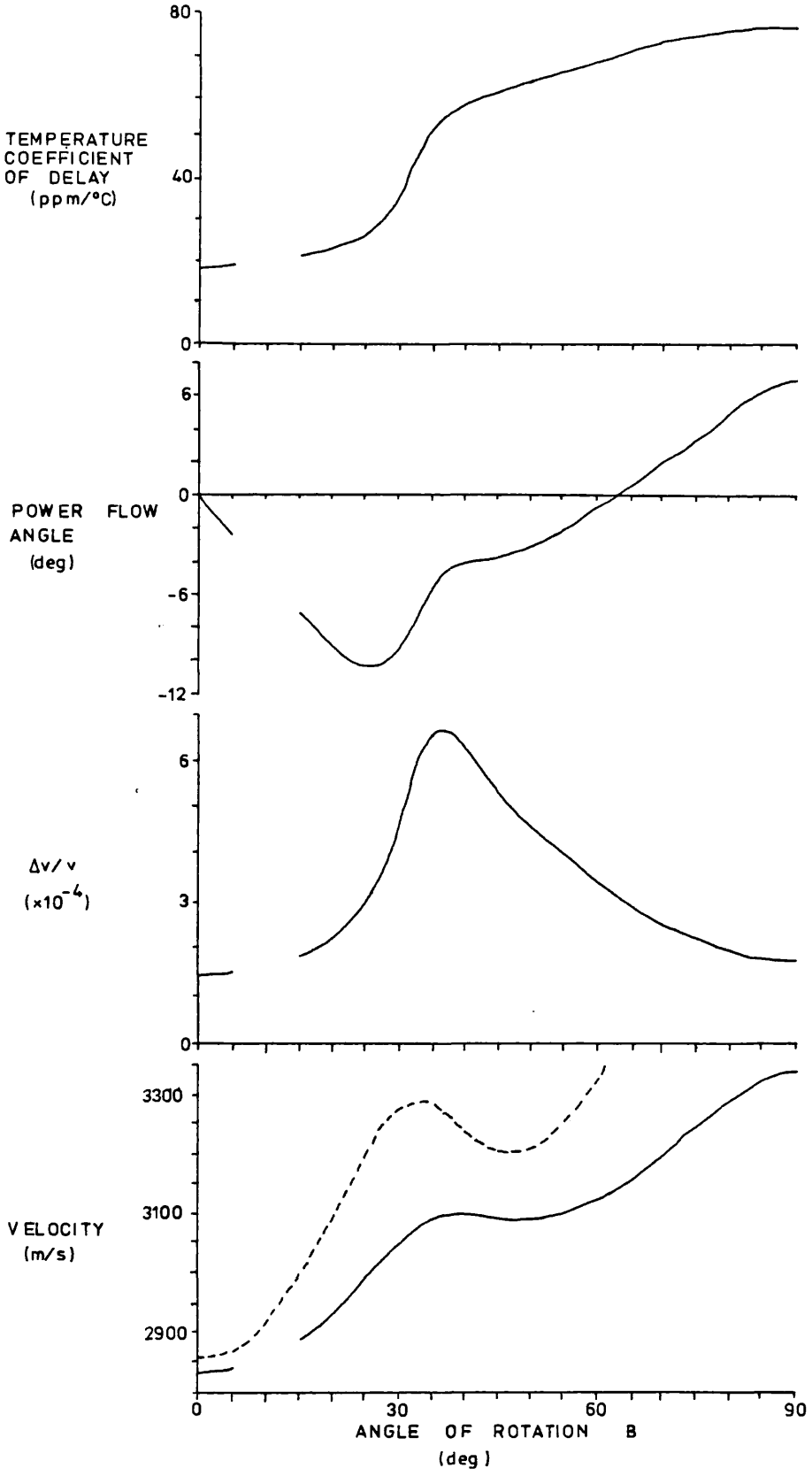

Figure 4.25

SAW PROPERTIES (A,90,90)

Z AXIS BOULE

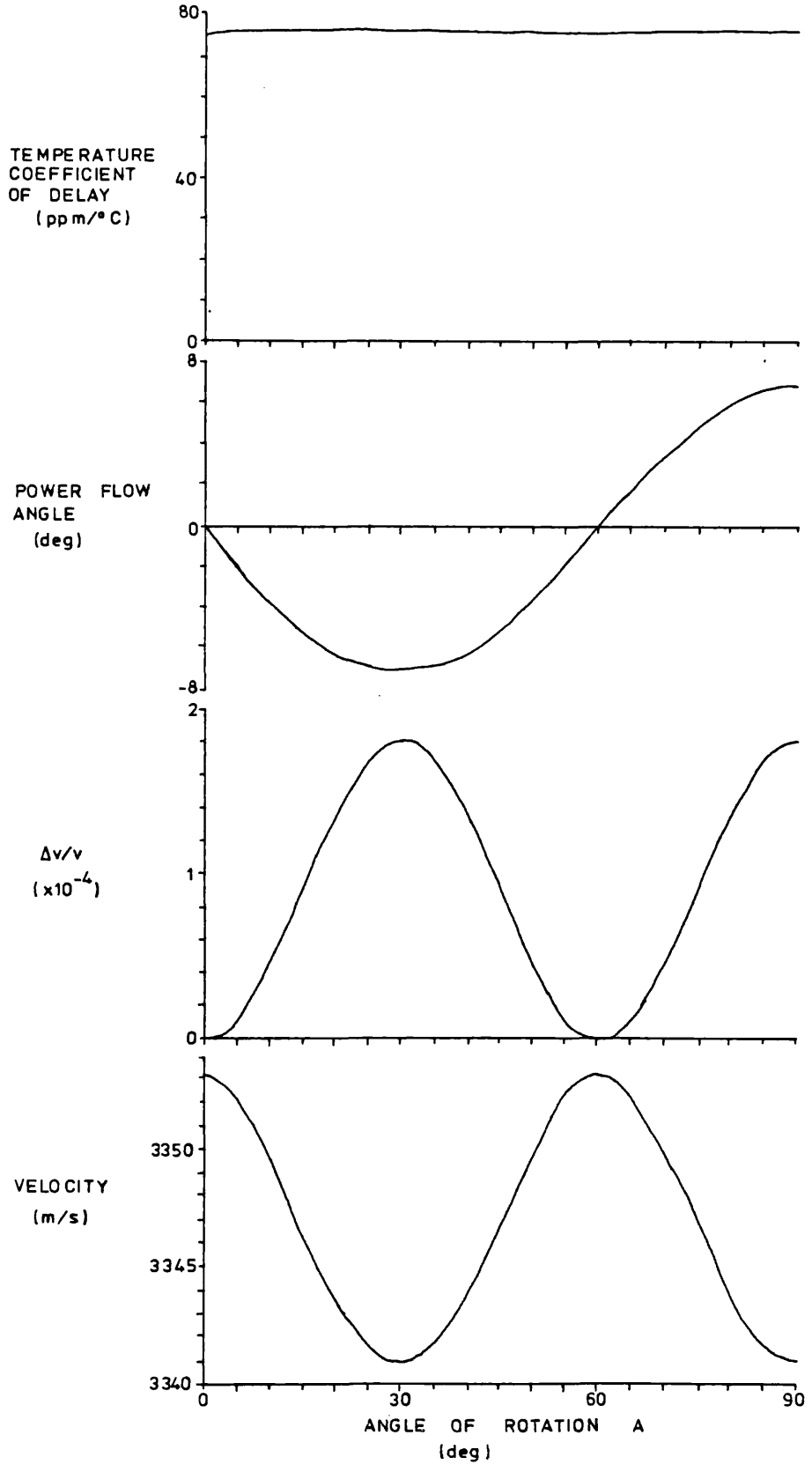

Figure 4.26

SAW PROPERTIES (90,90, G)

X CUT

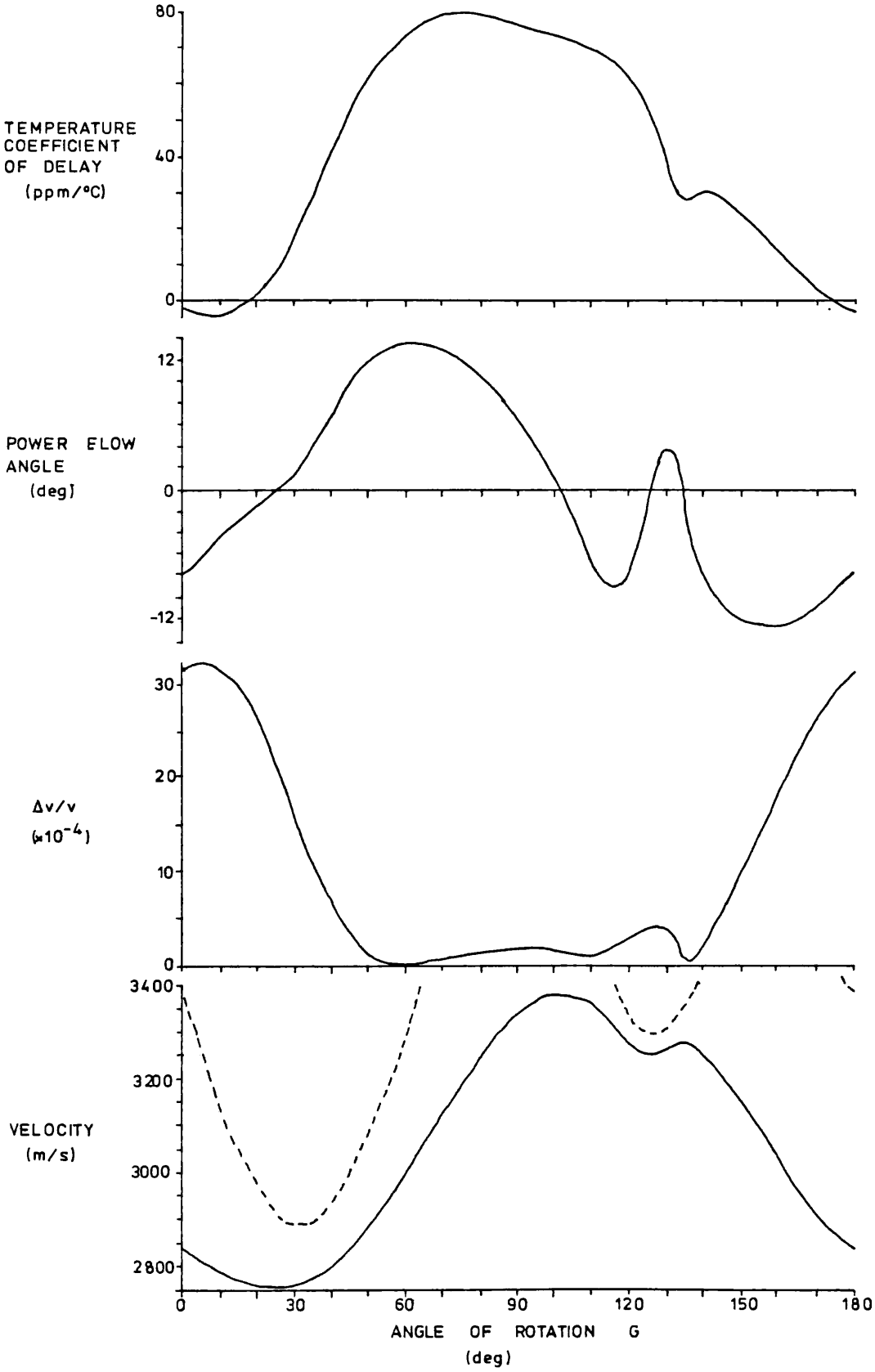

Figure 4.27

TEMPERATURE COMPENSATED CUTS IN PLANE (0, B, G)

Key

- ∘ Temperature Compensated orientation
- × Zero Power Flow Angle orientation
- □ No Surface Wave solution found for this orientation

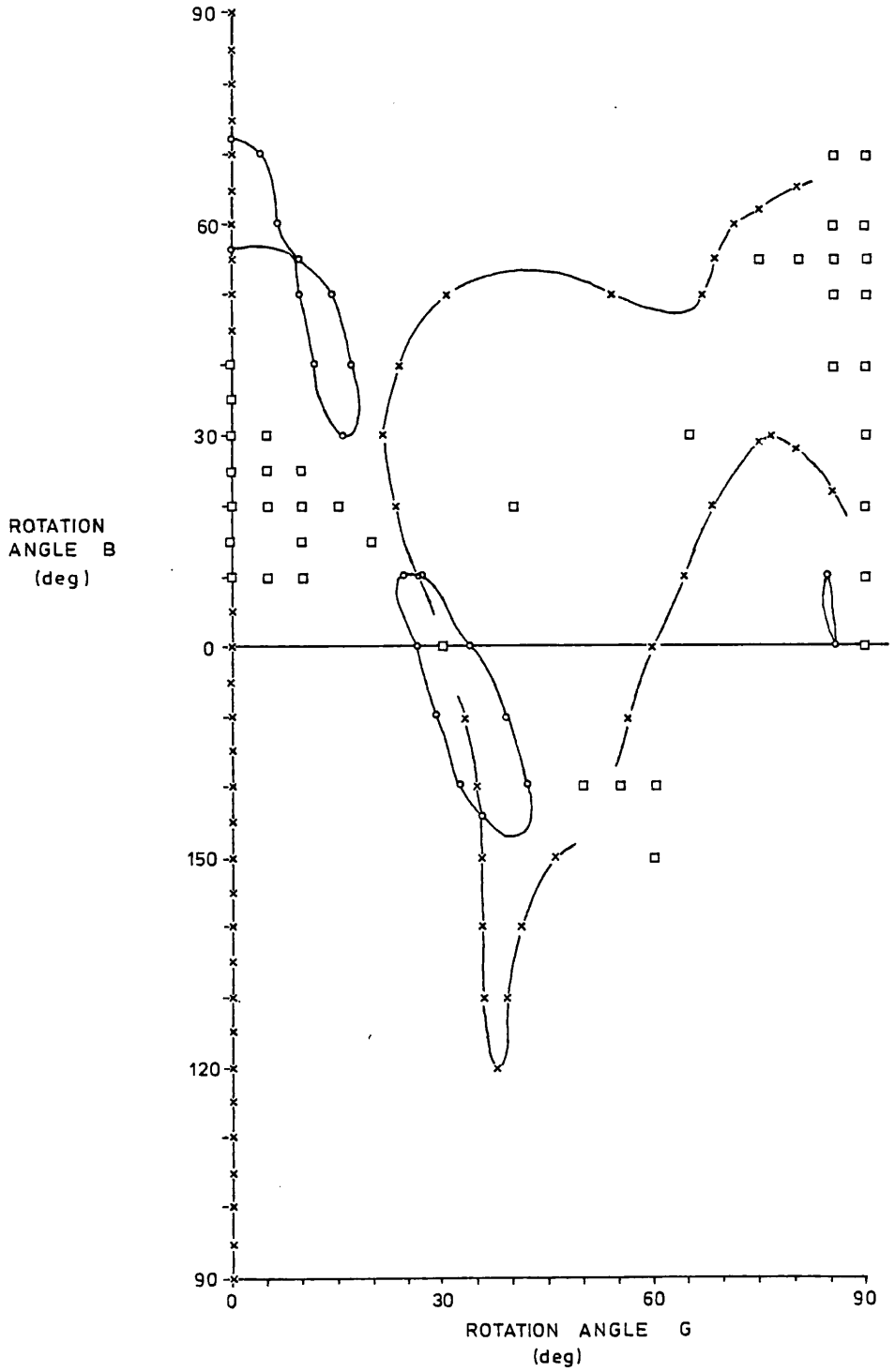

Chapter 5. Experimental results for surface acoustic waves on berlinite.

Section 1. Experimental results from other workers.

Three groups of workers other than ourselves have investigated the experimental properties of surface acoustic wave cuts on berlinite, these are Carr and O'Connell [44,58], Morency et al. [154, 155,156] and Detaint et al. [119].

Carr and O'Connell [44,58] used a crystal grown at the Naval Weapons Centre (USA) and looked at the 80.4° rotated Y cut (X axis boule) that they had predicted to be temperature compensated [151]. They constructed 3 devices which had 4 identical transducers arranged as two delay lines. Each transducer had 66 double electrode pairs with a line width of 1.26 μm and an aperture of 250 μm. The transducers on the three devices were seperated by 5.08 mm, 4.06 mm and 3.05 mm. The 5.08 mm delay line was used as a feedback element in an oscillator circuit. This enabled the SAW velocity and the frequency-temperature response to be determined. By allowing the oscillator to 'hop' between adjacent frequency modes, the SAW velocity was found to be 2739 m/s. From the geometry of the transducers and the synchronous frequency of the delay line a SAW velocity under the transducers of 2743 m/s was found.

The frequency-temperature response gave a turnover temperature at 25.4°C and a second order temperature coefficient of -264×10^{-9} °C^{-2}. The frequency response was measured over a range from 0°-48°C. The second order temperature coefficient is considerably larger than that of ST cut quartz (-31.5×10^{-9} °C^{-2} [11]).

The coupling coefficient k^2 was measured from the input impedance of the tuned 3.05 mm delay line, giving a value of 0.3% (i.e. $\Delta v/v \simeq 15 \times 10^{-4}$) which is much lower than they predicted [151].

Morency et al. [154,155,156] used a small crystal grown by Professor G. Lehmann in Germany. It was about 15 mm in the Z direction by 7 mm in the X direction. They used the X axis boule 92.75° orientation [154,155] that had been theoretically predicted by some of their group [27,152]. They fabricated a 10 finger pair, 90 MHz delay line having 1.82 mm seperation between input and output transducers. They measured the SAW velocity as 2747 m/s (compared with the prediction of 2733 m/s [27]). They measured k^2 by using a 30 finger pair 75 MHz transducer pattern and measuring the conductance at

resonance and the static capacitance [157]. They obtained a value of k^2 of approximately 0.3% ($\Delta v/v = 13 \times 10^{-4}$), compared with the theoretical prediction of 0.4% ($\Delta v/v = 22 \times 10^{-4}$ [27]).

The delay-temperature response of the delay line was measured using the oscillator method [158]. The delay line was matched by two air coils. The delay-temperature curve shows a turnover temperature of about 39°C, although they quote 32°C, and the response is noticably assymmetric. The temperature range used was from 15° - 55°C.

In a later paper [156] they also produce results for 80°, 85° and 87.25° X axis boule cuts. They measured $\Delta v/v$ by two methods, (i) by measuring the change in phase as a metal film was deposited [57] and (ii) by measurement of the conductance at resonance and the static capacitance of a 30 finger pair transducer [157]. The temperature coefficient of delay was measured with the delay lines matched by two air coils with copper screening between the transducers. Both black wax and black tape were used to dampen reflections. The results that they obtained are shown in Table 5.1. All the delay-temperature curves show a second order temperature coefficient of delay larger than that of ST cut quartz.

Detaint et al. [119] used some crystals that they had grown [119] and used the 90° X axis boule orientation (Y cut). They fabricated delay lines using two interdigital transducers of 181 and 361 fingers with a wavelength of 12.192 μm and an aperture of 0.5 mm. They obtained a value of k^2 of about 0.5% from impedance measurements which compares well with their prediction of 0.58%. The SAW velocity was measured as 2740 m/s, again close to their prediction of 2739.6 m/s, using a 'mode-hopping' technique. The frequency-temperature response was also measured and the turnover temperature varied between 14° and 24° C for the different crystal samples. The second order temperature coefficient of frequency was measured to be 210×10^{-9} °C^{-2}.

These results will be discussed further in Chapter 6.

Table 5.1 Experimental results from reference 156.

Property	80° cut		85° cut		82.25° cut	
	expt	theory	expt	theory	expt	theory
SAW velocity (m/s)	2728	2754	2836	2744	2747	2741
$\Delta v/v$ (10^{-4})		27	11	26	13	25
TCD (ppm/°C) at 25°C	-14.6	-2.9	-11.3	-1.8	-4.1	-1.1
Turnover temperature (°C)	44		38		32	
Temperature range (°C)	22-52		22-48		12-52	

Section 2. Details of the crystals used in these experiments.

The growth of the crystals used in our experiments was described in Chapter 3. The crystals were cut and lapped to the specified orientations of 80° X axis boule and 90° X axis boule. The slices obtained were etched in a 1% solution of HF for 10 minutes and photographs were then taken under polarised light to reveal grain boundaries between electrically twinned areas. The twinning revealed in the photographs showed that the spontaneously nucleated crystals,which had been grown through several growth cycles, to be much more heavily affected by twinning than the minor rhombohedrally grown crystal. This is shown in the photographs, Figures 5.1 to 5.6. Most writers have reported twinning in berlinite (see Chapter 3) and much effort is being put into improving the quality of the crystals currently being grown.

Most of the cut crystal plates had an area of surface which was free from major cracks of at least 10 mm by 5 mm. This enabled the larger type 2 mask to be used on crystal 2. This mask has three transducers as shown in Figure 5.7. Unfortunately this mask was not available in time to use it upon the slices from crystal 1 and a mask obtained from Marconi was used (see Figure 5.7). An ST cut quartz device was made up for the purposes of comparison, since the basic dimensional data for the Marconi mask was unavailable.

The crystals were repolished with ceri-rouge and processed for the photolithography of the transducer patterns. The transducers were placed to avoid areas of heavy twinning. The two crystals used and their details are listed in Table 5.2 together with the ST cut quartz crystal used for comparison.

Section 3. Details of the experiments :
(i) Oscillator experiments.

To measure the frequency-temperature response of the delay lines an oscillator loop was set up as shown in Figure 5.8. The amplification around the loop varied for some of the runs between 26 dB and 46 dB (see details of individual runs in Table 5.3).

The crystal slices were lightly glued into cast metal boxes with a small spot of Durofix which was placed well away from the region below the transducers to avoid any surface strains being introduced by different thermal expansion rates during the temperature cycling.

Table 5.2 Crystals used in experimental work.

Crystal	Slice	Mask	Device	Experimental run	Figure
1 Spontaneous	1	type 1	B1	X,XI,XIII	-
nucleation.	2	" 1	B2	I - VIII	-
(80° X axis	3	" 1	B3	Impedance	-
boule)	4	" 1	-	Not used	5.1
	5	" 1	-	" "	5.2
2. Minor	1	type 2	B4	Impedance	5.3
rhombohedral	2	" 2	-	Cracked	5.4
growth.	3	" 2	-	"	5.5
(90° X axis	4	-	-	"	5.6
boule)					
3. ST cut	1	type 1	Q1	IX,XII,XIV	-
quartz.	2	" 1	Q2	Impedance	-
	3	" 2	Q3	"	-

Figure 5.1

Crystal 1 Slice 4 80°X axis boule.

Figure 5.2

Crystal 1 Slice 5 80°X axis boule.

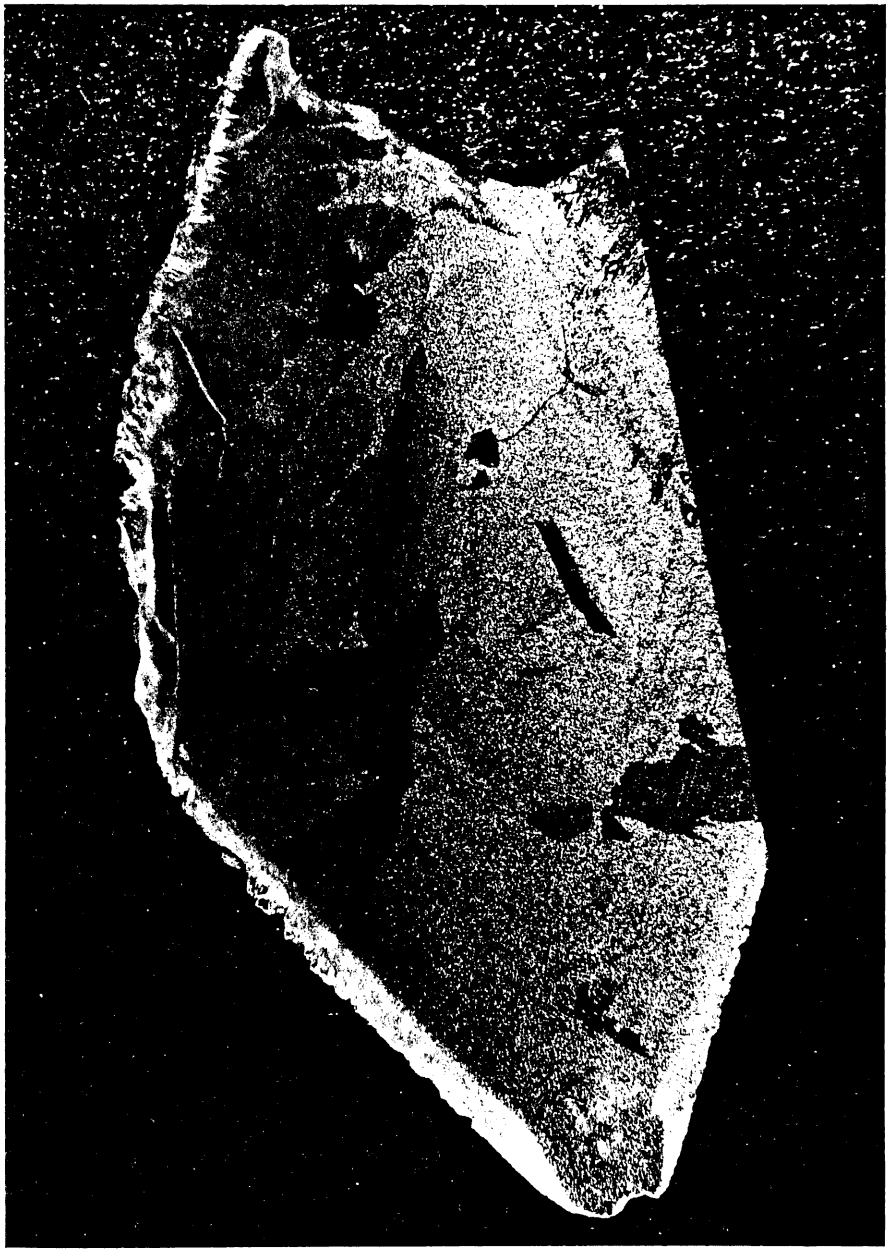

Figure 5.3

Crystal 2 Slice 1 90°X axis boule.

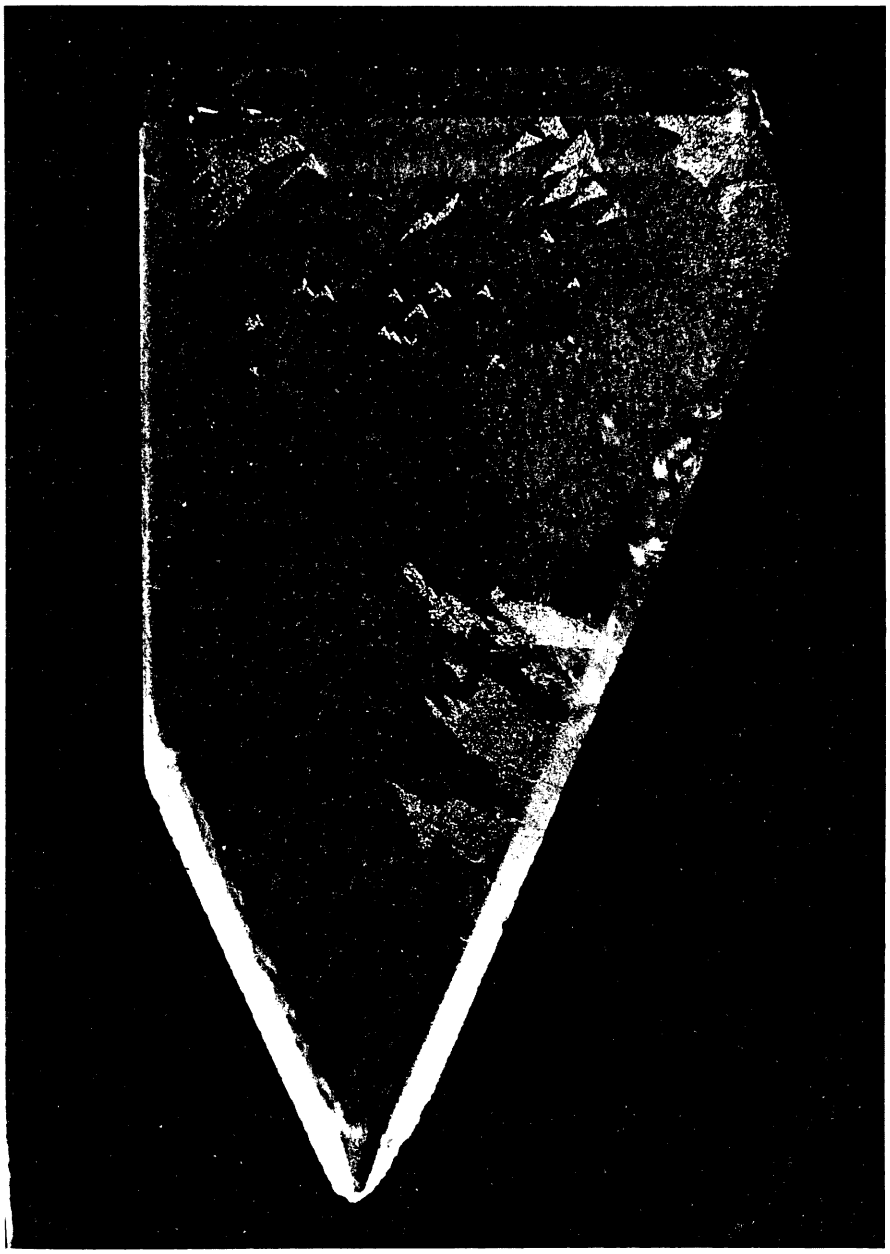

Figure 5.4

Crystal 2 Slice 2 90°X axis boule.

Figure 5.5

Crystal 2 Slice 3 90°X axis boule.

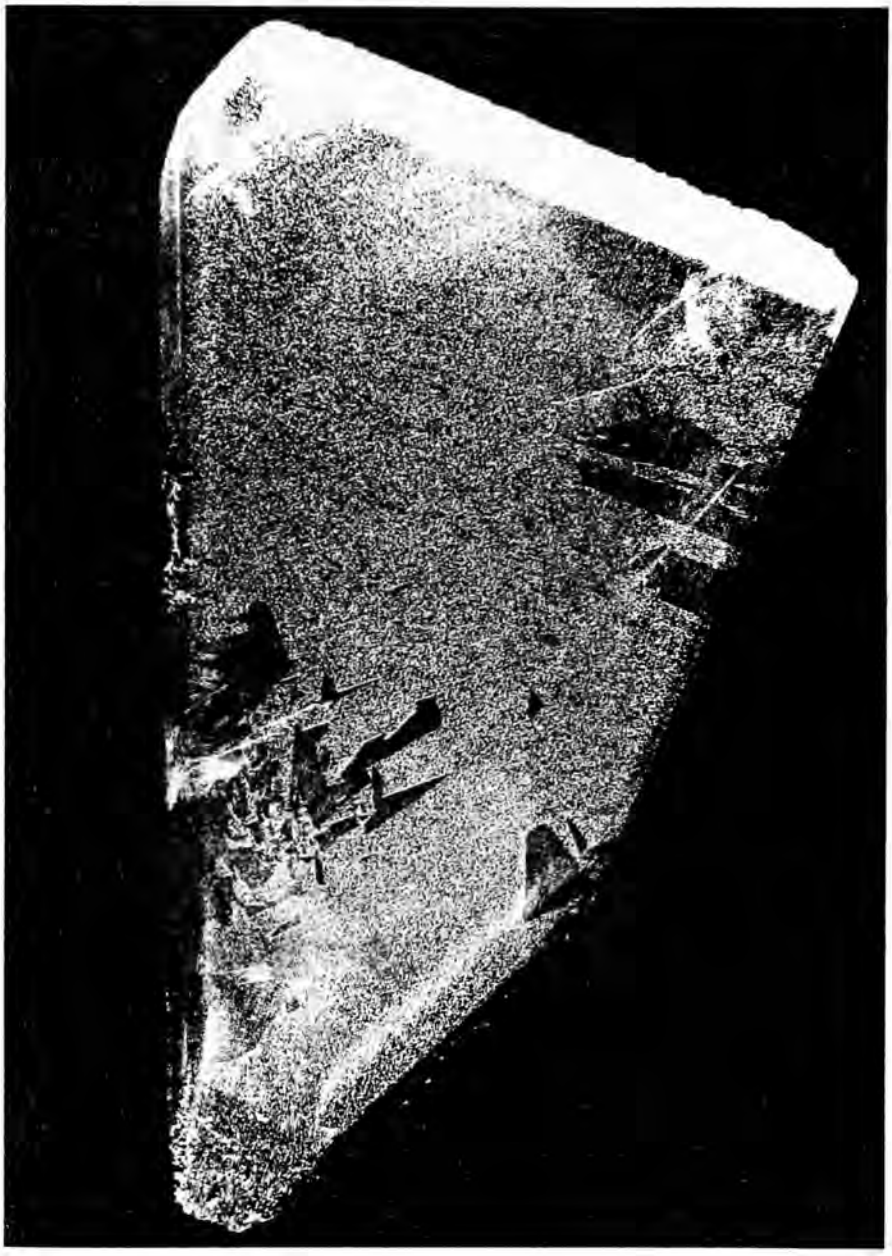

Figure 5.6

Crystal 2 Slice 4 90° X axis boule.

Figure 5.7

Type 2 transducer mask.

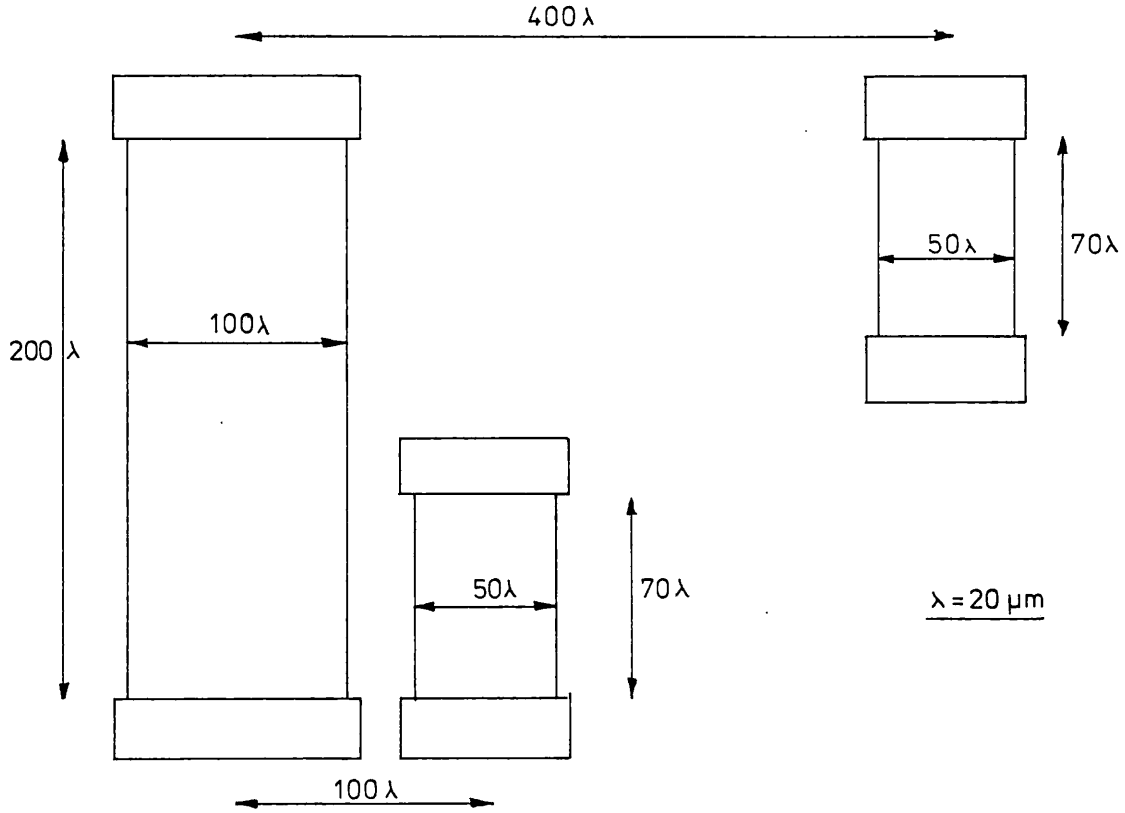

Type 1 transducer mask (Marconi).

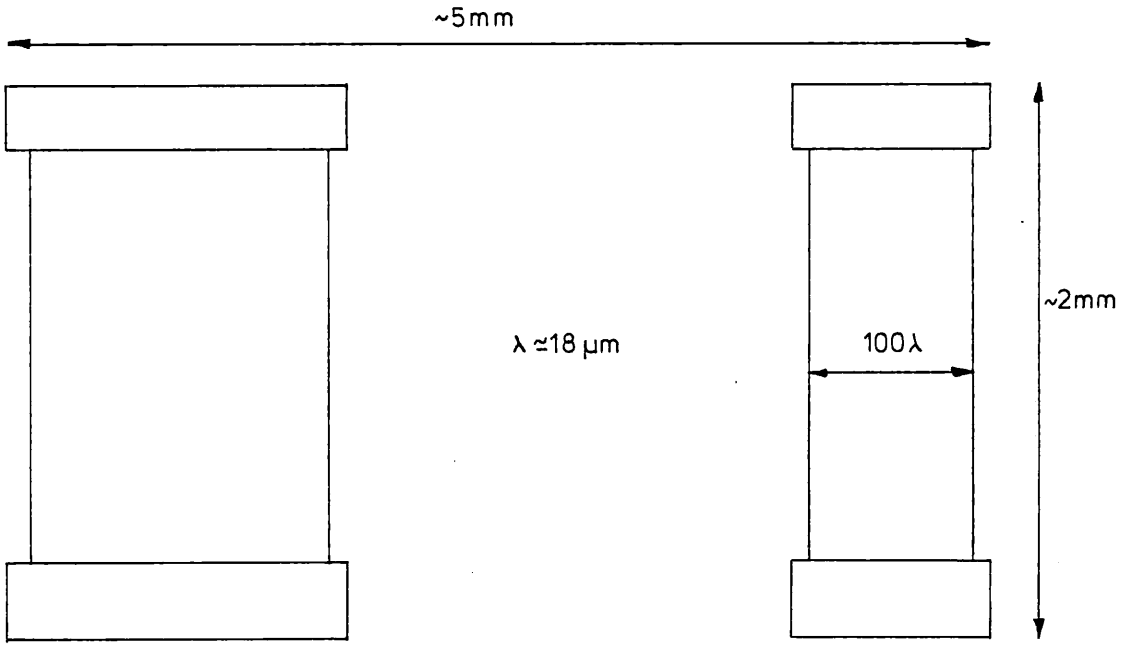

Table 5.3 Experimental runs for frequency-temperature responses.

Figure	Run	Device	Temperature (°C) Start	Finish	Amplification (dB)	Comments
-	I	B2	20	50		No external temperature control
-	II	B2	68	24		Thermocouple error
5.10	III	B2	75	31	46	
-	IV	B2	25	28	"	Stability test
-	V	B2	81	39	"	
-	VI	B2	80	18	"	Slow run to stabilise
5.11	VII	B2	106	32	26	164 mins, T_{ext} =25°C
5.12	VIIIa	B2	27	103	"	40 mins, " "
5.13	VIIIb	B2	106	32	"	170 mins, " "
-	IXa	Q1	22	95	"	78 mins, " " quartz control
-	IXb	Q1	90	30	"	137 mins, " "
5.14	X	B1	20	100	"	120 mins, T_{ext} =25°C
5.15	XIa	B1	18	100	"	69 mins, " "
5.16	XIb	B1	102	31	"	143 mins, " "
5.18	XIIa	Q1	19	101	"	52 mins, " "
-	XIIb	Q1	106	87	"	Bond wires broke
5.17	XIIIa	B1	82	25	"	159 mins, T_{ext} =25°C
5.19	XIVa	Q1	19	100	"	55 mins, " "
5.20	XIVb	Q1	103	30	"	137 mins, " "

Figure 5.8

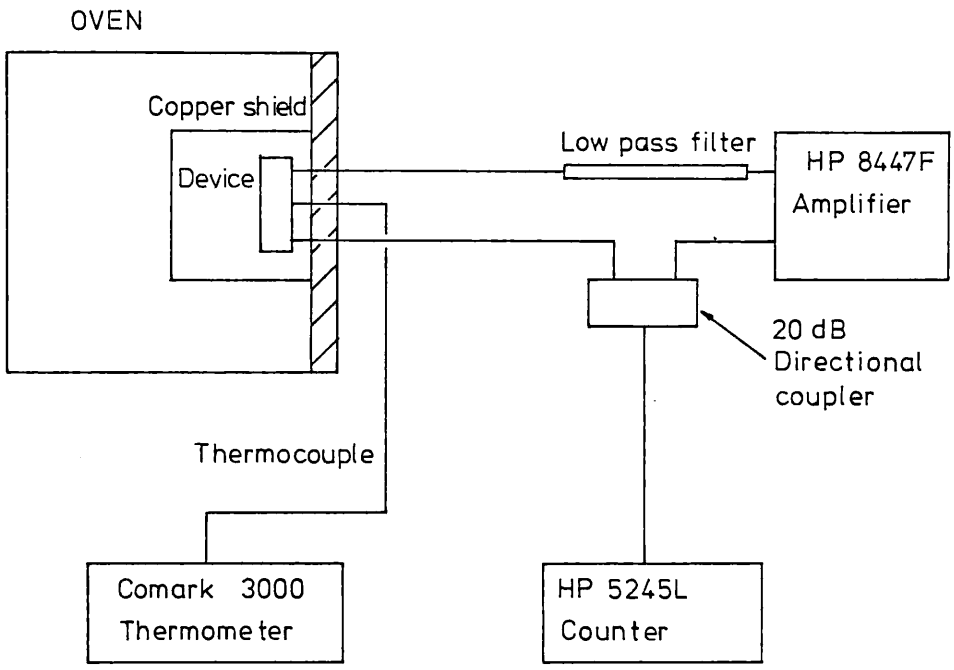

Experimental arrangement for freqency-temperature measurements

The transducers were bonded up using fine gold wire to pins connected to the external circuit. A thermocouple was firmly attached to the metal box to ensure that the correct temperature was recorded. The metal box was then attached to an asbestos oven door and covered by a copper box to shield the device from short term thermal variations and to try to ensure that the temperature of the device and the thermocouple were the same.

The oscillator loop makes use of the amplifier noise, this is filtered by the delay line and the low pass filter and reamplified around the loop. The oscillation frequency is characteristic to the delay line and transducer geometry and is measured by the frequency counter. The change in this oscillation frequency can then be measured for different temperatures.

The frequency of the modes of oscillation, f, must satisfy the phase condition :

$$2\pi f\tau + \phi_{ext} = 2\pi n \tag{5.1}$$

where τ is the delay time of the device, ϕ_{ext} is the phase shift of the external circuit and n is an integer.

Now if we rearrange and take temperature derivatives of the natural logs of both sides of equation (5.1) :

$$\frac{\partial}{\partial T} \ln(f\tau) = \frac{\partial}{\partial T} \ln(n - \frac{\phi_{ext}}{2\pi}) \tag{5.2}$$

$$\frac{1}{f}\frac{\partial f}{\partial T} + \frac{1}{\tau}\frac{\partial \tau}{\partial T} = \frac{1}{(n - \phi/2\pi)} \frac{\partial}{\partial T}(n - \phi/2\pi) \tag{5.3}$$

$$= 0 \tag{5.4}$$

since $\partial n/\partial T = 0$ (no 'mode hopping') and the external circuit is kept at constant temperature. Thus we have :

$$\frac{1}{f}\frac{\partial f}{\partial T} = -\frac{1}{\tau}\frac{\partial \tau}{\partial T} \tag{5.5}$$

(see equation (1.8)). Thus by measuring the temperature coefficient of frequency and reversing the sign we have the temperature coefficient of delay. It is much easier to measure frequencies accurately

than it is to measure small periods of time, thus we have chosen to measure and plot the changes in frequency with respect to temperature. On the graphs we plot $\Delta f/f$ against T and the slope of the graph gives the temperature coefficient of frequency and hence from equation (5.5) the temperature coefficient of delay.

Table 5.3 lists the details of the runs performed and some of these experimental runs are shown graphically in Figures 5.10 to 5.20 together with a least squares cubic frequency-temperature fit to the response. Three of the quartz runs are included with four runs from each of the two berlinite devices. These results will be discussed in Chapter 6.

(ii) Impedance measurements.

Two experimental arrangements were used to measure the electromechanical coupling coefficient k^2. Both involved the measurement of the magnitude and phase angle of the reflection coefficient of a transducer. Using the arrangement shown in Figure 5.9a we used a vector voltmeter to measure the magnitude and the phase angle of the transducer's reflection coefficient at the resonant frequency f_o of the transducer. The results plotted on a Smith's chart yielded the real and imaginary parts of the complex input impedance, Z.

The second method involved the use of the arrangement shown in Figure 5.9b and used a Hewlett Packard automatic network analyser to measure the magnitude and phase of the transducer's reflection coefficient over a small range of frequencies. From this it was possible to find the average phase angle at the resonant frequency f_o of the transducer. This average phase angle, together with the magnitude of the reflection coefficient, was used to calculate the complex input impedance, R-iX, of the transducer.

The reflection coefficient ρ is given by :

$$\rho = \frac{(R - R_o) - iX}{(R + R_o) - iX} \qquad (5.6)$$

where the system impedance $R_o = 50\ \Omega$.

The phase angle ϕ is given by :

$$\tan(\phi) = \frac{Im(\rho)}{Re(\rho)} = \frac{-2XR_o}{(R^2 - R_o^2) + X^2} \qquad (5.7)$$

Figure 5.9

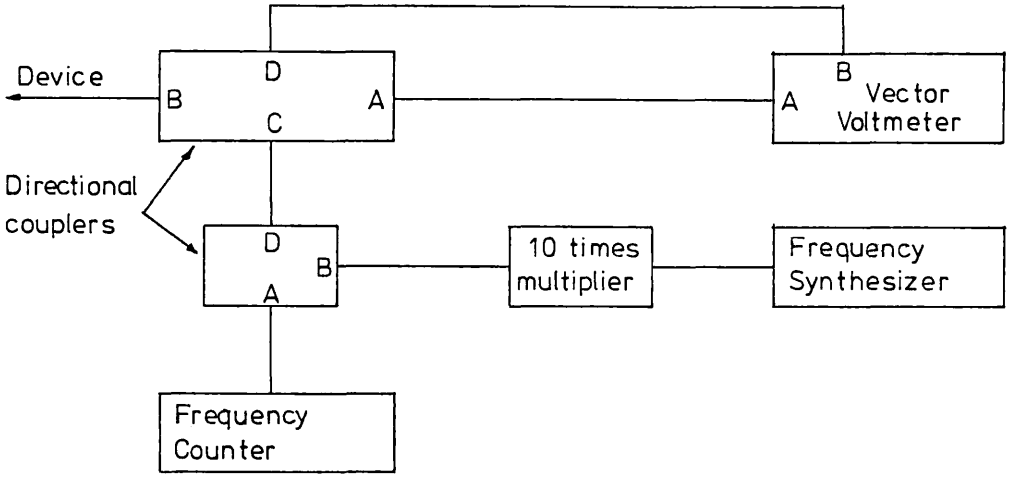

(a) Impedance measurements 1.

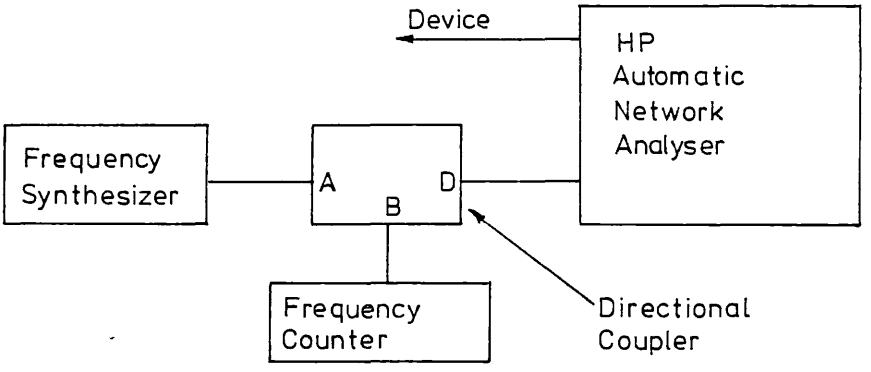

(b) Impedance measurements 2.

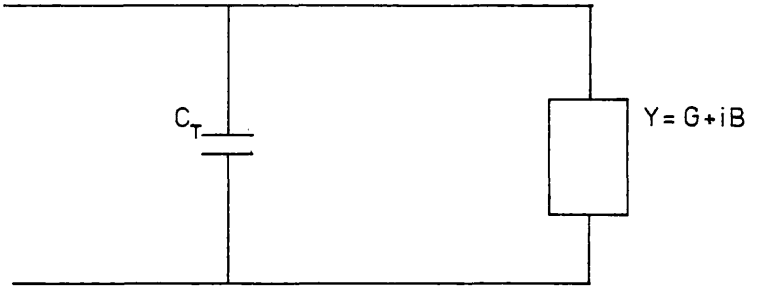

(c) Equivalent circuit of transducer.

We take ϕ to be the average phase angle shift due to piezoelectric coupling taken at the centre frequency f_o and we can then ignore the term R^2 in the denominator of equation (5.7).

$$\tan(\phi) = \frac{-2XR_o}{(R_o^2 + X^2)} \qquad (5.8)$$

The magnitude of the reflection loss x (in dB) is given by :

$$x = 10 \log_{10} (|\rho|^2) \qquad (5.9)$$

From equations (5.8) and (5.9) we can calculate R and X. Thus we have the complex input impedance of our transducer (R-iX). We have an equivalent circuit model for the transducer as shown in Figure 5.9c and we can obtain the complex admittance (G+iB) which is related to the electromechanical coupling factor k^2. From Figure 5.9c we have :

$$\frac{1}{R - iX} = G + iB + i\omega C_T \qquad (5.10)$$

and hence :

$$\frac{R}{X} = \frac{G}{(\omega C_T + B)} \qquad (5.11)$$

Both G and B are functions of ω. We have measured the mid-band conductance (i.e. at the resonant angular frequency ω_o) to reduce the frequency effects of the transducer. Auld [165] gives a relationship between the radiation conductance at resonance $G(\omega_o)$ and $\Delta v/v$:

$$G(\omega_o) = 2.87\ \omega_o C_T N.\ \Delta v/v \qquad (5.12)$$

and
$$B(\omega_o) = 0 \qquad (5.13)$$

where N is the number of finger pairs in the transducer (the finger width is equal to the width of the spaces between fingers). Using the approximation (1.8) ($k^2 \simeq 2\Delta v/v$) we obtain :

$$\frac{R}{X} = \frac{2.87}{2} N k^2 \qquad (5.14)$$

and hence :

$$k^2 = \frac{2}{2.87\ N}\ \frac{R}{X} \qquad (5.15)$$

The results of these measurements are shown in Table 5.4.

The frequency response of device B1 is shown in Figure 5.21 showing an untuned insertion loss of -18.7 dB (-40 dB + 21.3 dB). The corresponding untuned insertion loss for the quartz device Q1 is -28 dB.

(iii) Velocity measurements.

Since the dimensions of the Marconi mask were not known it was necessary to compare the resonant frequencies of the devices on ST cut quartz and on berlinite and then use the well known surface wave velocity for ST cut quartz (3157.8 m/s) to derive the surface wave velocity for berlinite. However, for the devices using the type 2 mask pattern we could calculate the velocity directly from the frequency and wavelength details. The results are compared to the theoretical predictions and other results in Table 5.5 and are discussed in Chapter 6.

Table 5.4 k^2 values from input impedance measurements.

Device	Finger pairs	$k^2(10^{-4})$	Method	Comments
Q2	100	9.8	1	ST cut quartz
Q2	"	9.7	1	" "
Q2	"	9.8	1	" "
B3	"	7.9	1	80° X axis boule crystal 1
B3	"	8.6	1	" " "
B3	"	8.8	1	" " "
B4	50	24.8	2	90° X axis boule crystal 2
B4	"	23.9	2	" " "
B4	"	28.4	2	" " "
B4	"	26.4	2	" " "
B4	"	28.2	2	" " "
B4	"	28.7	2	" " "
Q3	"	15.3	2	ST cut quartz

Table 5.5 Experimental SAW velocities on berlinite.

Device	Velocity (m/s)	Other results (m/s)				Original prediction (m/s)	Theory (Chap 4) (m/s)	Comments
B1	2767 ±2	2743	44	2728	156	2751	2753	80° X axis boule
B2	2766 ±2	"		"		"	"	" "
B3	2769 ±2	"		"		"	"	" "
B4	2743 ±1	2740	119			2736	2738	90° X axis boule

Figure 5.10

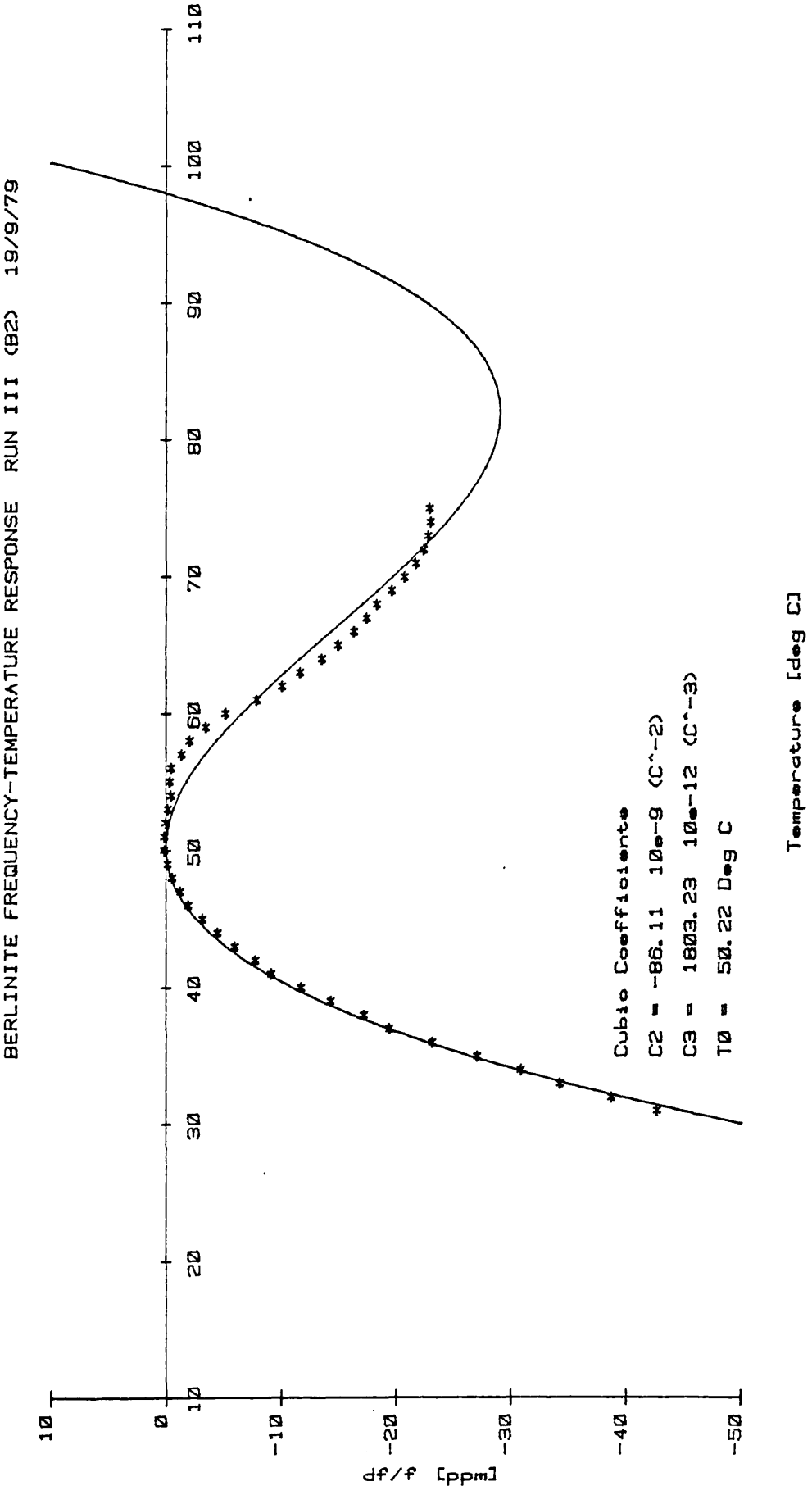
BERLINITE FREQUENCY-TEMPERATURE RESPONSE RUN III (B2) 19/9/79
Cubic Coefficients
C2 = -86.11 10e-9 (C^-2)
C3 = 1803.23 10e-12 (C^-3)
T0 = 50.22 Deg C
df/f [ppm]
Temperature [deg C]
10
0
-10
-20
-30
-40
-50
10
20
30
40
50
60
70
80
90
100
110

Figure 5.11

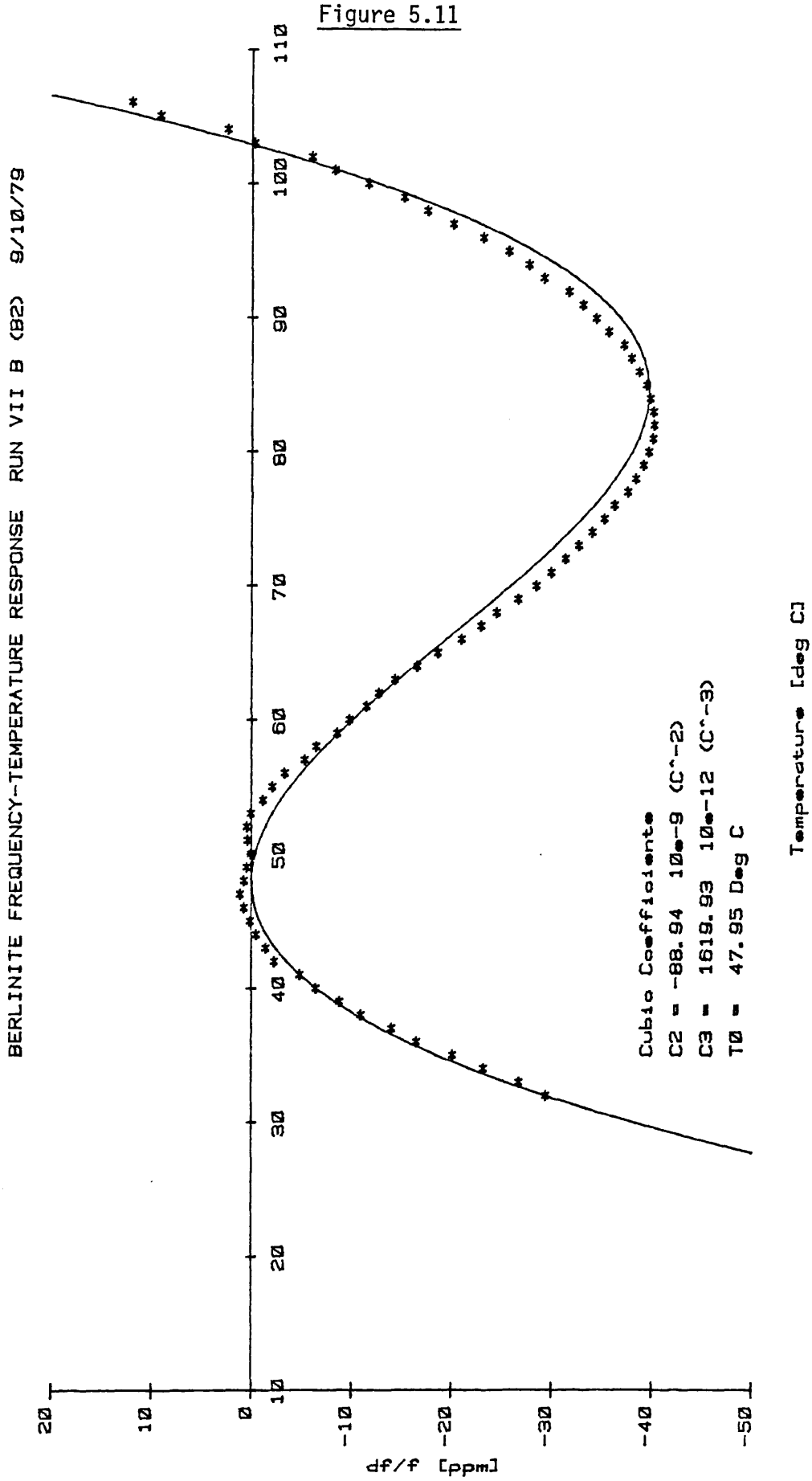
BERLINITE FREQUENCY-TEMPERATURE RESPONSE RUN VII B (B2) 9/10/79
Cubic Coefficients
C2 = -88.94 10e-9 (C^-2)
C3 = 1619.93 10e-12 (C^-3)
T0 = 47.95 Deg C
df/f [ppm]
Temperature [deg C]
20
10
0
-10
-20
-30
-40
-50
10
20
30
40
50
60
70
80
90
100
110

Figure 5.12

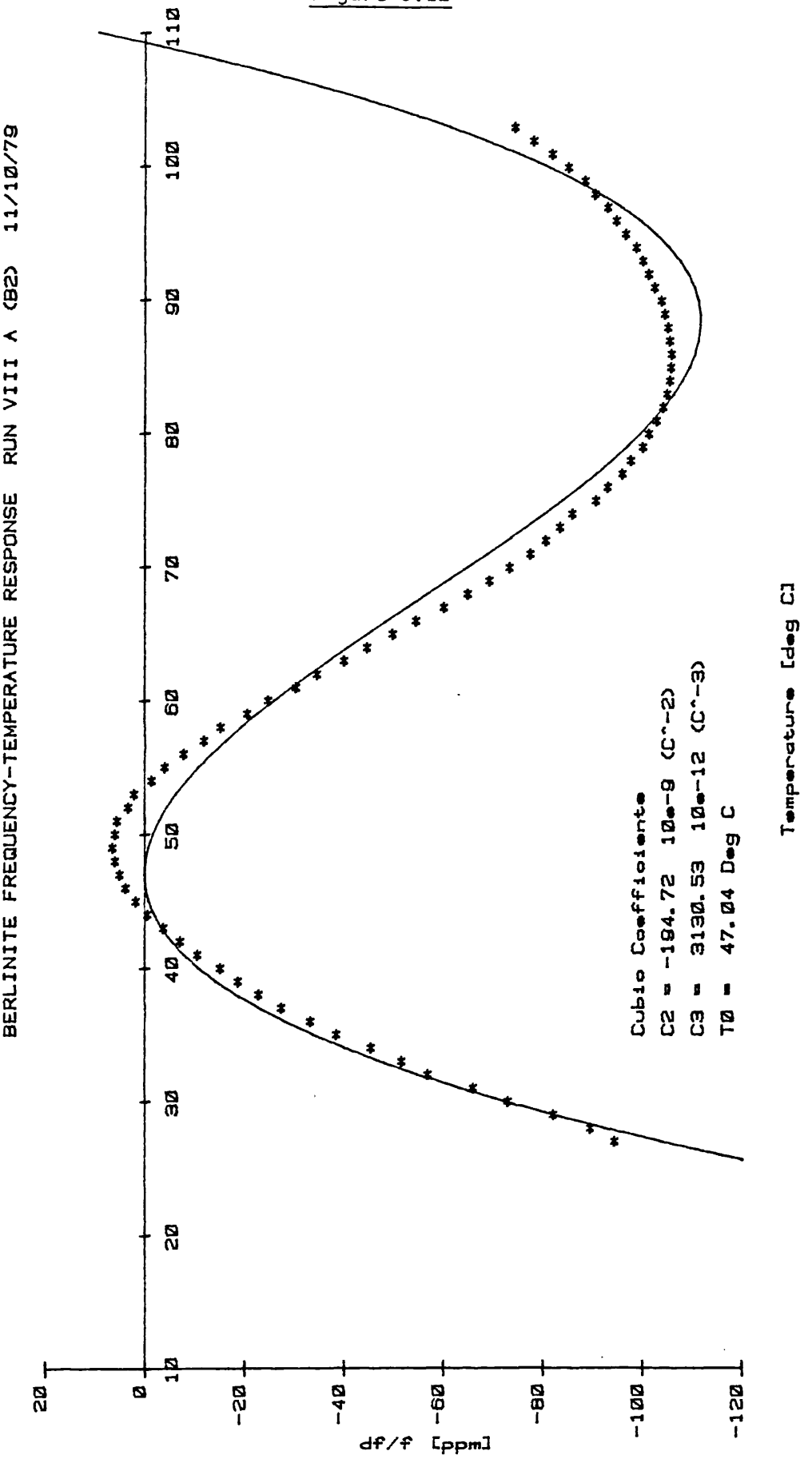
BERLINITE FREQUENCY-TEMPERATURE RESPONSE RUN VIII A (B2) 11/10/79
Cubic Coefficients
C2 = -194.72 10e-9 (C^-2)
C3 = 3130.53 10e-12 (C^-3)
T0 = 47.04 Deg C
df/f [ppm]
Temperature [deg C]
20
0
-20
-40
-60
-80
-100
-120
10
20
30
40
50
60
70
80
90
100
110

Figure 5.13

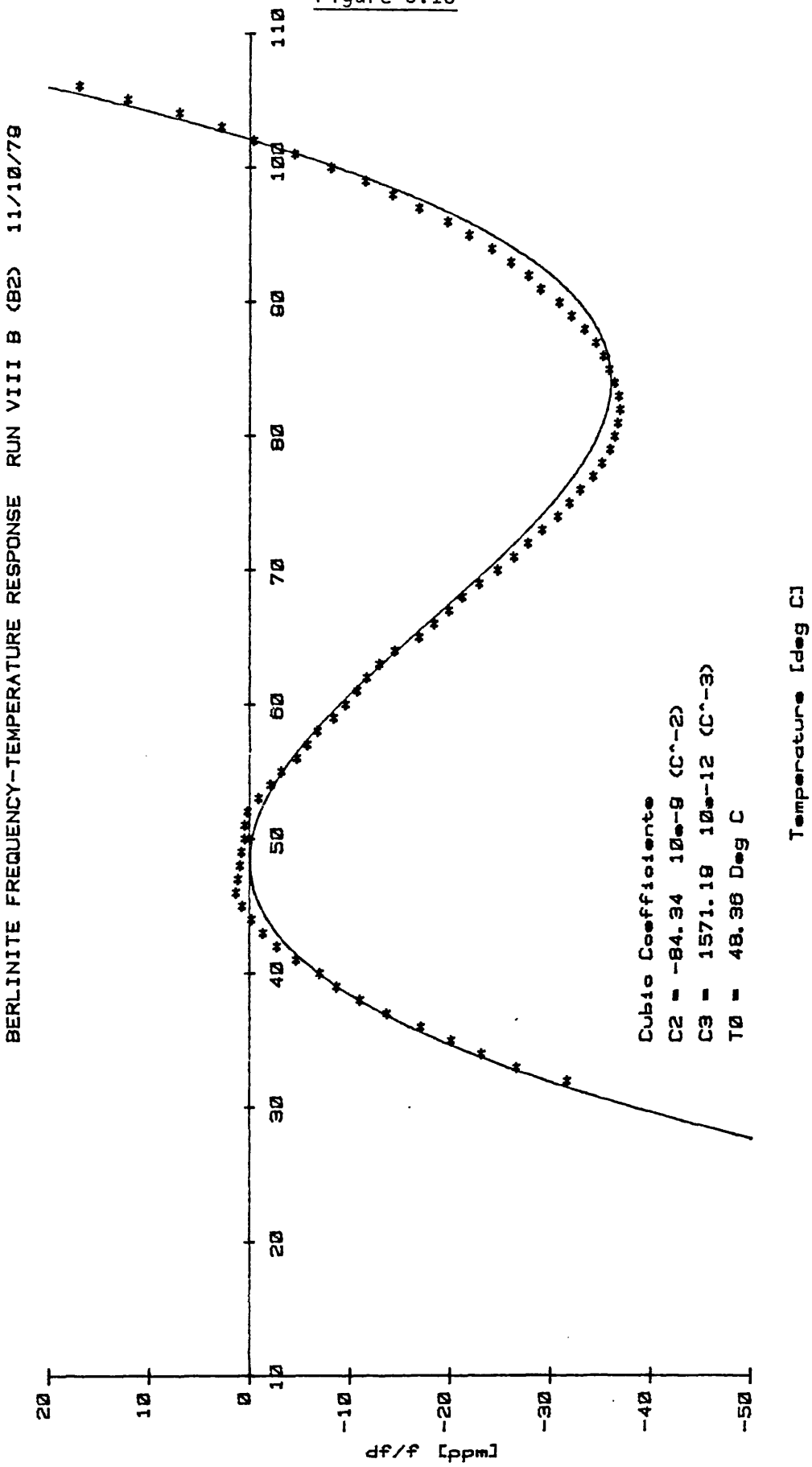
BERLINITE FREQUENCY-TEMPERATURE RESPONSE RUN VIII B (B2) 11/10/78
df/f [ppm]
Temperature [deg C]
20
10
0
-10
-20
-30
-40
-50
10
20
30
40
50
60
70
80
90
100
110
Cubic Coefficients
C2 = -84.34 10e-9 (C^-2)
C3 = 1571.18 10e-12 (C^-3)
T0 = 48.36 Deg C

Figure 5.14

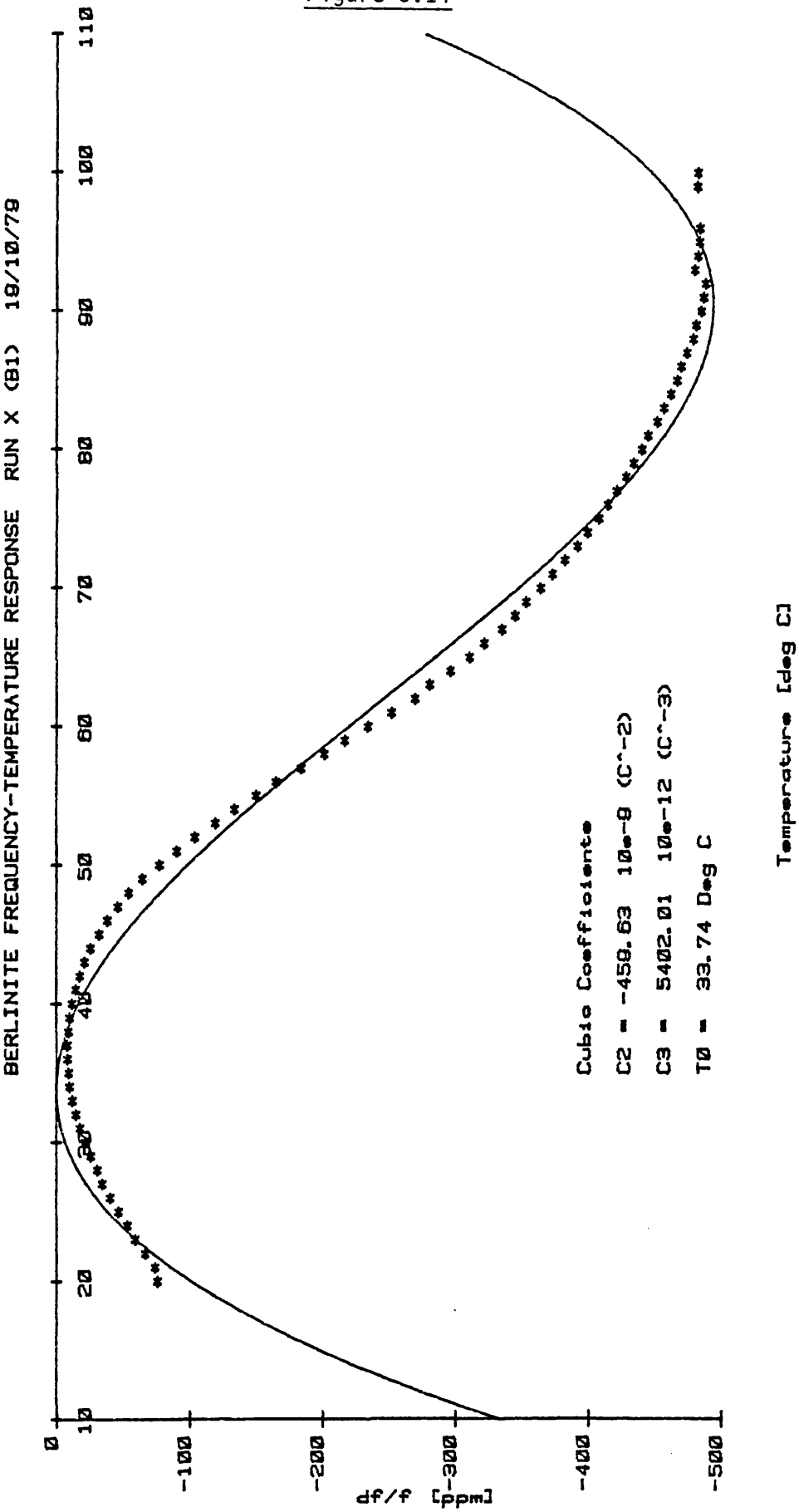
BERLINITE FREQUENCY-TEMPERATURE RESPONSE RUN X (B1) 19/10/79
df/f [ppm]
0
-100
-200
-300
-400
-500
10
20
30
40
50
60
70
80
90
100
110
Temperature [deg C]
Cubic Coefficients
C2 = -458.63 10e-9 (C^-2)
C3 = 5402.01 10e-12 (C^-3)
T0 = 33.74 Deg C

Figure 5.15

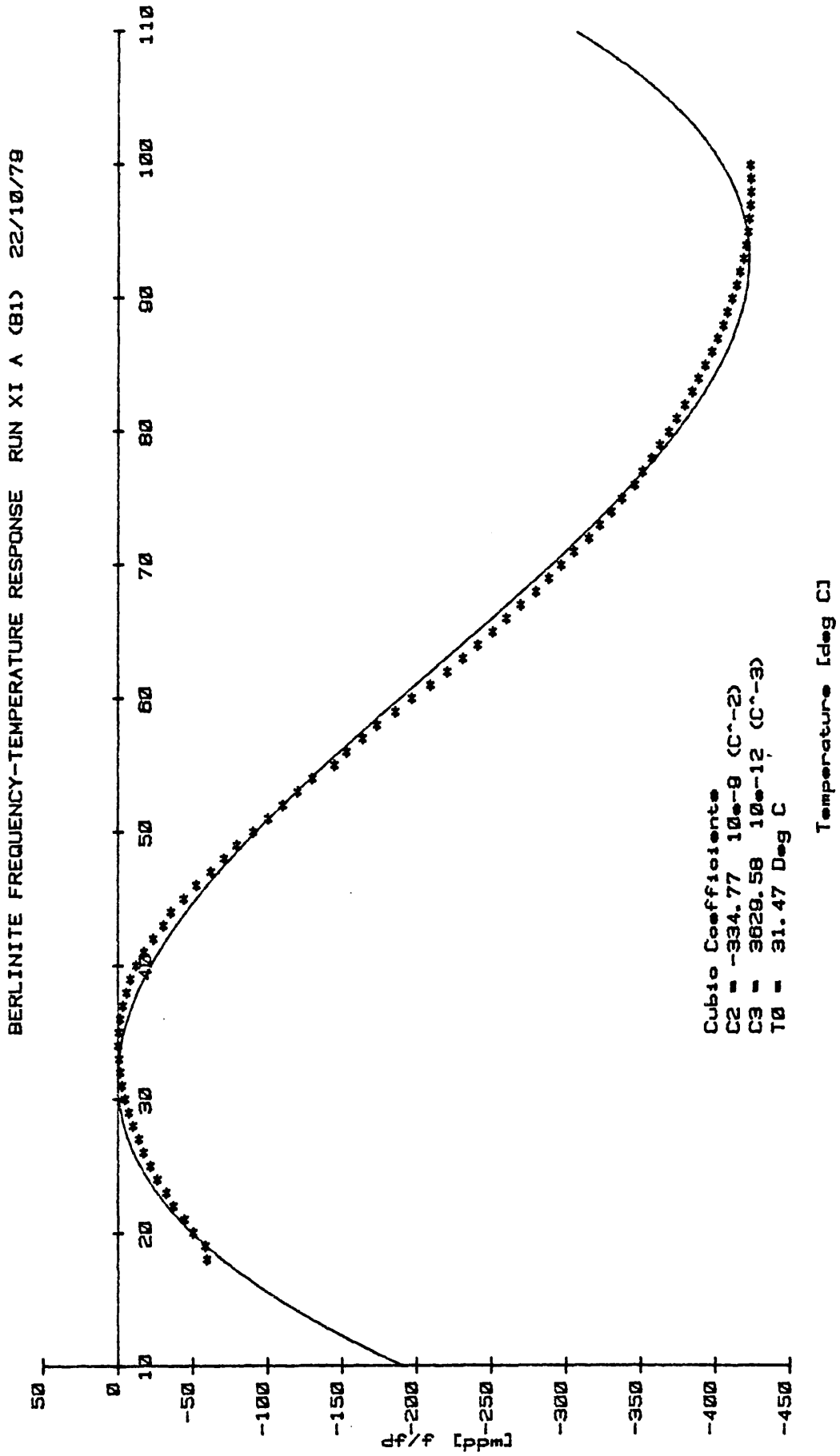
BERLINITE FREQUENCY-TEMPERATURE RESPONSE RUN XI A (B1) 22/10/79
df/f [ppm]
50
0
-50
-100
-150
-200
-250
-300
-350
-400
-450
10
20
30
40
50
60
70
80
90
100
110
Temperature [deg C]
Cubic Coefficients
C2 = -334.77 10e-8 (C^-2)
C3 = 3629.58 10e-12 (C^-3)
T0 = 31.47 Deg C

Figure 5.16

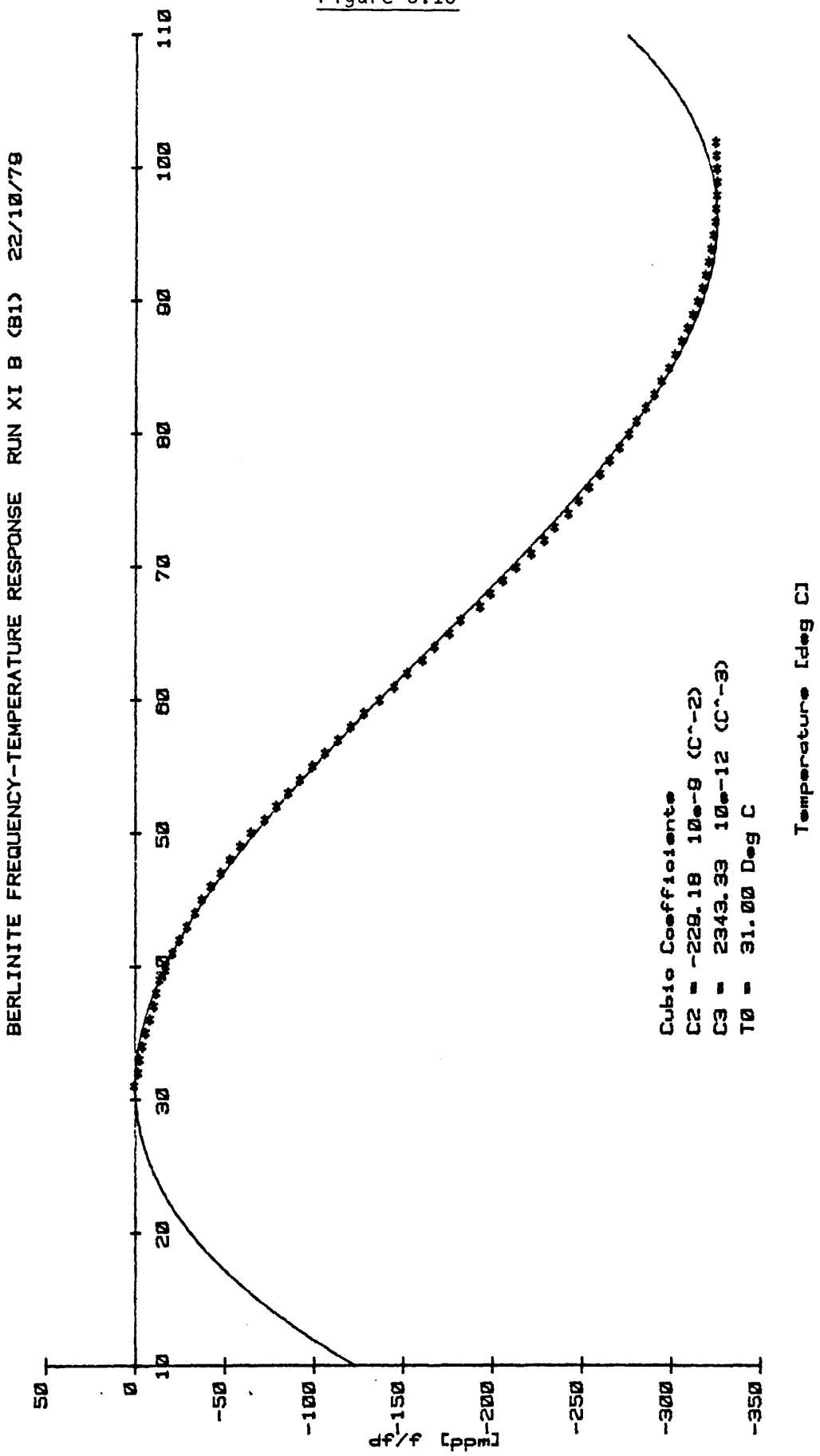
BERLINITE FREQUENCY-TEMPERATURE RESPONSE RUN XI B (B1) 22/10/79
df/f [ppm]
Temperature [deg C]
Cubic Coefficients
C2 = -228.18 10e-9 (C^-2)
C3 = 2343.33 10e-12 (C^-3)
T0 = 31.00 Deg C

Figure 5.17

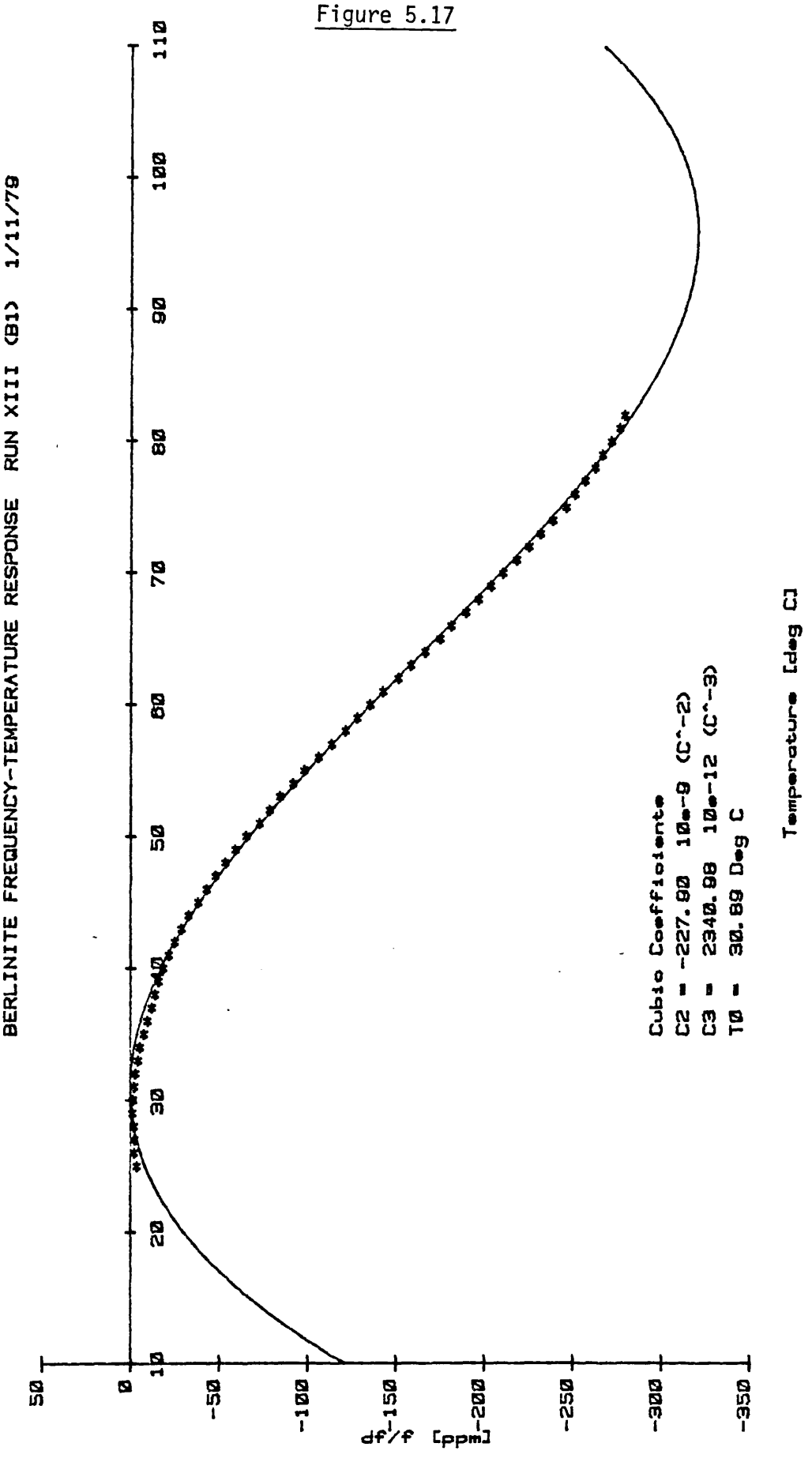
BERLINITE FREQUENCY-TEMPERATURE RESPONSE RUN XIII (B1) 1/11/79
Cubic Coefficients
C2 = -227.80 10e-9 (C^-2)
C3 = 2340.98 10e-12 (C^-3)
T0 = 30.89 Deg C
df/f [ppm]
Temperature [deg C]
50
0
-50
-100
-150
-200
-250
-300
-350
10
20
30
40
50
60
70
80
90
100
110

Figure 5.18

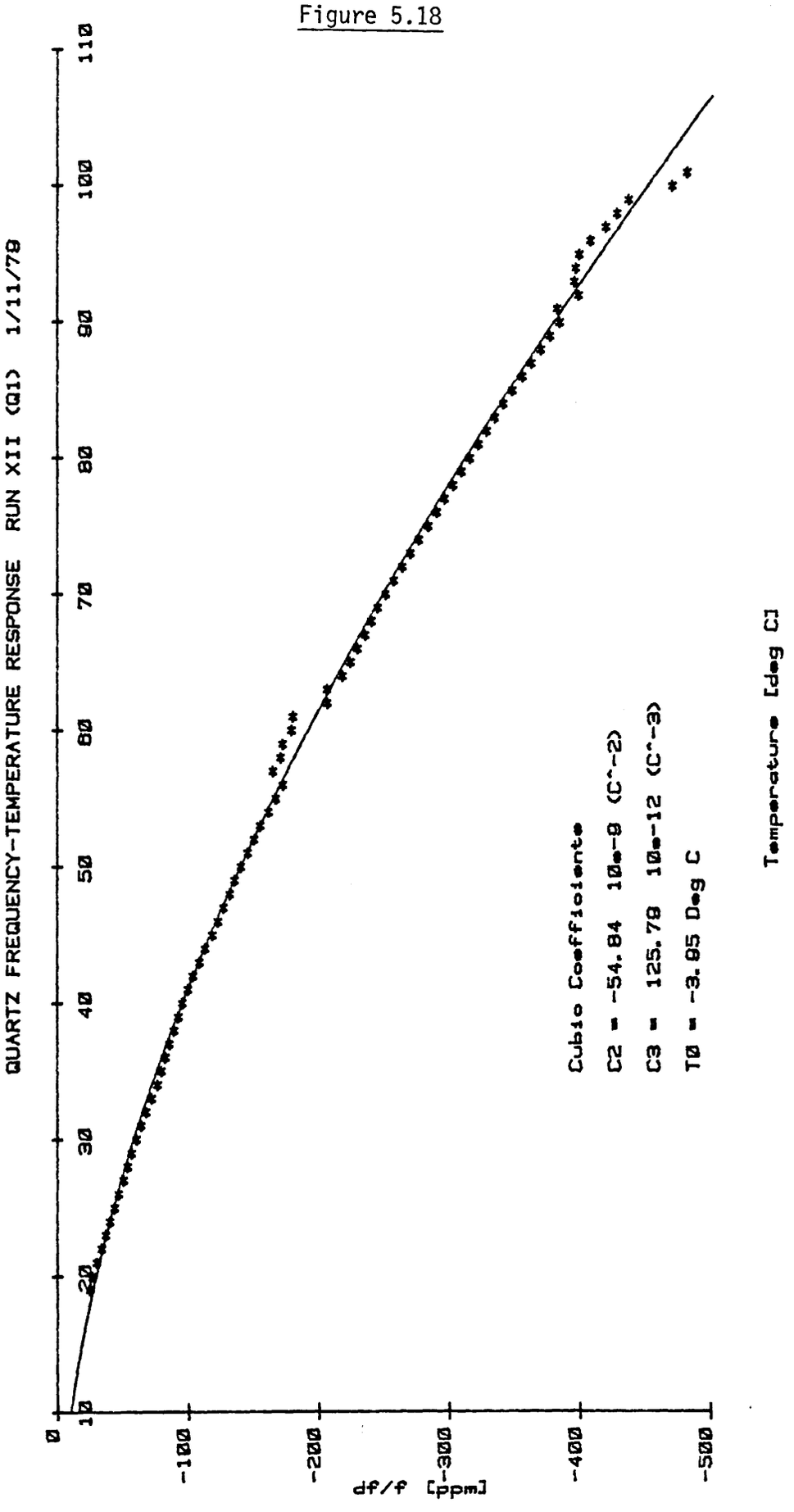
QUARTZ FREQUENCY-TEMPERATURE RESPONSE RUN XII (Q1) 1/11/79
0
10
20
30
40
50
60
70
80
90
100
110
-100
-200
-300
-400
-500
df/f [ppm]
Temperature [deg C]
Cubic Coefficients
C2 = -54.84 10e-9 (C^-2)
C3 = 125.79 10e-12 (C^-3)
T0 = -3.85 Deg C

Figure 5.19

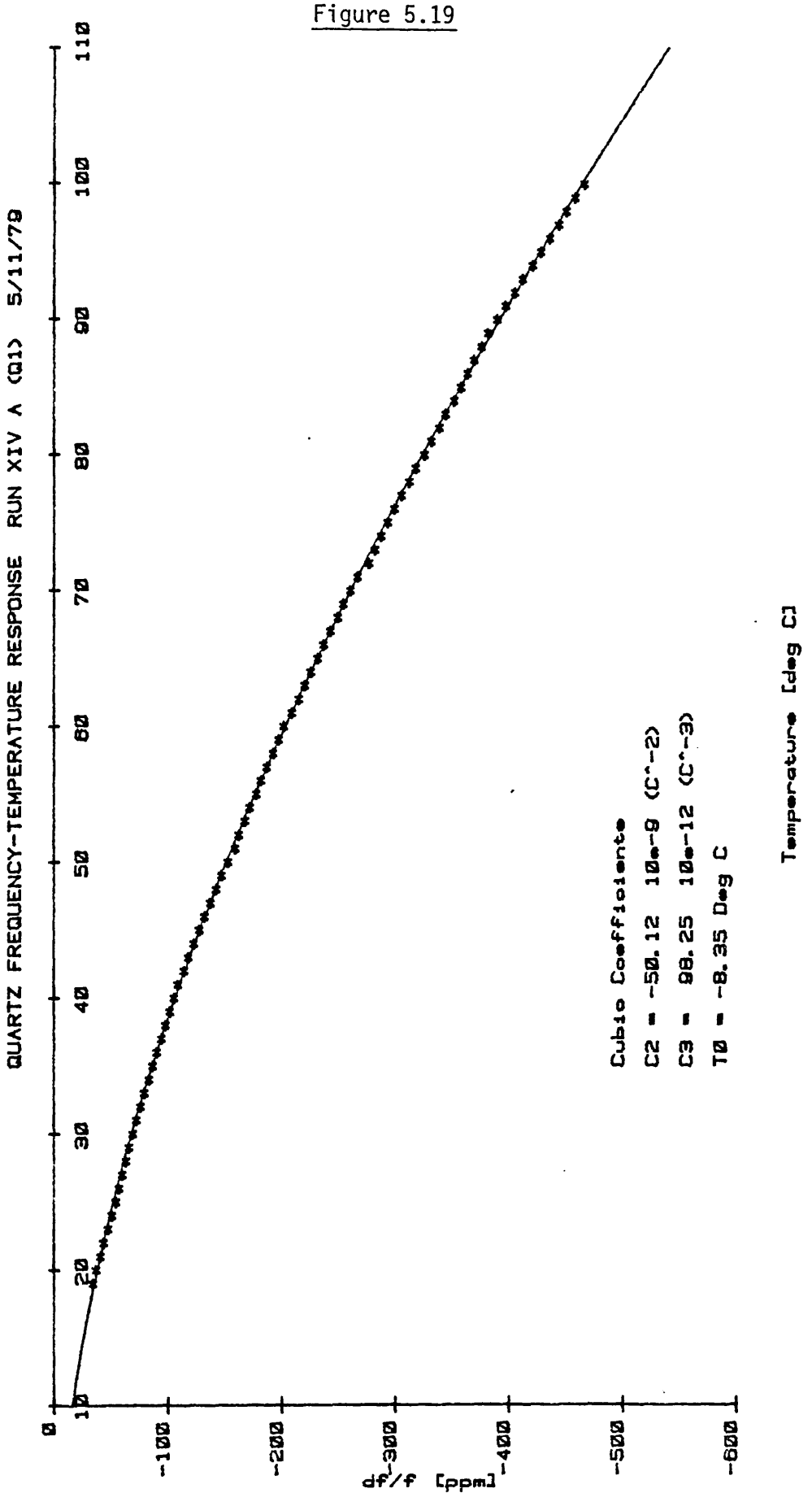
QUARTZ FREQUENCY-TEMPERATURE RESPONSE RUN XIV A (Q1) 5/11/79
Cubic Coefficients
C2 = -50.12 10e-9 (C^-2)
C3 = 88.25 10e-12 (C^-3)
T0 = -8.35 Deg C
df/f [ppm]
Temperature [deg C]
0
-100
-200
-300
-400
-500
-600
10
20
30
40
50
60
70
80
90
100
110

Figure 5.20

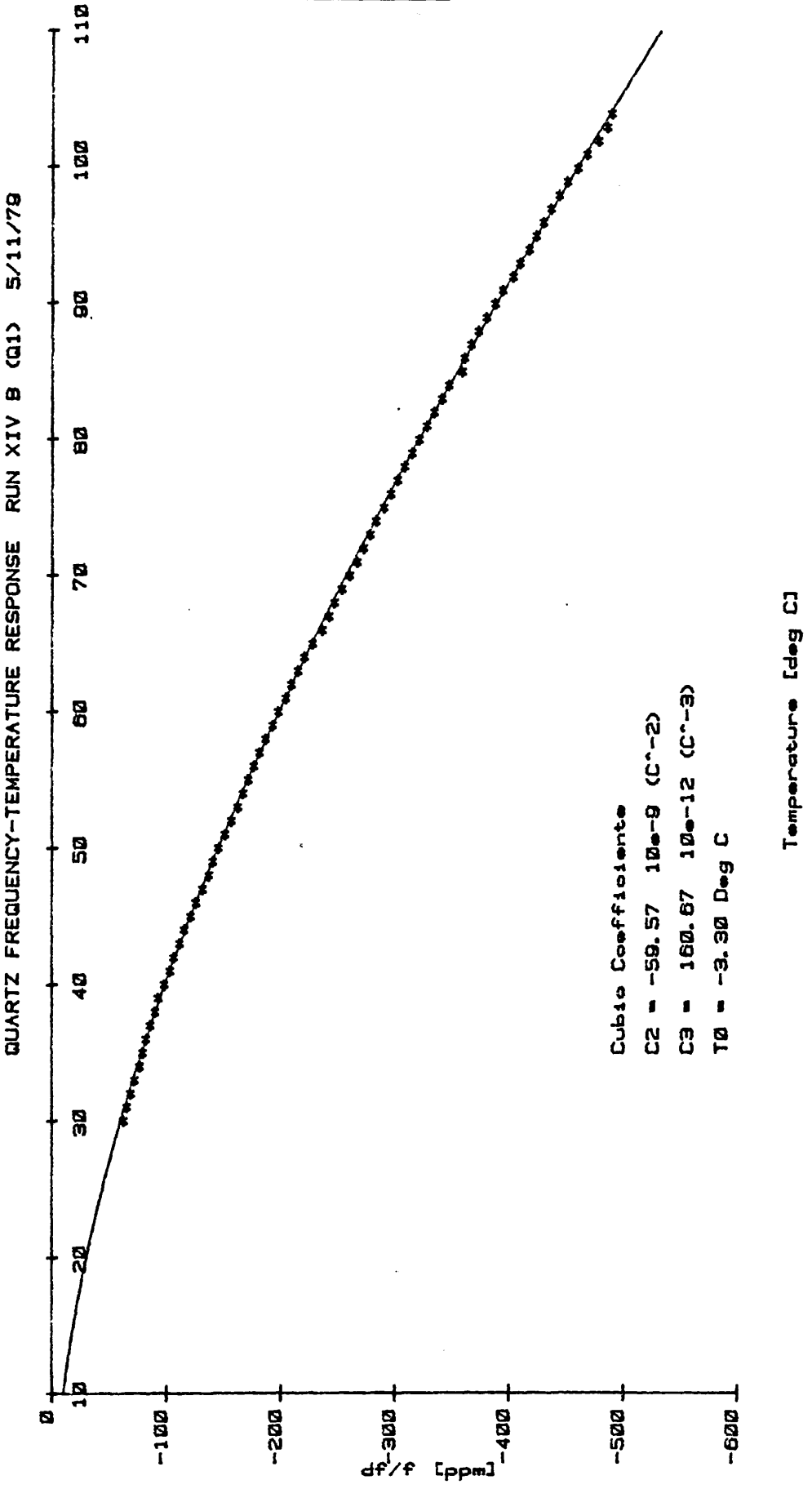
QUARTZ FREQUENCY-TEMPERATURE RESPONSE RUN XIV B (Q1) 5/11/79
0
10
20
30
40
50
60
70
80
90
100
110
-100
-200
-300
-400
-500
-600
df/f [ppm]
Temperature [deg C]
Cubic Coefficients
C2 = -59.57 10e-9 (C^-2)
C3 = 160.67 10e-12 (C^-3)
T0 = -3.30 Deg C

Figure 5.21

FREQUENCY RESPONSE DEVICE B1
(80.4° X AXIS BOULE BERLINITE)

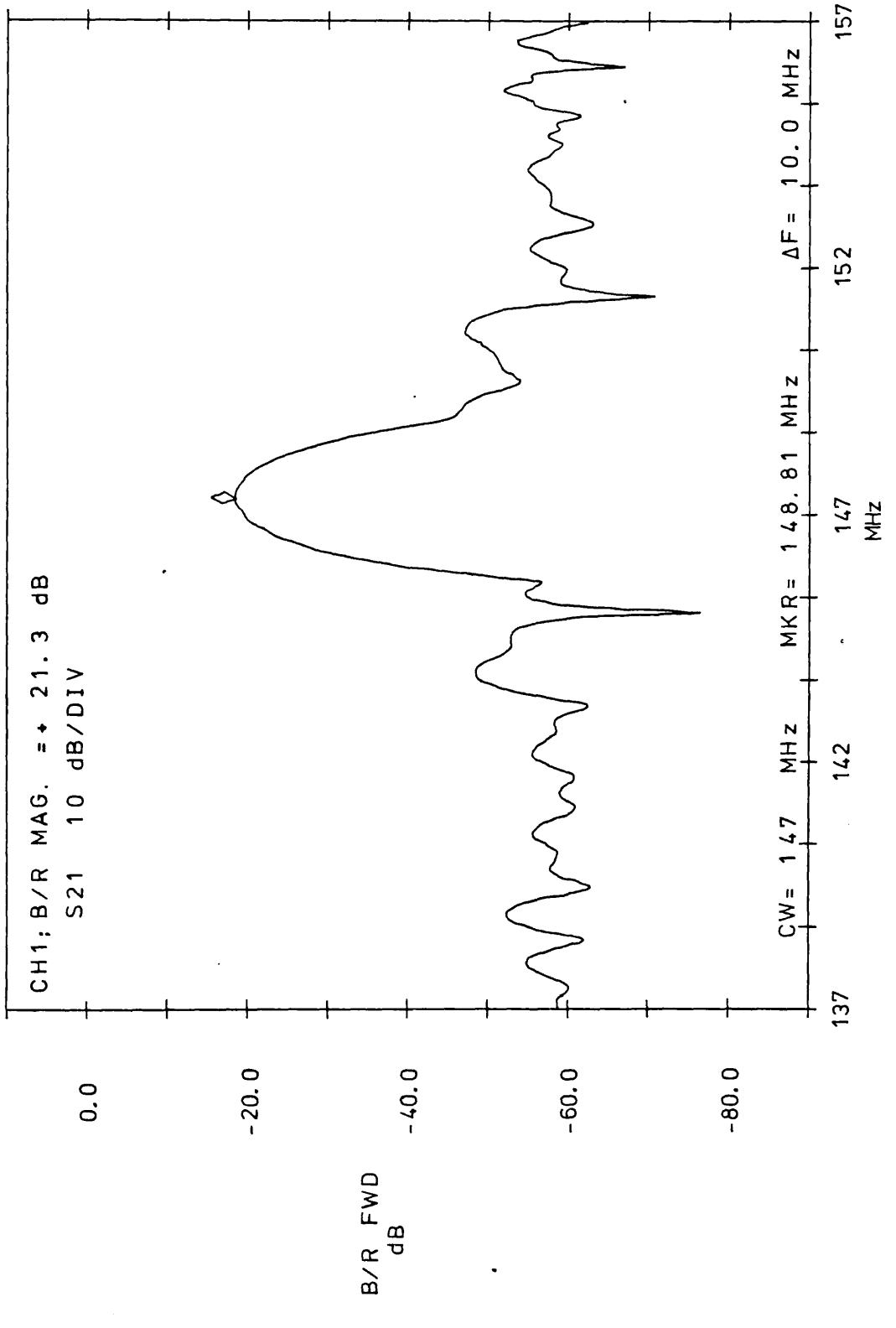

Chapter 6. Discussion and conclusions.

Section 1. Computer predictions.

The computer program described in Chapter 4 has been tested extensively and successfully against published results for quartz [62]. The program does not calculate pseudosurface wave solutions, but can give an indication of when they arise from the occurence of non zero power flow into the bulk of the crystal for orientations that fail to yield a SAW solution.

The differences between the results produced by Carr and O'Connell [42,43,44,49,151] and Jhunjhunwala et al. [27,152] are difficult to explain. We have tried to check their results using all the constants and temperature derivatives that can be obtained from Chang and Barsch [128] and also by omiting the temperature derivatives of the piezoelectric and dielectric constants. We still obtain differences of between 3 and 5 ppm/°C (at 25°C) for some of the orientations quoted (see Table 4.2). If we allow a temperature coefficient of delay of better than about ±2 ppm/°C, then, allowing for the quoted accuracies of the orientations (e.g. ±0.1°, or ±1°), most of the orientations shown in Table 4.2 are temperature compensated. However, the cuts predicted by Carr and O'Connell [151] have a persistent difference of about -3 ppm/°C which we cannot explain from the data that they claim to be using. There is also one orientation from Jhunjhunwala et al. [27,152] which did not yield a SAW solution at all for our calculations.

The results from Detaint et al. [119] were quite good, although the elastic constant data that they used is open to criticism (see Section 4). Most of their results are within ±1 ppm/°C of temperature compensation at 25°C.

For some orientations the rate of change of the temperature coefficient of delay with respect to orientation is large, (e.g. for the Z cut (0,0,24) orientation) and to the nearest 1° of rotation the orientations are temperature compensated, but have very large power flow angles. Thus any slight misorientation would greatly alter the properties of the cut, both as regards the power flow direction and the temperature coefficient of delay.

The orientations that have been investigated are the 9 standard singly rotated crystallographic cuts (see Appendix 2) , which includes one set of orientations for which the electromechanical

coupling is identically zero for the surface wave (the X axis cylinder orientations). We have also investigated a different doubly rotated plane of cuts to that investigated by Carr and O'Connell [151]. The singly rotated cuts would be the easiest to fabricate devices upon, although some of the doubly rotated orientations could be fabricated by incorporating one of the angles of rotation into the transducer pattern.

Of the orientations considered the most promising would appear to be the singly rotated X axis boule cuts analogous to the ST cut of quartz. The angle of rotation of this cut would appear to be somewhere between 70° and 95°. This cut has the advantage of high electromechanical coupling together with a power flow angle of zero. The actual angle chosen will depend upon the values of the elastic, piezoelectric, dielectric and lattice constants used in the calculations. It can be seen that there is quite a wide variation in the angles predicted :

71.8°	rotation	This work
80.4°	"	[151]
90°	"	[119]
92.75°	"	[27,152]

As improved measurements of the constants of berlinite become available we will be able to refine the predictions of this temperature compensated orientation.

The doubly rotated cuts which are both temperature compensated and have a zero power flow angle do not offer a sufficient improvement in electromechanical coupling to offset the increased difficulty of transducer orientation.

Section 2. Material parameters.

The quality of the crystals that have been used to determine the basic material parameters of berlinite has been very variable. Some of the crystals that have been used have been in existance for quite a long time and were grown before the growth techniques were completely reliable. As a result almost all the crystals appear to suffer from small size, twinning, impurities and defects. As the growth methods become more established the quality of the material should improve and more reliable measurements of the basic parameters of berlinite crystals may be made available. The poor quality of these

early crystals is evident from the lack of consistency between the measurements of the elastic constants made by Chang and Barsch [128] on Stanley's crystal and those made by Mason [140], together with the large differences between the theoretical predictions and the experimental results for surface waves. There are also differences between theoretical predictions and experimental results for bulk waves (C.D. Emin [unpublished]).

Section 3. The α-β transition, lattice parameters and density.

The α-β transition in berlinite is generally accepted to occur between 580°C and 585°C. This leads us to question the validity of the measurements that we have made (see Chapter 3) since our result indicates a transition temperature slightly over 600°C. We are not completely happy with the temperature calibration of the X ray powder photograph that we used. This would affect the measurements of the lattice parameters a and c at elevated temperatures by altering the horizontal temperature scale in Figure 3.1 and could give closer agreement with the results of Chang and Barsch [128].

The room temperature values of a and c that we measured (Table 3.2) are in good agreement with some of the more recent results from other workers. Again the differences in the results are probably due to impurities in the crystals. The more recent results seem to be more consistent for a range of crystal sources.

The density measurements by various authors give reasonably good agreement, again from a variety of crystal sources, to within about 4%. We have not measured the density, so we cannot compare the GEC grown crystals that we have used.

Section 4. Elastic constants.

As described in Chapter 3, we have fitted a cubic temperature dependence curve to the experimental results for the elastic constants obtained by Chang and Barsch [128]. We feel that this is an improvement on the straight line fit that Chang and Barsch suggested, although there are often large experimental errors quoted. The elastic constants were measured over a temperature range from -220°C to +25°C. This range is lower than the temperature regions that SAW devices are normally used at. Thus we have to have to work at the extreme top end of the temperature range measured and extrapolate to the higher temperatures of interest.

There are large differences between the elastic constants measured by Chang and Barsch [128] and those measured by Mason [140], which again suggests very variable crystal quality. The measurements made by Chang and Barsch are more recent and more comprehensive and we feel that they probably describe a better quality crystal.

The least squares cubic fits of temperature dependencies made by Detaint et al. [119] seem to bear little resemblance to the experimental results of Chang and Barsch [128] outside a small temperature range near room temperature (see Figures 3.3 to 3.9). For only two of the elastic constants (c_{44} and c_{12} ($=c_{11}-2c_{66}$)) do their cubic fits remain within the experimental errors quoted by Chang and Barsch [128]. We can place little reliance upon the theoretical results calculated using their temperature derivatives, although their first order temperature coefficients are generally similar to those from Chang and Barsch and our own calculations. This probably explains why their SAW predictions are not wildly different from those of other workers (see Section 1 and Chapter 4).

Section 5. Piezoelectric and dielectric constants.

Chang and Barsch [128] measured the piezoelectric constants of berlinite from bulk wave resonator measurements assuming that the dielectric constants ε_{11} and ε_{33} were equal and they used the value originally measured by Mason [140] for ε_{11} ($\varepsilon_{11} = 5.88\varepsilon_o$). Since Mason only measured ε_{11} all the results that followed are based upon that measurement and upon the validity of assuming that the two independent dielectric constants are equal. Since the surface acoustic wave electromechanical coupling is a function of both the piezoelectric and dielectric constants, it will be affected by any error arising in the calculation of the e_{ij} or the ε_{ij}. This could be part of the reason for the large differences between the theoretical predictions and the experimental measurements of $\Delta v/v$ and k^2.

The temperature coefficients of the dielectric constants of quartz are also used by Chang and Barsch [128] to calculate the temperature variations of both the piezoelectric and dielectric constants of berlinite. This makes the validity of these temperature coefficients doubtful. The temperature derivatives of e_{ij} and ε_{ij} make only a small alteration in the predicted temperature coefficients of delay. There is approximately 5 ppm/°C difference between using these coefficients and not using them to calculate the temperature coefficients

of delay for the orientations listed in Table 4.2 (see columns TCD1 and TCD2).

Section 6. Experimental measurements of SAW on berlinite.

The most striking aspect of the experimental results presented in Chapter 5 is the almost cubic frequency-temperature response of the SAW devices that were constructed on berlinite. The response shows temperature compensation as predicted, although at higher temperatures than the intended 25°C, together with a minimum in the frequency-temperature curve at a higher temperature. These results are the first observations of this effect in berlinite. It has not been observed by any of the other workers who measured the frequency-temperature response (or delay-temperature response) over more restricted temperature ranges as shown in Table 6.1. All workers have used a similar type of experimental arrangement to that which we have used (i.e. oscillator loops using surface wave delay lines).

It can be seen from Table 6.1 that the turnover temperatures T_o vary over a range from 14°C to 50°C and over a range of orientations between 80° and 92.75° rotated X axis boule cuts. This is shown graphically in Figure 6.1.

We would expect a certain amount of variation in T_o due to the differing orientations used [11] and the results show a slight change in T_o of about -1½°C per degree of X axis boule rotation [156]. However individual cuts give varying results for T_o which is probably due to the different quality crystals used for the experiments. All the results except that of Carr and O'Connell [46,58] and those of Detaint et al. [119] give a turnover temperature higher than 25°C which suggests that the temperature compensated orientation for 25°C lies at about 90° X axis boule (i.e. the Y cut).

It would appear that a cut very close to the 90° X axis boule orientation (or Y cut) with propagation along the X axis is the most useful temperature compensated orientation suggested by these experimental results.

Table 6.1 Temperature ranges, turnover temperatures and parabolic temperature coefficients from experimental results.

Cut	Temperature range (°C) T(low)	T(high)	Turnover temperature 1 (°C)	Turnover temperature 2 (°C)	$T_f^{(2)}$ ($°C^{-2}$)	reference
80.4°	0	48	25.4	-	-264×10^{-9}	44,58
92.75°	10	58	32	-	-	155
87.25°	12	52	32	-	-	156
85°	22	48	38	-	-	156
80°	22	52	44	-	-	156
90°	-20	40	14-24	-	-210×10^{-9}	119
92.75°	15	55	32(39° on graph)	-	-	154
80.4°	30	75	50	74	-86×10^{-9}	Fig 5.10
"	31	106	48	80	-88×10^{-9}	Fig 5.11
"	28	104	49	84	-195×10^{-9}	Fig 5.12
"	31	106	48	81	-84×10^{-9}	Fig 5.13
"	19	102	38	100	-460×10^{-9}	Fig 5.14
"	18	100	34	99	-335×10^{-9}	Fig 5.15
"	31	102	30	100	-229×10^{-9}	Fig 5.16
"	25	80	30	-	-228×10^{-9}	Fig 5.17

Figure 6.1

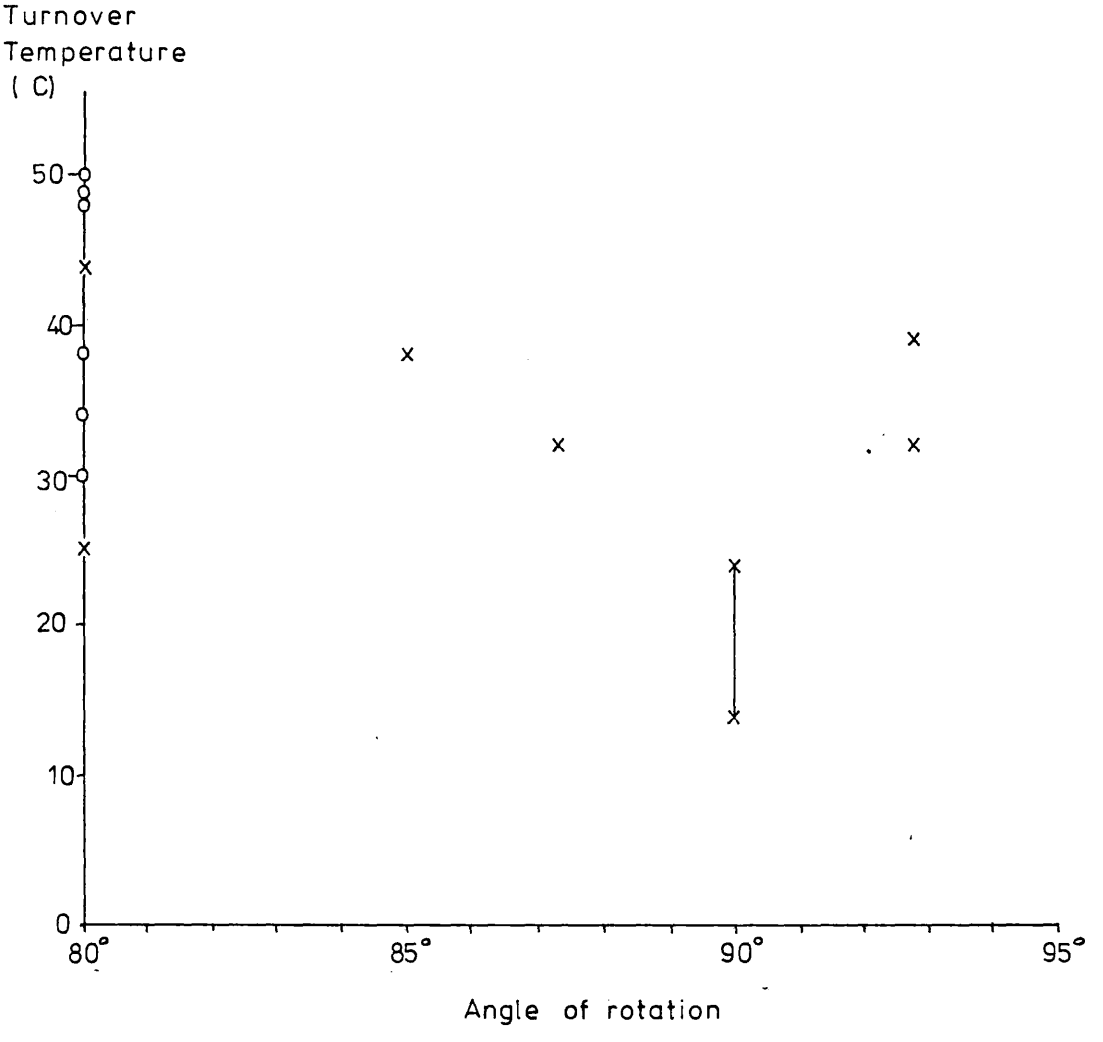

Temperature compensated cuts on Berlinite

o - our results
x - other workers

Section 7. Parabolic coefficients and cubic responses.

The parabolic temperature coefficients of delay obtained from the experimental results show a value which is about an order of magnitude larger than that for ST cut quartz (e.g. $30x10^{-9}\ °C^{-2}$ for ST cut quartz against around $300x10^{-9}\ °C^{-2}$ for 'ST' cut berlinite). However this seems to depend upon the rate of change of temperature. If we compare Figure 5.12(Run VIIIa (heating)) where the temperature sweep took 40 minutes with Figure 5.13(Run VIIIb (cooling)) where the temperature sweep took 170 minutes, we can see that the parabolic coefficients differ by a factor of two, with the slower cooling curve having a flatter frequency-temperature response. Ballato [159] has described a similar effect in bulk wave quartz oscillators where rapid heating increases the frequency deviation from a 'static' frequency-temperature curve, whereas slow cooling tends to decrease the frequency deviation. Thus the 'static' frequency-temperature response lies somewhere between the two results. This suggests a very approximate parabolic temperature coefficient of delay of $150x10^{-9}\ °C^{-2}$ for device B1 and $280x10^{-9}\ °C^{-2}$ for device B2.

Cubic frequency-temperature responses for SAWs have been noticed on quartz by Browning and Lewis [31] for their theoretical prediction of a 46° rotated X cut which showed an AT cut quartz like frequency-temperature behaviour. Shimizu et al. [23] have observed a cubic response on quartz which is caused by heavy metallisation. They report a change from a parabolic response to a cubic response and then to a response with a non zero first order temperature coefficient as the mass of the transducers increases. The metallisation also lowers the turnover temperature T_o. This has been noticed by other authors [160,161]. If this is happening with the berlinite samples then it implies much higher turnover temperatures (i.e. over 50°C).

Section 8. Electromechanical coupling.

There is very good agreement between all authors on the value of the electromechanical coupling coefficient k^2 of about 0.3%. This is much lower than predicted by the theoretical calculations. As mentioned earlier the theoretical calculations are based upon doubtful values of the dielectric constants and upon piezoelectric constants having large quoted errors. When improved measurements of these basic constants are available then new theoretical results may be more

accurate. Present theoretical results show trends and areas of interest for further study when the accuracy of the basic constants and their temperature derivatives is improved.

The magnitude of k^2 for berlinite is about twice that for ST cut quartz and hence shows that berlinite is a useful material for temperature compensated devices.

Section 9. General conclusions.

At the moment the samples of berlinite that are available are very variable in their quality and suffer from twinning and other defects. The crystals are not very large and much effort is being put into growing larger and better quality crystals. The variations in the quality of the crystals used for SAW measurements is apparent from the differing results obtained both by us and other workers and even within individual crystal samples. At present the most promising orientation would appear to be the 90° X axis boule orientation (or Y cut) with propagation along the X axis. This should have an electromechanical coupling coefficient of about 0.3% (about twice that of ST cut quartz). It should be temperature compensated at 25°C and have a surface acoustic wave velocity of about 2740 m/s.

Acknowledgements.

I would like to thank Dr. M.J. Lea of Bedford College and Dr. R.C. Peach of the GEC Hirst Research Centre for their help and supervision of the work described in this thesis and for their comments upon the manuscript.

I would also like to thank Drs. R.J. Biggs and C.D. Emin of the GEC Hirst Research Centre for helpful discussions on the surface wave and bulk wave work carried out at GEC and Dr. S. Gratz of Marconi for the loan of the Marconi transducer mask.

I would also like to thank the Science Research Council and the GEC Hirst Research Centre for the award of a Co-operative Award in Science and Engineering Studentship to carry out this work.

References.

1. Proc. London Maths. Soc. 17 4-11 (1885) J.W. Strutt (Lord Rayleigh).
2. Appl. Phys. Lett. 20 367-9 (1972) M.B. Schultz, J.H. Matsinger.
3. IEEE Sonics & Ultrasonics. SU15 209-17 (1968) J.J. Campbell, W.R. Jones.
4. Proc. IEEE 64 581-95 (1976) A.J. Slobodnik.
5. J. Appl. Phys. 41 2755-65 (1970) M.B. Schultz et al.
6. IEEE Sonics & Ultrasonics. SU20 240-51 (1973) T.L. Szabo, A.J. Slobodnik.
7. IEEE Ultrasonics Symp. 1979 612-22 (1979) M.F. Lewis.
8. Am. Ceramics Soc. Bull. 53 821-9 (1974) R.E. Newnham.
9. Proc. IRE 50 1812-22 (1962) R. Bechmann et al.
10. J. Appl. Phys. 42 476-7 (1971) M.F. Lewis et al.
11. Proc. IRE 58 1361-2 (1970) M.B. Schultz, M.G. Holland.
12. IEEE Sonics & Ultrasonics. SU22 46-50 (1975) J.F. Dias et al.
13. Bell Systems Tech. J. 19 74-93 (1940) W.P. Mason.
14. Bell Systems Tech. J. 30 366-80 (1951) W.P. Mason.
15. Appl. Phys. Lett. 31 315-7 (1977) D. Hauden et al.
16. IEEE Ultrasonics Symp. 1976 240-2 (1976) P. Hartemann.
17. Onde Electronique 56 189-96 (1976) J. Henaff.
18. Proc. 32nd Ann. Freq. Contr. Symp. 77-86 (1978) D. Hauden et al.
19. Appl. Phys. Lett. 34 817-9 (1979) B.K. Sinha, H.F. Tiersten.

20. J. Appl. Phys. 51 4659-65 (1980) B.K. Sinha, H.F. Tiersten.

21. Revue de Phys. Appliquée 12 1775-88 (1977) M. Feldmann, J. Henaff.

22. IEEE Ultrasonics Symp. 1979 632-6 (1979) C.O. Newton.

23. Trans. IECE of Japan E61 94-5 (1978) Y. Shimizu et al.

24. IEEE Ultrasonics Symp. 1979 595-7 (1979) P.H. Carr, R.M. O'Connell.

25. Appl. Phys. Lett. 35 217-9 (1979) R.M. O'Connell.

26. IEEE Ultrasonics Symp. 1978 662-6 (1978) B.K. Sinha, H.F. Tiersten.

27. J. Appl. Phys. 48 887-92 (1977) A. Jhunjhunwala et al.

28. J. Appl. Phys. 50 2732-9 (1979) B.K. Sinha, H.F. Tiersten.

29. Phys. Rev. 110 1060-1 (1958) R. Bechmann.

30. Phys. Rev. 109 1467-73 (1958) I. Koga et al.

31. Proc. 32nd Ann. Freq. Contr. Symp. 87-94 (1978) I. Browning, M. Lewis.

32. IEEE Ultrasonics Symp. 1979 797-801 (1979) T.J. Lukasek, A. Ballato.

33. IEEE Ultrasonics Symp. 1979 627-31 (1979) D.F. Williams, F.Y. Cho.

34. Proc 33rd Ann. Freq. Contr. Symp. 402-3 (1979) R.M. O'Connell.

35. Proc. IEEE 64 568-9 (1976) V.B. Jipson et al.

36. J. Appl. Phys. 41 2307-11 (1970) Y. Ohmachi, N. Uchida.

37. Ultrasonics 8 84-7 (1970) H. Schweppe.

38. J. Electronic Materials 4 67-75 (1975) T.J. Isaacs et al.

39. Electronics Lett. 12 683-4 (1976) A. Jhunjhunwala et al.

40. Electronics Lett. 13 300-2 (1977) J. Henaff, M Feldmann.

41. IEEE Ultrasonics Symp. 1977 696-700 (1977) J. Henaff, M Feldmann.

42. Optical Engineering 16 440-5 (1977) R.M. O'Connell, P.H. Carr.

43. Proc. 30th Ann. Freq. Contr. Symp. 129-31 (1976) P.H. Carr, R.M. O'Connell.

44. Proc. 32nd Ann. Freq. Contr. Symp. 189-95 (1978) R.M. O'Connell, P.H. Carr.

45. J. Electronics Materials 5 13-22 (1976) T.J. Isaacs, R.W. Weinert.

46. Electronics Lett. 13 661-2 (1977) J. Henaff, M Feldmann.

47. IEEE Ultrasonics Symp. 1974 286-90 (1974) P.H. Carr.

48. Air Force Cambridge Research Labs. AFCRL-TR-75-0609 G.R. Barsch, K.E. Spear.

49. Proc 31st Ann. Freq. Contr. Symp. 182-6 (1977) R.M. O'Connell, P.H. Carr.

50. J. Am. Ceramics Soc. 34 235-9 (1951) F.A. Hummel.

51. J. Am. Ceramics Soc. 42 175-7 (1959) F.H. Gillery, E.A. Bush.

52. American Mineralogist 58 681-90 (1973) W.W. Pillars, D.R. Peacor.

53. J. Appl. Phys. 46 4339-40 (1975) L.J. Bonczar, G.R. Barsch.

54. J. Appl. Phys. 46 2894-8 (1975) T. Yamada.

55. Appl. Phys. Lett. 23 213-4 (1973) T. Yamada.

56. J. Appl. Phys. 46 2361-5 (1975) J. Nakamo, T. Yamada.

57. J. Appl. Phys. 49 3324-7 (1978) R.M. O'Connell.

58. IEEE Ultrasonics Symp. 1978 590-3 (1978) R.M. O'Connell, P.H. Carr.

59. Appl. Phys. Lett. 32 599-600 (1978) H. Yamauchi.

60. Appl. Phys. Lett. 35 595-7 (1979) Y. Ito et al.

61. J. Appl. Phys. 41 4141-7 (1970) T. Yamada et al.

62. "Microwaves Acoustics Handbook Vol 1A 'Surface Wave Velocities'" (1973) A.J. Slobodnik et al.

63. Physica Status Solidi A 29 241-50 (1975) G.R. Barsch et al.

64. J. Appl. Phys. 50 3160-7 (1979) H. Yamauchi et al.

65. J. Appl. Phys. 49 6162-6 (1978) H. Yamauchi.

66. J. Appl. Phys. 48 2850-6 (1977) M. Kimura.

67. Appl. Phys. Lett. 32 203-5 (1978) J. Melngailis et al.

68. Acoustica 23 165-9 (1970) V.S. Hausseihl.

69. Proc. IEEE 65 1093 (1977) W. Soluch et al.

70. Appl. Phys. Lett. 26 75-7 (1975) T.E. Parker, M.B. Schültz.

71. IEEE Ultrasonics Symp. 1974 295-8 (1974) T.E. Parker, M.B. Schultz.

72. IEEE Ultrasonics Symp. 1975 261-3 (1975) T.E. Parker, M.B. Schultz.

73. IEEE Ultrasonics Symp. 1975 503-7 (1975) T.E. Parker, H. Wichansky.

74. J. Appl. Phys. 50 1360-9 (1979) T.E. Parker, H. Wichansky.

75. Wave Electronics 3 319-33 (1979) K. Yamanouchi et al.

76. Appl. Phys. Lett. 31 56-7 (1977) Y. Nakagawa.

77. Trans. IECE of Japan E62 790-1 (1979) Y. Nakagawa, O. Kanbara.

78. IEEE Ultrasonics Symp. 1979 940-4 (1979) S. Furukawa et al.

79. Appl. Phys. Lett. 33 217-8 (1978) S. Ono et al.

80. Electronics Lett. 8 439 (1972) M.T. Wauk, R.L. Zimmerman.

81. Electronics Lett. 10 109-10 (1974) M.T. Wauk.

82. IEEE Ultrasonics Symp. 1979 623-6 (1979) K. Hohkawa, S. Yoshikawa.

83. Appl. Phys. Lett. 35 678-80 (1979) L.A. Coldren.

84. Proc. 32nd Ann. Freq. Contr. Symp. 102-7 (1978) R.G. Kinsman.

85. IEEE Ultrasonics Symp. 1979 849-54 (1979) D.L. Lee.

86. IEEE Sonics & Ultrasonics. SU22 39-45 (1975) M. Toda, S. Osaka.

87. J. Appl. Phys. 39 4319-25 (1968) T.C. Lim, G.W. Farnell.

88. J. Acoustic Soc. Am. 45 845-51 (1969) T.C. Lim, G.W. Farnell.

89. Appl. Phys. Lett. 10 311-3 (1967) H. Egan et al.

90. Proc IRE 37 1378-95 (1949) -

91. IEEE Sonics & Ultrasonics. SU18 79-80 (1971) J. Zelenka, P.C. Lee.

92. IEEE Sonics & Ultrasonics. SU23 72-5 (1976) R. Holland.

93. J. Material Science 15 161-7 (1980) J.C. Brice.

94. Proc. Royal Soc. London A142 237-47 (1933) A.H. Jay.

95. J. de Physique - Lett. 39 295 (1978) E. Bertagnolli et al.

96. Physica Status Solidi A 30 K11-5 (1975) G. Van Tendeloo et al.

97. Physica Status Solidi A 33 723-35 (1976) G. Van Tendeloo et al.

98. J. Phys. Chem. of Solids 36 407-13 (1975) H. Grimm, B. Dorner.

99. Solid State Communications 8 1487-90 (1970) U.T. Höchli.

100. Solid State Communications. 17 11-14 (1975) E.J. Banda et al.

101. Canadian J. Phys. 55 1613-20 (1977) R. Lang et al.

102. Chem. Phys. Lett. 41 133-6 (1976) J.G. Bergman, G.R. Crane.

103. J. Appl. Phys. 49 5473-8 (1978) J.D. Jorgensen.

104. Mineral. Mag. 38 593-604 (1972) D. Taylor.

105. Z. Krist. 94 222-30 (1936) F. Machatschki.

106. Z. Krist. 152 119-33 (1980) K. Korsten, H. Arnold.

107. Z. Naturforsch. 30A 28-34 (1975) U. Krauss, G. Lehmann.

108. Z. Krist. 108 263-75 (1956) E.C. Schafer et al.

109. Z. Phys. Chem. 24 215-40 (1934) G.E.R. Schulze.

110. Acta Cryst. 12 820-1 (1959) F. Dachille, L.S. Dent Glasser.

111. J. Am. Ceramics Soc. 39 330-6 (1956) E.C. Schafer, R. Roy.

112. J. Am. Ceramics Soc. 39 83-8 (1956) A. Perloff.

113. Phys. Rev. B 11 1648-53 (1975) W. Dultz et al.

114. Z. Krist. 103 228-9 (1941) H. Strunz.

115. Mineral. Mag. 33 613-5 (1963) M.J. Gallagher, J.F. Gerrard.

116. Z. Krist. 90 508-16 (1935) H.F. Huttenlocher.

117. Chem. Erde. 16 75-112 (1953) W. Jahn, E. Kordes.

118. Indust. Eng. Chem. 46 1684-9 (1954) J.M. Stanley.

119. Proc. 33rd Ann. Freq. Contr. Symp. 70-9 (1979) J. Detaint et al.

120. J. Crystal Growth 43 313-9 (1978) E.D. Kolb, R.A. Laudize.

121. Proc. 31st Ann. Freq. Contr. Symp. 178-81 (1977) E.D. Kolb, R.A. Laudize.

122. Proc. 33rd Ann. Freq. Contr. Symp. 88-97 (1979) E.D. Kolb et al.

123. Proc. 33rd Ann. Freq. Contr. Symp. 80-7 (1979) E.J. Ozimek, B.H. T. Chai.

124. IEEE Ultrasonics Symp. 1979 577-83 (1979) B.H.T. Chai et al.

125. Proc. 2nd European Conf. on Crystal Growth (1979) D.F. Croxall et al.

126. Acta Cryst. 8 567-70 (1955) R. Brill, A.P. de Bretteville.

127. Phys. Lett. 30A 340-1 (1969) R. Lang et al.

128. IEEE Sonics & Ultrasonics. SU23 127-35 (1976) Z.P. Chang, G.R. Barsch.

129. University of Birmingham, Dept of Physics, Paper 72-02 (1973) J.I. Langford, G.F. Mariner.

130. J. Am Ceramics Soc. 32 147-51 (1949) W.R. Beck.

131. Fortschr. Min. 28 82-4 (1950) G. Trömmel, B. Winkhaus.

132. Neues. Jahrb. Min. Abh. 83 1-22 (1951) B. Winkhaus.

133. Nat. Bureau of Standards (U.S.) Circ.539 10 3 (1960) H.E. Swanson et al.

134. Crystal Structures Vol.3 (Interscience Pub) 31 (1965) R.W.G. Wyckoff.

135. J. Appl. Phys. 36 1674-7 (1965) W.L. Bond.

136. Acta Cryst. 17 82-5 (1964) B. Sharan, B.N. Dutta.

137. Z. Krist. 123 161-85 (1966) D. Schwarzenbach.

138. Naturwissen. 52 343 (1965) D. Schwarzenbach.

139. Acta Cryst. A35 658-64 (1969) N. Thong, D. Schwarzenbach.

140. "Piezoelectric Crystals and their Applications to Ultrasonics" (Van Nostrand) 208-9 (1950) W.P Mason.

141. American Mineralogist 58 796-8 (1973) L.H. Cohen, W. Klement.

142. Phys. Rev. B 4 1360-6 (1971) J.F. Scott.

143. Phys. Rev. Lett. 24 1107-10 (1970) J.F. Scott.

144. Canadian J. Phys. 54 638-47 (1976) H.N. Ng, C. Calvo.

145. Ber. Deutsch. Keram. Gesell. 39 55-62 (1962) V.O. Flörke, H. Lachenmayr.

146. Proc. 33rd Ann. Freq. Contr. Symp. 62-9 (1979) L.E. Halliburton et al.

147. J. Appl. Phys. 51 2193-8 (1980) L.E. Halliburton et al.

148. American Mineralogist 35 108-15 (1950) R.L. Manly (Jr).

149. Material Res. Bull. 14 603-12 (1979) H. Poignant et al.

150. J. Acoustic Soc. Am. 35 53-8 (1963) H.F. Tiersten.

151. IEEE Sonics & Ultrasonics. SU24 376-84 (1977) R.M. O'Connell, P.H. Carr.

152. IEEE Ultrasonics Symp. 1976 523-7 (1976) A. Jhunjhunwala et al.

153. Electronics Lett. 7 253-5 (1971) J.C. Crabb et al.

154. Appl. Phys. Lett. 33 117-9 (1978) D.G. Morency et al.

155. Proc. 32nd Ann. Freq. Contr. Symp. 196-201 (1978) D.G. Morency et al.

156. IEEE Ultrasonics Symp. 1978 594-7 (1978) D. Harmon et al.

157. IEEE Trans. Microwave Theory and Tech. MTT17 856-64 (1969) W.R. Smith et al.

158. Electronics Lett. 5 678-80 (1969) J.D. Maines et al.

159. IEEE Sonics & Ultrasonics. SU26 299-306 (1979) A. Ballato.

160. IEEE Ultrasonics Symp. 1979 606-11 (1979) R.S. Raghavan et al.

161. IEEE Ultrasonics Symp. 1976 519-22 (1976) Y. Shimizu et al.

162. Proc. IRE 46 764-78 (1958) -

163. Bull. Soc. Chim. France. 11 4256-9 (1967) M. Troccaz et al.

164. NAG FORTRAN Library Manual. Numerical Algorithms Group (Oxford).

165. "Acoustic Fields and Waves in Solids" Vol 2. (Wiley) 170-7 (1973) B.A. Auld.

Appendix 1. FORTRAN listing of the computer program.

```
      PROGRAM SAWVEL(INPUT,OUTPUT,TAPE5=INPUT,TAPE6=OUTPUT)
      DIMENSION C(6,6),CPRIME(81),E(3,6),EPRIME(3,3,3)
      DIMENSION EPSI(3,3),V(3,3),TRUE(81),ETRUE(27)
      DIMENSION C25(7),E25(2),EP25(2),ALPHA(3,3)
      DIMENSION TC1(7),TC2(7),TC3(7),TE1(2),TEP1(2)
      DIMENSION X(10,3),EP(3,3),ALPHAI(3,3),X2(11,5),X3(3,9)
      DIMENSION WKSP(4),WR(4),WI(4),EIGR(4,4),EIGIM(4,4)
      DIMENSION AI(9),ZIM(9),ZREAL(9),DET1(4,4),DET2(4,4)
      DIMENSION CR(4),CI(4),DMN2(4,4),DMN3(4,4),A2(9)
      DIMENSION CREAL(4,4),CIMAG(4,4),RWPOW(3),TE2(2),TE3(2)
      DIMENSION TA1(2),TA2(2),TA3(2),VS(102),ABSOL(101)
      DIMENSION VTEMP(3),DELAY(3),PHI1(3),PHI2(3)
      COMPLEX RL(3,4),DET(4,4),DMN(4,4),EIGVEC(4,4)
      COMPLEX ROOTS(8),UVECT(4),CVECT(4)
      COMPLEX FINT,FINT1,XST,YST,YST1,ZST,ZST1,EMN
      COMPLEX WPOW(3),SUMA(10)
      INTEGER P,Q,R,S,T,TIJ,QRST
C
      EPS0 = 8.854185E-12
      D = ASIN(1.0)/90.0
C     IDATA = 0
C1150 CONTINUE
      METAL = 0
      RLONG = 0.01
C
C     SET ROOTS RL(1,N) AND RL(2,N)
C
      DO 5 N=1,4
      RL(1,N) = CMPLX(1.0,0.0)
    5 RL(2,N) = CMPLX(0.0,0.0)
C
C
C     THIS PROGRAM IS TO CALCULATE THE SURFACE ACOUSTIC WAVE VELOCITIES
C     FOR PIEZO-ELECTRIC CRYSTALS
C
C
C     INPUT OF DATA
C
      READ (5,1000) (C25(I),I=1,7)
      READ (5,1000) (TC1(I),I=1,7)
      READ (5,1000) (TC2(I),I=1,7)
      READ (5,1000) (TC3(I),I=1,7)
      READ (5,1040) E25(1),TE1(1),TE2(1),TE3(1)
      READ (5,1040) E25(2),TE1(2),TE2(2),TE3(2)
      READ (5,1040) (EP25(I),I=1,2),(TEP1(J),J=1,2)
      READ (5,1040) RO0,TRO1,TRO2,TRO3
      READ (5,1080) TA1(1),TA1(2),TA2(1),TA2(2),TA3(1),TA3(2)
      READ (5,1085) NANGLE
      READ (5,1090) VSTART,DELV1,RKSP
      READ (5,1095) T0,T1,DT
C
 1000 FORMAT(7E11.4)
 1040 FORMAT(4E11.4)
 1080 FORMAT(6E11.4)
 1085 FORMAT(I2)
 1090 FORMAT(F9.3,2(1X,F5.2))
 1095 FORMAT(3(F5.1,1X))
C
      WRITE (6,5000) (C25(IOUT),IOUT=1,7)
      WRITE (6,5000) (TC1(IOUT),IOUT=1,7)
      WRITE (6,5000) (TC2(IOUT),IOUT=1,7)
      WRITE (6,5000) (TC3(IOUT),IOUT=1,7)
      WRITE (6,5004) E25(1),TE1(1),TE2(1),TE3(1)
      WRITE (6,5004) E25(2),TE1(2),TE2(2),TE3(2)
      WRITE (6,5004) (EP25(IOUT),IOUT=1,2),(TEP1(JOUT),JOUT=1,2)
      WRITE (6,5004) RO0,TRO1,TRO2,TRO3
      WRITE (6,5007) TA1(1),TA1(2),TA2(1),TA2(2),TA3(1),TA3(2)
C
 5000 FORMAT(1H0,20X,7(1PE11.4,2X))
 5004 FORMAT(1H0,20X,4(1PE11.4,2X))
 5007 FORMAT(1H0,20X,6(1PE11.4,2X))
C
C     PRINT THE HEADINGS
C
      WRITE (6,2000)
 2000 FORMAT(2(1H0/),31X,"THIS PROGRAM CALCULATES SURFACE WAVE ",
     1"VELOCITIES")
```

```
      C
            VS(1) = VSTART
 80         T2 = T1 - DT/2.0
            DELV = DELV1
      C
      C     READ IN THE ANGLES
      C
 85         DO 38 IRANGE=1,NANGLE
            INCRE = 101
            READ (5,1100) A,B,G
       1100 FORMAT(3(F5.1,1X))
            WRITE (6,2010) A,B,G
 90    2010 FORMAT(1H0,30X,"THE ANGLES ALPHA, BETA AND GAMMA ARE ",
           2(1H ,39X,"(",3(F6.2,2X),")   DEGREES ROTATED BERLINITE")
      C
      C     TRANSFORM TO RADIAN MEASURE
      C
 95         A = -A
            A = A*D
            B = B*D
            AINC = G - 0.1
      C
100   C     START ANGLE GAMMA ITERATIONS
      C
            DO 35 IANGLE=1,3
            AINC = AINC + 0.05
            G = AINC*D
105   C
      C     EVALUATE THE TRANSFORMATION MATRIX V(I,J)
      C
            V(1,1) = (COS(A)*COS(G)) + (SIN(A)*COS(B)*SIN(G))
            V(1,2) = (SIN(A)*COS(G)) - (COS(A)*COS(B)*SIN(G))
110         V(1,3) = -(SIN(B)*SIN(G))
            V(2,1) = -(COS(A)*SIN(G)) + (SIN(A)*COS(B)*COS(G))
            V(2,2) = -(SIN(A)*SIN(G)) - (COS(A)*COS(B)*COS(G))
            V(2,3) = -(SIN(B)*COS(G))
            V(3,1) = +(SIN(A)*SIN(B))
115         V(3,2) = COS(A)*SIN(B)
            V(3,3) = -COS(B)
      C
      C     CALCULATE AND PRINT THE TEMPERATURE T1 AND RELATE IT TO THE
      C     REFERENCE TEMPERATURE T0
120   C
            DO 35 ITEMP=1,3
            T2 = T2 + DT/2.0
            IF (IANGLE.NE.2.AND.ITEMP.NE.2) GO TO 37
      C
125         DELTA = T2 - T0
            IF (IANGLE.NE.2.OR.ITEMP.NE.2) GO TO 32
            WRITE (6,3000) T2
       3000 FORMAT(1H0,30X,"TEMPERATURE = ",F6.1," DEGREES CENTIGRADE")
         32 CONTINUE
130   C
      C     CALCULATE THE VALUES OF THE CONSTANTS (ADJUSTED FOR TEMPERATURE)
      C     BY USING FOUR SUBROUTINES
      C
            CALL CGEN(C25,TC1,TC2,TC3,DELTA,C)
135         CALL EGEN(E25,TE1,TE2,TE3,DELTA,E)
            CALL EPGEN(EP25,TEP1,DELTA,EPSI)
            CALL ALPGEN(TA1,TA2,TA3,DELTA,ALPHA1)
            F1 = DELTA*TRO1
            F2 = DELTA*DELTA*TRO2
140         F3 = DELTA*DELTA*DELTA*TRO3
            RO = RO0*(1.0 + F1 + F2 + F3)
      C
      C     CONVERT C(PQ) TO C(IJKL) AND E(IP) TO E(IJK)
      C
145         DO 60 I=1,3
            DO 60 J=1,3
            DO 60 K=1,3
            DO 70 L=1,3
            IF (I.EQ.J) P=I
150         IF (I.NE.J) P=9-(I+J)
            IF (K.EQ.L) Q=K
            IF (K.NE.L) Q=9-(K+L)
            IJKL = (27*(I-1)) + (9*(J-1)) + (3*(K-1)) + L
         70 TRUE(IJKL) = C(P,Q)
155   C
            KIJ = (9*(K-1)) + (3*(I-1)) + J
         60 ETRUE(KIJ) = E(K,P)
```

```
      C
      C     EVALUATE ROTATED CONSTANTS CPRIME(QRST),EPRIME(RST),EPSILON PRIME(ST)
160   C     AND ALPHA(ST)
      C
            DO 10 Q=1,3
            DO 10 IR=1,3
            EP(Q,IR) = 0.0
165         ALPHA(Q,IR) = 0.0
            DO 10 IS=1,3
            EPRIME(Q,IR,IS) = 0.0
            DO 10 T=1,3
            QRST = (27*(Q-1)) + (9*(IR-1)) + (3*(IS-1)) + T
170         CPRIME(QRST) = 0.0
            DO 20 I=1,3
            DO 20 J=1,3
            DO 30 K=1,3
            DO 30 L=1,3
175         IJKL = (27*(I-1)) + (9*(J-1)) + (3*(K-1)) + L
            X1 = V(Q,I)*V(IR,J)*V(IS,K)*V(T,L)*TRUE(IJKL)
         30 CPRIME(QRST) = CPRIME(QRST) + X1
      C
            TIJ = (9*(T-1)) + (3*(I-1)) + J
180         Y1 = V(Q,T)*V(IR,I)*V(IS,J)*ETRUE(TIJ)
         20 EPRIME(Q,IR,IS) = EPRIME(Q,IR,IS) + Y1
      C
            Z = V(Q,IS)*V(IR,T)*EPSI(IS,T)
            Z1 = V(Q,IS)*V(IR,T)*ALPHA(IS,T)
185         EP(Q,IR) = EP(Q,IR) + Z
         10 ALPHA(Q,IR) = ALPHA(Q,IR) + Z1
      C
            DIST = RLONG*ALPHA(1,1)
      C
190   C     ALLOCATE X(EQN,ORDER) TO SOLVE THE SECULAR EQUATION
      C     FIRST LEVEL OF COEFFICIENT MULTIPLICATIONS
      C
            X(1,2) = CPRIME(55) + CPRIME(3)
            X(1,3) = CPRIME(57)
195         X(2,1) = CPRIME(4)
            X(2,2) = CPRIME(58) + CPRIME(6)
            X(2,3) = CPRIME(60)
            X(3,1) = CPRIME(7)
            X(3,2) = CPRIME(61) + CPRIME(9)
200         X(3,3) = CPRIME(63)
            X(4,1) = EPRIME(1,1,1)
            X(4,2) = EPRIME(3,1,1) + EPRIME(1,3,1)
            X(4,3) = EPRIME(3,3,1)
            X(5,2) = CPRIME(67) + CPRIME(15)
205         X(5,3) = CPRIME(69)
            X(6,1) = CPRIME(16)
            X(6,2) = CPRIME(70) + CPRIME(18)
            X(6,3) = CPRIME(72)
            X(7,1) = EPRIME(1,1,2)
210         X(7,2) = EPRIME(3,1,2) + EPRIME(1,3,2)
            X(7,3) = EPRIME(3,3,2)
            X(8,2) = CPRIME(79) + CPRIME(27)
            X(8,3) = CPRIME(81)
            X(9,1) = EPRIME(1,1,3)
215         X(9,2) = EPRIME(3,1,3) + EPRIME(1,3,3)
            X(9,3) = EPRIME(3,3,3)
            X(10,1) = -EP(1,1)
            X(10,2) = -(EP(1,3) + EP(3,1))
            X(10,3) = -EP(3,3)
220   C
      C     START ITERATION PROCESS
      C
            ISTORE = 0
      430 CONTINUE
225   C
            IF (IANGLE.NE.2.OR.ITEMP.NE.2) GO TO 41
            IF (METAL.EQ.0) ISURF = 10HFREE
            IF (METAL.NE.0) ISURF = 10HMETALLIZED
            WRITE (6,6085) ISURF
230      6085 FORMAT(1H0,50X,"THE SURFACE IS ",A10)
         41 CONTINUE
      C
            IQ = 0
      440 CONTINUE
235   C
            IQ = IQ + 1
            X(1,1) = CPRIME(1) - (RO*VS(IQ)*VS(IQ))
            X(5,1) = CPRIME(13) - (RO*VS(IQ)*VS(IQ))
            X(8,1) = CPRIME(25) - (RO*VS(IQ)*VS(IQ))
```

```
      C
      C     ZERO THE COEFFICIENTS FOR SECOND LEVEL MULTIPLICATIONS
      C
            DO 80 I=1,11
            DO 80 J=1,5
   80 X2(I,J) = 0.0
      C
      C     CALCULATE SECOND LEVEL COEFFICIENTS
      C
            DO 90 M=1,3
            DO 90 N=1,3
            I = (M-1) + (N-1) + 1
            X2(1,I) = X2(1,I) + X(8,M)*X(10,N) - X(9,M)*X(9,N)
            X2(2,I) = X2(2,I) + X(6,M)*X(10,N) - X(9,M)*X(7,N)
            X2(3,I) = X2(3,I) + X(6,M)*X(9,N) - X(8,M)*X(7,N)
            X2(4,I) = X2(4,I) + X(3,M)*X(10,N) - X(9,M)*X(4,N)
            X2(5,I) = X2(5,I) + X(3,M)*X(9,N) - X(8,M)*X(4,N)
            X2(6,I) = X2(6,I) + X(3,M)*X(7,N) - X(6,M)*X(4,N)
            X2(7,I) = X2(7,I) + X(1,M)*X(5,N) - X(2,M)*X(2,N)
            X2(8,I) = X2(8,I) + X(3,M)*X(2,N) - X(1,M)*X(6,N)
            X2(9,I) = X2(9,I) + X(1,M)*X(7,N) - X(2,M)*X(4,N)
            X2(10,I) = X2(10,I) + X(2,M)*X(6,N) - X(3,M)*X(5,N)
   90 X2(11,I) = X2(11,I) + X(4,M)*X(5,N) - X(2,M)*X(7,N)
      C
      C     ZERO THE COEFFICIENTS FOR THIRD LEVEL MULTIPLICATIONS
      C
            DO 110 I=1,3
            DO 110 J=1,9
  110 X3(I,J) = 0.0
      C
      C     CALCULATE THIRD LEVEL COEFFICIENTS
      C
            DO 120 M=1,5
            DO 120 N=1,5
            I = (M-1) + (N-1) + 1
            X3(1,I) = X3(1,I) + X2(1,M)*X2(7,N) + X2(2,M)*X2(8,N)
            X3(2,I) = X3(2,I) + X2(3,M)*X2(9,N) + X2(4,M)*X2(10,N)
  120 X3(3,I) = X3(3,I) + X2(5,M)*X2(11,N) + X2(6,M)*X2(6,N)
      C
      C     CALCULATE THE COEFFICIENTS X3(I)
      C     A1(10-I) IS THE COEFFICIENT OF RL(3,N)**(I-1)     I=1,9
      C
            DO 125 I=1,9
  125 A1(10-I) = X3(1,I) + X3(2,I) + X3(3,I)
      C
      C     SOLVE THE SECULAR EQUATION POLYNOMIAL
      C
            N = 9
            TOL = 1.0E-15
            IFAIL = 0
            CALL C02AEF(A1,N,ZREAL,ZIM,TOL,IFAIL)
      C
            DO 140 I=1,8
            IF (ABS(ZREAL(I)).LT.1.0E-11) ZREAL(I) = 0.0
            IF (ABS(ZIM(I)).LT.1.0E-11) ZIM(I) = 0.0
  140 ROOTS(I) = CMPLX(ZREAL(I),ZIM(I))
      C
      C     ZERO THE MATRIX DMN
      C
            DO 200 I=1,4
            DO 200 J=1,4
  200 DMN(I,J) = CMPLX(0.0,0.0)
      C
      C     EVALUATE MATRIX DMN FOR ROOTS WITH IM(RL(3,N)),LT.ZERO
      C
            J = 0
            DO 210 I=1,8
            IF (AIMAG(ROOTS(I)).GT.0.0) GO TO 210
            IF (AIMAG(ROOTS(I)).EQ.0.0.AND.REAL(ROOTS(I)).GT.0.0) GO TO 210
      C
      C     ZERO THE MATRIX DET
      C
            DO 25 II=1,4
            DO 25 JJ=1,4
   25 DET(II,JJ) = CMPLX(0.0,0.0)
```

```
315         C
            C     CALCULATE THE MATRIX DET
            C
                  DO 205 IORDER=1,3
                  DET(1,1) = DET(1,1) + X(1,IORDER)*(ROOTS(I)**(IORDER-1))
320               DET(1,2) = DET(1,2) + X(2,IORDER)*(ROOTS(I)**(IORDER-1))
                  DET(1,3) = DET(1,3) + X(3,IORDER)*(ROOTS(I)**(IORDER-1))
                  DET(1,4) = DET(1,4) + X(4,IORDER)*(ROOTS(I)**(IORDER-1))
                  DET(2,2) = DET(2,2) + X(5,IORDER)*(ROOTS(I)**(IORDER-1))
                  DET(2,3) = DET(2,3) + X(6,IORDER)*(ROOTS(I)**(IORDER-1))
325               DET(2,4) = DET(2,4) + X(7,IORDER)*(ROOTS(I)**(IORDER-1))
                  DET(3,3) = DET(3,3) + X(8,IORDER)*(ROOTS(I)**(IORDER-1))
                  DET(3,4) = DET(3,4) + X(9,IORDER)*(ROOTS(I)**(IORDER-1))
            205   DET(4,4) = DET(4,4) + X(10,IORDER)*(ROOTS(I)**(IORDER-1))
            C
330         C     ALLOCATE RL(3,J) AND SYMMETRIC TERMS IN DETERMINANT GAMMA
            C
                  J = J + 1
                  RL(3,J) = ROOTS(I)
                  DET(2,1) = DET(1,2)
335               DET(3,1) = DET(1,3)
                  DET(4,1) = DET(1,4)
                  DET(3,2) = DET(2,3)
                  DET(4,2) = DET(2,4)
                  DET(4,3) = DET(3,4)
340         C
            C     SET TEMPORARY MATRICES
            C
                  DO 220 II=1,4
                  DO 220 JJ=1,4
345               DET2(II,JJ) = AIMAG(DET(II,JJ))
            220   DET1(II,JJ) = REAL(DET(II,JJ))
            C
            C     CHECK THAT AN EIGENVALUE OF DET IS ZERO
            C
350               IFAIL = 0
                  CALL F02AKF(DET1,4,DET2,4,4,WR,WI,EIGR,4,EIGIM,4,WKSP,IFAIL)
            C
                  DO 225 II=1,4
                  IF (ABS(WR(II)).LT.1.0E-08.AND.ABS(WI(II)).LT.1.0E-08) GO TO 226
355           225 CONTINUE
            C
                  GO TO 9999
              226 CONTINUE
            C
360         C     SOLVE FOR EIGENVECTORS OF MATRIX DET
            C
                  DO 227 K=1,4
              227 EIGVEC(K,J) = CMPLX(EIGR(K,II),EIGIM(K,II))
            C
365           210 CONTINUE
            C
            C     CALCULATE MATRIX DMN
            C
                  DO 230 J=1,3
370               DO 230 N=1,4
                  DO 230 K=1,3
                  DO 240 L=1,3,2
                  IJKL = 54 + (9*(J-1)) + (3*(K-1)) + L
            240   DMN(J,N) = DMN(J,N) + CPRIME(IJKL)*RL(L,N)*EIGVEC(K,N)
375         230   DMN(J,N) = DMN(J,N) + EPRIME(K,3,J)*RL(K,N)*EIGVEC(4,N)
            C
                  IF (METAL.NE.0) GO TO 291
            C
            C     FOR A FREE SURFACE
380         C
                  DO 295 N=1,4
                  DO 290 K=1,3
                  DO 300 L=1,3,2
            300   DMN(4,N) = DMN(4,N) + EPRIME(3,K,L)*RL(L,N)*EIGVEC(K,N)
385         290   DMN(4,N) = DMN(4,N) - (EP(3,K)*RL(K,N)*EIGVEC(4,N))
            295   DMN(4,N) = DMN(4,N) + CMPLX(0.0,EPS0)*EIGVEC(4,N)
                  GO TO 292
            C
            C     FOR A METALLIZED SURFACE
390         C
              291 CONTINUE
                  DO 293 N=1,4
              293 DMN(4,N) = EIGVEC(4,N)
            C
395           292 CONTINUE
            C
            C     EVALUATE THE DETERMINANT FOR A PARTICULAR SAW VELOCITY
            C
                  CALL DETER4(DMN,VALUE1)
400               ABSOL(IQ) = VALUE1
```

```
C
C     SET NEW SAW VELOCITY
C
      IJ = IQ + 1
405   VS(IJ) = VS(IQ) - DELV
      IF (ISTORE.NE.0) GO TO 500
C
      IF (IQ.NE.INCRE) GO TO 440
C
410   C     FIND MINIMUM OF DET(DMN) AND APPROX SAW VELOCITY VSTORE
C
      STORE = ABSOL(1)
      VSTORE = VS(1)
      DO 400 IK=2,INCRE
415   IF (ABSOL(IK).GE.STORE) GO TO 400
      STORE = ABSOL(IK)
      VSTORE = VS(IK)
  400 CONTINUE
C
420   C     EVALUATE COMPONENTS FOR THE FINAL SAW VELOCITY
C
      VS(1) = VSTORE + DELV
      ISTORE = 0
      IF (DELV.LE.1.0E-04) ISTORE = 1
425   IF (INCRE.EQ.101) INCRE = 7
      DELV = DELV/(FLOAT(INCRE-1)/2.0)
      IQ = 0
      IF (ISTORE.NE.1) GO TO 445
C
430   IF (METAL.EQ.1) GO TO 36
      VTEMP(ITEMP) = VSTORE
      DELAY(ITEMP) = DIST/VSTORE
   36 CONTINUE
C
435   IF (IANGLE.NE.2.OR.ITEMP.NE.2) GO TO 33
      WRITE (6,6000) VSTORE
 6000 FORMAT(1H0,40X,"THE SURFACE WAVE VELOCITY IS ",F10.4," M/S"/1H ,
     540X,43("*"))
   33 CONTINUE
440   C
      VS(1) = VSTORE
  445 CONTINUE
C
      GO TO 440
445   C
  500 CONTINUE
      IF (ITEMP.NE.2) GO TO 13
C
      C     CALCULATE EIGENVECTORS C(N)
450   C
      DO 450 I=1,4
      DO 450 J=1,4
      DMN2(I,J) = REAL(DMN(I,J))
  450 DMN3(I,J) = AIMAG(DMN(I,J))
455   C
      IFAIL = 0
      CALL F02AKF(DMN2,4,DMN3,4,4,CR,CI,CREAL,4,CIMAG,4,WKSP,IFAIL)
C
      C     CHECK THAT ONE OF THE EIGENVALUES IS ZERO
460   C
      DO 460 I=1,4
      IF (ABS(CR(I)).LT.5.0E-5.AND.ABS(CI(I)).LT.5.0E-5) GO TO 470
  460 CONTINUE
C
465   WRITE (6,6050)
 6050 FORMAT(1H ,50X,"EIGENVALUES OF C(N) ARE NON ZERO")
      GO TO 9999
C
  470 CONTINUE
470   DO 480 N=1,4
  480 CVECT(N) = CMPLX(CREAL(N,I),CIMAG(N,I))
C
      DO 485 N=1,4
  485 CVECT(N) = CVECT(N)/CVECT(4)
475   C
      C     CALCULATE PARTICLE DISPLACEMENTS U(J)
C
      DO 600 J=1,4
      UVECT(J) = CMPLX(0.0,0.0)
480   DO 600 N=1,4
  600 UVECT(J) = UVECT(J) + CVECT(N)*EIGVEC(J,N)
```

```
C
C     CALCULATE THE POWER FLOW DIRECTIONS
C
      FINT = CMPLX(0.0,1.0)*RKSP*VS(1)
      DO 610 I=1,3
      WPOW(I) = CMPLX(0.0,0.0)
      EMN = CMPLX(0.0,0.0)
      FINT1 = CMPLX(0.0,0.0)
C
      DO 620 N=1,4
      DO 620 M=1,4
      FINT1 = RL(3,N) * CONJG(RL(3,M))
      IF (CABS(FINT1).LT.1.0E-10) GO TO 620
      ZST = CMPLX(0.0,0.0)
      ZST1 = CMPLX(0.0,0.0)
C
      DO 630 J=1,3
      YST = CMPLX(0.0,0.0)
      YST1 = CMPLX(0.0,0.0)
C
      DO 635 K=1,3
      XST = CMPLX(0.0,0.0)
C
      DO 645 L=1,3,2
      IJKL = (27*(I-1)) + (9*(J-1)) + (3*(K-1)) + L
  645 XST = XST + CPRIME(IJKL)*EIGVEC(K,N)*RL(L,N)
C
      YST1 = YST1 + EPRIME(K,I,J)*EIGVEC(4,N)*RL(K,N) + XST
  635 YST = YST + EPRIME(I,J,K)*CONJG(EIGVEC(J,M))*CONJG(RL(K,M))
C
      ZST = ZST + CONJG(EIGVEC(J,M))*YST1
  630 ZST1 = ZST1 + (EP(I,J)*CONJG(EIGVEC(4,M))*CONJG(RL(J,M)) + YST)
     5              *EIGVEC(4,N)
C
      EMN = EMN + (ZST + ZST1)*CVECT(N)*CONJG(CVECT(M))/FINT1
  620 CONTINUE
C
      WPOW(I) = FINT*EMN
  610 RWPOW(I) = REAL(WPOW(I))*(-0.5)
C
      IF (RWPOW(1).EQ.0.0) GO TO 406
C
C     CALCULATE THE POWER FLOW ANGLES
C
      PHI1(IANGLE) = ATAN(RWPOW(2)/RWPOW(1))/D
      PHI2(IANGLE) = ATAN(RWPOW(3)/RWPOW(1))/D
      IF (IANGLE.NE.2) GO TO 13
C
      WRITE (6,6070) PHI1(2),PHI2(2)
 6070 FORMAT(1H0,30X,"THE SURFACE WAVE POWER FLOW ANGLE IS ",F9.3,
     4" DEG"/1H ,30X,"THE POWER FLOW ANGLE INTO THE BULK IS ",F8.3,
     5" DEG")
C
C     RESET FOR A METALLIZED SURFACE
C
      IF (METAL.NE.1) GO TO 405
      VMETAL = VS(1)
      GO TO 406
C
  405 VFREE = VS(1)
      VS(1) = VS(1) + DELV1
      DELV = (2.0*DELV1)/FLOAT(INCRE-1)
      ISTORE = 0
      METAL = 1
      GO TO 430
C
C     CALCULATE DV/V AND K SQUARED
C
  406 CONTINUE
      DVBYV = (VFREE - VMETAL)/VFREE
      EPT = (SQRT(EP(1,1)*EP(3,3) - EP(1,3)*EP(1,3)))/EPS0
      REK = DVBYV/(1.0 - DVBYV)
      REKSQ = 2.0*(1.0 + (1.0/EPT))*REK
      IF (IANGLE.NE.2.OR.ITEMP.NE.2) GO TO 13
C
      WRITE (6,6075) DVBYV,REKSQ
 6075 FORMAT(1H0,30X,"(DELTA V)/V = ",1PE11.4/1H ,30X,"K SQUARED = ",
     3E11.4)
```

```
C
C     COMPLETE TEMPERATURE AND ANGLE LOOPS
C
   13 METAL = 0
      VS(1) = VS(1) + DELV1
      DELV = (2.0*DELV1)/FLOAT(INCRE-1)
      ISTORE = 0
   37 IF (ITEMP.EQ.3) T2 = T1
   35 CONTINUE
C
C     CALCULATE THE TEMPERATURE COEFFICIENTS
C
      TCD = (DELAY(3)-DELAY(1))*(1.0E06)/DELAY(2)
      WRITE (6,8015) TCD
 8015 FORMAT(1H0,30X,"THE TEMPERATURE COEFFICIENT OF DELAY IS ",
     1F9.3," PPM/DEG C")
C
C     CALCULATE SLOPE OF THE POWER FLOW ANGLE
C
      DPHI1 = 10.0 * (PHI1(3) - PHI1(1))
      DPHI2 = 10.0 * (PHI2(3) - PHI2(1))
      WRITE (6,8020) DPHI1,DPHI2
 8020 FORMAT(1H0,30X,"SLOPE OF THE SURFACE WAVE POWER FLOW ANGLE ",
     9"IS ",F10.3/1H ,30X,"SLOPE OF THE BULK WAVE POWER FLOW ANGLE IS",
     8"  ",F10.3)
      GO TO 9998
C
C     FAILSAFE CATCHING ROUTINE
C
 9999 CONTINUE
      WRITE (6,9997)
 9997 FORMAT(1H0,30X,"THE PROGRAM HAS ABORTED"/1H ,30X,
     3"AN EIGENVALUE IS NON ZERO")
C
 9998 CONTINUE
      VS(1) = VSTART
      DELV = DELV1
      WRITE (6,130)
  130 FORMAT(1H0,5X,120("*"))
C
   38 CONTINUE
C     IDATA = IDATA + 1
C     IF (IDATA.NE.3) GO TO 1150
C
      STOP
      END
```

```
      SUBROUTINE CGEN(C25,X1,X2,X3,T,Y)
      DIMENSION C25(7),X1(7),X2(7),X3(7),Y(6,6),X(7)
      REAL Y
C
C     SUBROUTINE TO CALCULATE THE REAL VALUES OF C(P,Q) FOR CLASS 32
C
      DO 1 I=1,7
      FACT = 1.0 + (T*X1(I)) + (T*T*X2(I)) + (T*T*T*X3(I))
      X(I) = C25(I)*FACT
    1 CONTINUE
C
      DO 2 I=1,6
      DO 2 J=1,6
    2 Y(I,J) = 0.0
C
      Y(1,1) = X(1)
      Y(1,2) = X(2)
      Y(1,3) = X(3)
      Y(1,4) = X(4)
      Y(2,1) = X(2)
      Y(2,2) = X(1)
      Y(2,3) = X(3)
      Y(2,4) = - X(4)
      Y(3,1) = X(3)
      Y(3,2) = X(3)
      Y(3,3) = X(5)
      Y(4,1) = X(4)
      Y(4,2) = - X(4)
      Y(4,4) = X(6)
      Y(5,5) = X(6)
      Y(5,6) = X(4)
      Y(6,5) = X(4)
      Y(6,6) = X(7)
      RETURN
      END
```

```
      SUBROUTINE EGEN(E25,X1,X2,X3,T,Y)
      DIMENSION E25(2),X1(2),X2(2),X3(2),Y(3,6),X(2)
      REAL T
C
C     SUBROUTINE TO  CALCULATE THE REAL VALUES OF E(K,P) FOR CLASS 32
C
      DO 3 I=1,2
      FACT = 1.0 + (T*X1(I)) + (T*T*X2(I)) + (T*T*T*X3(I))
    3 X(I) = E25(I)*FACT
C
      DO 4 I=1,3
      DO 4 J=1,6
    4 Y(I,J) = 0.0
C
      Y(1,1) = X(1)
      Y(1,2) = - X(1)
      Y(1,4) = X(2)
      Y(2,5) = - X(2)
      Y(2,6) = - X(1)
      RETURN
      END
```

```
      SUBROUTINE EPGEN(EP25,X1,T,Y)
      DIMENSION EP25(2),X1(2),Y(3,3),X(2)
      REAL T
C
C     SUBROUTINE TO CALCULATE THE REAL VALUES OF EPSILON(I,J)
C     FOR CLASS 32
C
      DO 5 I=1,2
      FACT = 1.0 + (T*X1(I))
    5 X(I) = EP25(I)*FACT
C
      DO 6 I=1,3
      DO 6 J=1,3
    6 Y(I,J) = 0.0
C
      Y(1,1) = X(1)
      Y(2,2) = X(1)
      Y(3,3) = X(2)
      RETURN
      END
```

```
      SUBROUTINE ALPGEN(X1,X2,X3,T,X)
      DIMENSION X(3,3),X1(2),X2(2),X3(2),Y(2)
      REAL T
C
C     SUBROUTINE TO CALCULATE THE REAL VALUES OF ALPHA(I,J)
C     FOR CLASS 32
C
      DO 7 I=1,2
    7 Y(I) = 1.0 + (T*X1(I)) + (T*T*X2(I)) + (T*T*T*X3(I))
C
      DO 8 I=1,3
      DO 8 J=1,3
    8 X(I,J) = 0.0
C
      X(1,1) = Y(1)
      X(2,2) = Y(1)
      X(3,3) = Y(2)
      RETURN
      END
```

```
      SUBROUTINE DETER4(A,V)
      COMPLEX A(4,4),X(12),X2(4)
C
C     A SUBROUTINE TO EVALUATE A 4*4 DETERMINANT
C
      X(1) = A(1,1)*A(2,2) - A(1,2)*A(2,1)
      X(2) = A(3,3)*A(4,4) - A(3,4)*A(4,3)
      X(3) = A(1,3)*A(2,1) - A(1,1)*A(2,3)
      X(4) = A(3,2)*A(4,4) - A(3,4)*A(4,2)
      X(5) = A(1,1)*A(2,4) - A(1,4)*A(2,1)
      X(6) = A(3,2)*A(4,3) - A(4,2)*A(3,3)
      X(7) = A(1,2)*A(2,3) - A(1,3)*A(2,2)
      X(8) = A(3,1)*A(4,4) - A(3,4)*A(4,1)
      X(9) = A(1,4)*A(2,2) - A(1,2)*A(2,4)
      X(10) = A(3,1)*A(4,3) - A(3,3)*A(4,1)
      X(11) = A(1,3)*A(2,4) - A(1,4)*A(2,3)
      X(12) = A(3,1)*A(4,2) - A(4,1)*A(3,2)
C
      X2(1) = X(1)*X(2) + X(3)*X(4)
      X2(2) = X(5)*X(6) + X(7)*X(8)
      X2(3) = X(9)*X(10) + X(11)*X(12)
      X2(4) = X2(1) + X2(2) + X2(3)
C
      V = CABS(X2(4))
      RETURN
      END
```

APPENDIX 2
STANDARD CRYSTALLOGRAPHIC ORIENTATIONS

Key

N Plate Normal
P Propogation Direction
XYZ Axes of Crystal
ABG Rotation Angles

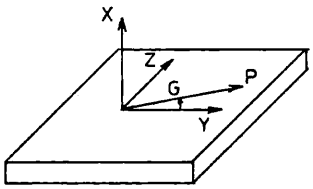

X CUT
(90,90,G)

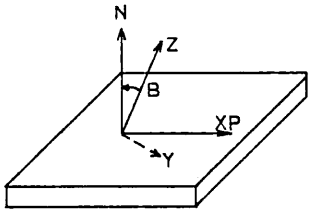

X AXIS BOULE
(0,B,0)

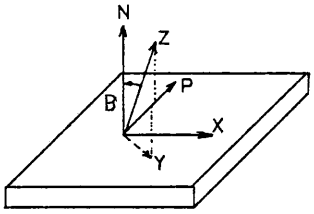

X AXIS CYLINDER
(0,B,90)

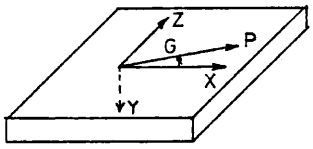

Y CUT
(0,90,G)

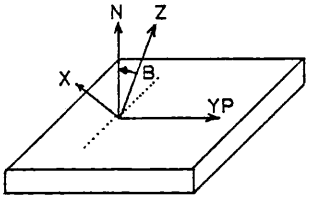

Y AXIS BOULE
(90,B,0)

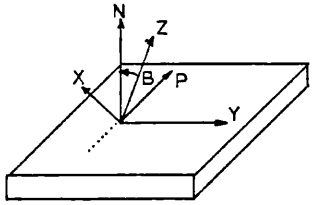

Y AXIS CYLINDER
(90,B,90)

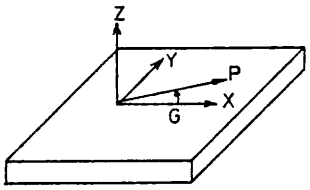

Z CUT
(0,0,G)

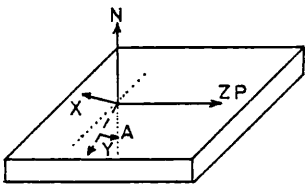

Z AXIS BOULE
(A,90,90)

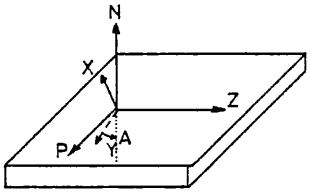

Z AXIS CYLINDER
(A,90,0)

Appendix 3.1 Berlinite SAW properties (0, β ,0) X axis boule.

α	β (deg)	γ	v(SAW) (m/s)	Δv/v (10^{-4})	φ (deg)	∂φ/∂θ (deg/deg)	TCD (ppm/°C)	v(bulk) (m/s)
0	0	0	2831.4	1.47	0	1.293	18.71	2856.9
0	5	0	2840.6	0.52	0	1.551	16.26	"
0	10	0	-					"
0	15	0	-					"
0	20	0	-					"
0	25	0	-					"
0	30	0	-					"
0	35	0	-					"
0	40	0	-					"
0	45	0	2851.9	11.62	0	3.066	3.96	"
0	50	0	2842.4	18.74	0	2.697	1.70	"
0	55	0	2828.7	23.94	0	2.257	0.25	"
0	60	0	2812.7	26.97	0	1.858	-0.36	"
0	65	0	2796.2	28.31	0	1.529	-0.41	"
0	70	0	2780.6	28.51	0	1.269	-0.06	"
0	75	0	2766.8	28.00	0	1.068	0.58	"
0	80	0	2755.1	27.09	0	0.912	1.50	"
0	85	0	2745.8	25.99	0	0.789	2.68	"
0	90	0	2738.9	24.81	0	0.691	4.09	"
0	95	0	2734.1	23.63	0	0.612	5.74	"
0	100	0	2731.1	22.46	0	0.548	7.57	"
0	105	0	2729.8	21.34	0	0.497	9.57	"
0	110	0	2729.8	20.24	0	0.459	11.66	"
0	115	0	2731.0	19.18	0	0.431	13.79	"
0	120	0	2733.3	18.15	0	0.414	15.90	"
0	125	0	2736.6	17.14	0	0.406	17.92	"
0	130	0	2741.0	16.12	0	0.409	19.81	"
0	135	0	2746.5	15.05	0	0.421	21.43	"
0	140	0	2753.0	13.89	0	0.443	22.75	"
0	145	0	2760.6	12.61	0	0.477	23.71	"
0	150	0	2769.2	11.18	0	0.525	24.30	"
0	155	0	2778.7	9.60	0	0.588	24.45	"
0	160	0	2788.8	7.91	0	0.671	24.22	"
0	165	0	2799.4	6.15	0	0.777	23.52	"
0	170	0	2810.3	4.41	0	0.912	22.39	"
0	175	0	2821.1	2.81	0	1.081	20.78	"

Appendix 3.2 Berlinite SAW properties (0,0,γ) Z cut plate.

α	β (deg)	γ	v(SAW) (m/s)	Δv/v (10^{-4})	φ (deg)	∂φ/∂θ (deg/deg)	TCD (ppm/°C)	v(bulk) (m/s)
0	0	0	2831.4	1.47	0	1.293	18.71	2856.9
0	0	5	2845.2	2.17	6.29	1.191	18.81	2881.0
0	0	10	2885.2	4.16	11.63	0.925	18.94	2950.5
0	0	15	2947.1	7.12	15.41	0.575	18.43	3057.5
0	0	20	3024.4	10.49	17.29	0.161	15.81	3189.0
0	0	25	3107.0	13.31	16.22	-0.892	5.04	3321.3
0	0	30	-					3390.2
0	0	35	3107.0	13.31	-16.22	-1.663	5.07	3321.3
0	0	40	3024.4	10.49	-17.29	0.161	15.84	3189.0
0	0	45	2947.1	7.12	-15.41	0.575	18.46	3057.5
0	0	50	2885.2	4.16	-11.63	0.925	18.99	2950.5
0	0	55	2845.2	2.17	-6.29	1.191	18.87	2881.0
0	0	60	2831.4	1.47	0	1.293	18.77	2856.9
0	0	65	2845.2	2.17	6.29	1.191	18.86	2881.0
0	0	70	2885.2	4.16	11.63	0.926	18.98	2950.5
0	0	75	2947.1	7.12	15.41	0.575	18.45	3057.5
0	0	80	3024.4	10.49	17.29	0.161	15.81	3189.0
0	0	85	3107.0	13.31	16.22	-0.892	5.02	3221.3
0	0	90	-					3390.2

Appendix 3.3 Berlinite SAW properties (0,10,γ).

α	β (deg)	γ	v(SAW) (m/s)	$\Delta v/v$ (10^{-4})	ϕ (deg)	$\partial\phi/\partial\theta$ (deg/deg)	TCD (ppm/°C)	v(bulk) (m/s)
0	10	0	-					2856.9
0	10	5	-					2886.2
0	10	10	-					2970.5
0	10	15	3012.7	5.98	20.61	2.518	12.93	3099.9
0	10	20	3118.1	9.10	21.71	-0.248	9.35	3258.0
0	10	25	3212.8	11.04	11.67	-6.129	-3.60	3419.6
0	10	30	3191.9	16.98	-13.10	-1.137	19.09	3519.7
0	10	35	3119.6	15.83	-15.60	-0.187	24.34	3477.4
0	10	40	3043.5	13.22	-15.77	0.104	25.13	3353.7
0	10	45	2971.7	9.99	-14.59	0.372	24.65	3215.0
0	10	50	2910.4	6.82	-12.05	0.641	23.62	3086.2
0	10	55	2864.9	4.32	-8.23	0.877	22.45	2981.6
0	10	60	2839.2	2.91	-3.43	1.023	21.43	2909.0
0	10	65	2835.6	2.76	1.77	1.029	20.55	2876.5
0	10	70	2854.0	3.83	6.60	0.880	19.48	2885.6
0	10	75	2891.9	5.93	10.32	0.583	17.31	2933.5
0	10	80	2943.3	8.75	12.05	0.037	11.81	3011.9
0	10	85	2994.4	10.45	8.91	-18.835	-2.21	3101.2
0	10	90	-					3149.8

Appendix 3.4 Berlinite SAW properties (0,20,γ).

α	β (deg)	γ	v(SAW) (m/s)	$\Delta v/v$ (10^{-4})	ϕ (deg)	$\partial\phi/\partial\theta$ (deg/deg)	TCD (ppm/°C)	v(bulk) (m/s)
0	20	0	-					2856.9
0	20	5	-					2890.3
0	20	10	-					2986.3
0	20	15	-					3133.1
0	20	20	3207.9	10.15	19.20	-1.466	6.05	3313.2
0	20	25	3230.2	16.91	-6.21	-1.996	24.89	3500.0
0	20	30	3185.0	18.24	-10.96	-0.456	30.47	3640.3
0	20	35	3127.4	17.42	-12.43	-0.173	31.76	3652.0
0	20	40	-					3560.1
0	20	45	3007.1	12.72	-12.28	0.195	30.44	3432.8
0	20	50	2953.6	9.68	-10.77	0.400	28.85	3299.5
0	20	55	2910.3	6.87	-8.30	0.584	27.01	3174.4
0	20	60	2880.5	4.78	-5.02	0.717	25.19	3067.6
0	20	65	2866.6	3.70	-1.28	0.759	23.34	2986.9
0	20	70	2869.1	3.76	2.35	0.666	21.12	2937.0
0	20	75	2885.9	4.95	5.05	0.373	17.57	2919.5
0	20	80	2910.3	7.14	5.39	-0.339	10.83	2930.1
0	20	85	2926.6	7.17	1.24	1.902	1.97	2956.2
0	20	90	-					2971.4

Appendix 3.5 Berlinite SAW properties (0,30,γ).

α	β (deg)	γ	v(SAW) (m/s)	Δv/v (10^{-4})	φ (deg)	∂φ/∂θ (deg/deg)	TCD (ppm/°C)	v(bulk) (m/s)
0	30	0	-					2856.9
0	30	5	-					2892.8
0	30	10	2990.1	2.32	25.87	3.779	6.36	2995.9
0	30	15	3134.3	11.84	28.57	-1.496	1.06	3153.8
0	30	20	3220.6	22.66	2.95	-3.772	11.11	3348.1
0	30	25	3208.7	20.85	-5.49	-0.706	26.58	3554.2
0	30	30	3175.6	19.41	-7.72	-0.282	32.82	3732.5
0	30	35	3135.5	18.10	-8.70	-0.123	35.75	3816.3
0	30	40	3093.0	16.51	-9.02	-0.008	36.88	3783.9
0	30	45	3050.7	14.46	-8.78	0.104	36.71	3689.5
0	30	50	3011.5	11.97	-7.98	0.218	35.53	3568.9
0	30	55	2977.9	9.27	-6.61	0.326	33.61	3438.3
0	30	60	2951.9	6.74	-4.76	0.406	31.09	3308.5
0	30	65	-					3188.1
0	30	70	2927.8	3.64	-0.78	-0.091	24.17	3083.8
0	30	75	2926.5	3.85	-0.16	-0.116	18.78	3000.4
0	30	80	2921.8	5.51	-2.49	-0.759	12.71	2940.6
0	30	85	2904.2	4.25	-4.52	3.016	12.89	2905.1
0	30	90	-					2893.4

Appendix 3.6 Berlinite SAW properties (0,40,γ).

α	β (deg)	γ	v(SAW) (m/s)	$\Delta v/v$ (10^{-4})	ϕ (deg)	$\partial\phi/\partial\theta$ (deg/deg)	TCD (ppm/°C)	v(bulk) (m/s)
0	40	0	-					2856.9
0	40	5	2892.0	6.40	15.62	5.105	6.03	2893.4
0	40	10	2992.3	14.37	25.59	1.063	3.28	2998.4
0	40	15	3117.5	30.90	20.55	-3.615	-3.92	3159.4
0	40	20	3173.1	28.84	3.92	-2.014	10.92	3359.1
0	40	25	3175.2	22.82	-1.93	-0.634	25.01	3575.6
0	40	30	3160.2	19.30	-3.95	-0.243	33.25	3780.4
0	40	35	3139.1	17.07	-4.71	-0.079	38.42	3929.9
0	40	40	3116.1	15.40	-4.85	0.016	41.72	3962.9
0	40	45	3093.6	13.87	-4.60	0.083	43.59	3850.0
0	40	50	3073.1	12.21	-4.05	0.134	44.17	3721.9
0	40	55	3055.9	10.26	-3.29	0.165	43.50	3583.6
0	40	60	3042.6	7.97	-2.45	0.161	41.42	3442.6
0	40	65	3032.8	5.39	-1.84	0.062	37.51	3306.9
0	40	70	3024.0	2.81	-2.28	-0.314	30.91	3183.9
0	40	75	3007.0	1.86	-5.84	-0.527	22.33	3080.1
0	40	80	2968.5	3.73	-10.14	-0.177	22.27	3001.3
0	40	85	-					2952.6
0	40	90	-					2935.3

Appendix 3.7 Berlinite SAW properties (0,50,γ).

α	β (deg)	γ	v(SAW) (m/s)	$\Delta v/v$ (10^{-4})	ϕ (deg)	$\partial\phi/\partial\theta$ (deg/deg)	TCD (ppm/°C)	v(bulk) (m/s)
0	50	0	2842.4	18.74	0	2.697	1.70	2856.9
0	50	5	2870.9	20.95	12.51	2.120	1.30	2892.1
0	50	10	2947.2	27.28	19.57	0.549	-0.18	2993.3
0	50	15	3038.0	32.60	17.02	-1.470	0.44	3149.4
0	50	20	3098.9	29.08	8.52	-1.553	10.14	3344.6
0	50	25	3124.2	22.57	2.78	-0.777	22.51	3560.6
0	50	30	3130.2	17.63	0.14	-0.322	32.36	3776.4
0	50	35	3128.0	14.31	-0.91	-0.111	39.70	3893.9
0	50	40	3122.9	12.05	-1.14	0.007	45.20	3779.5
0	50	45	3117.9	10.44	-0.92	0.075	49.30	3664.2
0	50	50	3114.6	9.15	-0.45	0.108	52.19	3552.0
0	50	55	3113.8	7.91	0.12	0.111	53.98	3446.5
0	50	60	3115.5	6.44	0.58	0.063	54.63	3351.2
0	50	65	3118.5	4.42	0.52	-0.136	53.73	3268.7
0	50	70	3117.1	1.58	-1.78	-0.967	49.70	3201.2
0	50	75	3092.3	0.85	-9.14	-1.386	42.14	3149.8
0	50	80	3040.3	2.54	-11.30	0.459	41.33	3114.3
0	50	85	-					3093.8
0	50	90	-					3087.1

Appendix 3.8 Berlinite SAW properties (0,60,γ).

α	β (deg)	γ	v(SAW) (m/s)	$\Delta v/v$ (10^{-4})	ϕ (deg)	$\partial\phi/\partial\theta$ (deg/deg)	TCD (ppm/°C)	v(bulk) (m/s)
0	60	0	2812.7	26.97	0	1.858	-0.36	2856.9
0	60	5	2832.1	27.78	8.71	1.516	-0.20	2888.9
0	60	10	2884.5	29.50	14.26	0.638	0.47	2981.3
0	60	15	2952.6	29.87	14.81	-0.392	2.99	3124.7
0	60	20	3013.9	26.58	11.22	-0.912	9.57	3305.5
0	60	25	3055.7	20.89	6.85	-0.764	19.60	3508.4
0	60	30	3086.1	15.49	3.83	-0.447	29.97	3713.7
0	60	35	3093.9	11.41	2.24	-0.206	39.00	3729.3
0	60	40	3102.7	8.57	1.62	-0.055	46.31	3616.9
0	60	45	3110.1	6.66	1.59	0.034	51.98	3512.5
0	60	50	3118.3	5.40	1.88	0.076	56.24	3422.5
0	60	55	3128.2	4.51	2.28	0.077	59.23	3350.7
0	60	60	3139.9	3.78	2.57	0.029	61.05	3299.6
0	60	65	3152.1	3.05	2.43	-0.103	61.78	3270.0
0	60	70	3161.6	2.35	1.26	-0.406	61.40	3261.0
0	60	75	3161.0	2.12	-1.89	-0.826	59.99	3269.1
0	60	80	3142.4	2.28	-5.46	-0.373	58.65	3287.6
0	60	85	-					3306.6
0	60	90	-					3314.7

Appendix 3.9 Berlinite SAW properties (0,70,γ).

α	β (deg)	γ	v(SAW) (m/s)	$\Delta v/v$ (10^{-4})	ϕ (deg)	$\partial\phi/\partial\theta$ (deg/deg)	TCD (ppm/°C)	v(bulk) (m/s)
0	70	0	2780.6	28.51	0	1.269	-0.06	2856.9
0	70	5	2793.8	28.52	6.06	1.100	0.34	2884.3
0	70	10	2830.5	28.27	10.53	0.650	1.62	2963.7
0	70	15	2882.0	27.05	12.34	0.068	4.19	3087.7
0	70	20	2936.2	24.06	11.37	-0.419	8.99	3245.2
0	70	25	2982.3	19.45	8.70	-0.586	16.68	3422.6
0	70	30	3015.8	14.46	6.01	-0.461	26.37	3589.9
0	70	35	3039.1	10.21	4.25	-0.243	36.24	3576.5
0	70	40	3056.8	7.07	3.53	-0.052	45.11	3478.4
0	70	45	3073.3	4.95	3.63	0.083	52.42	3394.1
0	70	50	3091.7	3.61	4.27	0.162	58.14	3333.8
0	70	55	3114.0	2.82	5.17	0.191	62.37	3301.0
0	70	60	3141.0	2.39	6.10	0.175	65.36	3296.6
0	70	65	3172.3	2.12	6.85	0.116	67.27	3319.1
0	70	70	3206.8	1.92	7.19	0.011	68.34	3364.8
0	70	75	3241.8	1.77	6.82	-0.182	68.99	3426.9
0	70	80	3272.0	1.75	4.96	-0.622	69.98	3494.9
0	70	85	-					3552.4
0	70	90	-					3576.1

Appendix 3.10 Berlinite SAW properties (0,80,γ).

α	β (deg)	γ	v(SAW) (m/s)	$\Delta v/v$ (10^{-4})	ϕ (deg)	$\partial\phi/\partial\theta$ (deg/deg)	TCD (ppm/°C)	v(bulk) (m/s)
0	80	0	2755.1	27.09	0	0.912	1.50	2856.9
0	80	5	2764.6	26.87	4.41	0.824	1.93	2878.8
0	80	10	2791.3	26.13	7.98	0.580	3.20	2942.6
0	80	15	2830.9	24.72	10.02	0.224	5.41	3042.6
0	80	20	2875.9	22.40	10.16	-0.163	8.92	3170.2
0	80	25	2918.2	19.06	8.59	-0.431	14.36	3312.7
0	80	30	2951.7	15.04	6.32	-0.426	22.26	3435.9
0	80	35	2976.3	11.10	4.71	-0.198	31.92	3431.1
0	80	40	2996.5	7.80	4.40	0.067	41.96	3356.9
0	80	45	3018.3	5.28	5.25	0.257	51.18	3298.1
0	80	50	3046.1	3.51	6.80	0.347	58.97	3270.3
0	80	55	3082.2	2.36	8.58	0.349	65.02	3276.7
0	80	60	3127.1	1.68	10.18	0.283	69.46	3316.3
0	80	65	3179.6	1.32	11.34	0.175	72.30	3385.3
0	80	70	3237.4	1.11	11.88	0.040	73.67	3477.3
0	80	75	3297.2	0.90	11.69	-0.123	73.79	3584.2
0	80	80	3354.7	0.62	10.53	-0.367	72.73	3694.9
0	80	85	3402.7	0.25	7.47	-0.961	70.48	3790.7
0	80	90	-					3833.7

Appendix 3.11 Berlinite SAW properties (0,90,γ) Y cut plate.

α	β (deg)	γ	v(SAW) (m/s)	$\Delta v/v$ (10^{-4})	ϕ (deg)	$\partial\phi/\partial\theta$ (deg/deg)	TCD (ppm/°C)	v(bulk) (m/s)
0	90	0	2738.9	24.81	0	0.691	4.09	2856.9
0	90	5	2746.0	24.60	3.37	0.639	4.46	2873.1
0	90	10	2766.5	23.97	6.23	0.488	5.53	2920.4
0	90	15	2797.4	22.95	8.10	0.249	7.25	2994.8
0	90	20	2834.1	21.49	8.60	-0.056	9.62	3089.6
0	90	25	2870.0	19.47	7.56	-0.347	13.12	3193.4
0	90	30	2898.9	16.73	5.49	-0.426	18.69	3278.2
0	90	35	2919.3	13.39	3.89	-0.168	27.01	3285.3
0	90	40	2936.2	9.97	4.02	0.216	37.39	3239.9
0	90	45	2957.9	6.93	5.81	0.466	48.15	3207.9
0	90	50	2990.0	4.48	8.34	0.515	57.84	3210.1
0	90	55	3034.3	2.69	10.70	0.408	65.65	3249.8
0	90	60	3089.0	1.53	12.28	0.213	71.24	3324.1
0	90	65	3150.0	0.87	12.77	-0.018	74.71	3427.0
0	90	70	3211.7	0.53	12.10	-0.250	76.33	3549.9
0	90	75	3268.1	0.33	10.30	-0.464	76.60	3683.8
0	90	80	3313.5	0.17	7.51	-0.643	76.10	3819.4
0	90	85	3342.9	0.05	3.97	-0.764	75.47	3947.4
0	90	90	-					4059.3

Appendix 3.12 Berlinite SAW properties (0,100,γ).

α	β (deg)	γ	v(SAW) (m/s)	$\Delta v/v$ (10^{-4})	ϕ (deg)	$\partial\phi/\partial\theta$ (deg/deg)	TCD (ppm/°C)	v(bulk) (m/s)
0	100	0	2731.1	22.46	0	0.548	7.57	2856.9
0	100	5	2736.8	22.35	2.68	0.513	7.85	2867.2
0	100	10	2753.1	22.02	5.01	0.408	8.63	2899.9
0	100	15	2778.0	21.54	6.64	0.231	9.73	2930.1
0	100	20	2808.1	20.96	7.20	-0.018	11.10	3013.6
0	100	25	2837.9	20.17	6.39	-0.306	12.85	3081.1
0	100	30	2861.6	18.76	4.36	-0.456	16.06	3132.8
0	100	35	2876.2	16.23	2.54	-0.196	22.32	3140.8
0	100	40	2887.1	12.77	2.84	0.317	32.09	3118.1
0	100	45	2904.6	9.19	5.35	0.628	43.58	3108.1
0	100	50	2935.8	6.08	8.54	0.598	54.47	3131.6
0	100	55	2980.6	3.68	10.97	0.352	63.27	3191.5
0	100	60	3034.5	2.05	11.97	0.050	69.46	3282.6
0	100	65	3090.7	1.06	11.55	-0.205	73.24	3394.7
0	100	70	3142.9	0.52	10.06	-0.378	75.23	3515.1
0	100	75	3186.7	0.25	7.90	-0.475	76.07	3629.5
0	100	80	3219.4	0.10	5.39	-0.522	76.32	3723.7
0	100	85	3239.4	0.02	2.72	-0.541	76.35	3785.4
0	100	90	-					3806.9

Appendix 3.13 Berlinite SAW properties (0,110,γ).

α	β (deg)	γ	v(SAW) (m/s)	$\Delta v/v$ (10^{-4})	ϕ (deg)	$\partial\phi/\partial\theta$ (deg/deg)	TCD (ppm/°C)	v(bulk) (m/s)
0	110	0	2729.8	20.24	0	0.459	11.66	2856.9
0	110	5	2734.5	20.22	2.25	0.432	11.81	2863.8
0	110	10	2748.2	20.20	4.23	0.350	12.20	2883.6
0	110	15	2769.3	20.23	5.65	0.208	12.70	2914.5
0	110	20	2794.8	20.38	6.19	-0.005	13.08	2952.6
0	110	25	2820.4	20.61	5.48	-0.285	13.34	2990.8
0	110	30	2840.0	20.44	3.44	-0.494	14.35	3016.1
0	110	35	2849.9	18.87	1.30	-0.263	18.26	3015.9
0	110	40	2854.9	15.53	1.54	0.373	26.73	3001.4
0	110	45	2867.5	11.53	4.56	0.751	38.11	3001.9
0	110	50	2895.9	7.92	8.19	0.630	49.48	3033.5
0	110	55	2938.4	5.07	10.45	0.257	58.71	3096.6
0	110	60	2987.6	3.05	10.82	-0.089	65.18	3182.0
0	110	65	3035.8	1.74	9.80	-0.296	69.17	3275.9
0	110	70	3077.9	0.95	8.06	-0.383	71.43	3364.2
0	110	75	3111.4	0.47	6.07	-0.407	72.68	3437.0
0	110	80	3135.5	0.20	4.03	-0.407	73.34	3489.6
0	110	85	3150.0	0.05	2.01	-0.402	73.66	3521.0
0	110	90	-					3531.4

Appendix 3.14 Berlinite SAW properties (0,120,γ).

α	β (deg)	γ	v(SAW) (m/s)	$\Delta v/v$ (10^{-4})	ϕ (deg)	$\partial\phi/\partial\theta$ (deg/deg)	TCD (ppm/°C)	v(bulk) (m/s)
0	120	0	2733.3	18.15	0	0.414	15.90	2856.9
0	120	5	2737.5	18.21	2.03	0.391	15.93	2861.2
0	120	10	2749.5	18.44	3.83	0.320	15.99	2873.6
0	120	15	2769.0	18.81	5.14	0.146	15.88	2892.5
0	120	20	2792.3	19.49	5.67	0.004	15.36	2914.9
0	120	25	2815.8	20.45	5.04	-0.270	14.33	2935.0
0	120	30	2833.6	21.27	2.98	-0.528	13.36	2943.8
0	120	35	2840.8	20.66	0.51	-0.344	14.89	2934.7
0	120	40	2841.7	17.67	0.58	0.411	21.53	2919.3
0	120	45	2851.0	13.49	4.09	0.881	32.11	2921.0
0	120	50	2878.3	9.65	8.19	0.662	43.36	2952.7
0	120	55	2920.3	6.57	10.22	0.146	52.88	3011.8
0	120	60	2966.6	4.27	9.91	-0.228	59.67	3086.1
0	120	65	3008.8	2.66	8.35	-0.362	63.93	3161.0
0	120	70	3043.2	1.58	6.49	-0.370	66.47	3225.7
0	120	75	3069.3	0.85	4.71	-0.343	67.97	3275.8
0	120	80	3087.5	0.37	3.06	-0.319	68.86	3310.8
0	120	85	3098.2	0.09	1.50	-0.304	69.34	3331.3
0	120	90	-					3338.0

Appendix 3.15 Berlinite SAW properties (0,130,γ).

α	β (deg)	γ	v(SAW) (m/s)	Δv/v (10^{-4})	φ (deg)	∂φ/∂θ (deg/deg)	TCD (ppm/°C)	v(bulk) (m/s)
0	130	0	2741.0	16.12	0	0.409	19.81	2856.9
0	130	5	2745.2	16.23	2.01	0.387	19.72	2860.6
0	130	10	2757.5	16.59	3.79	0.320	19.50	2871.1
0	130	15	2776.5	17.23	5.12	0.202	18.89	2887.1
0	130	20	2799.9	18.25	5.70	0.019	17.63	2905.6
0	130	25	2823.7	19.65	5.15	-0.254	15.49	2921.3
0	130	30	2842.1	21.12	3.09	-0.556	12.83	2926.0
0	130	35	2849.2	21.25	0.28	-0.435	12.01	2913.5
0	130	40	2848.4	18.62	0.10	0.436	16.38	2895.3
0	130	45	2856.6	14.50	4.20	1.065	25.19	2896.1
0	130	50	2886.5	10.84	9.11	0.754	35.63	2930.1
0	130	55	2932.9	7.94	10.95	-0.016	45.73	2994.3
0	130	60	2980.5	5.53	9.60	-0.435	53.54	3073.4
0	130	65	3019.4	3.66	7.30	-0.446	58.41	3148.8
0	130	70	3048.4	2.28	5.29	-0.357	61.25	3209.3
0	130	75	3069.2	1.28	3.68	-0.290	62.92	3253.2
0	130	80	3083.3	0.58	2.34	-0.251	63.91	3282.4
0	130	85	3091.4	0.15	1.14	-0.232	64.44	3299.2
0	130	90	-					3304.6

Appendix 3.16 Berlinite SAW properties (0,140,γ).

α	β (deg)	γ	v(SAW) (m/s)	Δv/v (10^{-4})	φ (deg)	∂φ/∂θ (deg/deg)	TCD (ppm/°C)	v(bulk) (m/s)
0	140	0	2753.0	13.89	0	0.443	22.75	2856.9
0	140	5	2757.6	14.05	2.18	0.420	22.62	2862.0
0	140	10	2771.0	14.55	4.12	0.350	22.18	2876.6
0	140	15	2791.9	15.41	5.60	0.231	21.25	2899.0
0	140	20	2819.8	16.69	6.32	0.046	19.47	2925.7
0	140	25	2844.7	18.42	5.89	-0.236	16.46	2950.7
0	140	30	2866.6	20.28	3.82	-0.591	12.25	2962.7
0	140	35	2876.2	20.72	0.53	-0.564	9.01	2949.6
0	140	40	2875.4	17.95	-0.15	0.384	10.56	2922.3
0	140	45	2882.8	13.60	4.33	1.293	16.01	2914.6
0	140	50	2917.3	10.26	11.08	1.195	23.21	2948.6
0	140	55	2977.1	8.67	13.84	-0.271	34.52	3027.1
0	140	60	3033.5	6.81	9.89	-0.935	47.26	3137.9
0	140	65	3070.5	4.68	6.25	-0.525	53.94	3253.8
0	140	70	3094.8	3.05	4.24	-0.312	57.00	3343.9
0	140	75	3111.5	1.78	2.92	-0.231	58.58	3400.8
0	140	80	3122.8	0.82	1.86	-0.198	59.46	3434.4
0	140	85	3129.4	0.21	0.91	-0.184	59.92	3452.4
0	140	90	-					3458.2

Appendix 3.17 Berlinite SAW properties (0,150,γ).

α	β (deg)	γ	v(SAW) (m/s)	$\Delta v/v$ (10^{-4})	ϕ (deg)	$\partial\phi/\partial\theta$ (deg/deg)	TCD (ppm/°C)	v(bulk) (m/s)
0	150	0	2769.2	11.18	0	0.525	24.30	2856.9
0	150	5	2774.7	11.42	2.58	0.498	24.17	2865.2
0	150	10	2790.7	12.13	4.89	0.418	23.68	2889.1
0	150	15	2815.7	13.29	6.67	0.285	22.62	2926.2
0	150	20	2847.1	14.92	7.64	0.088	20.56	2971.8
0	150	25	2880.5	17.02	7.37	-0.219	16.78	3017.0
0	150	30	2909.2	19.17	5.17	-0.677	10.82	3042.7
0	150	35	2923.3	19.24	0.99	-0.857	4.44	3019.6
0	150	40	2920.4	14.96	-1.62	-0.099	2.73	2963.7
0	150	45	2914.7	8.11	-0.50	0.496	4.90	2927.0
0	150	50	2921.2	1.97	4.27	1.459	8.32	2937.3
0	150	55	2958.9	0.35	12.62	1.824	11.29	3002.4
0	150	60	-					3119.1
0	150	65	3120.2	4.98	12.67	-0.690	44.38	3277.7
0	150	70	3160.1	4.59	5.56	-0.638	55.82	3462.7
0	150	75	3181.2	2.87	3.45	-0.303	57.17	3643.2
0	150	80	3194.7	1.36	2.15	-0.223	57.43	3731.5
0	150	85	3202.4	0.35	1.04	-0.212	57.48	3756.0
0	150	90	-					3762.6

Appendix 3.18 Berlinite SAW properties (0,160,γ).

α	β (deg)	γ	v(SAW) (m/s)	$\Delta v/v$ (10^{-4})	ϕ (deg)	$\partial\phi/\partial\theta$ (deg/deg)	TCD (ppm/°C)	v(bulk) (m/s)
0	160	0	2788.8	7.91	0	0.671	24.22	2856.9
0	160	5	2795.9	8.27	3.29	0.634	24.13	2869.8
0	160	10	2816.5	9.33	6.23	0.531	23.74	2907.2
0	160	15	2848.7	10.98	8.51	0.369	22.79	2965.2
0	160	20	2889.5	13.16	9.81	0.140	20.59	3036.9
0	160	25	2933.9	15.75	9.69	-0.224	15.98	3109.2
0	160	30	2973.0	18.02	6.95	-0.963	7.00	3147.9
0	160	35	2989.9	15.93	-0.24	-1.738	-4.35	3100.4
0	160	40	2969.7	9.10	-8.33	-1.325	-4.02	3006.7
0	160	45	2924.4	3.61	-9.92	-0.639	5.21	2931.9
0	160	50	-					2902.1
0	160	55	2891.2	0.05	4.16	22.054	5136.97	2926.7
0	160	60	-					3006.0
0	160	65	2998.1	2.66	17.64	2.674	20.36	3133.4
0	160	70	3088.7	6.34	19.28	-0.164	29.16	3297.5
0	160	75	3177.4	8.26	15.78	-1.171	43.32	3483.3
0	160	80	3239.8	5.32	9.26	-1.257	55.26	3671.2
0	160	85	3271.9	1.46	3.95	-0.883	59.87	3830.2
0	160	90	-					3900.5

Appendix 3.19 Berlinite SAW properties (0,170,γ).

α	β (deg)	γ	v(SAW) (m/s)	$\Delta v/v$ (10^{-4})	ϕ (deg)	$\partial\phi/\partial\theta$ (deg/deg)	TCD (ppm/°C)	v(bulk) (m/s)
0	170	0	2810.3	4.42	0	0.912	22.39	2856.9
0	170	5	2820.0	4.95	4.46	0.855	22.37	2875.3
0	170	10	2848.2	6.48	8.39	0.700	22.24	2928.5
0	170	15	2892.1	8.81	11.35	0.475	21.51	3010.8
0	170	20	2947.8	11.66	13.03	0.185	19.25	3112.4
0	170	25	3008.5	14.74	12.88	-0.320	13.04	3214.5
0	170	30	3060.2	15.91	7.58	-2.285	-3.85	3255.0
0	170	35	3061.5	9.09	-7.05	-2.745	-14.62	3196.4
0	170	40	3003.0	7.78	-15.56	-0.377	2.85	3075.1
0	170	45	2932.1	4.67	-14.18	0.727	11.53	2966.5
0	170	50	2878.7	2.12	-9.16	1.236	14.53	2894.7
0	170	55	2853.2	0.64	-2.23	1.493	15.79	2871.4
0	170	60	2859.9	0.63	5.28	1.461	16.87	2900.7
0	170	65	2898.6	2.08	11.94	1.169	18.32	2980.7
0	170	70	2964.9	4.97	16.74	0.737	20.46	3103.4
0	170	75	3051.2	8.62	19.26	0.269	23.52	3256.8
0	170	80	3147.4	11.41	19.40	-0.222	28.48	3424.1
0	170	85	3239.4	10.09	16.57	-1.065	40.16	3577.7
0	170	90	-					3651.8

Appendix 3.20 Berlinite SAW properties (α,90,0) Z axis cylinder.

α	β (deg)	γ	v(SAW) (m/s)	Δv/v (10^{-4})	ϕ (deg)	∂ϕ/∂θ (deg/deg)	TCD (ppm/°C)	v(bulk) (m/s)
0	90	0	2738.9	24.81	0	0.691	4.09	2856.9
5	90	0	2743.6	25.05	1.85	0.676	3.86	2881.0
10	90	0	2757.3	25.78	3.62	0.633	3.15	2950.5
15	90	0	2778.3	27.08	5.25	0.564	1.84	3057.5
20	90	0	2802.7	28.70	6.61	0.478	0.05	3189.0
25	90	0	2823.7	30.43	7.54	0.399	-1.85	3321.3
30	90	0	2832.2	31.22	7.88	0.352	-2.80	3390.2
35	90	0	2823.7	30.43	7.54	0.399	-1.85	3321.3
40	90	0	2802.7	28.70	6.61	0.478	0.07	3189.0
45	90	0	2778.3	27.02	5.25	0.564	1.90	3057.5
50	90	0	2757.3	25.78	3.62	0.633	3.17	2950.5
55	90	0	2743.6	25.05	1.85	0.676	3.88	2881.0
60	90	0	2738.9	24.81	0	0.691	4.13	2856.9
65	90	0	2743.6	25.05	-1.85	0.676	3.88	2881.0
70	90	0	2757.3	25.78	-3.62	0.633	3.17	2950.5
75	90	0	2778.3	27.02	-5.25	0.564	1.88	3037.5
80	90	0	2802.7	28.70	-6.61	0.478	0.05	3189.0
85	90	0	2823.7	30.43	-7.54	0.399	-1.87	3321.3
90	90	0	2832.2	31.22	-7.88	0.352	-2.78	3390.2

Appendix 3.21 Berlinite SAW properties (90,β,0) Y axis boule.

α	β (deg)	γ	v(SAW) (m/s)	Δv/v (10^{-4})	ϕ (deg)	∂ϕ/∂θ (deg/deg)	TCD (ppm/°C)	v(bulk) (m/s)
90	0	0	-					3390.2
90	5	0	3144.8	14.83	8.00	-4.295	-10.81	"
90	10	0	3116.5	18.15	11.17	-1.498	6.12	"
90	15	0	3085.1	19.52	10.96	-0.806	12.51	"
90	20	0	3055.1	20.75	10.09	-0.557	14.99	"
90	25	0	3027.3	22.02	9.04	-0.434	15.84	"
90	30	0	3001.8	23.34	7.90	-0.360	15.79	"
90	35	0	2978.3	24.68	6.68	-0.311	15.12	"
90	40	0	2956.7	25.98	5.37	-0.275	14.01	"
90	45	0	2936.7	27.20	3.93	-0.247	12.48	"
90	50	0	2918.1	28.31	2.36	-0.221	10.60	"
90	55	0	2900.8	29.26	0.67	-0.188	8.43	"
90	60	0	2884.9	30.03	-1.10	-0.139	6.10	"
90	65	0	2870.5	30.60	-2.87	-0.066	3.77	"
90	70	0	2857.7	30.97	-4.51	0.034	1.60	"
90	75	0	2847.1	31.16	-5.92	0.149	-0.24	"
90	80	0	2839.0	31.22	-6.99	0.258	-1.64	"
90	85	0	2834.0	31.23	-7.66	0.335	-2.49	"
90	90	0	2832.2	31.22	-7.88	0.364	-2.78	"

Appendix 3.22 Berlinite SAW properties (90,β,90) Y axis cylinder.

α	β (deg)	γ	v(SAW) (m/s)	Δv/v (10^{-4})	ϕ (deg)	∂ϕ/∂θ (deg/deg)	TCD (ppm/°C)	v(bulk) (m/s)
90	0	90	2831.4	1.47	0	1.293	18.71	2856.9
90	5	90	2837.6	1.51	-2.51	1.269	18.92	2873.1
90	10	90	-					2920.4
90	15	90	2887.4	1.84	-7.20	1.978	20.71	2994.8
90	20	90	2930.6	2.24	-9.12	0.867	22.83	3089.6
90	25	90	2984.7	2.97	-10.32	0.542	26.83	3193.4
90	30	90	3044.4	4.49	-9.69	-0.024	35.57	3278.2
90	35	90	3088.4	6.63	-5.83	-0.331	51.56	3285.3
90	40	90	3094.8	6.36	-4.07	-0.343	58.92	3239.9
90	45	90	3090.0	5.37	-3.69	-0.412	61.16	3207.9
90	50	90	3090.9	4.57	-2.98	-0.414	63.40	3210.1
90	55	90	3101.7	3.94	-1.97	-0.405	65.87	3249.8
90	60	90	3123.4	3.40	-0.76	-0.402	68.40	3324.2
90	65	90	3155.4	2.93	0.60	-0.409	70.83	3427.0
90	70	90	3196.3	2.53	2.06	-0.425	72.94	3549.9
90	75	90	3243.1	2.20	3.58	-0.446	74.60	3683.8
90	80	90	3289.8	1.97	5.07	-0.462	75.62	3819.4
90	85	90	3326.6	1.84	6.29	-0.467	75.96	3947.4
90	90	90	3341.0	1.80	6.79	-0.465	75.99	4059.3

Appendix 3.23 Berlinite SAW properties (α,90,90) Z axis boule

α	β (deg)	γ	v(SAW) (m/s)	Δv/v (10^{-4})	ϕ (deg)	∂ϕ/∂θ (deg/deg)	TCD (ppm/°C)	v(bulk) (m/s)
0	90	90	-					4059.3
5	90	90	3352.2	0.12	-1.99	-0.776	75.26	"
10	90	90	3349.8	0.46	-3.73	-0.698	75.43	"
15	90	90	3346.7	0.91	-5.10	-0.607	75.62	"
20	90	90	3343.8	1.36	-6.05	-0.530	75.82	"
25	90	90	3341.7	1.68	-6.61	-0.481	75.94	"
30	90	90	3341.0	1.80	-6.79	-0.465	75.99	"
35	90	90	3341.7	1.68	-6.61	-0.481	75.94	"
40	90	90	3343.8	1.36	-6.05	-0.530	75.82	"
45	90	90	3346.7	0.91	-5.10	-0.607	75.62	"
50	90	90	3349.8	0.46	-3.73	-0.698	75.43	"
55	90	90	3352.2	0.12	-1.98	-0.776	75.26	"
60	90	90	-					"
65	90	90	3352.2	0.12	1.98	-0.776	75.25	"
70	90	90	3349.8	0.46	3.73	-0.698	75.42	"
75	90	90	3346.7	0.91	5.10	-0.607	75.61	"
80	90	90	3343.8	1.36	6.05	-0.530	75.80	"
85	90	90	3341.7	1.68	6.61	-0.481	75.95	"
90	90	90	3341.0	1.80	6.79	-0.465	75.99	"

Appendix 3.24 Berlinite SAW properties (90,90,γ) X cut plate.

α	β (deg)	γ	v(SAW) (m/s)	$\Delta v/v$ (10^{-4})	ϕ (deg)	$\partial\phi/\partial\theta$ (deg/deg)	TCD (ppm/°C)	v(bulk) (m/s)
90	90	0	2832.2	31.22	-7.88	0.364	-2.78	3390.2
90	90	5	2802.2	32.11	-6.01	0.378	-3.99	3264.9
90	90	10	2780.6	31.58	-4.19	0.344	-3.82	3149.8
90	90	15	2766.3	29.49	-2.63	0.276	-2.02	3056.2
90	90	20	2757.9	25.83	-1.38	0.237	1.91	2971.4
90	90	25	2754.7	20.92	-0.07	0.310	8.67	2918.0
90	90	30	2758.2	15.56	1.88	0.474	18.44	2893.3
90	90	35	2771.6	10.66	4.58	0.587	30.32	2899.2
90	90	40	2797.4	6.68	7.52	0.569	42.59	2935.3
90	90	45	2835.7	3.68	10.11	0.455	53.72	2999.2
90	90	50	2884.8	1.63	12.02	0.308	62.87	3087.1
90	90	55	2942.0	0.45	13.20	0.165	69.81	3194.1
90	90	60	3004.3	0.02	13.70	0.040	74.65	3314.7
90	90	65	3068.9	0.12	13.62	-0.068	77.65	3443.7
90	90	70	3133.2	0.53	13.04	-0.160	79.14	3576.1
90	90	75	3194.8	1.04	12.04	-0.240	79.45	3707.3
90	90	80	3251.4	1.48	10.65	-0.313	78.87	3833.7
90	90	85	3300.8	1.74	8.91	-0.385	77.63	3951.9
90	90	90	3341.0	1.80	6.79	-0.465	75.99	4059.3
90	90	95	3369.4	1.69	4.23	-0.567	74.14	3943.1
90	90	100	3383.3	1.49	1.05	-0.709	72.35	3806.9
90	90	105	3378.9	1.35	-2.88	-0.851	76.75	3665.0
90	90	110	3353.3	1.48	-6.99	-0.707	69.20	3531.4
90	90	115	3311.0	2.11	-8.93	0.013	66.47	3418.7
90	90	120	3269.9	3.18	-6.69	0.846	60.74	3338.0
90	90	125	3249.4	4.15	-1.18	1.252	51.21	3298.2
90	90	130	3257.9	3.64	4.00	0.480	37.94	3304.6
90	90	135	3272.2	0.21	-0.70	-2.097	28.52	3358.9
90	90	140	3246.9	1.85	-8.24	-0.830	30.43	3458.2
90	90	145	3198.6	5.73	-10.82	-0.317	28.28	3596.0
90	90	150	3142.6	9.78	-11.94	-0.149	23.61	3762.6
90	90	155	3083.8	13.96	-12.41	-0.043	18.18	3943.7
90	90	160	3025.0	18.19	-12.39	0.051	12.71	3900.5
90	90	165	2968.5	22.31	-11.90	0.144	7.61	3779.5
90	90	170	2916.5	26.05	-10.95	0.233	3.17	3651.8
90	90	175	2870.6	29.12	-9.58	0.311	-0.35	3520.7